https://ntrs.nasa.gov/search.jsp?R=19770022406 2020-03-22T07:52:33+00:00Z

NASA CR- 152579

(NASA-CR-152579) TDRSS TELECOMMUNICATIONS SYSTEM, PN CODE ANALYSIS Final Report (Gold (Robert) Associates, Los Angeles, Calif.) 442 p HC A19/MF A01 CSCL 17B

N77-29350

Unclas
G3/32 44209

RGA

RECEIVED
NASA STI FACILITY
INPUT BRANCH
AUG 1977

ROBERT GOLD ASSOCIATES

435 SOUTH LA CIENEGA BOULEVARD • LOS ANGELES, CALIFORNIA 90048

FINAL REPORT

TDRSS TELECOMMUNICATIONS SYSTEM PN CODE ANALYSIS

Contract NAS 5-22546

Prepared for

NATIONAL AERONAUTICS AND SPACE ADMINISTRATION
GODDARD SPACE FLIGHT CENTER
Greenbelt, Maryland 20771

August 31, 1976

Robert Dixon
Robert Gold
Fred Kaiser

Robert Gold Associates
435 South La Cienega Boulevard
Los Angeles, California 90048

TABLE OF CONTENTS

Table of Contents (continued)

Table of Contents (continued)

LIST OF TABLES

List of Tables (continued)

LIST OF FIGURES

List of Figures (continued)

List of Figures (continued)

List of Figures (continued)

1.0 INTRODUCTION

1.1 General

This document is the final report on TDRSS Telecommunications System PN Code Analysis, performed by Robert Gold Associates for NASA Goddard Space Flight Center under Contract NAS 5-22546, and represents the work accomplished during the reporting period October 1975 through July 1976.

The purpose of this study was to perform parametric analysis of the pseudo noise (PN) codes required to support the TDRSS telecommunications services and to assess the impact of alternate coding techniques on the user transponder equipment, the TDRSS equipment, and all factors that contribute to the acquisition and performance of these telecommunication services. Specifically, possible alternatives to the currently proposed hybrid FH/direct sequence acquisition procedures have been considered and compared relative to acquisition time, implementation complexity, operational reliability, and cost. The hybrid FH/direct sequence technique was analyzed in detail and rejected in favor of the approach described in this report. The recommended approach minimizes acquisition time and user transponder complexity while maximizing probability of acquisition and overall link reliability.

1.1.1 Contents of Report

The remaining sections of this introduction provide a brief overall description of the TDRSS and a communication link analysis upon which the overall study conclusions were based. In Section 2, the recommended signal structure and associated codes are given. Code characteristics and taps selected to provide the desired characteristics are given. A description of the user transponder subsystem and specifications for system parameters are provided. Both the forward and return link signals and their operation are described in this section. The emphasis of Section 2 is to provide an overview of the system, its characteristics, and operational capabilities as they are laid out in the selected design.

Subsystem design is described in Section 3. User transponder and ground receiver designs are described, and block diagrams and operational descriptions of these subsystems are given. U er transponder design in postulated on the NASA Standard Transponder as a baseline. This permits a familiar transponder configuration to be considered for ready extension of expected complexity.

Phase-shift-keyed signals are employed throughout the system, in all modes, and in forward and return links. The signal format chosen has been based on system performance in acquisition, data tra nission, and ranging operations, and has also been oriented to minimizing overall system complexity—especially in the user transponder subsystem. Signal design and employment of dual PSK signal structures are discussed in detail in Appendix A. 2.

The recommended synchronization techniques of the user transponder for the forward link and the ground receiver of the re urn link are discussed and analyzed in Section 4. Emphasis is placed on the multiple access links which, for both the forward and return channels, have the lowest threshold. The code search algorithm requires the largest amount of the overall synchronization time. Hence, little emphasis was placed upon the code loops and carrier loops which are activated upon acquisition. It is estimated that the pull-in, settlir and tracking times associated with these loops are less than 1 second and hence are almost insignificant contributors to the overall synchronization time.

Section 4 begins with an outline of candidate acquisition techniques. A summary table is given of the candidate techniques which is the result of a first-level analysis documented in the Interim Report.* As a result

---

*<u>Interim Report, TDRSS Telecommunications System PN Code Analysis</u>, Robert Gold Associates (under Contract NAS 5-22546), April 30, 1976.

of this preliminary study, two techniques were selected for more detailed analysis. In Section 4.3, the basic theory and associated analysis of the fixed length and sequential detection tests is presented. The functional models of the detectors, as well as the derivations of the mean acquisition times, is given. The results are extended to include a dual state detection algorithm. Several supplementary analyses are also given. These include a code doppler analysis, interfering signal analysis, and bandlimiting analysis. The subsection concludes with a discussion of multiple filter acquisition techniques for doppler resolution.

The application of the developed theory to the user transponder is given in Section 4.4 and to the ground receiver in Section 4.5. In each case, the discussion begins with a distribution of error and minimum threshold summary. Desired performance requirements are summarized and these parameters are used as inputs and applied to the theoretical development of Section 4.3. The overall performance is then summarized in tables and graphs.

The impact of multipath upon the synchronization parameters is summarized in Section 4.6. The basic multipath characteristics were established in a special study performed by the Boeing Company. A short summary of this study is presented herein with further details given in the Interim Report. The impact of these various parameters is discussed relative to the acquisition of the 3 Mcps PN signal on the forward link to the user receiver. The section concludes with the discussion of an algorithm developed to preclude false lock to a multipath signal.

Code generation techniques and recommended code libraries for the recommended TDRSS signal designs are presented in Section 5. Sections 5.1 through 5.4 discuss the general principles and techniques for the selection of the bandspread codes for TDRSS and Section 5.5 contains an analysis of the effect of clock error on acquisition. Specific code libraries for TDRSS are developed in Section 5.6. The Forward Link Multiple Access Library consists of 100 long codes of period $2^{18}-1$. These may be selected from the family of Gold codes of the period which are generated as described in Section 5.6.1.1, or from the library of maximal PN codes of this period listed in Appendix G.5. The technique for the generation of the code library for the Mode 2 return link is described in Section 5.6.2 and the correlation properties of this family are analyzed and documented in Appendix A.5. The code library for the dedicated Mode 1 return link consists of maximal PN codes of period $2^{18}-1$. The codes selected are those such that phase-shifted versions in excess of 20,000 chips may be generated by adding the output of two stages of the 18-stage code generated. This code library, together with the taps which must be added and the resultant phase shift, are contained in Appendix C.5.

1.2 System Design Considerations

TDRSS is a satellite communication signal relay system intended to provide almost complete earth coverage to users wishing to transmit or receive messages to and from earth stations located within the United States. The system is illustrated in figure 1.2-1.

"The Tracking and Data Relay Satellite System (TDRSS) will consist of two geosynchronous relay satellites, 130 degrees apart in longitude, and a ground terminal located in the continental United States. Additionally, the system will include two spare satellites; one in orbit, and one in configuration for a rapid replacement launch. The purpose of the TDRSS is to provide telecommunications services which will relay communications signals between low earth-orbiting user spacecraft and the user control and/or data processing facilities. A real-time, bent-pipe concept is utilized in the operation of the TDRSS telecommunications services. The system will be capable of transmitting data to, receiving data from, or tracking user spacecraft over at least 85 percent of the user orbit."*

Services provided by TDRSS are:

Multiple Access - "The multiple access (MA) communication service system is designed to provide simultaneous real-time and dedicated return link service to low earth-orbiting user spacecraft with real-time data rates to ___ bps. Forward and return link service will be provided to all system users."*

Single Access - "The single access (SA) communication service system is designed to provide a high data rate return link to users with real-time, playback, or science data requirements. The system will be utilized on a priority scheduled basis, and will not normally be used for dedicated support to any mission (with the exception of Space Shuttle)."*

Cross-support - "Any mission which is compatible with the MA system can receive forward or return link support from either the MA or SSA systems."*

*TDRSS User's Guide, May 1975.

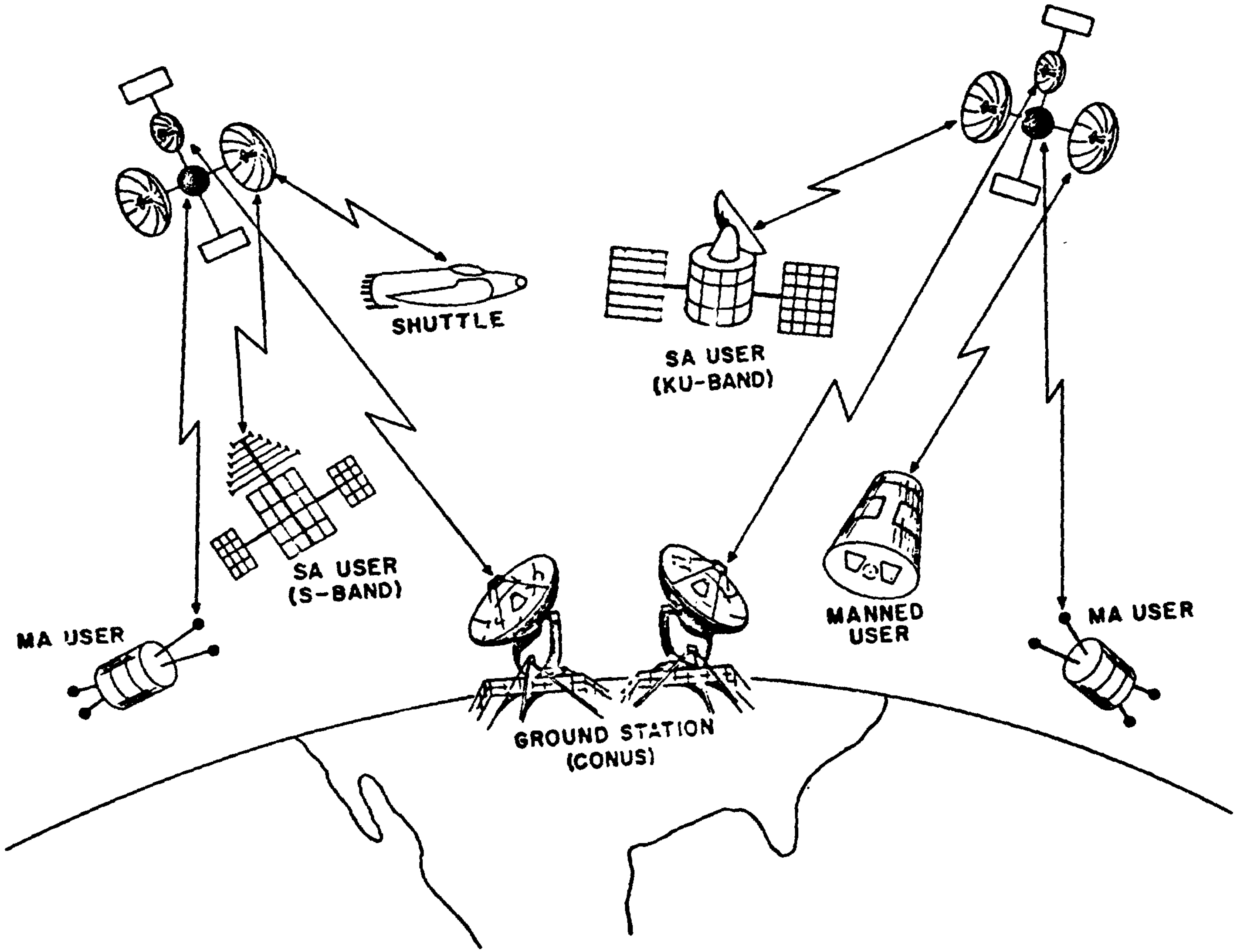

Figure 1.2-1. TDRSS Concept

Tracking - All service systems can provide range rate tracking data for the users supported. Tracking accuracy will be comparable to that currently available from the ground-based STDN (Spacecraft Tracking and Data Network).

Operating Frequencies

TDRS to User

SMA	2106.4 MHz
SSA	2.2 to 2.3 GHz
KSA	15.0086 GHz

User to TDRS

SMA	2287.5 MHz
SSA	2025 to 2120 MHz
KSA	13.775 GHz

The various subsystems and their requirements are described in the sections of this report that follow. Each subsystem is considered, together with its signals, and its functions in handling and/or generating those signals.

1.3 Link Analysis

1.3.1 Introduction

One of the objectives of this investigation as to determine, based on the link an. lyses, the minimum received signal level by the user receiver for each of the TDRSS forward links and, similarly, for the ground receiver for each of the return links. One of the primary assumptions was the user antenna gain. Values assumed are those given in the performance specification for the simulation service.* For both the MA and SSA service, an antenna gain of -9 dB was used. For the KSA service, +17 dB gain was assumed.

1.3.2 Discussion of Results

Forward Links. A summary of the forward link analyses is given in tables 1.3-1 through 1.3-3. Considering first the MA forward link, we find the minimum received signal level is approximately -137 dBm. This is the required receiver sensitivity. Continuing on through the link analysis of table 1.3-1, we find that with no design margin the link is just on the edge of being able to support a data rate of 100 bps, the desired objective for the minimum data rate. By increasing the receiver antenna gain, the link is capable of supporting a higher data rate.

The SSA forward link does not require the receiver sensitivity of the MA forward link. It has a minimum received signal level as shown in table 1.3-2 of -127.8 dBm. This link is capable of supporting a data rate in excess of 400 bps with a 3 dB design margin. Compared with the multiple access system, the S-band single access system is characterized by higher S/N_0 values due to the gain of a dish antenna on the TDRS. Thus, synchronization acquisition on the forward link is less of a problem than with the multiple access system.

---

*Performance Specification for Telecommunications Service Via the Tracking and Data Relay Satellite System, Goddard Space Flight Center, S-805-1, June 1975, p. 25.

Table 1.3-1. Link Analysis for MA Forward Link, S-Band

f_c = 2106.4 MHz

TDRS Antenna Gain (dB)	23.0	
TDRS Transmit Power (dBw)	13.0	
RF Transmit Loss (dB)	-1.0	
Transmitted EIRP (dBw)	35.0	
TDRS Transponder Loss (dB)	-1.0	
Antenna Pointing Loss (dB)	0	
Signal EIRP (dBw)	34.0	
Space Loss (dB)	-191.6	
User Antenna Gain (dB)	-9.0	
Polarization Loss (dB)	-0.5	
P_s - Signal Power Out of User Antenna (dBw)	-167.1	
P_s - Signal Power Out of User Antenna (dBm)	-137.1	
T_s (Antenna Output) (824^oK) (dB)	29.2	
KT_s (dBw/Hz)	-199.4	
P_s/KT_s (dB-Hz)	32.3	
Required E_b/N_0 = 9.9 dB @ 10^{-5} BER	-9.9	
Demodulation Loss (dB)	-1.5	
PN Loss (dB)	-1.0	
Achievable Data Rate (dB), No Margin	19.9	implies 98 bps
Achievable Data Rate (dB), 3 dB Margin	16.9	implies 49 bps

Table 1.3-2. Link Analysis for SSA Forward Link, S-Band

f_c = 2106.4 MHz

TDRS Antenna Gain (dB)	35.4
TDRS Transmit Power (dBw)	11.6
RF Transmit Loss (dB)	-2.0
Transmitted EIRP (dBw)	45.0
TDRS Transponder Loss (dB)	-1.0
Antenna Pointing Loss (dB)	-0.5
Signal EIRP (dBw)	43.5
Space Loss (dB)	-191.6
User Antenna Gain (dB)	-9.0
Polarization Loss (dB)	-0.5
P_s - Signal Power Out of User Antenna (dBw)	-157.8
P_s - Signal Power Out of User Antenna (dBm)	-127.8
T_s (Antenna Output) (824^{o}K) (dB)	29.2
KT_s (dBw/Hz)	-199.4
P_s/KT_s (dB-Hz)	41.8
Required E_b/N_0 = 9.9 dB @ 10^{-5} BER	-9.9
Demodulation Loss (dB)	-1.5
PN Loss (dB)	-1.0
System Margin (dB)	-3.0
Achievable Data Rate (dB)	26.4 implies 436 bps

Table 1.3-3. Link Analysis for KSA Forward Link

f_c = 13.775 GHz

TDRS Antenna Gain (dB)	52.0	
TDRS Transmit Power (dBw)	-3.0	
RF Transmit Loss (dB)	-2.0	
Transmitted EIRP (dBw)	47.0	
TDRS Transponder Loss (dB)	-1.0	
Antenna Pointing Loss (dB)	-0.5	
Signal EIRP (dBw)	45.5	
Space Loss (dB)	-208.6	
User Antenna Gain (dB)	17.0	
Polarization Loss (dB)	-0.5	
P_s - Signal Power Out of User Antenna (dBw)	-146.6	
P_s - Signal Power Out of User Antenna (dBm)	-116.6	
T_s (Antenna Output) (893°K) (dB)	29.5	
KT_s (dBw/Hz)	-199.1	
P_s/KT_s (dB-Hz)	52.5	
Required E_b/N_0 = 9.9 dB @ 10^{-5} BER	-9.9	
Demodulation Loss (dB)	-1.5	
PN Loss (dB)	-1.0	
System Margin (dB)	-3.0	
Achievable Data Rate (dB)	37.1	implies 5128 bps

The link analysis for the KSA forward link is given in table 1.3-3. The received signal power is the greatest of the three links, -116.6 dBm. With a 3 dB design margin, the link is capable of sustaining a data rate in excess of 5 kbps.

One area of investigation which was not considered in the link analyses given in the above reports is that of ionospheric scintillation. Recent investigations have found that it does have an effect on the signal in the 2-4 GHz region. This effect occurs only if the signal penetrates the ionosphere. If the signal does penetrate the ionosphere, peak-to-peak amplitude fluctuations of 2 to 5 dB, as well as phase perturbations, can occur at certain times during a 24-hour time period. The fluctuations will be the greatest if the propagated signal comes within the influence of the earth's magnetic equator or the aurora zones. The intensity of the scintillation effects is also correlated with the sunspot activity. To obtain a point of reference, an analysis was made to determine the range from the TDRS satellite to a user in a 2000 km orbit at which the signal would penetrate the edge of the ionosphere. Referring to Figure C-7 on page C-16 of the User's Guide,* we see the geometry depicting the range selected for the link calculations. At this range, the closest distance to the earth's surface is 1829 km. For the satellite to be within 500 km of the earth's surface, which would be the outer edge of the ionosphere, the range to the user satellite is 46,550 km. It is at this range and beyond for the spatial relationships given in Figure C-7 that the scintillation effects can be observed.

Return Links. A summary of the multiple access, single access and Ku-band single access return link analyses is given in table 1.3-4. These results are taken from the User's Guide and are included here for completeness.

---

*Tracking and Data Relay Satellite System (TDRSS) User's Guide, Goddard Space Flight Center, STDN No. 101.2, Rev. 2, May 1975, pp. C5-C16.

Table 1.3-4. Return Link Analysis

S-Band: f_c = 2287.5 MHz

Ku-Band: f_c = 15 GHz

	S-Band		Ku-Band
Link Parameters	Multiple Access	Single Access	Single Access
BER	10^{-5}	10^{-5}	10^{-5}
User EIRP (dBw)	EIRP	EIRP	EIRP
Space Loss (dB)	-192.2	-192.2	-209.2
Polarization Loss (dB)	-1.0	-0.5	-0.5
Pointing Loss (dB)	---	-0.5	-0.5
TDRS Antenna Gain (dB)	28.0	36.0	52.6
P_s at Output of Antenna (dBw)	-165.2 + EIRP	-157.2 + EIRP	-157.6 + EIRP
T_s (Antenna Output Terminals) (°K)	824	586	893
T_i (Due to Other User Interference)(°K)	255	---	---
$K\ (T_s + T_i)$ (dBw/Hz)	-198.3	-200.9	-199.1
$P_s/K(T_s + T_i)$ (dB-Hz)	33.1 + EIRP	43.7 + EIRP	41.5 + EIRP
Transponder Loss (dB)	-2.0	-2.0	-2.0
Demodulation Loss (dB)	-1.5	-1.5	-1.5
PN Loss (dB)	-1.0	---	---
Antenna Beam Forming Loss (dB)	-0.5	---	---
System Margin (dB)	-3.0	-3.0	-3.0
Required E_b/N_0 (dB) PSK	-9.9	-9.9	-9.9
Achievable Data Rate (dB)	15.2 + EIRP	27.3 + EIRP	25.1 + EIRP
FEC Gain (dB) R = 1/2, K = 7	5.2	5.2	5.2
Achievable Data Rate (dB)	20.4 + EIRP	32.5 + EIRP	30.3 + EIRP

Data rates on the return link multiple access spread spectrum signal from a user can range up to 50 kbps and rate 1/2 error correction establishes the maximum symbol rate at 100 kbps. Return link performance for a given multiple access user is affected by interference from other users within the receive beam. An analysis of this degradation is given in Section 4.3.5.

The S-band single access return link may have telemetry data rates in the range from 100 bps up to 6.3 Mbps. As with the multiple access return link, the rates are a function of the operational mode, the EIRP, whether the data is biphase formatted or convolutionally coded, and whether spectrum spreading is utilized.

The Ku-band single access return link is intended to handle telemetry data rates from 1 kbps to 300 Mbps. The data rates are functions of the same factors as given above for the single access return link.

2.0 SUMMARY OF RESULTS

This report section describes the results of studies carried out by Robert Gold Associates. Signal design descriptions are given for both forward and return links, together with recommended system and subsystem parameters.

2.1 Forward Link Multiple Access

2.1.1 Recommended Parameters

Signal Design

The recommended signal design is a dual format, wherein a pair of PSK (phase-shift-keyed) signals are sent on quadrature-related versions of the same carrier signal. This is illustrated by the modulator of Figure 2.1-1. (It is noted that the modulator shown is different from a standard quadriphase PSK modulator only in that one of the two biphase PSK signals generated internally to the modulator is held to a level 10 dB below the other.) The signal employed can be considered to be a composite of two signals, one of which has 10 dB less power than the other, whose carriers happen to be at the same frequency and whose carrier phases are in quadrature. The quadrature phase relationship is assured by actually employing only one carrier signal source and routing properly phase-shifted versions of this carrier to the right place. Frequency coherence is assured by this employment of phase-separated versions of the same carrier reference for the two signals.

The forward link multiple access signal is an unbalanced quadriphase pair of signals, as shown in Figure 2.1-2. This signal is made up of a pair of bi-phase signals related in such a way that their combined structure has a constant envelope. That is, in the steady state, the signal always takes one of the four phases as shown in Figure 2.1-2, and the radius vector has the same value in all four phases as long as the two bi-phase signals are maintained in phase quadrature. Constant envelope

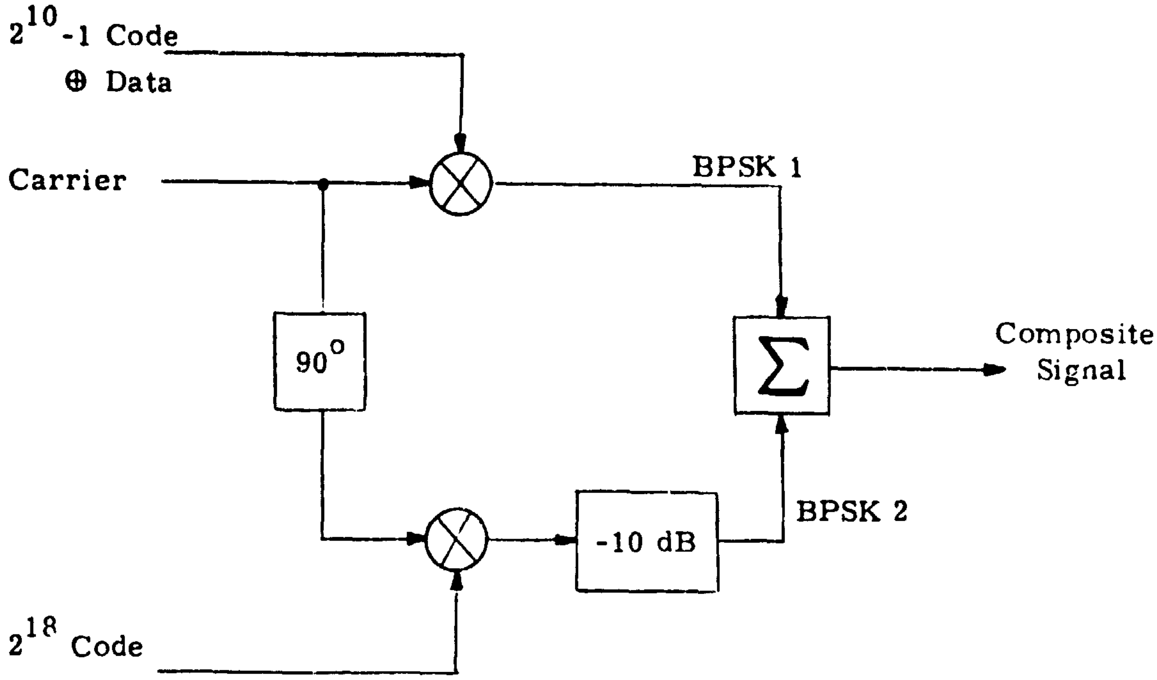

Figure 2.1-1. Composite Signal Modulator

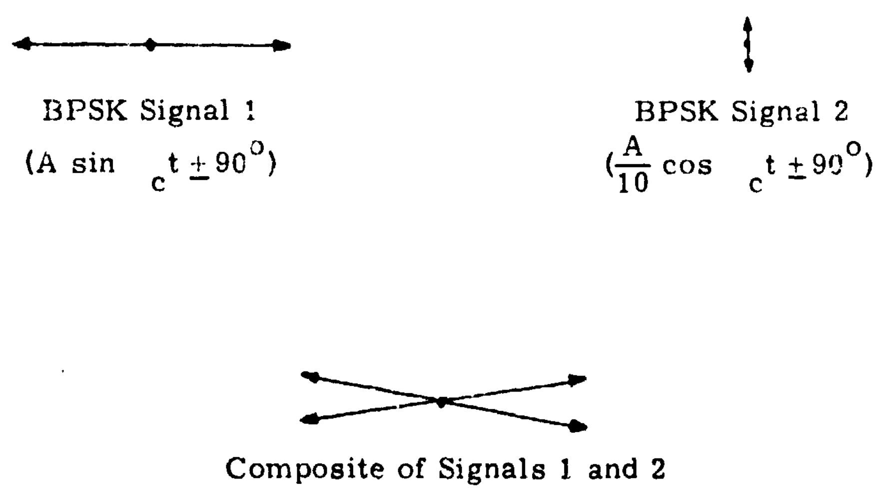

Figure 2.1-2. Composite Signal Structure

power is important in systems employing either traveling wave tube or solid-state power amplifiers, as these exhibit AM-to-PM conversion in the range of 6 to 10 degrees for each 1 dB signal amplitude change. Thus, incidental phase modulation may be caused by unintended amplitude modulation, and this phase modulation can approach the level of the desired signal, causing serious loss or degradation of the intended signal.

A dual bi-phase signal format has been chosen in preference to dual quadriphase because of the relative simplicity of the bi-phase structure from the hardware point of view. In addition, it is necessary to limit the allowable phase states assumed by the smaller signal in a dual-QPSK modulator, to avoid incidental AM modulation.

Direct sequence spread spectrum modulation is employed in the forward link for several reasons:

1. The spread spectrum modulated signal has relatively low power density, which is necessary to meet system requirements for signal flux density at the earth's surface* due to TDRSS transmissions,

2. The coded modulation provides for code division multiple access operation.

3. The system has reduced sensitivity to interference, as well as furnishing low interference to other link users.

4. Good range resolution is facilitated by the coded modulation.

Demodulation of the dual signals must be accomplished by synchronizing the receiver to both transmitted code sequences. For all practical

---

*S-band

-154 dBw/m^2 in 4 kHz for 0^o to 5^o arrival angle.
-154 + (0-5)/2 dB BW/m^2 in 4 kHz for 5^o to 25^o
-144 dBw/m^2 in 4 kHz for 25^o to 90^o

Ku-band

-152 dBw/m^2 in 4 kHz, 0^o to 5^o
-152 + (0-5)/2 dBw/m^2 in 4 kHz, 5^o to 25^o
-142 dBw/m^2 in 4 kHz, 25^o to 90^o.

purposes, the signal received is treated as if it were two unrelated signals. Therefore, the optimum receiver is actually a pair of bi-phase PSK receivers rather than a single quadriphase receiver for two unequal signals; even though the two signals are in phase quadrature just as are other quadriphase PSK signals.

As the coded modulation is a key to range resolution, multiple access, interference rejection, and low spectrum density, the codes employed must be plentiful, readily generated, and have good correlation properties. The larger of the dual signal pair is modulated by a 3.077799 Mbps, 1023-bit code sequence of the "Gold" type. This signal is employed for initial acquisition and for data transmission. The second, smaller signal is modulated by a longer code ($2^{18}-256$ bits) at the same bit rate, and is employed for range measurement.

The code sequences employed in the forward link (Codes 1 and 2 of figure 2.1-1) are of lengths 1023 bits and (1023 · 256) bits, at a bit rate of 3.077799 Mbps. Gold sequences will be employed for the 1023-bit codes to insure that a large family of usable codes is available. The long code is specifically chosen to have a length which is an integral multiple of the shorter code length, which aids in the long code synchronization process.

In the return link, the f_1 signal used as a reference for carrier frequency generation may be coherent or noncoherent with the f_1 signal used in the forward link. This depends on the mode in which the system is operating (see table 2.1-1). In all cases, code rates are related to carrier frequency in the following ratios:

Operation	Ratio	Bit Rate
SMA, SSA	$\frac{31\ fc\ (fwd)}{221 \times 96}$	3.077799479 Mbps
KSA	$\frac{31\ fc\ (fwd)}{1469 \times 96}$	3.02803069 Mbps

The section that follows lists the specific codes that have been selected for use in this program.

Table 2.1-1. PN Code Lengths

Mode	Q Channel Code	I Channel Code	f_1/f_2
1	1023 bits	(1023 · 256) bits	Coherent
2	2047 bits	2047 bits	Noncoherent
3	None	(1023 · 256) bits	Coherent

Codes recommended are listed in the following paragraph.

2.1.2 User Transponder Description

This section describes a user transponder design used to implement tradeoffs in signal structure and signal selection. Further information and details may be found in Robert Gold Associates Interim Report for Contract NAS 5-22546, TDRSS PN Code Analysis, April 30, 1976.

2.1.2.1 Figure 2.1.3 shows the simplified block diagram of a transponder design based on the NASA Standard Transponder configuration. The necessary spread spectrum blocks have been added to the standard transponder to provide the desired signal characteristics (i.e., wideband, low-power-density signals in the modulated signal band).

A signal at 2106.40625 MHz (221 f_1) is received and mixed with a local oscillator at 1982.5 MHz (208 f_1) to produce a 193.90625 MHz IF signal. At this IF frequency, the signal is split and applied to two second mixers along with two local code-modulated reference signals. One of these local reference codes (No. 1) is the 2^{10}-1 bit synchronization and data sequence, and the other (No. 2) is the 2^{18}-256 bit ranging sequence. Both local reference signals are centered at 136.15625 MHz, so that when local codes are synchronous with either received signal, the corresponding IF2 output signal is 12.25 MHz, output to either $IF2_A$ or $IF2_B$ depending on which code is synchronous (either one or both may be synchronized at any given time).

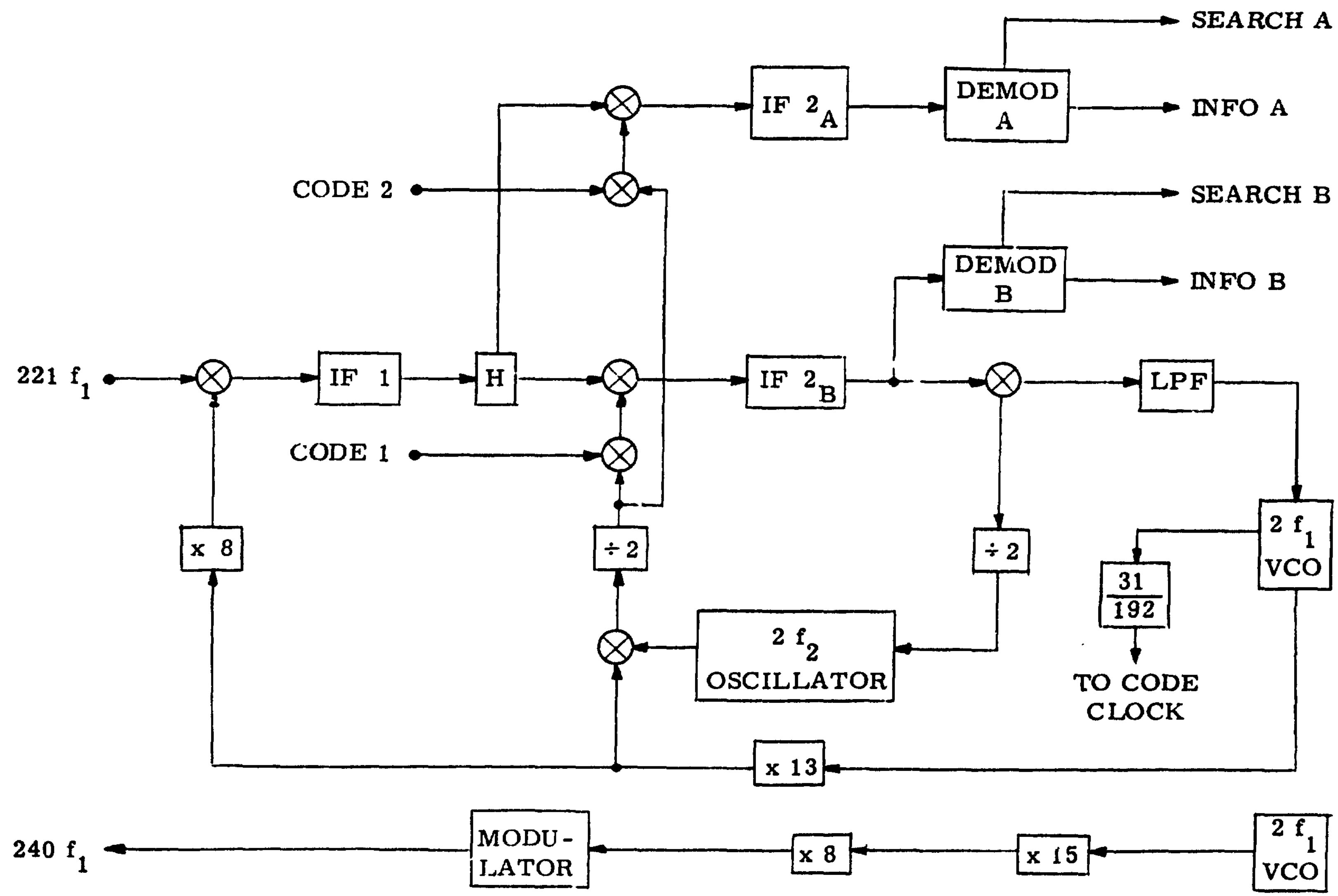

Figure 2.1-3. Transponder Block Diagram

A synchronized signal output in $IF2_B$ is from the 1023 bit code channel, which includes forward link data in its modulation. The synchronized signal output then is a carrier (at 12.25 MHz) that is PSK modulated by the desired data. This signal is then demodulated and the data employed as required.

The $IF2_A$ signal is an unmodulated carrier employed in ranging. Since this signal is unmodulated, the design of Demod A is greatly simplified by a carrier detector. Further, since the $IF2_B$ signal will be acquired prior to the $IF2_A$ signal, coherent carrier detection is facilitated, as a carrier reference is available from Demod B. If desired, low rate data such as commands might be sent as baseband modulation on the signal in $IF2_A$. Of course, this would impact the demodulator design since it would then be required to accept data, and this would in turn bring about the need for a somewhat wider bandwidth (at least as great as the data rate).

Either coherent or noncoherent signal transmission at 240 f_1 is facilitated to allow for turnaround ranging or any other operation that might require a return link signal that is coherent with the forward link signal.

Two separate oscillators are provided as $2f_1$ sources. One, a VCO, is phase locked to the forward link signal, which provides a coherent $2f_1$ source for generating (after multiplication by 120) the return link carrier. In the noncoherent mode, a separate $2f_1$ oscillator is used to generate the return link carrier. In some instances, the noncoherent mode is necessary to prevent retransmission of a return link signal that is perturbed by forward link carrier phase noise.

Code clock is also derived by operation on the $2f_1$ VCO or $2f_1$ oscillator. Again, the decision as to which is used depends on whether coherent or noncoherent turnaround must be employed. The clock rate is 31/96 f_1, or 3.077799479 Mbps when the return link carrier frequency is 2287.5 MHz. Code rate does vary as carrier frequency is changed, but within the range of carrier frequencies expected, the code rate will be close to 3.0 Mbps.

Basic code generator design is illustrated in figure 2.1-4. A number of codes must be generated simultaneously for full forward and return link operational capability. The use of a number of codes and availability of a large library of well-defined and carefully selected codes is a feature of the system design and a specific goal of this study program.

The most prominent features of the user transponder design selected are given in table 2.1-2.

2.1.2.2 Estimates of the number of components required to implement the portions of the user transponder that are beyond the subsystem included in present standard transponder design (i.e., code generators, code modulators, and other circuitry associated specifically with spread spectrum modulation and demodulation) are given in table 2.1-3. Also included in this table is an estimate of the additional power required to operate these additional components. Overall power estimated for a transponder is given in tables 2.1-4 and 2.1-5.

Table 2.1-6 shows overall weight estimated for a spread spectrum user transponder.

It is apparent from considerations of available alternatives that the selected direct sequence approach meets TDRSS requirements and is the best available method for doing so.

Further descriptions of the user transponder and the signal structure employed in TDRSS may be found in section 3.1 of this report.

Table 2.1-7 lists the overall characteristics of the recommended subsystem.

2.1.3 System Performance

The results obtained for the S-band multiple access and single access forward link synchronization study are summarized below. We begin by summarizing the performance objectives and the system constraints.

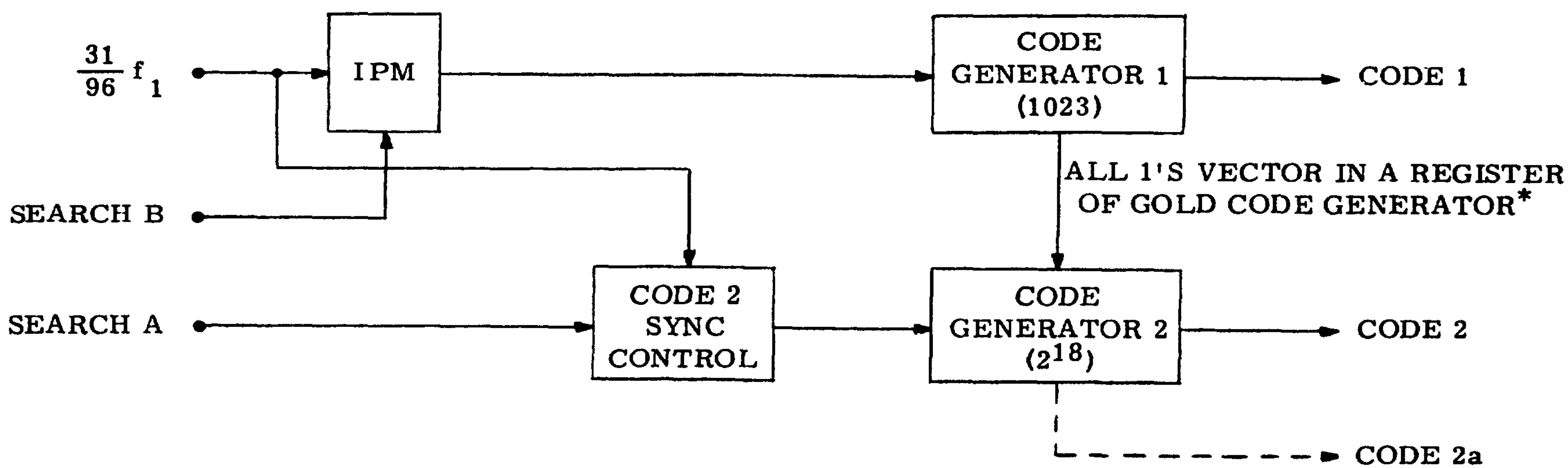

*See Figu 'e 5.6-2, page 5-23.

Figure 2.1-4. Transponder Code Generator

Table 2.1-2. User Transponder Design

Synchronization Technique	1-23 bit sequence Sequential acquisition with doppler resolution filters
Data Transmission	By sequence inversion modulation of the 1023 bit sequence
Ranging Code	2^{18}-256 bit sequence ranging code acquisition by derivation from short code timing. Used for ranging only
Signal Format	Unbalanced QPSK, synchronization/ data transmission code on (90,270) degree carrier, range co e on (0,180) degree carrier. Range carrier 10 dB below data carrier
Code Rate	3.07799 Mbps
Average Synchronization Time	Sequential Search Short code 14.2 seconds Long code 1.5 seconds
User can synchronize any time, no specific synchronization mode	
Additional Hardware Required (transponder)	75 components
Power Estimated (transponder)	7.4 watts (not including P.A.) MIC constuction 12.0 watts (not including P.A.) Hybrid construction
Development Risks	No new transponder circuitry needed. Code generators, frequency synthesizers, modulators, and demodulators use proven circuits and techniques

Table 2.1-3. Component Estimate

	Circuits		Power
Transmitter			
Coders	8	33 f-f	0.33 w
	2	8 mod 2	0.08
	3	3 nor	0.03
Modulator	12	2 B.M.	0
	1	1 90° hybrid	0
	1	1 Σ	0
	1	1 10-dB atten.	0
	28 components		0.44 w
Receiver			
	36	6 B.M.	0
	2	2 Σ	0
	6	6 IF I.C.	0.6 w
	30	30 resistors	0
	25	25 capacitors	0
	2	2 BPF	0
	12	45 f-f	0.45
	1	1 comparator	0.1
	1	1 diff. amp.	0.1
	1	1 4 Q mult.	0.1
	2	7 gates	0.07
	2	8 mod 2	0.08
	2	2 VCO I.C.	0.1
	122 components		1.6 w

Assumes: 10 mw/digital I.C.; 100 mw/analog I.C.

28 + 122 = 150 total parts

0.44 + 1.6 = 2.04 w total

Table 2.1-4. Total Power Estimate

SS	2.04 w
Hybrid IF/RF	10.0 w
MIC IF/RF	5.5 w
Hybrid	12.04 w total
MIC	7.54 w total
	(No PA)

Table 2.1-5. Power Amplifier Estimate

Power Amplifier (20 watts)

TWT	6.5 lb	80-133 w prime power
Trapatt	<4 lb	50-80 w prime power
Transistor	<4 lb	50-67 w prime power

Table 2.1-6. Total Weight

SS	1.6 lb
Hybrid IF/RF	2.25 lb
MIC IF/RF	1.6 lb
Hybrid	3.85 lb total
MIC	3.2 lb total

Table 2.1-7. Transponder Specifications

RECEIVER CHANNEL	
Center Frequency	2106.40625 MHz
Noise Figure	2.5 dB max
Bandwidth (3 dB)	5 MHz min (at 2nd IF)
VSWR	1.1:1 to ± 2.25 MHz
Phase Response	Linear to within $\pm 5^{\circ}$ $\pm$ 1.50 MHz
Amplitude Response	Flat to within 1/2 dB $\pm$ 1.50 MHz
Dynamic Signal Range	40 dB
Maximum Signal and Noise	-130 dBW
Minimum Signal	-180 dBW
SYNCHRONIZATION PREAMBLE	
Code:	
Type	Pseudorandom, Gold-type
Code Generation	Linear
Code Length	1023 bits
Code Loop:	
Dither	τ_d = 0.5 chip (if τ dither used), delay lock preferred
Order	1st
Bandwidth (B_L)	0.1 Hz
Dynamics Aiding	From carrier loop
Acquisition:	
Search Steps	1/2 chip
Average Search Rate	75 chips/second
Signal Detector	Sequential detector
Detector Bandwidth	± 3 kHz
Frequency Uncertainty	700 Hz nominal, 3000 Hz maximum
Time Uncertainty	1023 PN chips maximum

Table 2.1-7. (continued)

PN Losses:	
Bandwidth	Negligible
Channel Distortion	0.5 dB
Imperfect Tracking	0.3 dB
CARRIER ACQUISITION AND TRACKING	
Type of Loop	Costas/PLL or Squaring
Loop Order	2nd
Loop Bandwidth (B_L)	32 Hz
Damping Factor	0.707
Frequency Offset (Max)	
Acquisition	$\pm$ 3 kHz
Tracking	$\pm$ 60 kHz
Incidental FM	6^{o} RMS in 10 Hz with good S/N, maximum
Carrier Tracking Losses:	
Incidental FM	0.2 dB
Nonlinearities	0.5 dB at threshold
AGC Noise	0.3 dB at threshold
COMMAND DATA DEMODULATION	
Demodulator	Costas Loop
Fixed Data Rate	125, 1000 bps
Data Processing	Integrate and dump
Telemetry Data:	
Rate	1 kbs - 50 kbs
Clock	Asynchronous, user supplied
External Interface	TTL compatible
EDAC Encoding	
Type	Convolutional
Constraint Length	7
Rate	1/2
Transmission Encoding	
Type	Differential

Table 2.1-7. (continued)

User Oscillator Phase Noise	$\leq 3^{o}$ RMS; BW - 6 Hz - 100 kHz
Modulator/Demodulator Phase Imbalance	$\leq 4^{o}$
Modulator/Demodulator Amplitude Imbalance	≤ 0.5 dB
Data Asymmetry	≤ 1 percent
Data Skew	≤ 0.1 bit time
Data Decoding	Differential
Data Clock	Derived from PN code
Data Interface	TTL
Implementation Losses:	
Carrier Reference at Threshold	1 dB at 100 bps
Nonlinearity	0.3 dB
Bandlimiting	0.2 dB
TRANSMIT CHANNEL	
Transmitter:	
Type	Solid State or TWT
Center Frequency	2287.5 MHz
Bandwidth (3 dB)	6 MHz minimum
Amplitude Response	Flat to within 1/2 dB bandwidth
Phase Response	Linear to within $\pm 5^{o}$
Modulator:	
Modulation	Unbalanced QPSK
Code Families	Gold code pairs
PN Chip Rate	3.077799 MHz
Code Lengths	
Forward Link	2^{18} - 256, 1023
Return Link	2^{18} - 256, 1023
Bandwidth	3 MHz
Filter Type	Butterworth, 4-pole

Table 2.1-7. (continued)

Carrier Suppression	30 dB or greater
Spurious Responses	20 dB down outside of ± 3 MHz
AM/PM Conversion	< 10°/dB
Cross-Modulation	≥ 10 dB below signal
Code Epoch	82 msec, 322 μsec
Local Reference:	
Bandwidth (3 dB)	3 MHz
Phase Response	Linear to within ± 5° over ± 1.5 MHz
Amplitude Response	Flat to within 1/2 dB over ± 1.5 MHz
Spurious Responses	20 dB down outside ± 3 MHz
Acquisition:	
Signal Bandwidth	3.077 MHz x 2 (null-null)
Signal Detector	Sequential detector
Detection Bandwidth	± 1500 Hz
Average Search Rate	136 chips/second
Frequency Uncertainty	700 Hz nominal, 3000 Hz maximum
PN DEMODULATION	
PN Code:	
Type	SQPN (Staggered Quadriphase Pseudonoise)
Code Family	Maximal code pairs truncated by 255 bits
Code Period	2^{18} - 256, 1023
PN Chip Rate	3.077 MHz
Repetition Interval	82.432 ms, 322 μsec
Local Reference:	
Bandwidth (3 dB)	3 MHz
Phase Response	Linear to within ± 5° over ± 1.5 MHz
Amplitude Response	Flat to within 1/2 dB over ± 1.5 MHz
Carrier Suppression	45 dB or greater

Performance Objectives

Short Code - 1023 chips

Mean Acquisition Time	20 seconds (including long code)
Probability of Detection	0.9
Probability of False Alarm	10^{-6}

Long Code - 2^{18}-256 chips

Mean Acquisition Time	Included in 20 seconds
Probability of Detection	0.9
Probability of False Alarm	10^{-6}

Multipath rejection algorithm required

System Constraints

Multiple Access Mode:	C/N_0	= 32.3 dB-Hz
	Data Rate	= 125 bps
Single Access Mode:	C/N_0	= 41.8 dB-Hz
	Data Rate	= 125 bps

Total Doppler and Frequency Uncertainty: 3000 Hz

The recommended synchronization approach for the short code is to use a noncoherent sequential search strategy. The theory and functional description of this search strategy is given in section 4.3.2. The analysis of the technique as applied to the forward link is given in section 4.4.

Both the noncoherent fixed length strategies and sequential test strategies were considered in the study. In order to meet the performance objectives, multiple IF contiguous doppler resolving filters are required. The technique analyzed was a completely parallel processing approach. Techniques for simplifying the hardware, such as the implementation of a maximum detector, are possible. However, with the use of the sequential search strategy, only two doppler cells are required. The same performance could be obtained by using two despreaders with each local reference stepping through a different set of cells simultaneously. In this case, only one IF filter covering the total uncertainty band would be associated with each despreader.

The performance of the S-band multiple access and single access forward links is summarized in tables 2.1-8 and 2.1-9, respectively. The fixed length test analysis was not performed for the single access link. However, rough estimates indicate that the average acquisition time exceeds the sequential test acquisition time by an order of magnitude.

Either the coherent or noncoherent sequential test strategy can be used for the long code acquisition of the multiple access forward link. Code tracking and carrier lock are obtained at the conclusion of the short code acquisition. Therefore, two possibilities exist. The first is that the long code can be coherently acquired. The second is that the local reference can be doppler corrected permitting the use of a narrowband IF filter which precedes a noncoherent detector. Clearly, the performance is a function of how narrow an IF filter can be utilized. The average acquisition times for a range of IF bandwidth filter cases for the two approaches suggested above are summarized in Table 2.1-10.

The third aspect of the performance analysis was to assess the nature of the multipath between a low orbiting user satellite and the synchronous TDRS satellite (cf. Section 4.6.7). The primary problem is one of false locking to a multipath component. The differential doppler is small enough that most of the multipath energy will fall within the receiver bandwidth. The basic nature of the multipath signal is diffuse rather than specular. The multipath energy tends to be smeared over several tap positions. The degree of smearing is a function of the elevation angle and the antenna polarizations relative to the multipath signal.

Several techniques for avoiding false lock to a multipath signal are suggested. These techniques take advantage of the basic properties of the multipath signal at the output of the despreader. The one approach takes advantage of the diffuse nature of the multipath energy in frequency, thus making it very difficult to falsely code lock and carrier lock to the multipath

Table 2.1-8. Comparative Summary of Average Acquisition Times for the MA Forward Link Short PN Code

Number of Doppler Cells	IF Bandwidth per Cell (Hz)	SNR in Frequency Cell (dB)	Noncoherent Fixed Length Test Strategy		Noncoherent Sequential Test Strategy	
			$\overline{T}_{acq}$ (sec)	Average Search Rate (chips/sec)	$\overline{T}_{acq}$ (sec)	Average Search Rate (chips/sec)
1	6000	-9.3	42.9	23.8	28.6	35.8
2	3000	-6.3	27.5	37.2	14.2	72
5	1200	-2.3	16.5	62.0	5.7	179
10	600	0.7	13.7	74.7	2.9	353

Table 2.1-9. Summary of Average Acquisition Times for the SA Forward Link Short PN Code

Number of Doppler Cells	IF Bandwidth per Cell (Hz)	SNR in Frequency Cell (dB)	Noncoherent Sequential Test Strategy	
			$\overline{T}_{acq}$ (sec)	Average Search Rate (chips/sec)
1	6000	0.2	0.8	1279
2	3000	3.2	0.8	1279

Table 2.1-10. Comparative Summary of Mean Acquisition Times for Multiple Access Forward Link Long PN Code

IF Bandwidth (Hz)	SNR in IF Bandwidth (dB)	Sequential Test Strategy* Coherent		Sequential Test Strategy Noncoherent	
		$\overline{T}_{acq}$ (sec)	Mean Search Rate (chips/sec)	$\overline{T}_{acq}$ (sec)	Mean Search Rate (chips/sec)
6000	-17.2	1.4	182.9	276	0.93
3000	-14.2	1.35	189.6	138	1.9
1200	-10.2	1.3	196.9	55	4.7
600	-7.2	1.3	196.9	27	9.5

*Assumes local reference stepped in 1/2 chip increments.

signal. The other approach makes use of the time spread of the multipath signal. The energy is almost flat across several adjacent time cells. This is in contrast to the direct signal whose cross-correlation function peaks at its in-phase position, and is almost negligible at adjacent cell positions. The sequence of steps in the acquisition process for both the short and long codes is given below:

Step 1	Short Code Acquisition
Step 2	Short Code Verification
Step 3	PN Code Tracking with Multiple Test
Step 4	Carrier Lock Search with Coherent Amplitude Detection Multipath Test
Step 5	Long Code Acquisition
Step 6	Long Code Verification
Step 7	Direct Signal Verification

2.2 Return Link

The return link consists of a path from the user transponder, through TDRS as a relay, and to the ground receiver. Signals employed in the return link are similar to those employed in the forward link, but differ somewhat in their particulars. The paragraphs that follow delineate these differences.

Figure 2.2-1 shows both forward and return links and the frequencies employed in those links. (Figure 2.2-1 is from TDRSS User's Guide, dated May 1975.)

2.2.1 System Parameters

The user transponder portion of the return link consists of the $2f_1$ source, multipliers to develop the 2287.5 MHz trnnsmitted signal center frequency, and a modulator for impressing the data transmitted on the signal carrier. It is of some interest to note that the PSK modulation employed in TDRSS cannot be followed by multiplication as in the NASA Standard Transponder, since multiplication of such PSK signals removes the modulation and produces an unmodulated carrier signal at the desired output frequency. For this reason, the return link blocks shown in figure 2.1-3 are reversed in order from those usually seen in the Standard Transponder.

Three signalling modes are provided in the return link. Mode 1, which employs coherent turn-around of the forward link carrier signal, uses a 1023 bit synchronization and data transmission coded signal, together with a reduced-power 2^{18}-256 bit range code modulated signal (actually the turn-around ranging signal). This signal is, of course, identical to the structure of the forward link signal, with the exception of the use of different code sequences where required for multiple access operations.

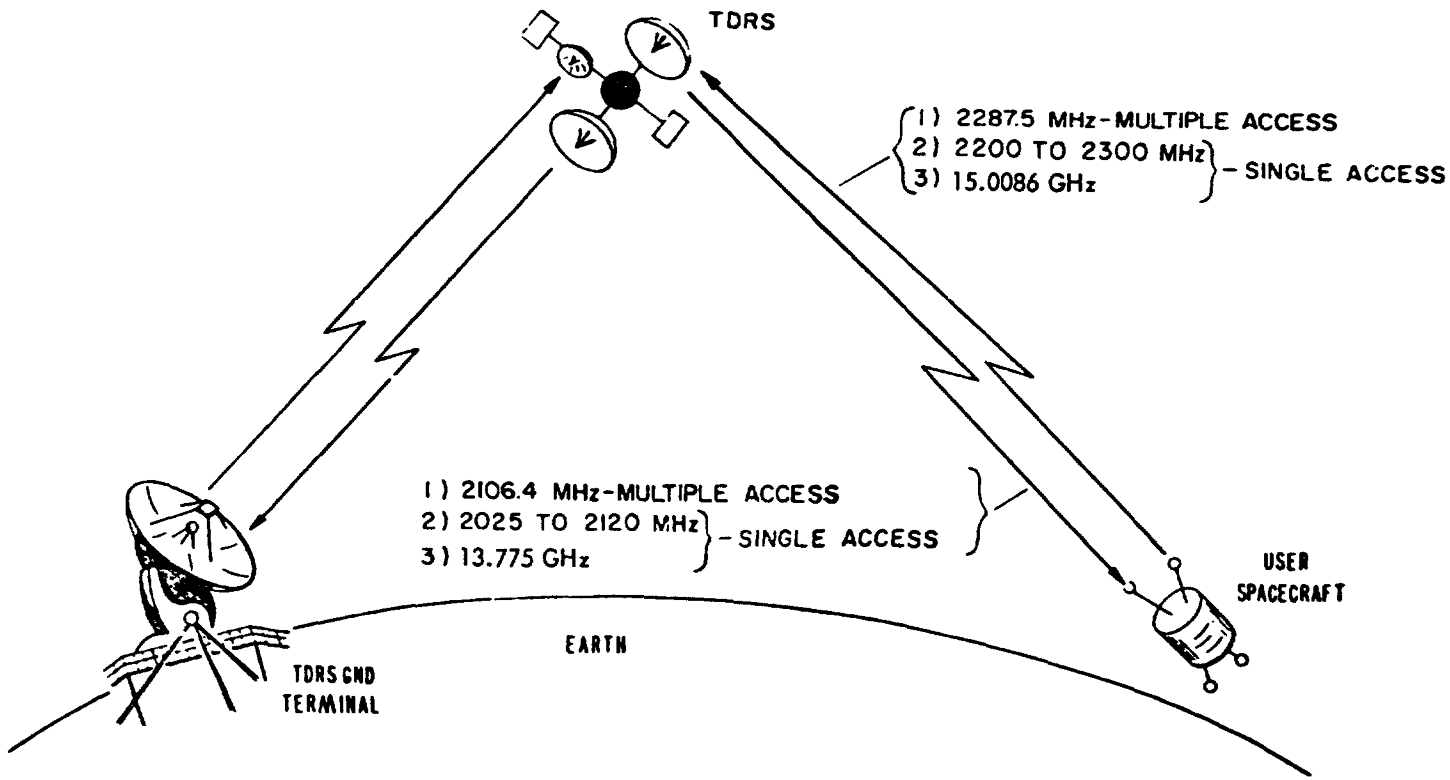

Figure 2.2-1. TDRSS Frequency Plan

Noncoherent turnaround is employed in Mode 2. That is, the independent $2f_1$ oscillator shown in figure 2.1-3 is used to generate the carrier signal. Also in Mode 2, the code length employed is $2^{11}-1$ (2047 bits).

Mode 3 employs a coherent carrier, with a $2^{18}-256$ bit coded ranging signal being present, but the primary signal (transmitted instead of the Mode 1, 1023 bit data and synchronization code) is a clear PSK data signal transmitted at data rates higher than those that could be supported by the Mode 1 PN signal transmission. It is expected that such data will be at rates sufficient to reduce signal power density below critical levels with respect to meeting flux density criteria.

The various signal structures corresponding to Modes 1, 2, and 3 are shown in figure 2.2-2.

2.2.2 Ground Receiver

The TDRS ground receiver system performs three basic receiving functions:

1. Receives multiple access and single access sent to the TDRS relay satellite on both S-band and K-band, at K-band (i.e., both are translated to K-band).

2. Receives test signals returned from the TDRS satellite, when the system is in the test mode.

3. Receives TTNC signals when they are being sent during launch operations.

Figure 2.2-3 illustrates the frequencies used by the TDRS system in links to and from the ground to the satellite, and to and from the TDRS relay satellite to the user satellite (or other user, such as Space Shuttle). TDRS-to-ground signals are:

13.937 GHz	K-band signal access. 225 MHz bandwidth provided. May be split into two 88 MHz-BW channels.
13.7 to 13.725 GHz	S-band single access signals. Two 10 MHz bands provided, with 5 MHz guard band (25 MHz total)

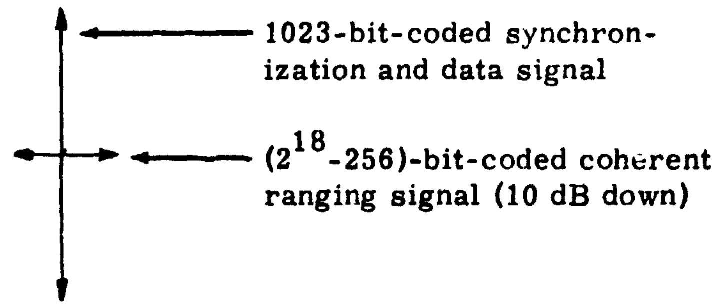

a. Mode 1 Signal Structure (Coherent Turnaround)

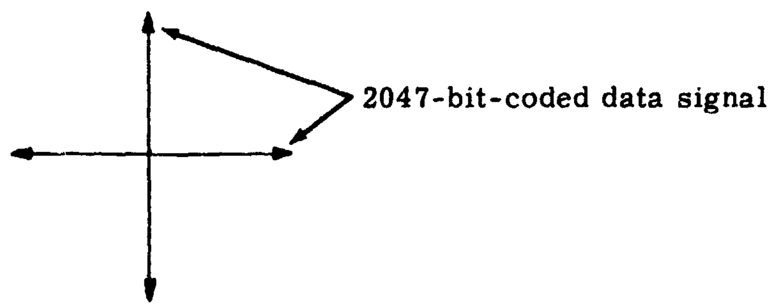

b. Mode 2 Signal Structure (Noncoherent Turnaround)

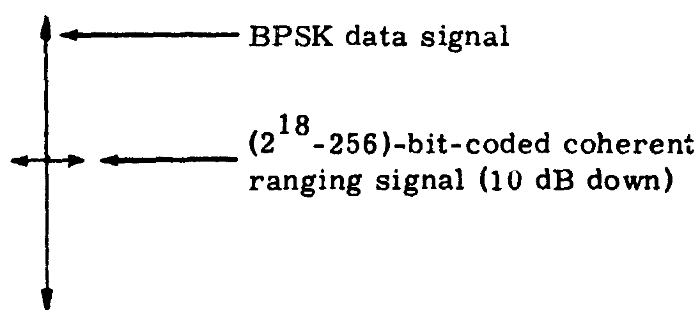

c. Mode 3 Signal Structure (Coherent Turnaround)

Figure 2.2-2. Signal Structure

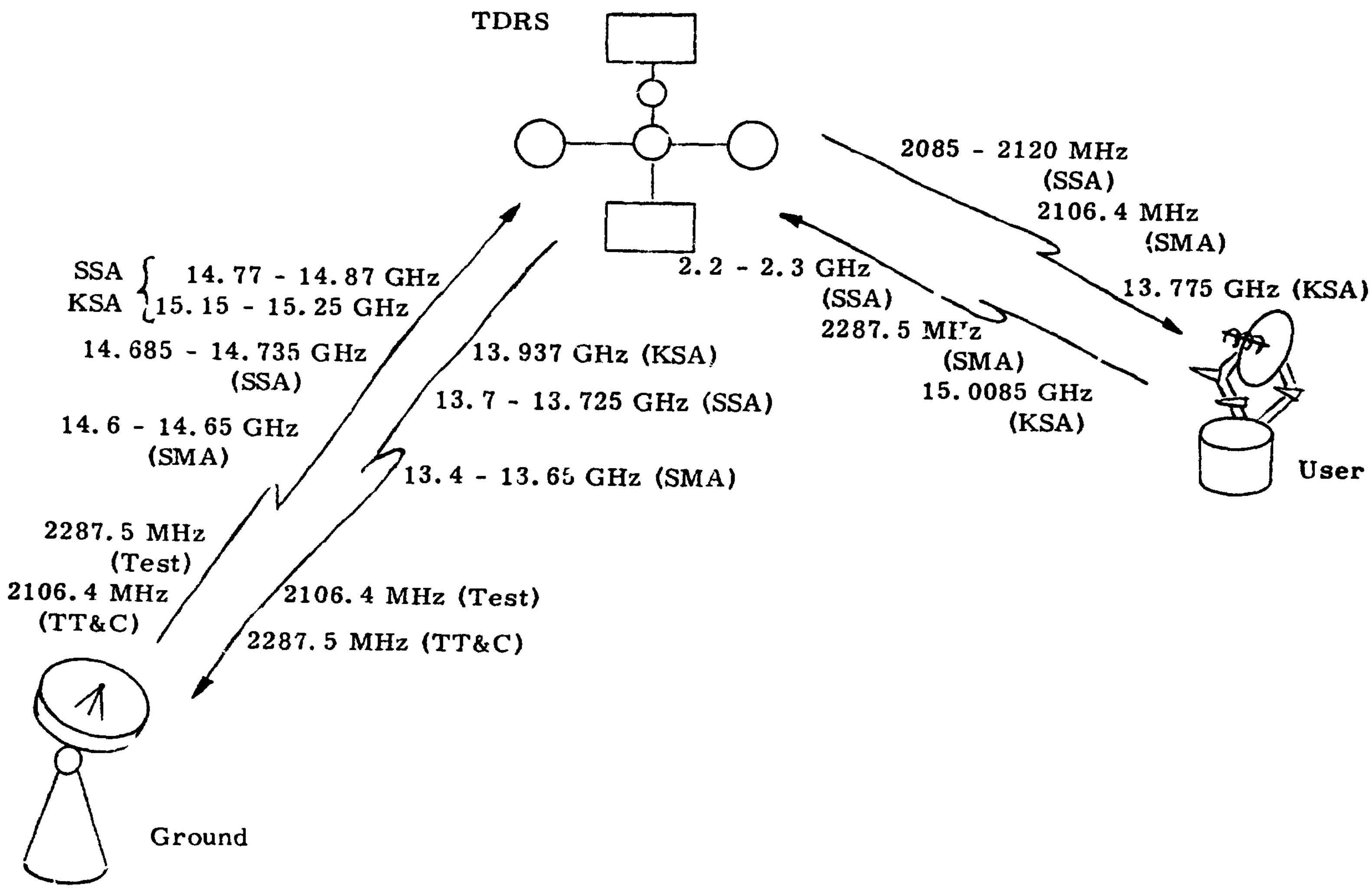

Figure 2.2-3. Frequencies Used in TDRS for Various Links

13.4 to 13.65 GHz	S-band multiple access users. 42 channels provided. 41 at 6 MHz spacing and one at 4 MHz spacing. 40 slots with 4.5 MHz BW for downlink user signals, 2 slots for turn-around ranging.
2106.4 MHz	Test receive frequency for TDRS satellite transmitter (same frequency as TDRS-to-user)
2287.5 MHz	Receive frequency for TT&C signals used during satellite launch period. Same frequency as user-to-TDRS.

Figure 2.2-4 illustrates a receiver design that could serve to meet the requirements of the TDRS-to-ground link. It provides for both K-band and S-band reception of signals, using as much common circuitry and subsystems as possible. A more detailed version of this receiver is described in section 3.2 of this report.

2.2.3 System Performance

The results obtained for the S-band multiple access return link Mode 2 synchronization analysis are summarized below. One of the objectives in the study was to establish the required length of the PN code sequence. A code length of 2047 chips was recommended. The performance objectives are:

Mean Acquisition Time	15 seconds
Probability of Detection	0.9
Probability of False Alarm	10^{-6}
Probability of Detecting Interfering Signal	10^{-2}

The results are obtained for the case where the signal is uncoded and for the case where a half-rate convolutional code with a Viterbi decoding algorithm is employed. One of the major steps in the analysis was the interfering signal analysis and the likelihood of false locking to an interfering signal.

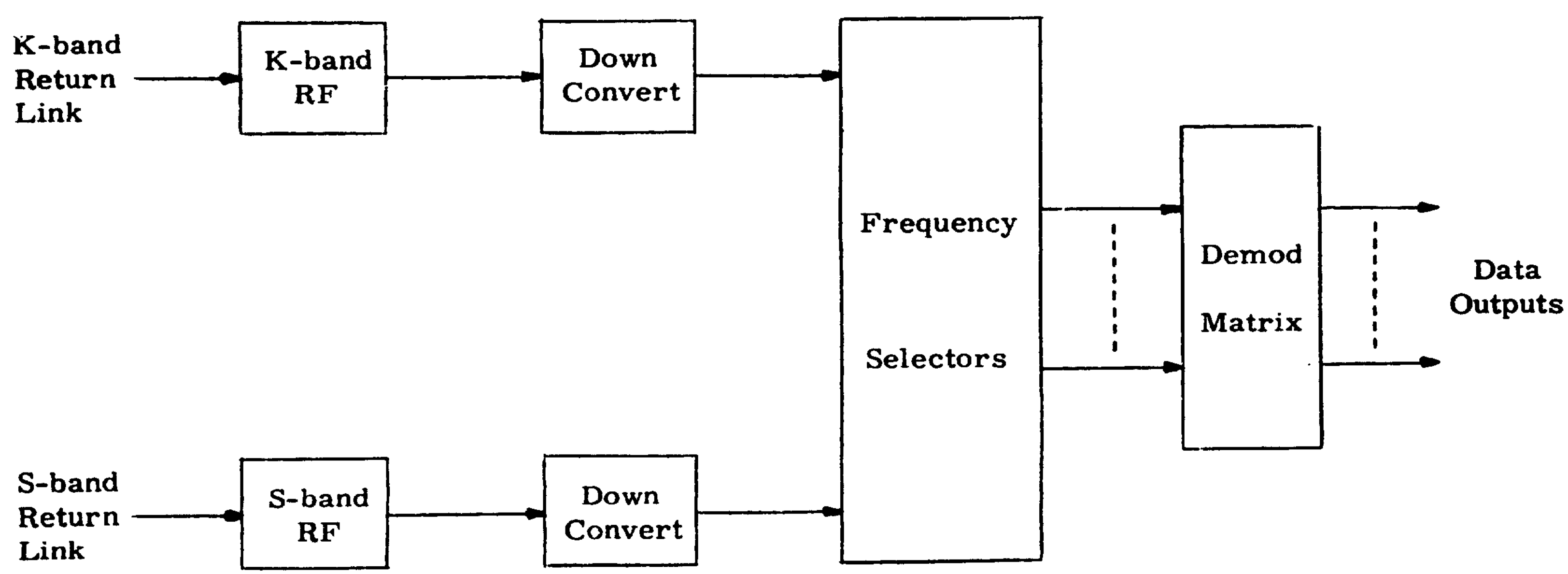

Figure 2.2-4. Simplified Block Diagram of Ground Receiver

The system constraints are:

C/N_0 (without coding)	39.9 dB-Hz
C/N_0 (with coding)	34.9 dB-Hz
Total doppler and frequency uncertainty	$\pm$ 2.5 kHz

A fixed length test strategy was employed for the ground receiver synchronization analysis. The detection performance analysis results for both the desired and interfering signals is summarized in table 2.2-1. Although through the verification state, neither the detection probability objective of 0.9 nor the false alarm probability objective of 10^{-6} is satisfied, the code tracking and carrier lock thresholds can be set to achieve the above requirements. The average acquisition time analysis at threshold is summarized in table 2.2-2 for the dual mode fixed length test strategy. A single 5 kHz IF bandpass filter covering the total doppler and frequency offset uncertainty is assumed. Clearly, the acquisition times can be reduced considerably by multiple doppler resolution filters as recommended for the user transponder. For a code length of 2047 chips, both with and without coding, the average acquisition time objectives of 15 sec are achieved.

Table 2.2-1. Detection Performance of Desired and Interfering Signals
Code Length $N = 2^{11}-1$

Link Condition \ Performance	Desired Signal				Undesired Signal			
	Acquisition		Verification		Acquisition		Verification	
	P_{FA}	P_D	P_{FA}	P_D	P_{FA}	P_D	P_{FA}	P_D
Without Coding	10^{-2}	0.58	10^{-4}	0.95	10^{-2}	1.0*	10^{-4}	2×10^{-4}
With Coding	10^{-1}	0.47	10^{-2}	0.74	10^{-1}	1.0*	10^{-2}	7×10^{-2}

*This assumes one searches through all possible cell positions.

Table 2.2-2. Average Acquisition Time vs. Code Length

Link Condition \ Code Length N	Average Acquisition Time, T_{ACQ} (sec)		
	$2^{11} - 1$	$2^{13} - 1$	$2^{15} - 1$
Without Coding	3.9	15.4	61.5
With Coding	14.7	58.6	234.5

APPENDIX A.2

GENERAL COMPARISON OF BIPHASE AND QUADRIPHASE (DOUBLE-BINARY) MODULATION

A.2.1 Modulation

Biphase modulation is readily accomplished through use of a simple diode-balanced mixer. These are available from a number of manufacturers (Relcom, H-P, Mini-Circuits Lab, Vari-L, and others). Their equivalent circuit is shown in figure A.2-1.

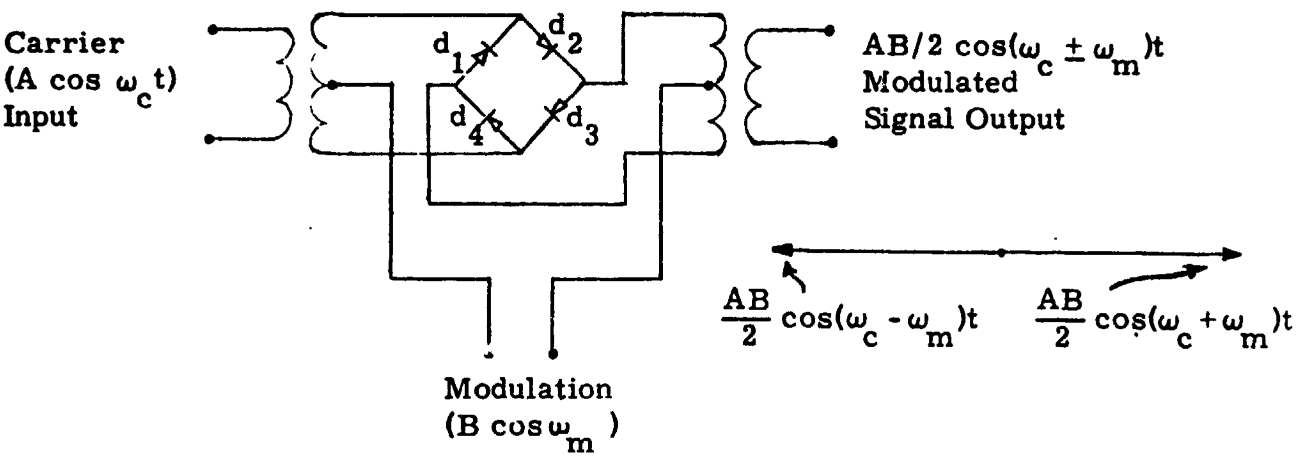

Figure A.2-1. Biphase Modulator

Operation is such that the modulation input causes either d_1 and d_3 or d_2 and d_4 to conduct at any given time, with the other diode pair cut off. Thus, either one phase of the input carrier or the opposite phase (0° or 180°) is coupled to the output. If $B \cos \omega_m t$ is a code sequence, then a carrier, biphase modulated with the code, is the output signal.

The output signal has a power spectrum which has an envelope having a $(\sin x/x)^2$ shape, where the main lobe is $2R_c$ wide (R_c is the code sequence clock rate) and the sidelobes are R_c wide. The first side lobes are 13 dB down, and the envelope falls off at a 6 dB per octave rate thereafter.

Approximately 10 percent* of the energy falls outside the main lobe.

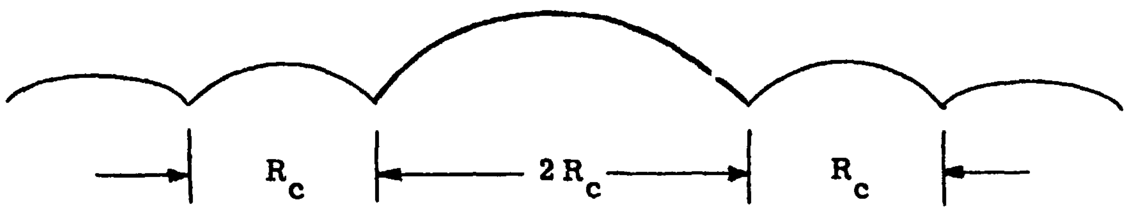

Quadriphase modulators are approximately three to four times as complex, on the basis of components required, as biphase modulators. (This is true whether the modulator is simple quadriphase or some form of offset quadriphase.) A quadriphase modulator commonly is constructed as in the following diagram (figure A.2-2).

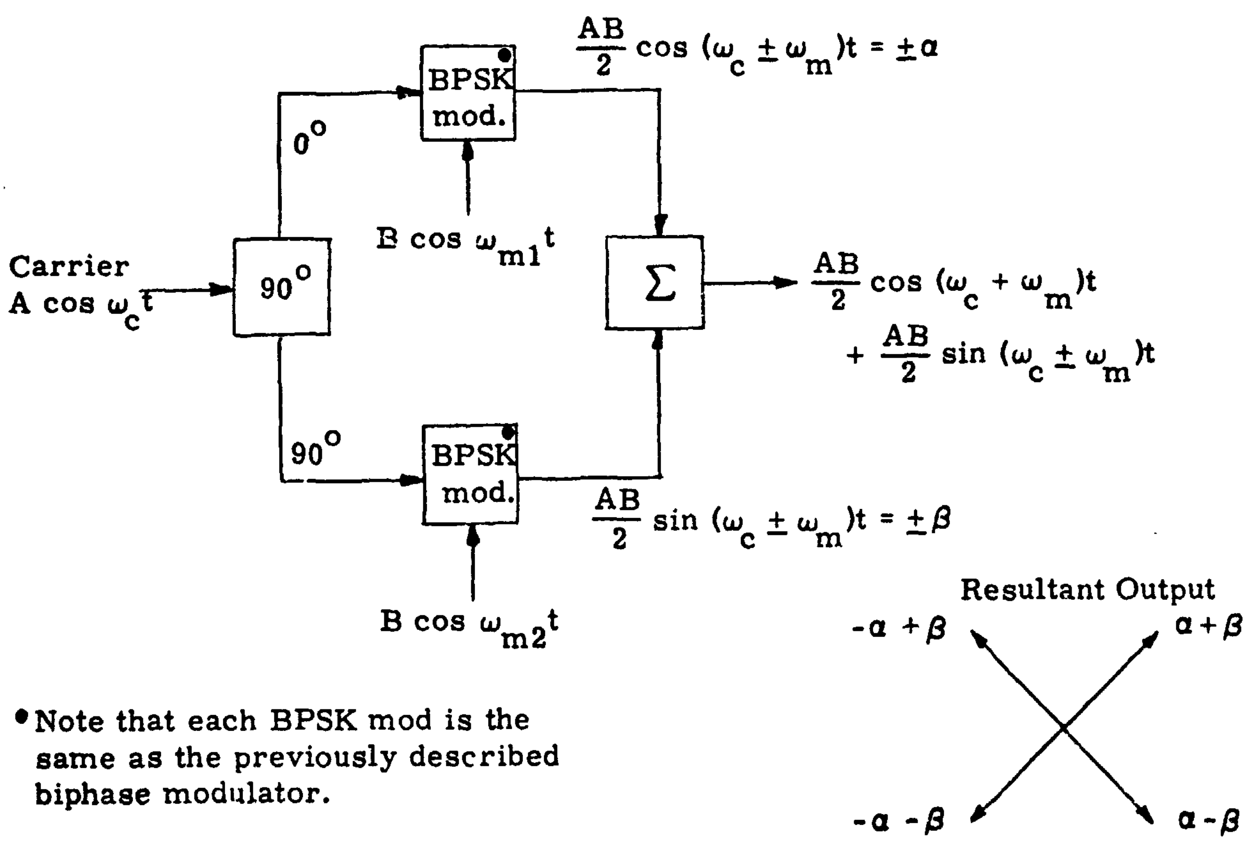

Figure A.2-2. QPSK Modulator

*R. C. Dixon, Spread Spectrum Systems, John Wiley & Sons, 1976, p. 21, 234.

The power spectra for both simple quadriphase and double-binary are the same as for biphase (when all modulating signals are at equal rates). Two advantages exist for the quadriphase signals, however:

1. They can tolerate passage through a limiter simultaneously with a narrowband coherent carrier, which a BPSK signal cannot do.

2. They can be filtered and subsequently limited, without appreciable reconstitution of the undesired sidebands, which is not true of BPSK signals. (In fact, this is true only of the double-binary or offset QPSK signal format.)

The offset quadriphase signal can be filtered to a desired BW and then passed through a saturated power amplifier. This is not practical for BPSK or simple QPSK signals, however. Therefore, in a spacecraft that employs a saturating TWT power amplifier, one must pay the hardware penalty for implementing QPSK modulation and demodulation, but the transmitted signal is more efficient, due to all of the relevant energy being packed into a $\pm R_c$ bandwidth around the carrier. Where 10 percent of the BPSK signal goes into sidelobe energy, only 5 percent or less goes into sidelobe energy in the offset QPSK format. Therefore, the savings in signal power can be translated into a direct signal improvement for offset QPSK signals.

A. 2. 2 Demodulation

Demodulators for BPSK and QPSK signals are similar. Where data is sent phase-shift-keyed, a Costas demodulator or squaring demodulator is normally employed, and there is little difference* in them, whether they are for BPSK or QPSK signals.

The amount of hardware needed is similar, so no further receiver demodulator comparison will be made.

The received signal bandpass filter should be considered in the light of sending either QPSK or BPSK signals. That is, if the power amplifier transmits a BPSK signal, it will have a $(\sin x/x)^2$ distribution whether it filters before amplification or not. For the offset QPSK signal, however, only the main lobe of the signal may be transmitted. If the

*Costas and squaring demodulators are different, but there is little difference in a Costas demod for BPSK or one for QPSK. Squaring demods are in a similar vein.

receiver bandwidth is just wide enough to accept the main lobe, then it throws away the BPSK sidelobe energy. An increase in bandwidth to include the first two sidelobes causes a net signal loss, since the increase in receiver noise is greater than the increase in received signal. Therefore, it is seen that the BPSK signal format is advantageous from the standpoint of transmitter simplicity, but it loses in the area of effective transmitter power. This is illustrated in the patterns of figure A. 2-3, one of which is the spectrum of a BPSK signal after limiting, whether filtered or not, and the other shows an offset or staggered QPSK signal spectrum after filtering and limiting. This comparison is at the heart of the tradeoff between BPSK and QPSK, with the possible improvement in signal-to-noise ratio being a maximum of 0.9 dB for SQPN over simple biphase signal transmission.

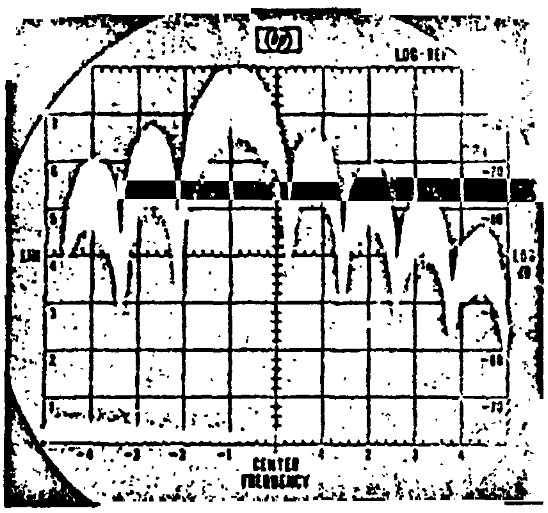

a. Filtered and limited QPSK signal. Note that the sidelobe level is the same as if filtering had not occured. (This reaction is typical of both biphase and quadriphase direct sequence signals.) Filter bandwidth = 2 R_{clock}.

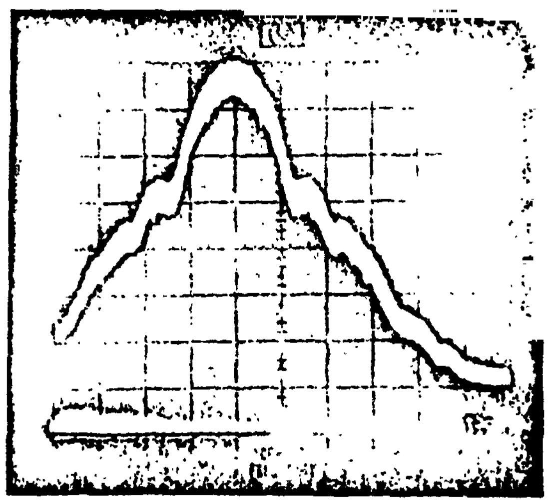

b. Identical filtering and limiting of a double-binary or staggered quadriphase signal. First sidelobe level is now down 25 dB, or 12 dB below the level of the signal in (a) above.

Figure A.2-3. Comparison of Normal and Offset QPSK Signal Spectra

We have not considered filtering after the power amplifier, as this does nothing to preserve signal power in any case.

A. 2. 3 PSK Modulation Considerations for Simultaneous TDRSS Signals

Phase shift keyed (PSK) modulation offers significant performance and implementation advantages in communication systems when compared to other forms of modulation. Phase shift keying provides the lowest threshold performance available. In addition, this modulation form is directly applicable in the spread spectrum and high data rate areas required in TDRSS.

Two forms of PSK are of primary interest for use in TDRSS: biphase and quadriphase modulation, wherein the information is conveyed as either one of two or one of four phases for each information symbol. These are of interest not only because of their spread spectrum and/or high data rate compatibility but because they lend themselves to transmission of multiple signals with minimal mutual interference between those being sent.

In the following paragraphs, we will examine various combinations of biphase and quadriphase signals to determine the effects of operating with them simultaneously in linear and saturating channels.

Modulation Possibilities

Signal 1	Signal 2
QPSK	QPSK
QPSK	BPSK
BPSK	QPSK
BPSK	BPSK

Let us first consider that one signal (2) is always 10 dB smaller than the other signal (1). (See figures A. 2-4 through A. 2-7.)

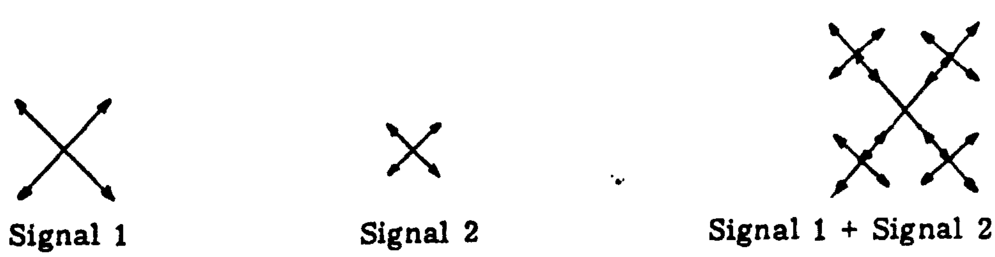

Figure A. 2-4. Case 1 - Linear Summation, Two QPSK Signals

Note that amplitude modulation occurs for some phase states of signal 2. That is, signal 2 may add or subtract from signal 1.

Figure A. 2-5. Case 2 - One QPSK and One BPSK (10 dB Smaller) Signal

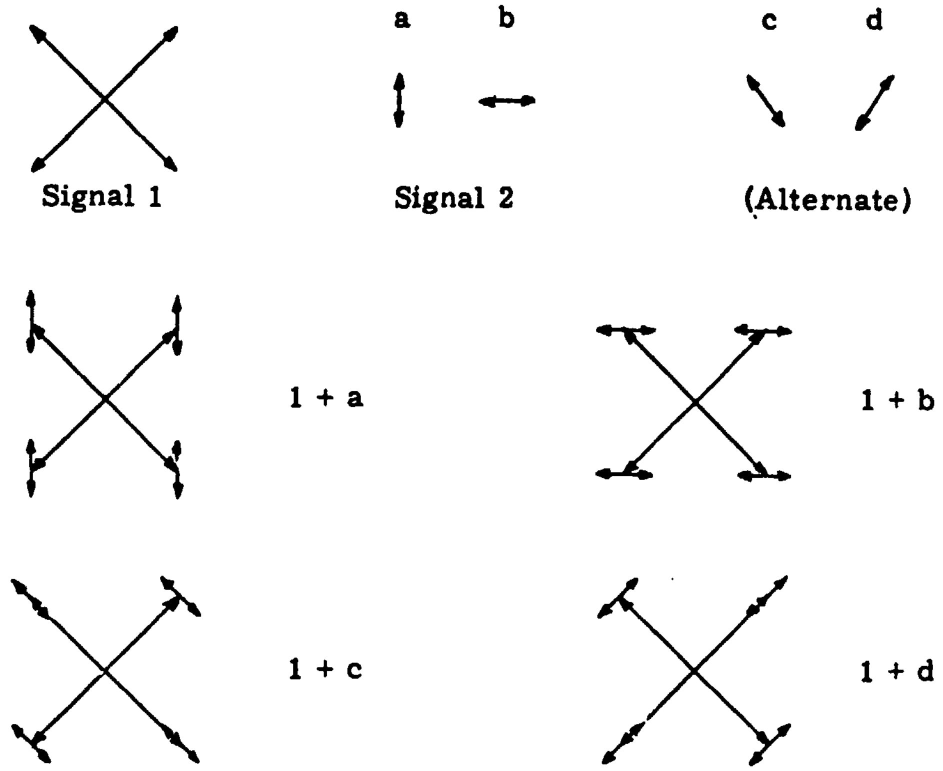

Figure A. 2-6. Case 3 - BPSK Signal with Smaller QPSK Signal

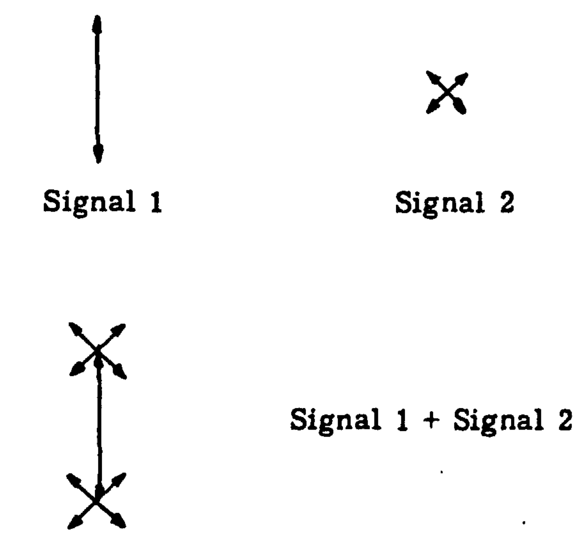

Amplitude modulation occurs for all phase states of case 3.

Figure A. 2-7. Case 4 - Two BPSK Signals, Different Amplitudes

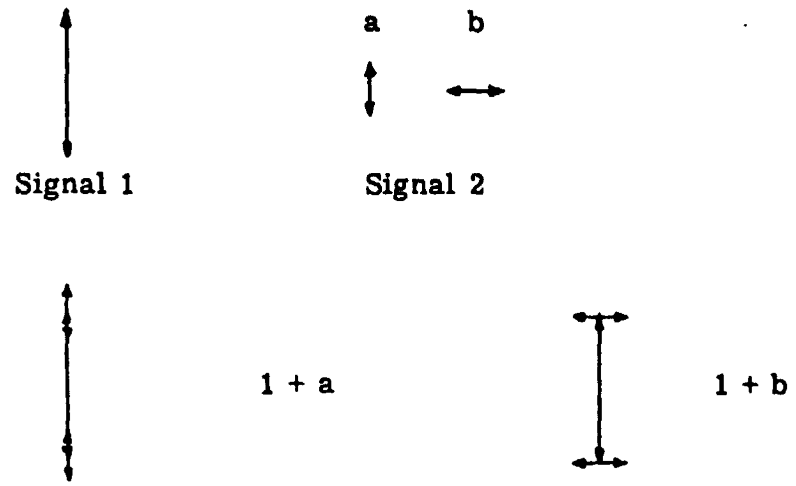

Note that no amplitude modulation* is produced by combining the orthogonal signal pair $\{90, 270\}$ and $\{0, 180\}$.

How, then, can a signal be modified to produce a constant-amplitude* signal (steady state) when the desire is to transmit two QPSK signals?

The following signal combination would be satisfactory (figure A. 2-8):

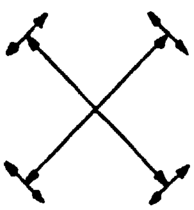

Figure A. 2-8. QPSK Combined with Selected-Phase QPSK (Combined Signal)

---

*These signals are constant-amplitude only in their steady-state condition. Incidental amplitude modulation does occur in the transition from one phase state to another. Where a phase shift is ϕ degrees, the incidental amplitude modulation that can be expected is

$$\% \text{ AM} = (1 - \cos \phi/2) \times 100 .$$

That is, the carrier signal can be expected to drop to an amplitude equal to $\cos \phi/2$ times its steady state value during a phase transition. Thus, it is easy to see the advantage of SQPN modulation (90° phase shifts) over standard QPSK modulation (90° and 180° phase shifts) since the incidental AM produced is 30% rather than 100%.

This signal can be generated from a pair of QPSK signals, but the signals must be properly managed.

Incidentally, it does not matter whether the signals in question are QPSK or SQPSK. The same considerations hold--since SQPSK differs from QPSK only in that the order of phase shifts is changed by modifying the data (or code) fed to the phase modulators used.

A further modification to the code used by the smaller signal (signal 2) can produce the desired orthogonal pair of QPSK signals.

If the phase mapping for signal 1 is:

Data	
0 0	45°
1 0	135°
1 1	225°
0 1	315°

let the phase mapping for signal 2 be the same.

To produce the desired combined signal, the overall phase mappings allowable are:

Signal 1	Signal 2
45°	135° or 315°
135°	45° or 225°
225°	135° or 315°
315°	45° or 225°

This means that only certain code states may be permitted for code pair 2, based on the state of code pair 1. These are:

Code pair 1	Code pair 2
00	10 or 01
10	00 or 11
11	10 or 01
01	00 or 11

This can be accomplished by modifying one code in one of the code pairs used in a double-quadriphase signal set (two quadriphase signals) on the basis of the other code pair. Such a technique is illustrated in the example that follows.

Code pair 1	0	0	1	1	1	0	1	0	1	1	0	0	1	0	0	1	0	...
	0	1	0	0	1	1	0	0	0	1	1	0	1	1	1	0	1	...
Code pair 2 (unmodified)	1	0	1	1	0	0	0	1	0	1	1	1	0	1	0	1	1	...
	0	1	0	1	1	0	1	1	1	0	0	0	1	0	1	1	0	...
(Δ signifies not-allowed state)		Δ	Δ				Δ	Δ	Δ		Δ			Δ	Δ		Δ	
Code pair 2 (modified)	1	0	1	1	0	0	0	1	0	1	1	1	0	1	0	1	1	...
	0	0	1	1	1	0	0	0	0	0	1	0	1	1	0	1	1	...

The only question is - what happens to the correlation properties of the long code. An alternate coding rule would be to repeat the last allowed state when a not-allowed state is next. This would change the code also, but would be a more complex rule.

To summarize, where two unequal level signals are to be transmitted simultaneously, then it is recommended that both be either biphase or quadriphase. Combinations of biphase and quadriphase signals do not readily adapt to constant-amplitude signalling. Where saturating amplifiers are employed, both constant-amplitude signals and minimum incidental AM are desirable. For those cases where a combination of two signals produces AM, that AM would be lost in transmission through a saturating amplifier. The case for minimum incidental AM is made because bandpass filtering ahead of the saturating amplifier can suppress small amplitude modulation to an extent that it is not restored to any significant degree in the nonlinear amplification process. This in turn reduces transmitter sidelobe energy and improves signalling efficiency.

The signals that result from combining either two BPSK or two QPSK signals are shown in figure A. 2-9. (One of the two in each case is 10 dB smaller than the others.)

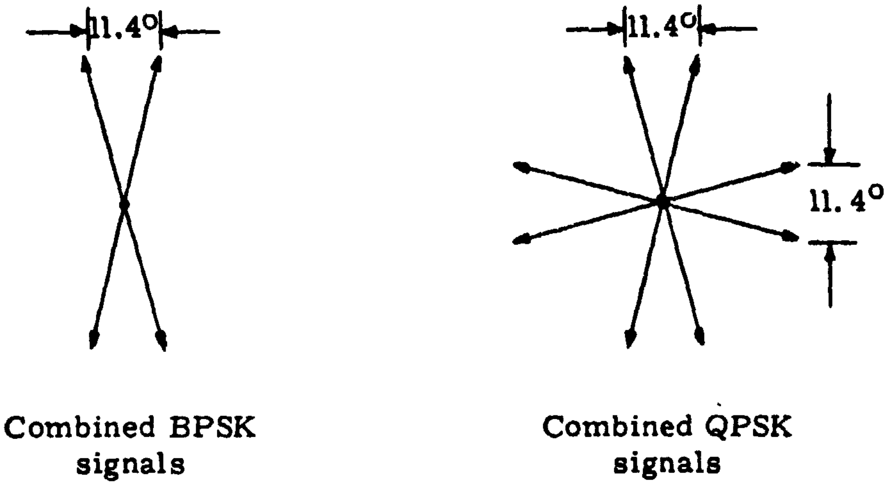

Figure A. 2-9. Comparison of Combined BPSK and QPSK Phase Diagrams

In both cases, incidental AM due to the combining of signals is only 0.49%. Incidental AM for the individual signals is the same, however, as if the other signal were not there (i.e., 100% for the biphase signals and 30% for staggered quadriphase signals).

II. Consider now the case of equal amplitude carriers, but those having arbitrary phase and/or frequency relationships. (It is considered that the phase and/or frequency of carriers used is known and controlled, but our interest here is in the effect of the relationships between the pair of postulated carriers.)

We will consider that this is the case for transmission of data group 1 and data group 2 signals. Data group 1 and 2 signal characteristics are summarized as follows:

<u>Data Group 1</u>

PN modulated (SQPN)

6 Mbps code, 2^{19} long

Data rate: 1-300 kb/sec

same on I and Q

data embedded in 6 Mbps code

Data Group 2

No PN modulation

Data QPSK

Data rate:	1 kb - 300 Mbps total
I:	1 kb - 150 Mbps
Q:	1 kb - 150 Mbps

I and Q rates independent and either synchronous or asynchronous

The Data Group 2 carrier may be asynchronous with the Data Group 1 carrier.

Assume the two following QPSK signals (figures A. 2-10 and A. 2-11):

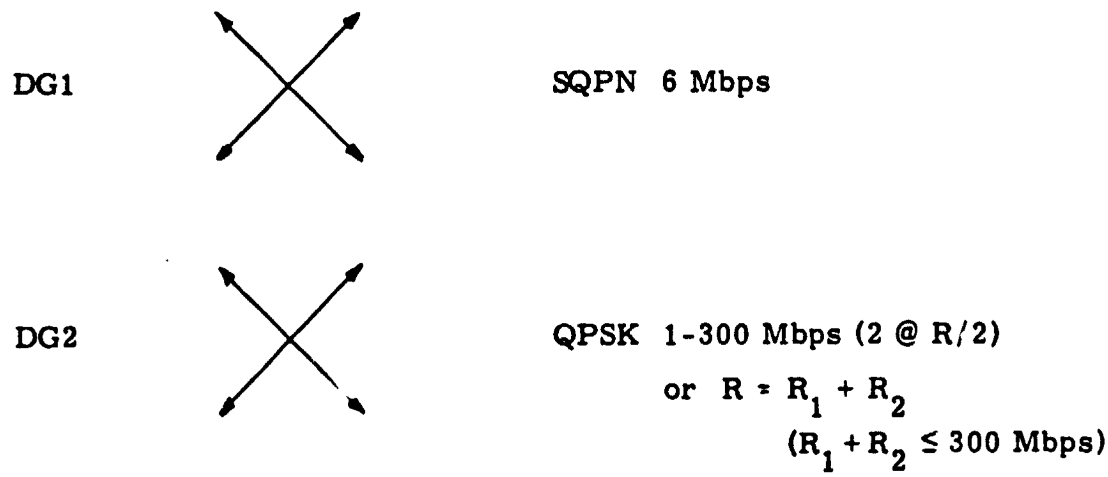

Figure A. 2-10. DG1 and DG2 Signals

Data rate has little effect except to determine the rate of phase shifts. QPSK/SQPN also has little bearing except to determine rate of phase shifts and phase difference from shift to shift. (SQPN allows only 90° shifts. QPSK can shift 180° or 90°.)

Carrier amplitude, frequency, and relative phase have much more effect.

Let DG1 power = DG2 power

$\phi_1 = \phi_2$

DG1 carrier = DG2 carrier

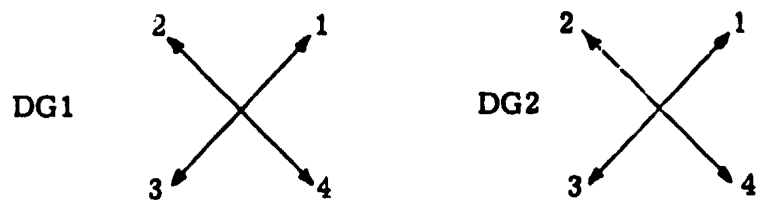

Linear channel:

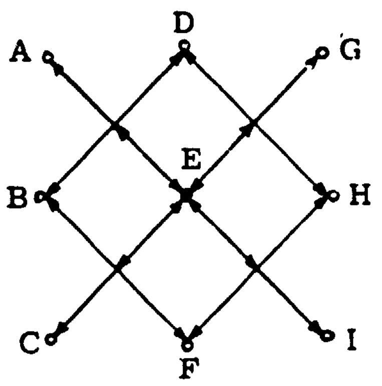

Loci of possible phase positions for two equal-value 4-phase signals, linearly added. (Note ambiguity.)

Figure A. 2-11. Combination of Two Equal QPSK Signals

The same combined phase mapping results if the two carriers are offset in phase, except that the combined phase map is itself rotated.

There are $4^2 = 16$ possible combinations of two four-phase signals. The combined, linearly-added signals have only 9:

$1_1 + 2_1 = G$ $\qquad$ $G = 2P \angle 45$

$1_1 + 2_2 = D$ $\qquad$ $D = \sqrt{2}\,P \angle 90$

$1_1 + 2_3 = E$ $\qquad$ $E = 0 \angle 0$

$1_1 + 2_4 = H$ $\qquad$ $H = \sqrt{2} \angle 0$

$1_2 + 2_1 = D$

$1_2 + 2_2 = A$ $\qquad$ $A = 2P \angle 135$

$1_2 + 2_3 = B$ $\qquad$ $B = \sqrt{2}\,P \angle 180$

$1_2 + 2_4 = E$

$1_3 + 2_1 = E$

$1_3 + 2_2 = B$

$1_3 + 2_3 = C \qquad C = 2P\,\angle 225$

$1_3 + 2_4 = F \qquad F = \sqrt{2}\,\angle 270$

$1_4 + 2_1 = H$

$1_4 + 2_2 = E$

$1_4 + 2_3 = F$

$1_4 + 2_4 = I \qquad I = 2P\,\angle 315$

Occurrences: A = 1, B = 2, C = 1, D = 2, E = 4, F = 2, G = 1, H = 2, I = 1

This is not the case in the saturating or limiting channel (figures A. 2-12 and A. 2-13):

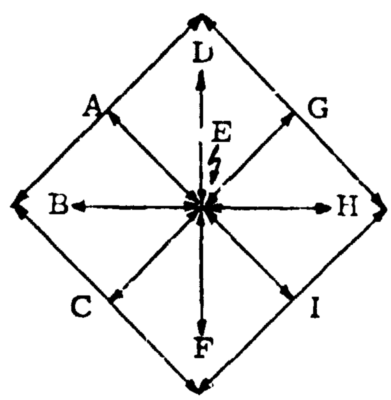

Figure A. 2-12. Combined QPSK Signals in a Limiting Channel

This phase table is the same as for the linear channel, but the amplitude table is different:

$G = P\,\angle 45 \qquad B = P\,\angle 180$

$D = P\,\angle 90 \qquad C = P\,\angle 225$

$E = 0\,\angle 0 \qquad F = P\,\angle 270$

$H = P\,\angle 0 \qquad I = P\,\angle 315$

$A = P\,\angle 135$

(letters correspond to linear channel phase diagram)

Occurrences: Same as linear channel if amplitudes of DG1 and 2 carriers are precisely equal.

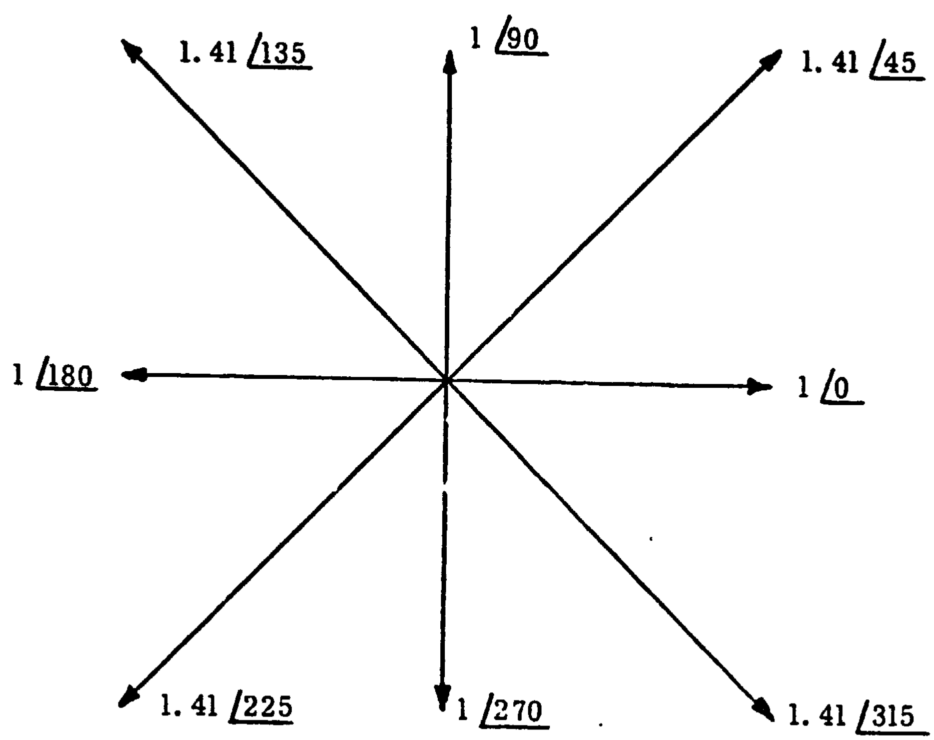

Figure A.2-13. Eight-Phase Phase/Amplitude Resultant of Summed Equal-Amplitude QPSK Signals (Carriers Coherent)

If carriers are not equal in amplitude (and they seldom would be), then whichever is larger will dominate in positions A, C, G, and I, as in the following phase tables.

(Remember that the saturating amplifier we are discussing tends to drive any signal above a value α to the point of amplitude limiting. In such a case, if two carriers are not exactly equal, and their difference is $\geq \alpha$, then the larger signal will dominate and suppress the smaller signal.)

Assume PDG1 > PDG2:

$$1_1 + 2_1 = P\angle 45$$
$$1_1 + 2_2 = P\angle 90$$
$$1_1 + 2_3 = P\angle 45$$
$$1_1 + 2_4 = P\angle 0$$
$$1_2 + 2_1 = P\angle 90$$
$$1_2 + 2_2 = P\angle 135$$
$$1_2 + 2_3 = P\angle 180$$
$$1_2 + 2_4 = P\angle 135$$
$$1_3 + 2_1 = P\angle 225$$
$$1_3 + 2_2 = P\angle 180$$
$$1_3 + 2_3 = P\angle 225$$
$$1_3 + 2_4 = P\angle 270$$
$$1_4 + 2_1 = P\angle 0$$
$$1_4 + 2_2 = P\angle 315$$
$$1_4 + 2_3 = P\angle 270$$
$$1_4 + 2_4 = P\angle 315$$

Occurrences: 0 = 2, 45 = 2, 90 = 2, 135 = 2, 180 = 2, 225 = 2, 270 = 2, 315 = 2

Assume PDG2 > PDG1: PDG2 - PDG1 $\geq \alpha$: $\alpha K \geq P$

$1_1 + 2_1 = P \angle 45$
$1_1 + 2_2 = P \angle 90$
$1_1 + 2_3 = P \angle 225$
$1_1 + 2_4 = P \angle 0$
$1_2 + 2_1 = P \angle 90$
$1_2 + 2_2 = P \angle 135$
$1_2 + 2_3 = P \angle 180$
$1_2 + 2_4 = P \angle 315$
$1_3 + 2_1 = P \angle 45$
$1_3 + 2_2 = P \angle 180$
$1_3 + 2_3 = P \angle 225$
$1_3 + 2_4 = P \angle 270$
$1_4 + 2_1 = P \angle 0$
$1_4 + 2_2 = P \angle 135$
$1_4 + 2_3 = P \angle 270$
$1_4 + 2_4 = P \angle 315$

Occurrences: 0 = 2, 45 = 2, 90 = 2, 135 = 2, 180 = 2, 225 = 2, 270 = 2, 315 = 2

It is most notable that, for a pair of quadriphase signals of equal amplitude, passing through either linear or limiting channels, the combined phase mappings result in ambiguities that cause loss of information. That is, where two quadriphase signals separately represent 16 possible symbol-pairs (and thereby four bits of information), only eight phases result from their combination, with the same phase resulting from more than one signal pairing.

The examples shown consider that the two signals of interest maintain a constant phase relationship. What if the two carriers are not at the same frequency? Where this is true, then the same two QPSK phase diagrams hold, but one of the two may be considered to rotate with respect to the other. This then effectively causes the signal that is rotating to add a continuous phase shift component, with rotation at the difference frequency between the two carrier signals. The combined phase diagram for two QPSK signals with different carrier frequencies would be (figure A. 2-14):

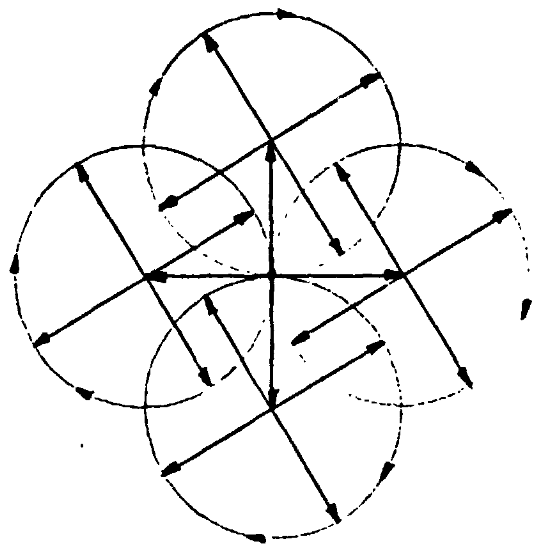

Figure A. 2-14. Rotating Phase Combination of Two Equal Value But Frequency Offset QPSK Signals

and 100 percent amplitude modulation would result, as well as phase rotation of 360° at the difference frequency rate. This would occur [illegible]ddition to independent discrete phase modulation by the two data signals

Such a signal would be difficult to handle in the linear channel and could degrade in the saturating channel to the point of being unusable.

Extending Case 1 (the pairing of a QPSK signal with a second QPSK which is smaller by 10 dB and whose carrier is at 90 degrees), Case 1a, which follows, considers the same QPSK carriers but shifts the smaller signal so that it is at a 45^{o} angle with respect to the larger signal.

The resulting composite signal is an amplitude- and phase-modulated resultant that has very small phase shifts, together with amplitude modulation of approximately 9 percent. Such signals are not useful in a system employing saturated traveling wave tubes (or even solid state RF power amplifiers) that exhibit AM/PM conversion on the order of 4 to 12 degrees per dB of amplitude shift, since the phase modulation produced by the incidental AM is larger than that produced by the intended phase modulation.

Case 1a (see figure A. 2-15) illustrates the problem faced with any form of modulation in TDRS that produces incidental amplitude shifts due to addition of two or more signals, where the composite signal is to be processed in a power amplifier. This especially applies to the two-signal or simultaneous signal approach to TDRS user synchronization and data transmission, whether the signals being sent are direct sequence signals (data group 1) or high speed data signals (data group 2).

Typical AM/PM conversion in a saturated TWT PA is as much as 6 to 8 degrees per dB. For this modulation, amplitude difference is 1.48 - 1.35 = 0.12 or 0.13/1.48 x 100 = 8.78 percent. This would be a 0.399 dB difference, for a 2.4^{o} phase shift. Thus, a phase shift produced by an amplitude change would be greater than that produced by modulation of the phase by the data being sent.

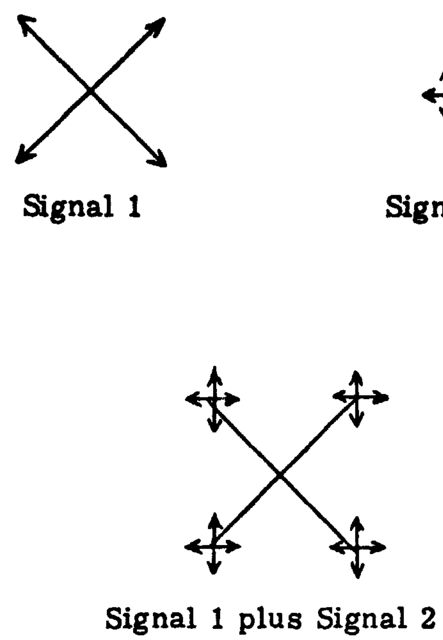

Figure A. 2-15. Case 1a - Two QPSK Signals

Signals produced are:

$1.35 \angle 42$	$1.35 \angle 222$
$1.48 \angle 42.3$	$1.48 \angle 222.3$
$1.48 \angle 47.7$	$1.48 \angle 227.7$
$1.35 \angle 48$	$1.35 \angle 228$
$1.35 \angle 132$	$1.35 \angle 312$
$1.48 \angle 132.3$	$1.48 \angle 312.3$
$1.48 \angle 137.7$	$1.48 \angle 317.7$
$1.35 \angle 138$	$1.35 \angle 318$

Phase mapping would be:

$1.35\ \underline{/42}$

$1.48\ \underline{/44.7}$

$1.48\ \underline{/50.1}$

$1.35\ \underline{/48}$

Compare this phase mapping with the first signal set:

$1.35\ \underline{/42}$

$1.48\ \underline{/42.3}$

$1.48\ \underline{/47.7}$

$1.35\ \underline{/48}$

In this quadrant, the unintended phase modulation due to AM/PM conversion would be 2.4° greater than the intended modulation, for the conservative estimate of 6 degrees per dB of amplitude shift.

3.0 SUBSYSTEM DESIGN

This report section describes user transponder and ground receiver subsystem designs that are postulated for TDRSS use. These subsystem designs do not represent either final recommendations or optimal designs, but are presented as practical configurations that may, in turn, be used as bases for comparison and for system configuration.

3.1 User Transponder

This section presents a transponder design which reflects possible implementation with contemporarily available components; that is, none of the subsystems presented depends on development of new or higher performance components than those presently available.

The selected approach for TDRS signal structure is the use of a direct sequence waveform for acquisition, as well as data transmission. A pair of direct sequence modulated signals will be transmitted simultaneously. One signal is BPSK modulated with a 1023 bit code sequence that is, in turn, sequence-inversion-modulated with data. The second signal is BPSK modulated with a 2^{18}-256 bit code sequence, and has no data modulation. The second signal is transmitted at a level 10 dB below the first, and on a carrier signal phase-shifted by 90 degrees from it.

Both the 1023 bit (short) and 2^{18}-256 bit (long) codes will use the same $31f_1/96$ = 3.077799 Mbps clock, and the all-ones vectors in both the generators will be set to coincide at a given point in time. Thus, the long code will repeat in exactly 256 repetitions of the short code all-ones vector.

The receiver will then have to search a maximum of 1023 bits to acquire short code synchronization; once short code synchronization is achieved, the long code ambiguity is reduced to 1/256. This is true because a receiver synchronized to the short code knows when the long code all-ones vector will occur, except that it occurs only once every 256 short code all-ones occurrences. If the receiver then resets its long code at each short code all-ones vector, and monitors its correlator for synchronization until the next one, then all it needs to do is decide if it is synchronized. If so, then it does not reset; but if not, then it resets and tries again during the next interval.

Actually, the long code monitoring or integration period is not just one but may be many periods of the short code. This is done to make up for the reduced (-10 dB) power in the long code modulated signal. If, for example, the integration period is an average of 10 short code periods, then long code acquisition time is $256 \times 10 \times 322$ μsec = 824 msec. (Actual long code acquisition time is expected to be <2 seconds.) This time is in addition to short code acquisition time, since the short code must be acquired first.

The short code modulated acquisition signal employed will be the data transmission signal, and will be transmitted continuously. Therefore, a user may acquire the signal at any time without a need for any special transmission or procedure. The long code modulated signal will be used only to resolve range and multipath ambiguities.

Figure 3.1-1 is a simplified block diagram showing the modulator and demodulator configuration for the selected TDRSS signal acquisition approach.

3.1.1 Overall Design

Figure 3.1-2 illustrates a transponder configuration using a 221/240 frequency turn-around ratio. The configuration shown departs from the Standard Transponder design, in that the second IF is a function of the f_1 reference oscillator frequency rather than an auxiliary f_2 oscillator. This configuration has the advantage that it does not employ an f_2 oscillator (about 12.25 MHz for a standard transponder) but it does have a second IF frequency that changes if the operating frequency is changed. For TDRS, with 221 f_1 at 2106.40625 MHz, f_1 and the second IF would be 9.53125 MHz.

A demodulator is part of this configuration. When relaying data, that data would preferably be demodulated to baseband and used to remodulate the relayed signal. This remodulation would be accomplished by modulo-2 addition with the transmit code. The alternative is to preserve

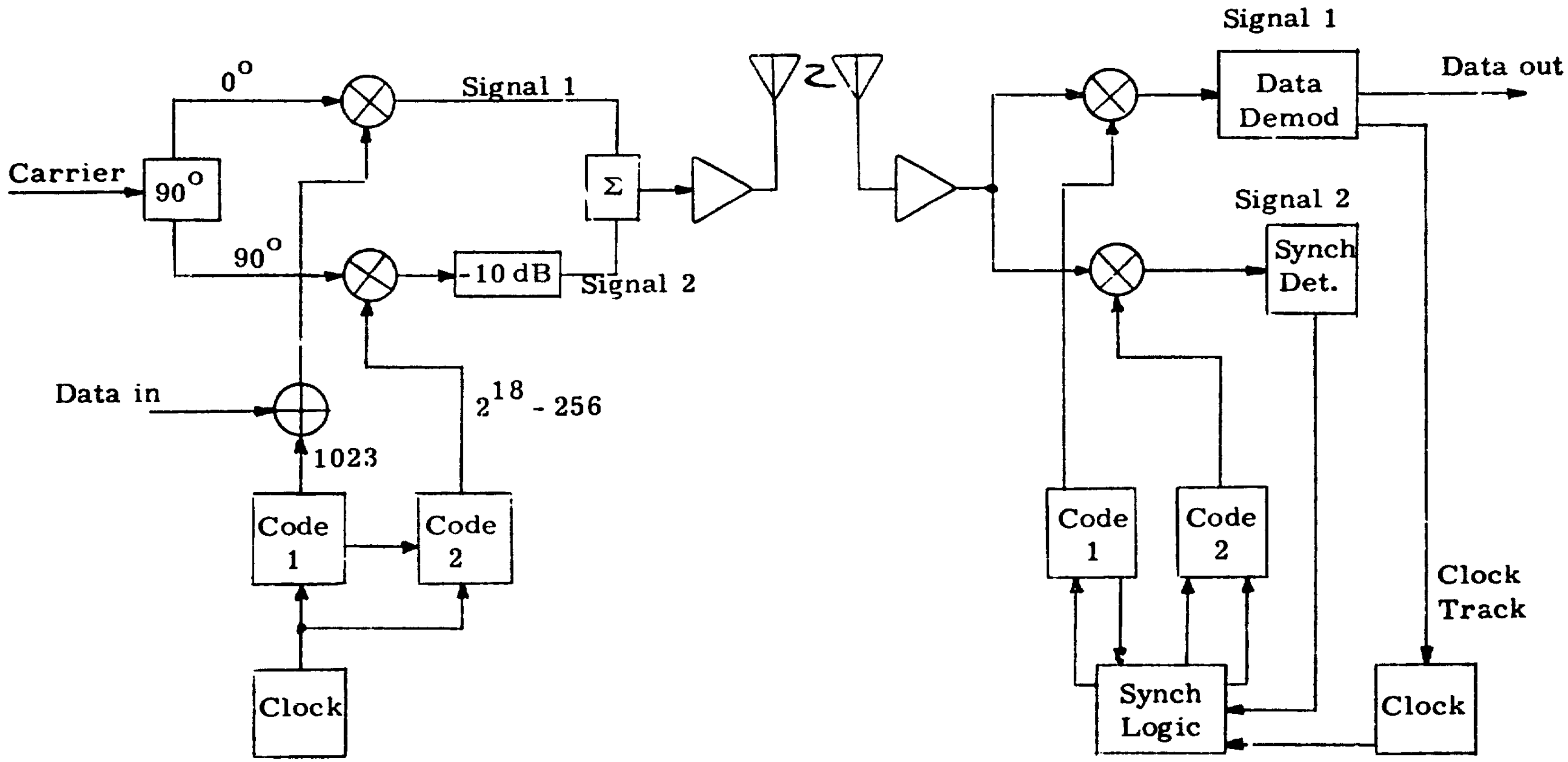

Figure 3.1-1. Simplified Modulator and Demodulator Using Simultaneous Signal Approach

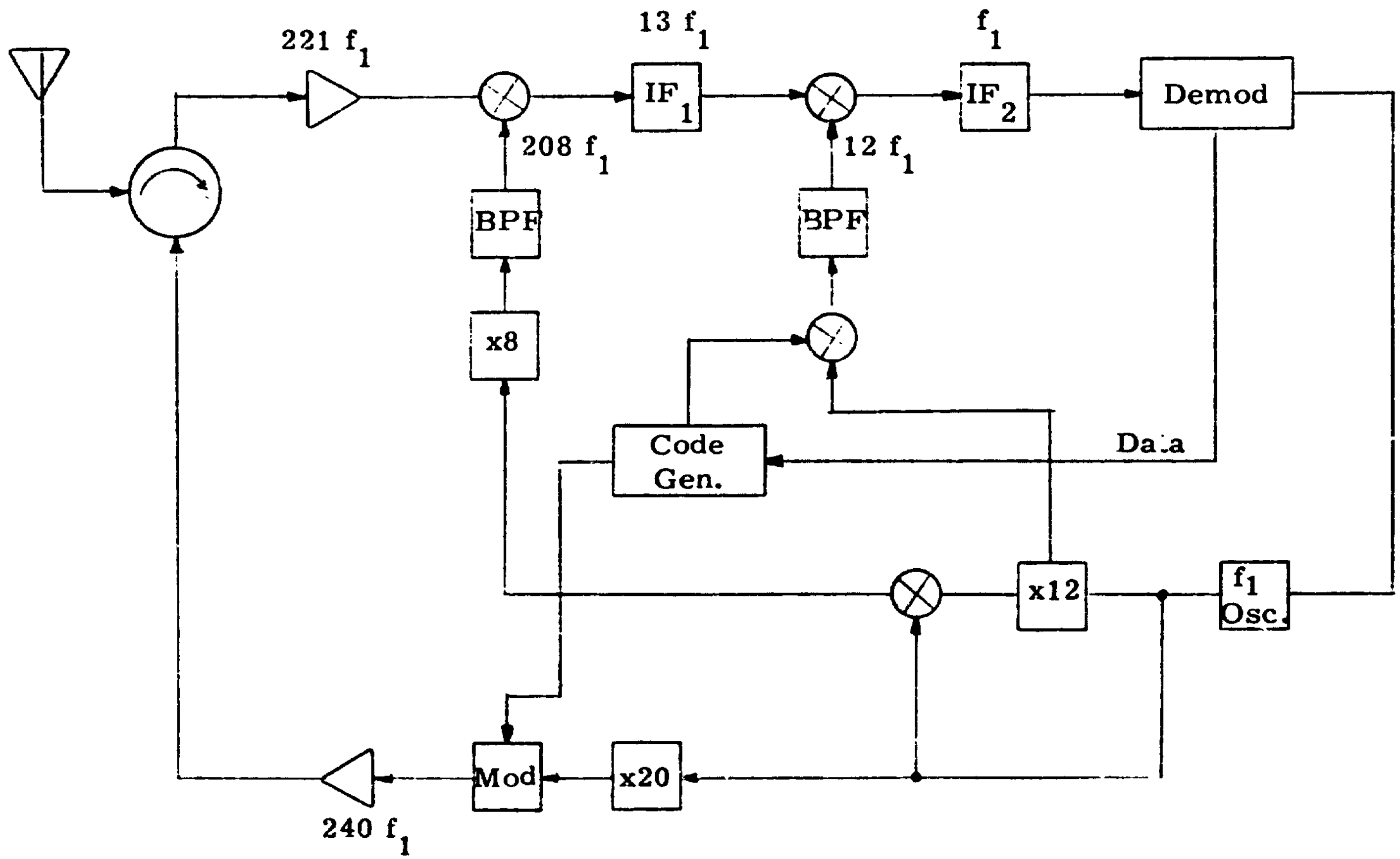

Figure 3.1-2. Basic Transponder Frequency Scheme and Signal Flow

the data as carrier PSK, translate this signal to 240 f_1, and overlay it with code modulation.

In practice, the data would not go directly from the demodulator to be used as a signal for the modulator, but would be processed as required within the spacecraft.

Figure 3.1-3 shows a more detailed block diagram of the data demodulation channel. A 221 f_1 received signal would be converted to 13 f_1, where it would be power-divided (by 4). One signal would be multiplied with a local reference (BPSK modulated with the 1023 bit code) which would, when synchronized, produce a signal PSK modulated with data at the IF2 frequency. This would then be demodulated by a squaring loop, and the data signal output for processing. A squaring-loop demodulator is shown because it is somewhat simpler than a Costas demodulator, although a Costas loop could readily be substituted for it. Performance of Costas and squaring loop demodulators has been shown to be the same.* The squaring loop VCO would be multiplied to produce the 240 f_1 frequency.

One of the signals from the IF1 power divider would be applied to a balanced mixer along with the range code (2^{18}-128 bits). When the range code signal is synchronized, a CW output signal appears at the mixer output, passes through a bandpass filter, is amplified and envelope detected, integrated and applied to a threshold detector. When a signal is detected, the range code generator is allowed to continue without reset, and is traced by the data code loop. This range channel subsystem is illustrated in Figure 3.1-4.

The other two signals from the IF1 power divider are fed to a pair of balanced mixers (see Figure 3.1-5) whose reference inputs are a pair of time-offset codes. These produce a differential in correlation output signals when filtered and detected, which are differentially amplified, filtered, and used to control the code clock frequency. Thus, the receiver code

---

*R. L. Didday and W. C. Lindsey, "Subcarrier Tracking Methods Communication System Design," JPL Report 32-1317, August 1968.

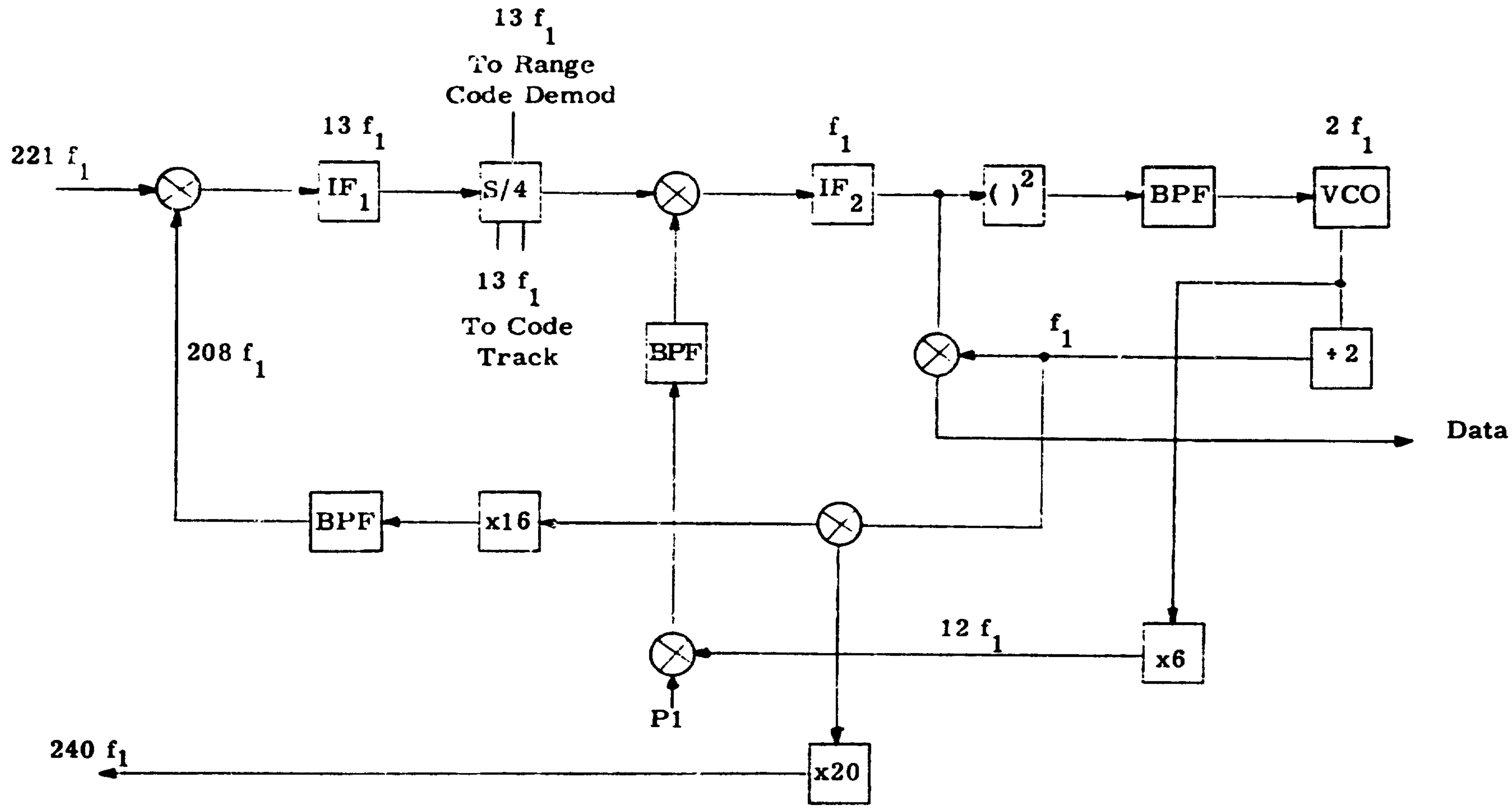

Figure 3.1-3. Data Channel Block Diagram and Frequency Scheme

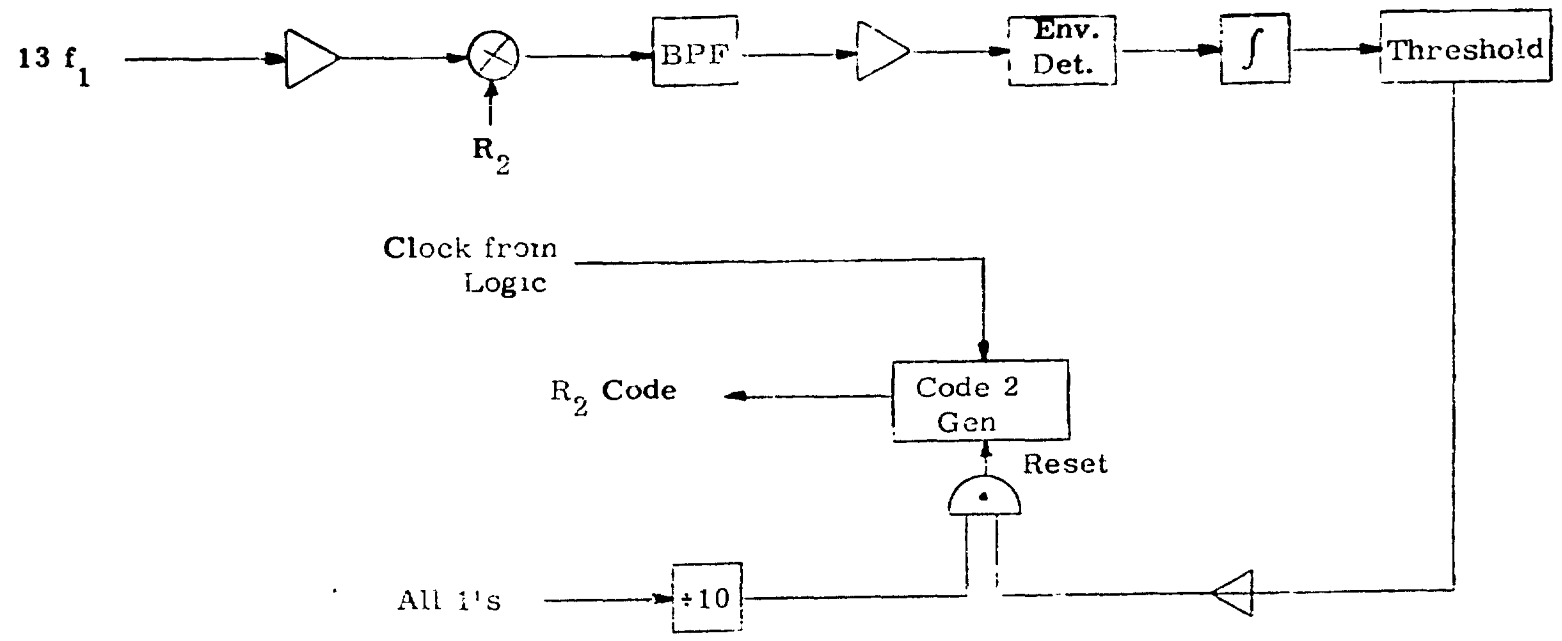

Figure 3.1-4. Range Channel Block Diagram

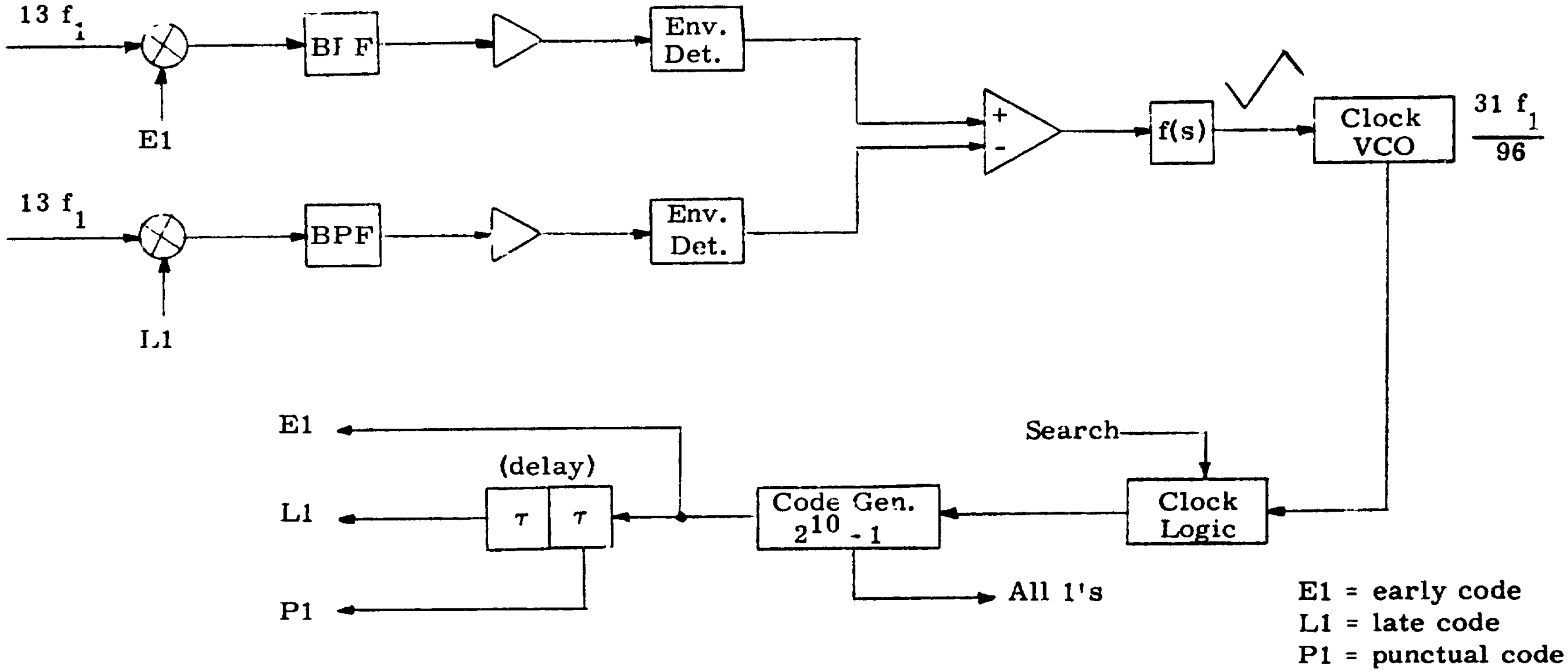

Figure 3.1-5. Tracking Channel Block Diagram

rate is tracked with the incoming signal's code rate. (This subsystem is a conventional delay-lock loop.) An alternate technique would be to employ an incremental phase modulator instead of the VCO. This incremental phase modulator would modify the phase of a $31 f_1/96$ signal derived from the demodulator's f_2 VCO.

An accurate clock source is vital to any spread spectrum system, since code drift can drastically affect synchronization time. The quartz crystal oscillators appear to have the edge for on-board spacecraft use, because of their size, weight, power, and reliability. (It is interesting to note that a hydrogen maser has been flown as a frequency source.) One of the atomic standards (cesium or rubidium) would be good for ground use.

3.1.2 Electrical Specifications for User Transponders

A number of electrical specifications for user transponders may directly affect the performance of the TDRSS with respect to achievable data rate(s). Some of these are examined in the following pages, with their effects, in order to arrive at minimal specifications without causing the implementation task to be too difficult.

In addition to analysis oriented to determining the effects of the parameters of interest, prospective transponder designers have also been contacted for comments with respect to their estimates of difficulty of implementation. These comments have also been considered in determining specifications.

The specifications of specific interest, with suggested specification limits, are given in table 2.1-7. Considerations in determining these specifications are described in the following pages.

User Oscillator Phase Noise

It is desirable to hold user oscillator phase noise to as low a value as is practical for a voltage controlled oscillator. The noise produced by the oscillator is multiplied, and appears at both receive local oscillator frequencies and transmit frequencies as a much larger amount of random phase noise. Investigation of the capability to hold phase noise down shows that present systems are capable of $<15^{\circ}$ phase noise, at S-band, where the measurement is made with integration over a 6 Hz to 2.5 MHz bandwidth.

Modulator/Demodulator Phase Imbalance

Phase imbalance is especially important to a quadriphase modulator. (It is equally important to a biphase modulator, but phase between halves of a transformer winding is difficult to maintain at anything other than 180°, which is that desired for BPSK.) Quadriphase modulation, on the other hand, can easily exhibit phase imbalance—usually occasioned by an offset in the carrier phase input to the two biphase modulators included in a QPSK modulator.

Phase offset in a QPSK modulator would be exhibited by producing signals similar to those seen in figure 3.1-6.

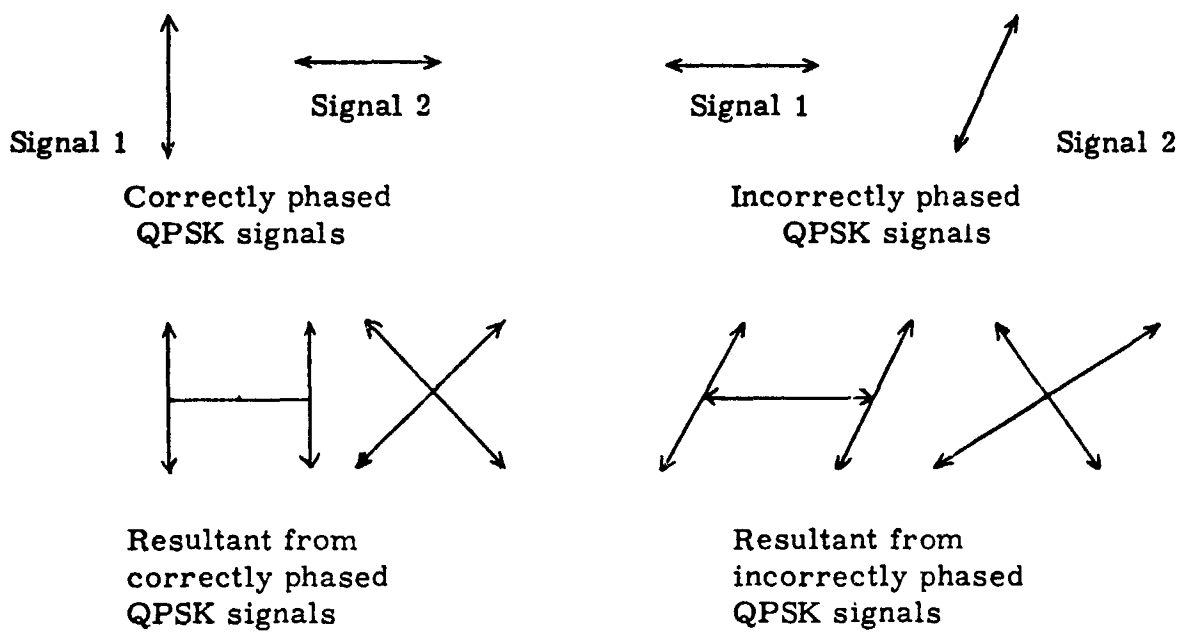

Figure 3.1-6. Signals Due to Phase Offset

This phase imbalance would produce an amplitude imbalance that could, in turn, cause large incidental phase shifts in the signal at the power amplifier output (see page 3-13).

It is suggested that amplitude imbalance be held to a maximum of 1 dB total, for both direct amplitude shifts and for incidental AM caused by paired-signal phase shifts. If 0.5 dB is allocated to each cause, then signal amplitude would vary from 1 (normalized) to 0.891. Therefore, the maximum phase shift allowable would be approximately 6.5 degrees.*

Modulator/Demodulator Amplitude Imbalance

Where a pair of signals are unbalanced in amplitude, the signal resulting from their being combined is affected in both amplitude and phase angle. In a previous section of this memorandum, it was considered that amplitude balance could be held to within 0.5 dB. In that same section, it was shown that a 0.5 dB amplitude shift corresponds to a 6.5 degree phase shift.

Data Asymmetry

In a biphase or quadriphase modulator, the effect of data asymmetry is to cause a DC bias in the output, which in turn causes unbalance at the second harmonic of the data. (For code-driven modulators, the code is unbalanced.) This then produces a strong carrier component at the code sequence bit rate, which appears as a signal at the nulls of the output signal spectrum. (See figure 3.1-7.)

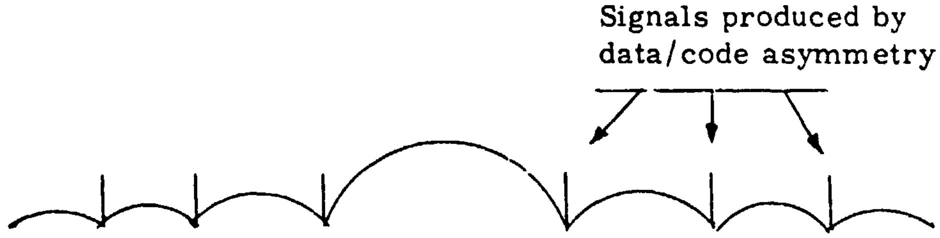

Figure 3.1-7. Direct Sequence Signal with Data/Code Symmetry

*From the formulae derived on page 3-13:

$$(\sin 6.5 + 1) + j \cos 6.5 = 1.492 \angle 41.75$$

$$(\sin 6.5 - 1) + j \cos 6.5 = 1.331 \angle 131.75$$

$$\frac{1.331}{1.492} = 0.892 .$$

If data signals are held to symmetry within 1%, then the signals seen at spectrum nulls should be ≥10 log 100 = 20 dB below the unsuppressed carrier signal.

Data Skew

Data skew primarily affects the signal shaping, since the effect of such skew is one of causing signal transitions to occur at times other than those for which the system is designed. As long as data transitions are not skewed to the point that both data transitions in a QPSK modulator occur simultaneously, there is no effect. (We restrict this argument, however, to one in which the receiver may separately track the two data streams. Where only one of the two signals is tracked, data skew should be avoided to as great a degree as practical.)

AM-to-PM Conversion

AM/PM conversion and distortion experienced by an amplitude modulated signal in being processed by a TWT power amplifier is discussed on page 3-16. For some of the signals proposed, this AM/PM conversion can produce phase shifting signals that are larger than those that convey the desired information. Therefore, the aim in choosing modulation formats has been to choose a format that has minimum steady-state amplitude shifts. (We note that some amplitude shifting is inevitable during phase transitions, but that proper signal selection can provide minimum amplitude shift after setting to a new phase.)

Phase Characteristics

Both sinusoidal and quadratic phase characteristics and their effect on PSK signals have been well defined by Jones.* The curves given by Jones may be employed to specify the allowable signal distortion, given a maximum allowable signal degradation or loss in performance.

---

*J. J. Jones, "Filter Distortion and Intersymbol Interference Effects on QPSK," Proc. Hawaii Conf. Syst. Sci., January 1970.

Effect of Phase Shift Between Orthogonal Signal Pairs

A balanced biphase modulator's output (in the modulated signal band of interest) may be written as (see figure 3.1-8):

$$A^* \cos \omega_c t \pm \omega_m t$$

where the input carrier is $B \cos \omega_c t$ and the modulating signal for the case of interest here is $C \cos \omega_m t$.

The modulating signal is $\phi(t)$, where ± 90 degrees is the only accepted modulation, and the period of the modulating signal ω_m is that of either a coded signal or data modulation. That is, a +1 is represented by $A \cos \omega_c t + 90^\circ$, and a -1 is represented by $A \cos \omega_c t - 90^\circ$.

This signal format may be extended to quadriphase (QPSK) modulation by realizing that the QPSK modulator is a pair of biphase modulators (figure 3.1-9) whose outputs are summed. The QPSK signal may be expressed as

$$A \cos \omega_c t \pm 90^\circ + D \sin \omega_c t \pm 90^\circ$$

which results in four possible output signals

$$A \cos \omega_c t + 90^\circ + D \sin \omega_c t + 90^\circ$$

$$A \cos \omega_c t + 90^\circ + D \sin \omega_c t - 90^\circ$$

$$A \cos \omega_c t - 90^\circ + D \sin \omega_c t + 90^\circ$$

$$A \cos \omega_c t - 90^\circ + D \sin \omega_c t - 90^\circ$$

which correspond to signals

$$\sqrt{A^2 + D^2} \ \angle 135^\circ$$

$$\sqrt{A^2 + D^2} \ \angle 225^\circ$$

——— input
– – – output

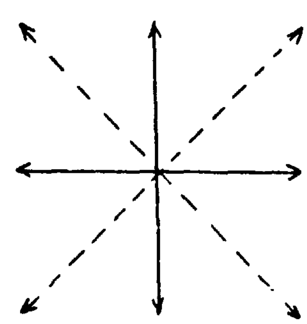

*$B \cos \omega_c t \ C \cos \omega_m t = (BC)/2 \cos \omega_c t \pm \omega_m t = A \cos \omega_c t \pm \omega_m t$.

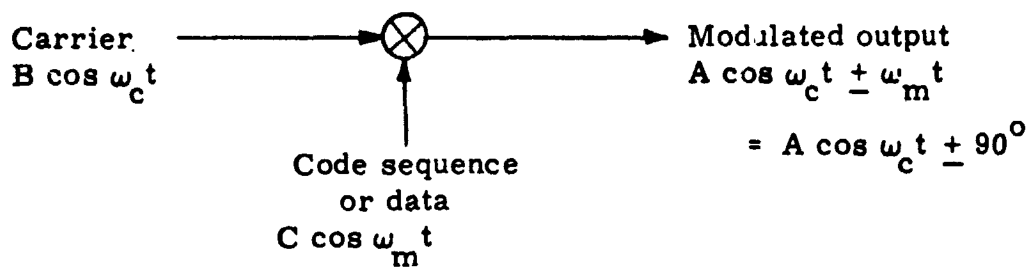

Figure 3.1-8. Biphase PSK Modulator

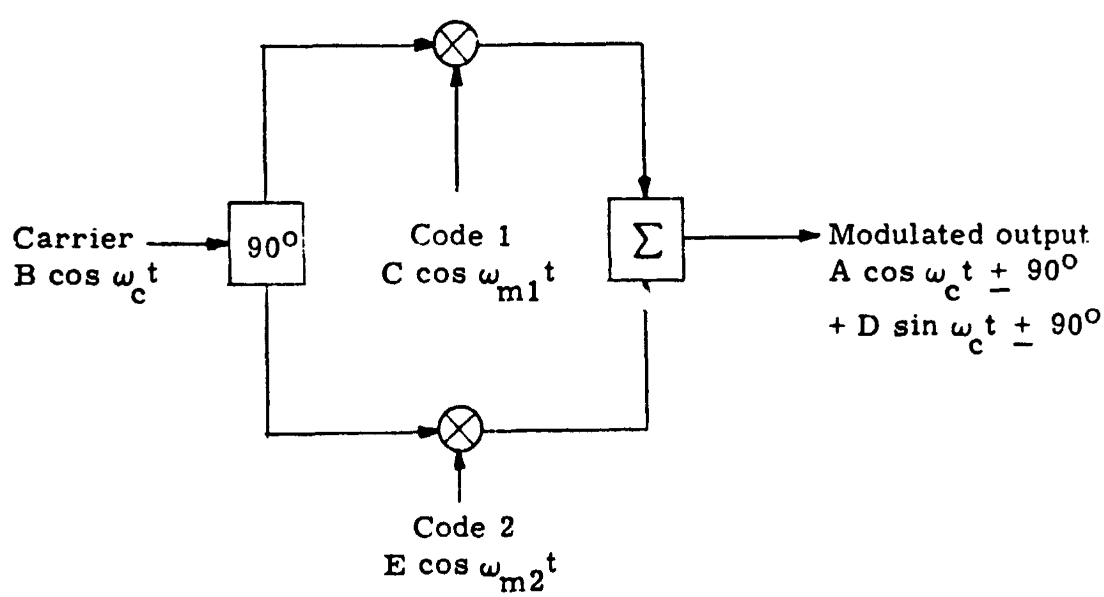

Figure 3.1-9. Quadriphase PSK Modulator

$$\sqrt{A^2 + D^2}\ \angle 45^\circ$$

$$\sqrt{A^2 + D^2}\ \angle 315^\circ,$$

respectively.

Now if there is a phase shift (other than 90 degrees) between the carriers applied to the two biphase modulators contained in the QPSK modulation, then there is no longer a phase and/or amplitude balance in the output signal. Instead, the input and output signals will be

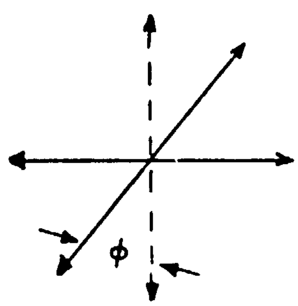

Input signal

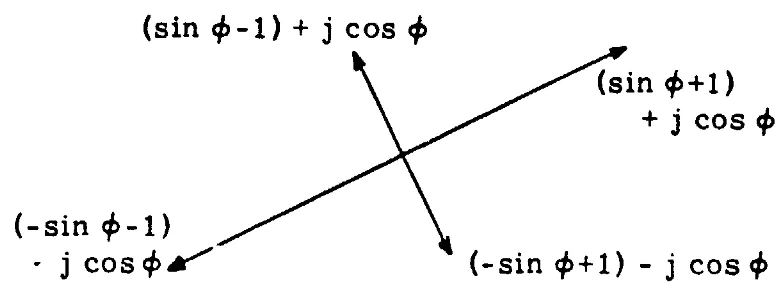

Resultant output

If, for example, we choose ϕ as 45 degrees, then the output signal resulting from a pair of equal amplitude input signals is

$$(\sin 45 + 1) + j \cos 45 = 1.847\ \angle 22.5$$

$$(\sin 45 - 1) + j \cos 45 = 0.765\ \angle 112.5$$

$$(\sin 45 - 1) - j \cos 45 = 1.847\ \angle 202.5$$

$$(\sin 45 + 1) - j \cos 45 = 0.765\ \angle 292.5$$

For this kind of signal, there is a large amplitude shift between output positions, which is highly undesirable because of the difficulty which could be engendered due to AM/PM conversion.

Here, for convenience, we have analyzed biphase and quadriphase modulators. We hasten to point out, however, that the signals existing in a quadriphase modulator are identical to those that exist in a linear channel wherein two biphase signals are processed.

AM-to-PM Conversion and Intermodulation Distortion in Spacecraft-Type Traveling Wave Tube Amplifiers

It is of interest in satellite systems, where traveling wave tube (TWT) amplifiers are employed, to be able to define the incidental phase modulation, and the intermodulation products resulting from processing one or more signals in a communication channel. This is especially true with respect to incidental phase modulation when the signals being processed contain low-deviation FM or PM signals.

Traveling wave tubes exhibit phase modulation as a function of their input signal level. This phase modulation is a result of a change in beam velocity in the TWT as input signal changes.

The signals of most interest in TDRS are phase-modulated, and therefore, if they are selected properly should be constant-envelope signals. This is true, however, only in the steady-state case, and amplitude modulation does exist during the transitions from one state to another. Some signal alternatives do exhibit both steady-state amplitude and phase shift and these must be carefully considered before use, since it is possible that the phase modulation introduced by amplitude changes in the signal may be grater than the desired phase modulation.

In addition to characterization of AM/PM conversion, it is also of interest to know the degree of cross-modulation that may be expected when two signals are to be passed through a single TWT amplifier. This parameter is a measure of the self-generated noise that may be expected under the two-signal condition.

Table 3.1-1 shows typical AM/PM conversion measurements for TWT amplifiers for various frequencies and power levels. It is apparent that, depending on the tube type and its operation, AM/PM conversion may vary widely. For data considered, values covered a range from 1.5°/dB to 8.4°/dB, with a tendency for low power tubes to exhibit higher AM/PM conversion.*

Cross-modulation in the saturated mode appears to produce third-order products that are approximately 8 to 12 dB below the desired signals in the two-signal case.

---

*It is of some interest to note that a preliminary check with JPL brought a quotation of 12^{o}/dB for the tube type employed on the typical spacecraft transponder. This agrees with Hughes data.

Source	TWT	Output Power	AM/PM Conversion: Saturated	AM/PM Conversion: Linear
"Improved TWT's for Broadband Jamming," Microwaves, November 1969	WJ 440	440 w (sat) (5-10 GHz)	6^{o}/dB	6^{o}/dB
"New Data Eases TWT Use in Communications," MSN, July 1971	STC-5215 & 52161 (Sperry)	250 w (sat) (4-8 GHz)	$2.5^{o} - 3.5^{o}$/dB	Same
		100 w (sat) (8-12 GHz)	---	---
		50 w (sat)	---	---
RCA Technical Bulletin MWD-109, September 1969	RCA 4054	20 w (sat) (1.7 - 2.7 GHz)	$7^{o} - 8^{o}$/dB	3.5^{o}/dB
"Designing High Efficiency TWT's", Microwaves, July 1973	219 HX (Hughes)	28 w (sat) (7.7 - 8.0 GHz)	4.1^{o}/dB	8.4^{o}/dB
"Traveling Wave Tube for Satellite Applications," MW Journal, November 1972	Thomson-CSF	20 w (sat) (10.95 - 11.20, 11.45 - 11.7 GHz)	1.5^{o}/dB	Same
"High Power Broadband T-W Tubes," MW Journal, April 1969	M5312 (Teledyne-MEC)	150 w (sat) (3.4 - 3.6 GHz)	2^{o}/dB	1.6^{o}/dB

Table 3.1-1. Measured AM/PM Conversion for Various Traveling Wave Tube Amplifiers (Linear 6 dB below saturation)

3.2 Ground Receiver

The TDRSS receiver serves the function of receiving and demodulating all of the information sent down from the various user transponders on the return links. These signals are listed in section 2.2.2 of this report. The receiver description given here is for the purpose of clarifying the design, and does not represent a specified receiver, nor does it represent an "optimum" design. Figure 3.2-1 illustrates a possible receiver for the multiple signals expected, and the remainder of this section describes the operation of this receiver. Block diagrams are given to illustrate possible implementations of the subsystems of this receiver.

The receiver block diagram shown is for reception of signals in either (or both) K-band and S-band, since TDRSS is capable of and is expected to operate in both bands.

K-band signals would be amplified, split into two components, one of which would be taken for other K-band users. The second signal would be mixed with an 11.2375 GHz signal, producing a 2287.5 MHz intermediate frequency which is passed through a bandpass filter of 250 MHz BW (to pass the 225 MHz KSA signal). The signal is then amplified, mixed with a 1.975 GHz local oscillator, and output as a signal centered at 312.5 MHz. (The signal consists of a number of SMA signals separated at 6 MHz intervals.) After amplification again, the signal i[illegible]d by 22 and applied to 22 separate demodulations, each of which is c[illegible] of demodulating one downlink signal. These demodulators are not d[illegible] for demodulation of all signals encountered, however. Instead, [illegible] demodulation bandwidths are distributed as follows:

Demodulator	Demodulator Data Rate
1 through 8	100 bps to 10 kbps
9 through 12	10 kbps to 25 kbps
12 through 20	25 kbps to 40 kbps
21 and 22	40 kbps to 50 kbps

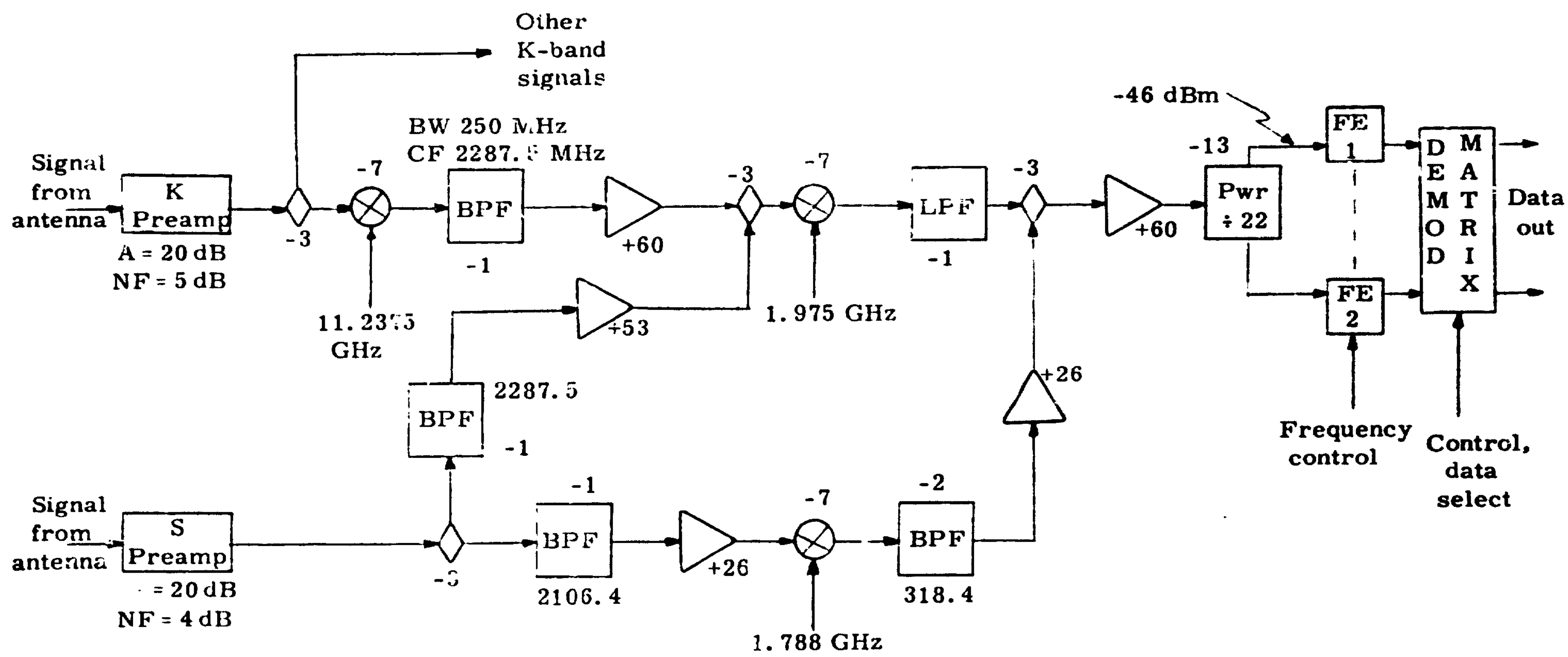

Figure 3.2-1. Block Diagram of Ground Receiver for TDRSS SMA, TT&C, and Test Signals

Each selector at the output from the ÷22 power divider would have channel selection capability which would be controllable from the TDRS console in the ground station. A demodulator matrix would steer the signal outputs from the selectors to the right signal demodulator and then to the correct user output.

The second signal path in figure 3.2-1 is for S-band signals. Signals arriving at the S-band preamp would be amplified, split and routed to both the first IF in the receiver and to a second path that eventually reaches the ÷22 power divider. These alternate paths provide for use of the same subsystems for demodulation and signal switching, thus minimizing the ground receiver complexity. Signals at 2287.5 MHz would be routed to the second mixer and 312 MHz IF, while those at 2106.4 MHz would be routed to a mixing process which converts them to 318.4 MHz. Thus, if desired, these signals can be received simultaneously.

After power division, all input signals are applied to a set of tunable selectors (labeled FE1 through FE22) which are modified UHF communications receiver front ends. (The modifications entail broadening their frequency synthesizers by approximately 20%.) Each would be individually controllable to receive at any of the possible 42 MA and/or turn-around ranging channels. After signal selection, the signals would be routed to a demodulator and output data matrix, which allows the proper demodulator to be connected to any incoming signal frequency and the resulting data to be routed to the proper output.

Figure 3.2-2 shows the method for providing downlink frequency selection and demodulation of the single access signals, as a simplified block diagram. Figure 3.2-3 is a block diagram showing the modified UHF receiver front end and spread spectrum code correlator. Spread spectrum receivers at UHF (225 to 400 MHz) presently exist to perform this exact function. Therefore, it is suggested that a modified version of one of the existing receiver subsystems be investigated.

c-2

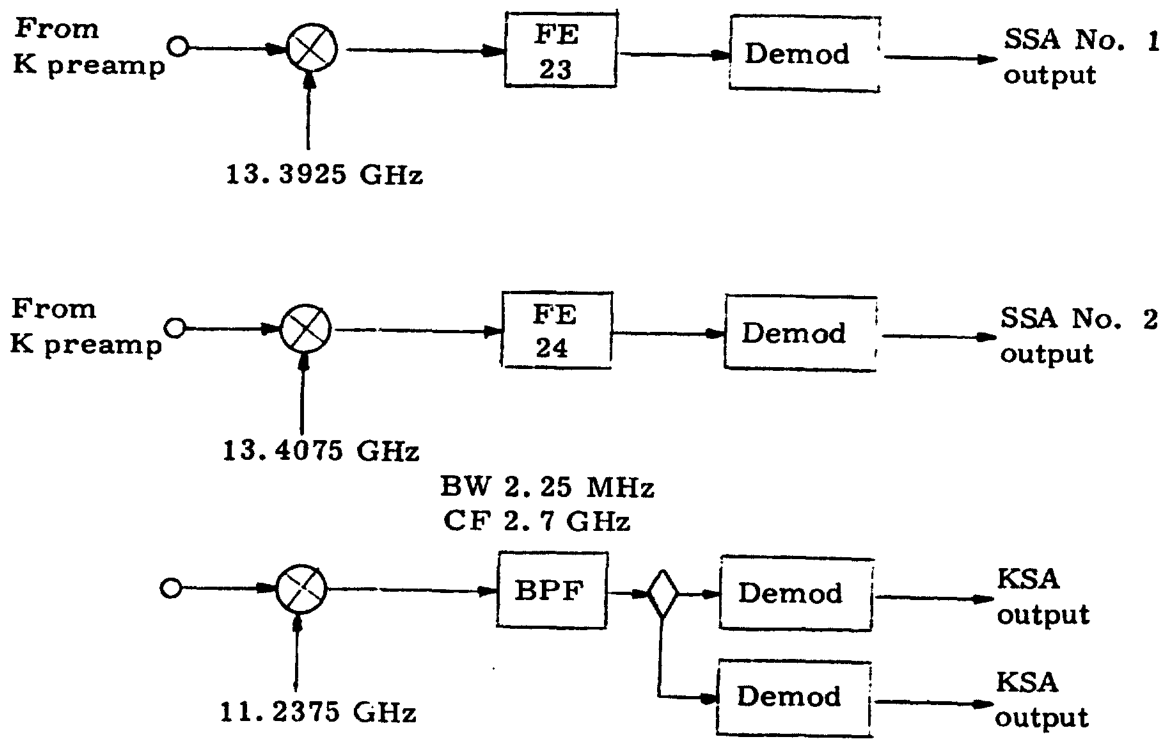

Figure 3.2-2. Block Diagram of Ground Receiver for SA Signals

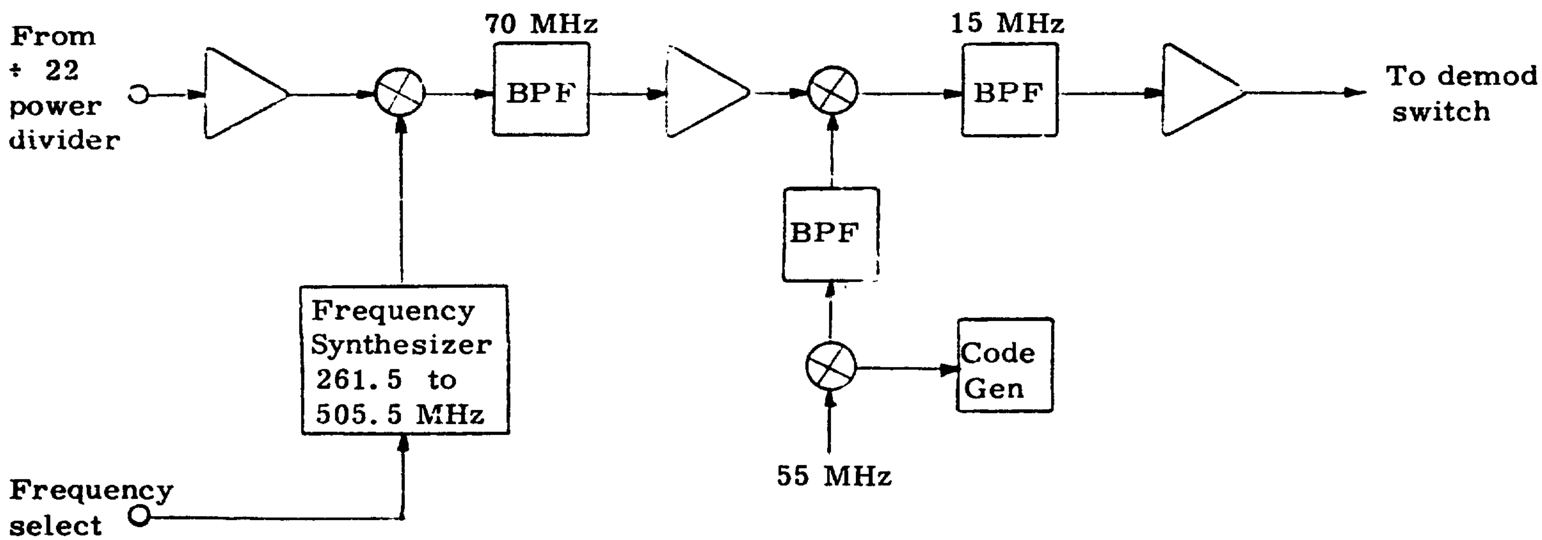

Figure 3.2-3. Modified UHF Front End (One of 22)

The demodulator matrix is shown in block diagram form in figure 3.2-4. This matrix would route incoming signals, after frequency selection, to the proper demodulator. Twenty-two demodulators are shown, with varying data rate capabilities. This number could readily be modified or the type of demodulator could be changed to accommodate different requirements.

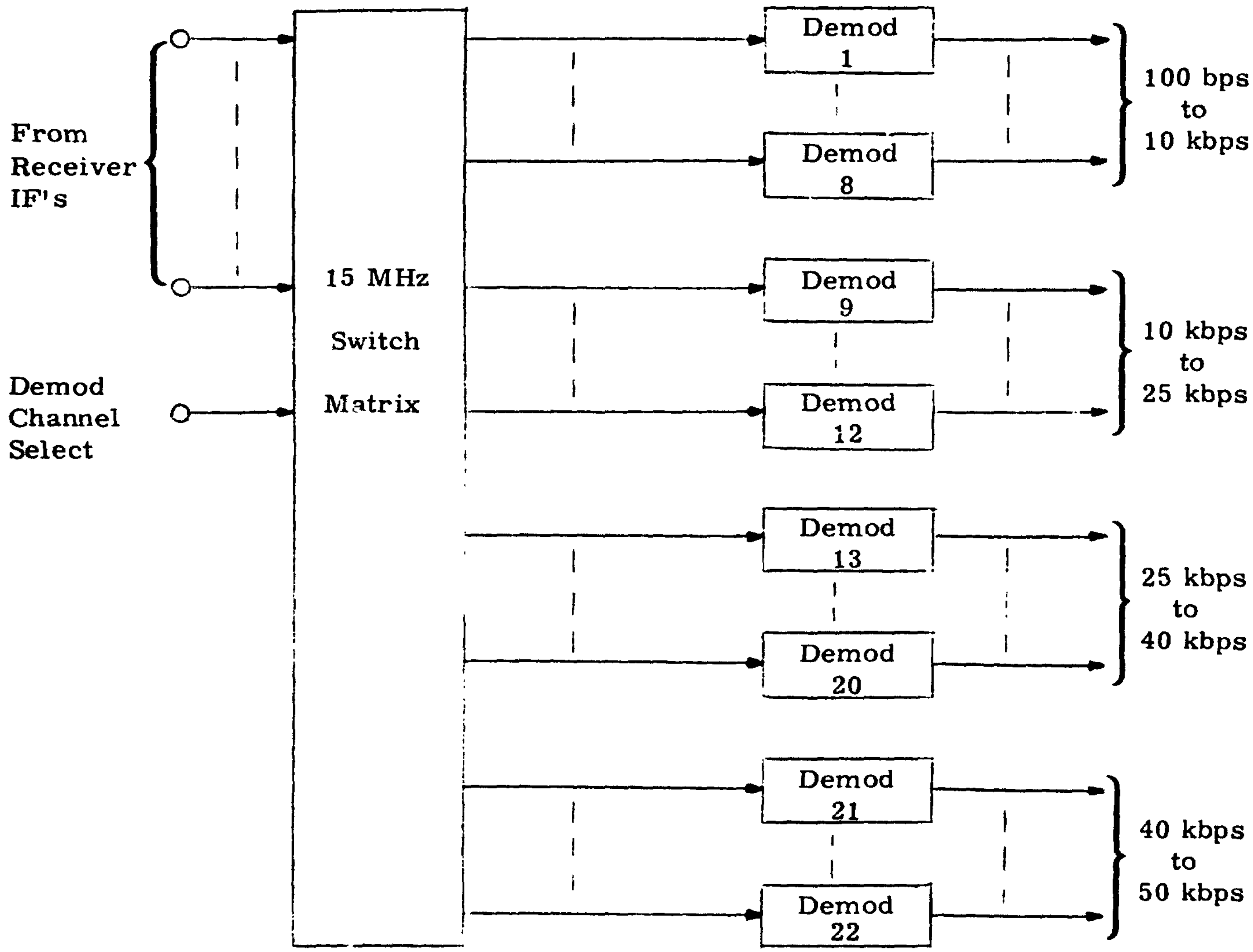

Figure 3.2-4. Demod Matrix for Ground MA Subsystem

4.0 SYNCHRONIZATION TECHNIQUES AND ANALYSIS

4.1 Introduction

One of the purposes of this investigation was to establish basic system parameters and signal design techniques for both the S-band forward link and the return links, with particular emphasis on the multiple access modes. Clearly, the synchronization requirements play a pivotal role in establishing the signal design parameters. Among the goals established at the beginning of this investigation were the desire to eliminate the requirements for a synchronization preamble, to limit the average synchronization time of the multiple access forward link to 20 seconds and on the return link to 15 seconds, and to limit the design to technologies for which there are space-qualified components. An additional consideration was the minimization of hardware complexity, in particular, in the user transponder.

In the first step to achieve the above objectives, a set of candidate techniques was selected for which a first-level analysis was performed. This analysis focused on the multiple access forward link to the user, as this is the link with the lowest threshold of performance. The acquisition techniques can be divided into two classes. The first class is termed component (composite) code acquisition. The second class is direct sequence code acquisition. Within each of these classifications, several approaches were analyzed. These include techniques such as serial search with fixed length tests and sequential tests, parallel search, and both digital and analog matched filtering techniques. From the preliminary assessment, a more detailed study was made of the techniques with the greatest likelihood of achieving the desired acquisition time performance goals and those which could be implemented with relatively low risk technology. The analysis and tradeoffs associated with the candidate techniques are detailed in the Interim Report.[1]

From these various candidate approaches, the fixed length and sequential test strategies of the direct sequence codes were selected for more detailed investigation. The details include a multiple mode acquisition strategy, doppler resolution, and the consideration of bandlimiting losses, subchannel power losses, and multiple access interference. Most of the details of this second-level analysis are given below.

The study concludes with an analysis of the impact of multipath on the recommended acquisition approach. Several ideas are presented for mitigating the effects of multipath. The actual mutlipath parameters were obtained from the Boeing Company under a subcontract to Robert Gold Associates. These multipath parameters were obtained through a simulation program with the specific TDRSS parameters as input data. The simulation model was verified by Boeing through extensive experimental testing for a satellite-to-aircraft link.

Even the more detailed analysis discussed in this section of the report is not optimized. With the use of a computer simulation, a "fine tuning" of the analysis could be performed to further reduce the mean acquisition times.

Both the delay lock chip tracking loop and carrier lock loops have lock times which contribute to the overall acquisition time. It is estimated that the code tracking and carrier pull-in and settling times are less than 1 second and hence are largely insignificant contributors the overall synchronization time. It is for this reason that the major emphasis in this study is directed toward the code acquisition analysis.

4.2 Synchronization of Receive System

4.2.1 Statement of the Problem

To demodulate the transmitted wideband noiselike signal, the receiver must have knowledge of the pseudorandom code employed during modulation. The receiver not only needs to know which particular code was used by the transmitter, but also the exact code epoch or phase. This is the synchronization problem of the receiver.

A model of the synchronization circuitry is given in Figure 4.2-1.

The receiver removes the pseudorandom code from the received signal by cross-correlating the received signal plus noise with a reference signal. This involves first multiplying the signal plus noise with a reference signal generated by a local PN code generator. The locally generated replica is cross-correlated with the received signal plus noise and integrated in different relative phase positions until the correlation value indicates the two sequences are in phase. The number of correlations which must be performed depend upon the initial phase uncertainty of the received sequence, the length of the sequence before it repeats, the frequency offset between the local reference and the incoming signal, and the specified acquisition probabilities (i.e., probability of detection and false alarm). The acquisition time is a function of the number of correlations required.

Once the acquisition of the received signal is obtained, the codes are close enough in phase to enable the delay lock loop to begin tracking. During this time, the carrier recovery circuit or phase lock loop also begins operating and the data demodulation process can begin.

4.2.2 Outline of Candidate Acquisition Techniques

The basic direct sequence acquisition techniques considered as candidates for the TDRS receivers are summarized in Table 4.2-1.

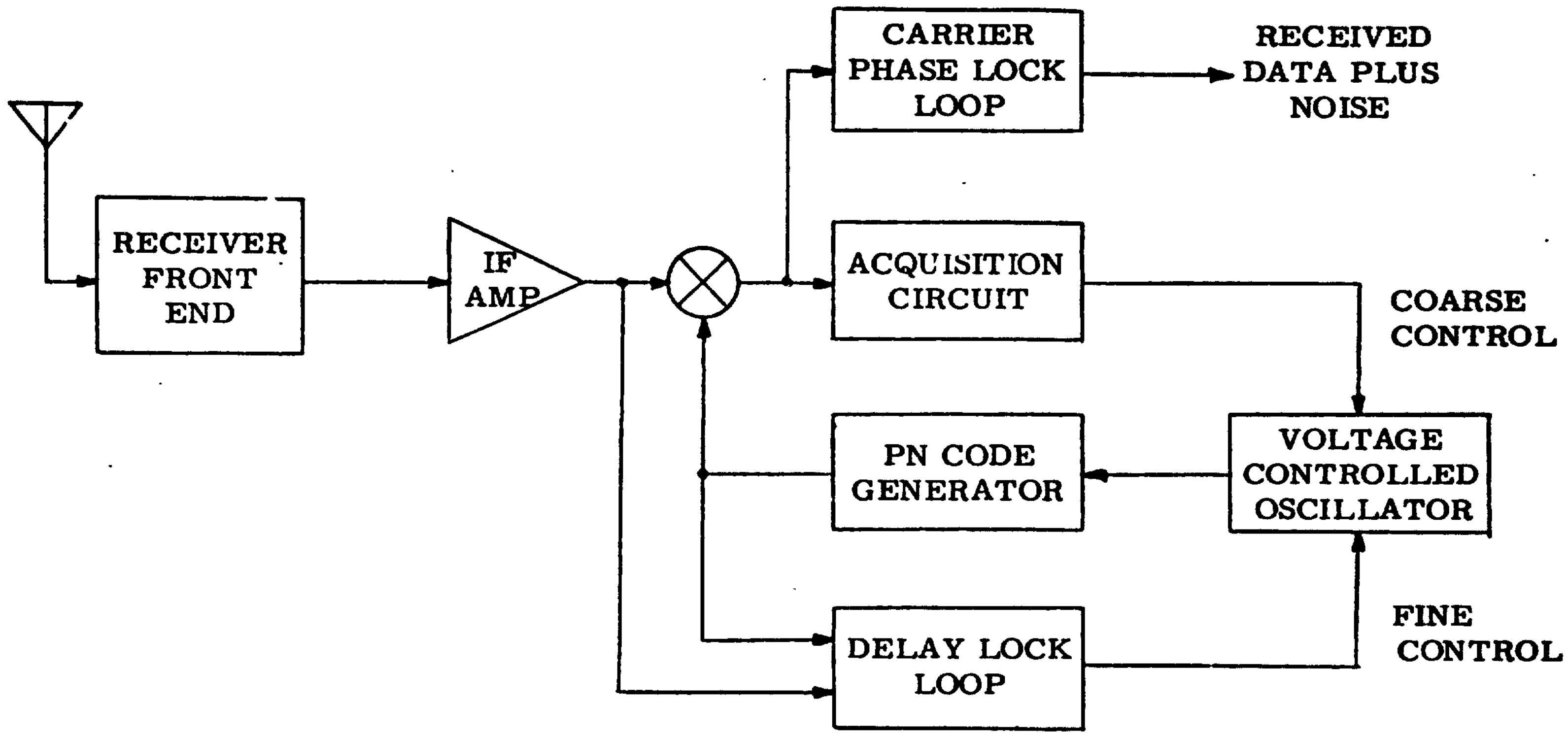

Figure 4.2-1. Pseudo Noise Synchronization Circuits

Table 4.2-1. Candidate Acquisition Techniques

Serial Search Techniques
- Component codes
- Direct sequence - PN code

Parallel Search Techniques
- Component codes
- Direct sequence - PN code

Matched Filter Techniques
- Analog
- Digital

A simplified model for each of these techniques is given in Figure 4.2-2. In each of these techniques, some form of post-detection integration was employed. During the course of the study, each of the above techniques was analyzed and compared. A first-level summary of this comparison is given in Table 4.2-2. As a consequence of this analysis, the component code techniques were rejected because of their inherent complexity. The matched filter techniques were rejected because of their development risk. Hence, the direct sequence serial search techniques were analyzed in greater depth. The basic concepts and analyses of the techniques which were rejected for further consideration are documented in the Interim Report[1] and several of the monthly reports.

4.2.3 Basic Steps in the Acquisition Procedure

As noted above, the receiver must perform a search in time to find the correct code epoch to demodulate the transmitted signal.

There are a couple of basic assumptions for the synchronization model. One assumption is that the apriori distribution of the true code position is uniform over the entire PN code period. Another assumption made for the first-level analysis of the candidate techniques is that only

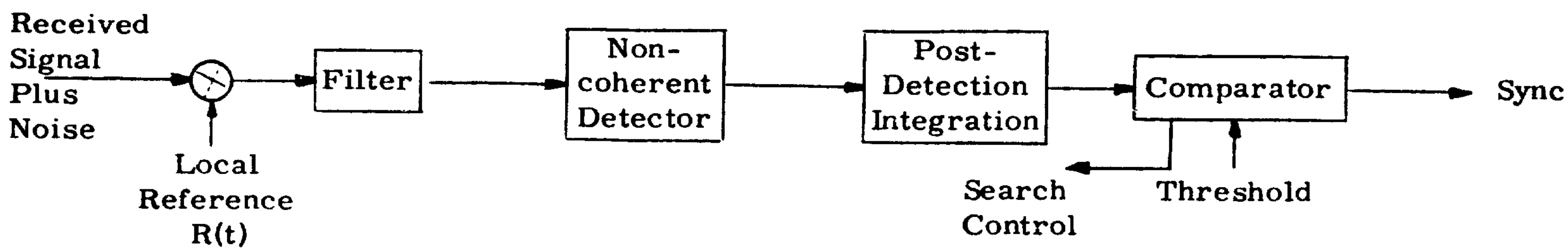

(a) Serial Search Technique

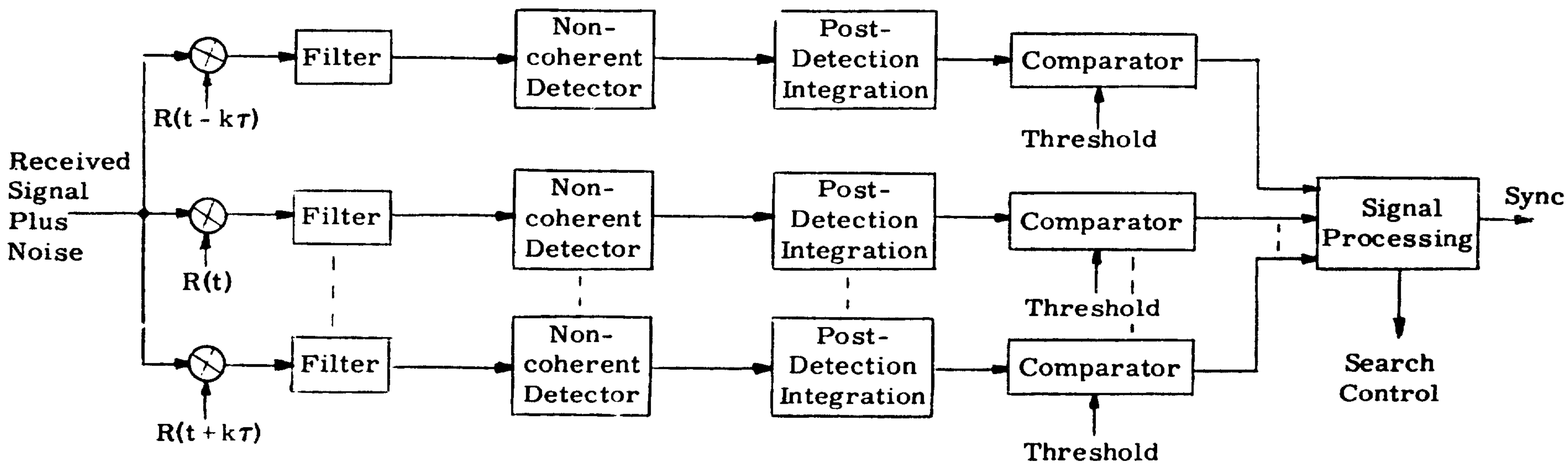

(b) Parallel Search Technique

Figure 4.2-2. Models of Candidate Acquisition Techniques

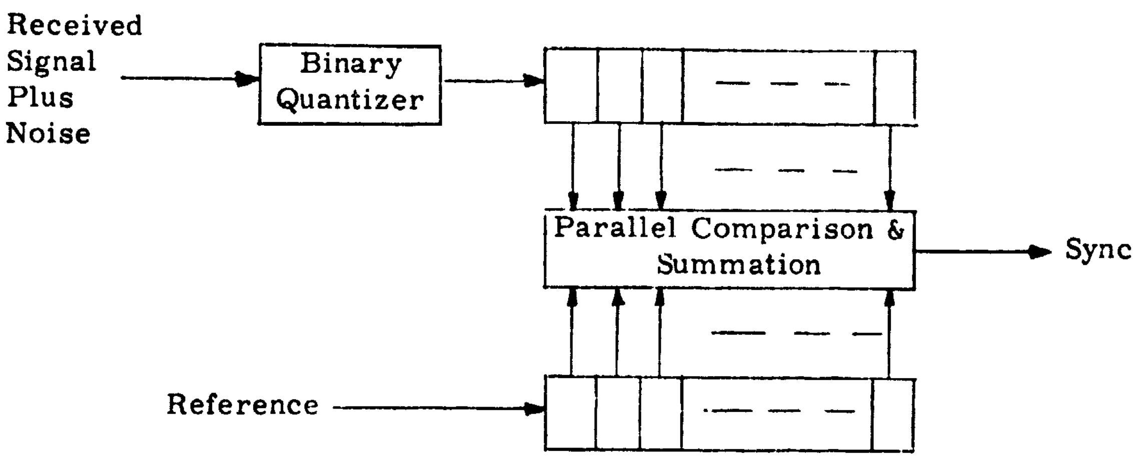

(c) Matched Filter with Binary Quantization

Figure 4.2-2. Models of Candidate Acquisition Techniques (continued)

Table 4.2-2. Comparative Evaluation of Candidate Acquisition Techniques

Acquisition Code Type	Acquisition Detection Technique	Received Signal Level (dBm)	Length of Code (chips)	Chip Rate (chips/sec)	Average Acquisition Time (sec)	Complexity	Development Risk
3 Component	Serial search	-137.1	47, 63, 73	3×10^6	41.5	Moderate	Low
	Parallel search	-137.1	47, 63, 73	3×10^6	10.5	High	Low
	Parallel matched filter Coherent combining	-137.1	47, 63, 73	3×10^6	0.23	High	High
	Parallel matched filter Noncoherent combining	-137.1	47, 63, 73	3×10^6	1000	High	High
Direct Sequence PN	Digital matched filter Noncoherent combining	-137.1	1000	3×10^6	0.13	High	Moderate
	Digital matched filter Majority detector	-137.1	8000	3×10^6	0.15	High	Moderate
	Serial search 1/2 chip increments (fixed length test)	-137.1	1000	3×10^6	110	Low	Low
	Serial search 1/2 chip increments (sequential test)	-137.1	1000	3×10^6	16.5	Low	Low

one code chip or time cell is the true synchronization position. This particular code position is the signal chip, and all other code positions are the noise positions. This assumption is removed in the second-level analysis of the recommended synchronization technique.

The most important parameter of the synchronization process for the present study is the average synchronization time, $\overline{T}_{acq}$, which is obviously to be minimized. A complete statistical description of the synchronization time would entail the calculation of higher order statistics which would allow confidence limits to be defined for the synchronization time. This is an area of future work which can come directly from the synchronization model developed below. The optimization or minimization of $\overline{T}_{acq}$ was not performed.

The overall synchronization process can be broken down into a sequence of steps, as illustrated in Figure 4.2-3. The synchronizer dwells in a particular cell position for a fixed duration of time, T, or a variable length of time, t, in the case of the sequential test. In the fixed length test, a cell is rejected if no threshold crossing occurs after integrating for T seconds. In the sequential test, a cell is rejected if a lower threshold is crossed.

When cell rejection occurs, the synchronizer advances to the next time cell and repeats the above process. If there is a threshold crossing in the fixed length test and an upper threshold crossing in the sequential test, the synchronizer enters the verification mode in which it tries to arrive at a temporary decision as to whether the time cell under examination is indeed the true synchronization position. If it decides there was no signal, it resumes the search in the next time cell. If it decides there was a signal, it enters the tracking or demodulation mode with the possibility of having made a false lock in a no-signal cell. If a false lock is recognized in the tracking mode, the loops are unlocked and the synchronizer again resumes the search.

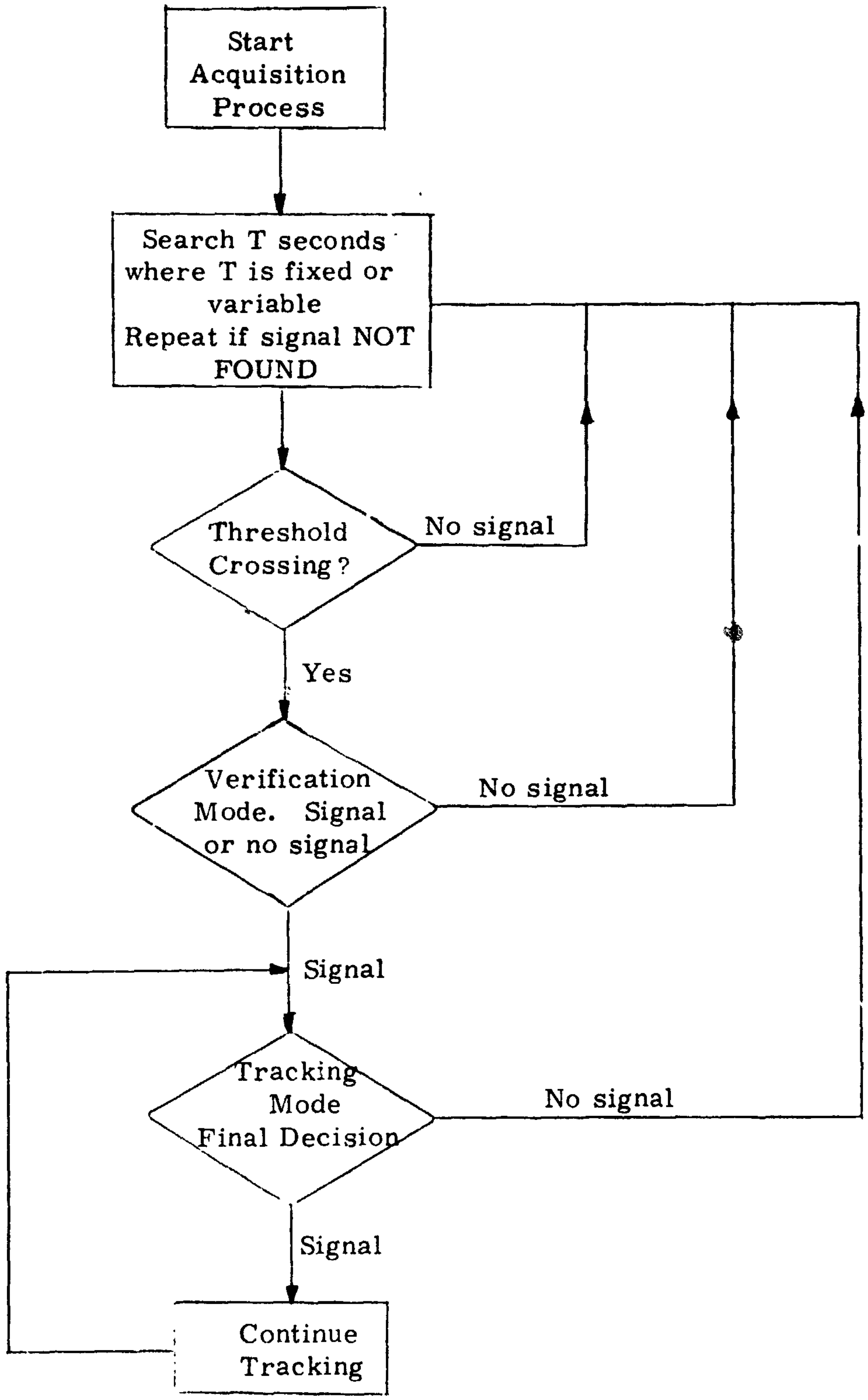

Figure 4.2-3. Overall Synchronization Process

In the initial acquisition process, there is no apriori knowledge limiting the number of cells which may contain the signal. However, during reacquisition, a different strategy should be implemented. The reacquisition search should begin from the cell position where synchronization was last detected and proceed tc search from that point to its nearest neighbors and continue searching cells radiating out from that position. This technique of ınsuring that the cells are searched in order of their likelihood of containing the signal yields the optimum performance.

4.3 Analysis of Acquisition Techniques

4.3.1 Fixed Length Test

A block diagram of a noncoherent acquisition detector using an envelope detector and an adaptive threshold is shown in Figure 4.3-1. The search procedure of the fixed length test is relatively straightforward. The local code is correlated with the received signal for a period of time, T, after which the output is compared with a threshold and a decision is made. (The test is of fixed length because the integration period T is a constant.) If the output of the integrator falls below the threshold, the code phase is advanced (or retarded) by 1/2 chip time and another test is made. If the output at the sample time is above the threshold, additional tests are made according to the verification mode algorithm. A step size of 1/2 chip time is selected so that, for at least one step in the search sequence, the two codes will be within 1/4 chip of correct synchronization. Since the chip cross-correlation function is a triangular waveform, the basic effect of the synchronization error is to reduce the power spectral density of the despread signal. One can show that the power spectral density is reduced by a factor of $(1 - |\varepsilon|/T_c)^2$, where $|\varepsilon| \leq \Delta$. Hence, for a maximum phase error of 1/4 chip, the degradation is $(0.75)^2$ or -2.5 dB. Thus, the signal-to-noise ratio during acquisition is reduced by 2.5 dB.

The bandpass filter following the despreader is designed to maximize the predetection signal-to-noise ratio. It must be wide enough to accommodate the data modulation bandwidth and both the doppler and frequency uncertainty offsets.

When the local code is in synchronism with the incoming code, the output is a CW waveform which is envelope detected. If the codes are out of phase by more than one chip period, the signal-to-noise ratio is greatly reduced because the signal bandwidth will be spread at the filter input. The extent to which this occurs is investigated in Section 4.3.5.

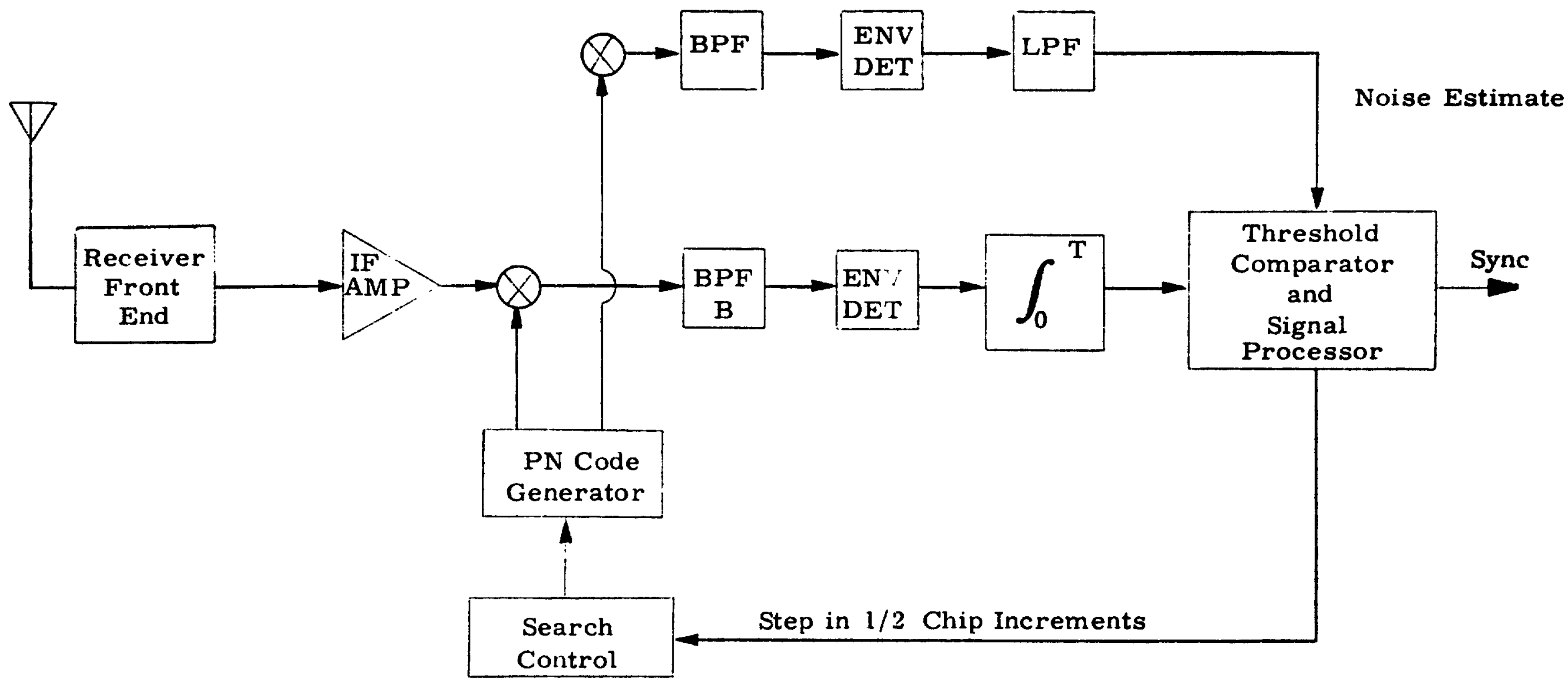

Figure 4.3-1. Functional Diagram of Acquisition Circuit for Fixed Length Test

4.3.1.1 Theoretical Analysis

For the fixed length test, the time required to search a given code phase is the integration time, T. Its value is determined by the requirements for the detection probability, P_D, and the false alarm probability, P_{FA}. The probability density of the noise and signal plus noise required to calculate these probabilities depends upon the BT product. For BT = 1, i.e., no post-detection filtering, the probability density functions (PDF) are Rayleigh and Rician. For BT ≈ 10, the PDFs can be approximated very accurately by Gaussian densities for both noise only and signal plus noise. We now evaluate the signal-to-noise ratio required to provide a given P_D and P_{FA} as a function of BT.

Consider first the case for BT = 1, or no post-detection filtering. If the detector is assumed to be a perfect envelope detector, the PDF of the output noise in the absence of a signal (e.g., when the receiver is out of synchronization) is Rayleigh. Therefore, the probability of false alarm is

$$P_{FA} = e^{-Th^2/2\sigma^2} \tag{4.3-1}$$

where Th = threshold voltage

$\sigma^2 = N_0 B$ = input noise power.

The PDF of the detector output when synchronization is obtained is Rician and the probability of detection is given by

$$P_D = \int_{Th}^{\infty} \frac{V}{\sigma^2} \exp\left[\frac{-V^2 + 2S_0}{2\sigma^2}\right] I_0\left(\frac{V\sqrt{2S_0}}{\sigma^2}\right) dV\,. \tag{4.3-2}$$

This is the Marcum Q function,

$$P_D = Q\left(\sqrt{\frac{S_0}{\sigma^2}}, \frac{Th}{\sigma}\right). \tag{4.3-3}$$

For the range of P_D of interest, an asymptotic expansion of the Q function yields

$$P_D \approx 1 - \frac{1}{2}\,\text{erfc}\left(\frac{\sqrt{S_0} - \text{Th}}{\sqrt{2}\,\sigma}\right) \qquad (4.3\text{-}4)$$

where

$$\text{erfc}\,(x) = 1 - \frac{2}{\sqrt{\pi}} \int_0^x e^{-t^2}\,dt\,. \qquad (4.3\text{-}5)$$

For large BT products, we may use the Central Limit Theorem to approximate the output PDF as Gaussian for both the in-synchronization and out-of-synchronization cases. Consider first the out-of-synchronization case, and assume that the detector is a square-law device. One can show that the mean value of the detector output signal is given by

$$M_n = 2\,BTN_0 \qquad (4.3\text{-}6)$$

and the variance is given by

$$\sigma_n^2 = \frac{(2\,BTN_0)^2}{BT} = 4\,BTN_0^2\,. \qquad (4.3\text{-}7)$$

The false alarm probability is therefore

$$P_{FA} = \frac{1}{2}\left[1 - \text{erf}\left(\frac{\text{Th} - M_n}{\sqrt{2}\,\sigma_n}\right)\right]. \qquad (4.3\text{-}8)$$

When the local reference is in synchronism with the received signal, then the mean and variance of the detector output can be shown to be

$$M_s = 2\,BTN_0\left[1 + \frac{S_0}{N_0 B}\right], \qquad (4.3\text{-}9)$$

$$\sigma_s^2 = 4\,BTN_0^2\left(1 + \frac{2\,S_0}{N_0 B}\right). \qquad (4.3\text{-}10)$$

Thus, the probability of detection is given by

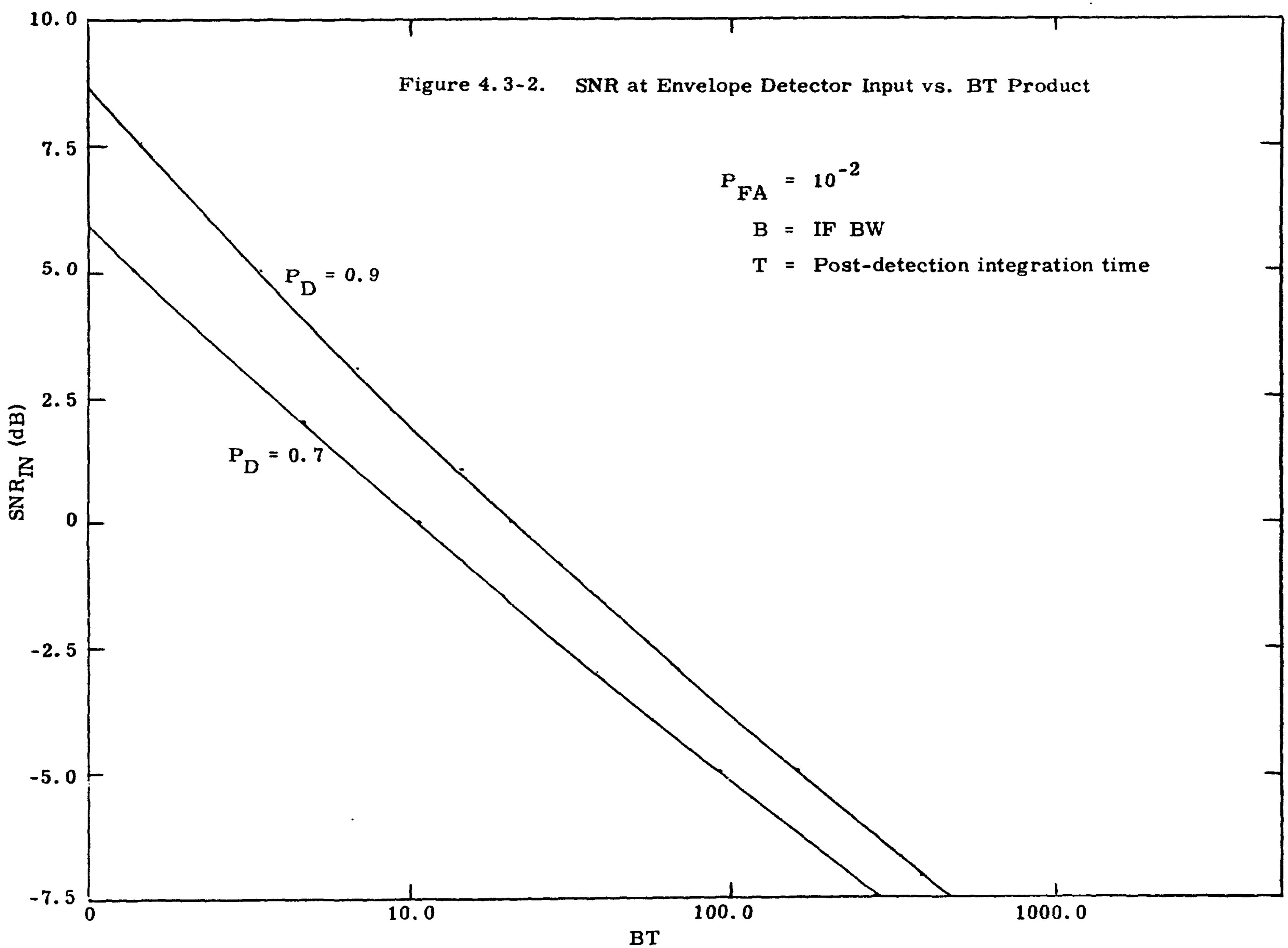

Figure 4.3-2. SNR at Envelope Detector Input vs. BT Product

$$P_D = \frac{1}{2}\left[1 - \text{erf}\left(\frac{Th - M_s}{\sqrt{2}\ \sigma_s}\right)\right] . \tag{4.3-11}$$

If we equate the thresholds, Th, in (4.3-8) and (4.3-11), we can plot the signal-to-noise ratio at the input to the detector, $S_0/N_0B = SNR_{in}$, as a function of BT. This relationship is plotted in Figure 4.3-2 for a $P_{FA} = 10^{-2}$ and two values for P_D, 0.9 and 0.7.

4.3.2 Sequential Detection Test

Introduction

Since it is important in the multiple access forward link to speed up the detection proces,, consideration was given to the sequential tests because of their optimum nature.[2] For such tests, the procedure is simply to introduce two thresholds at the detector output such that the signal in a particular cell position is declared present if one threshold is exceeded and declared absent if the other is exceeded. The length of the detection process or integration time is not fixed in advance, but is a random variable which depends upon the progress of the test. The major feature of this technique, which is referred to as sequential detection, is that it minimizes the average detection time.

The sequential detection procedure is illustrated functionally in Figure 4.3-3.

Basic Theory

This acquisition technique is constructed to decide between two alternative hypotheses, these hypotheses being the absence or presence of a signal. However, the amplitude of the signal is usually not known a priori, so that the "signal present" hypothesis does not correspond to a unique statistical distribution of the received data. This is usually circumvented by choosing a "design" signal amplitude on the basis of which the sequential test is constructed. The probabilities of false alarm and detection are pre-chosen for this design signal amplitude.

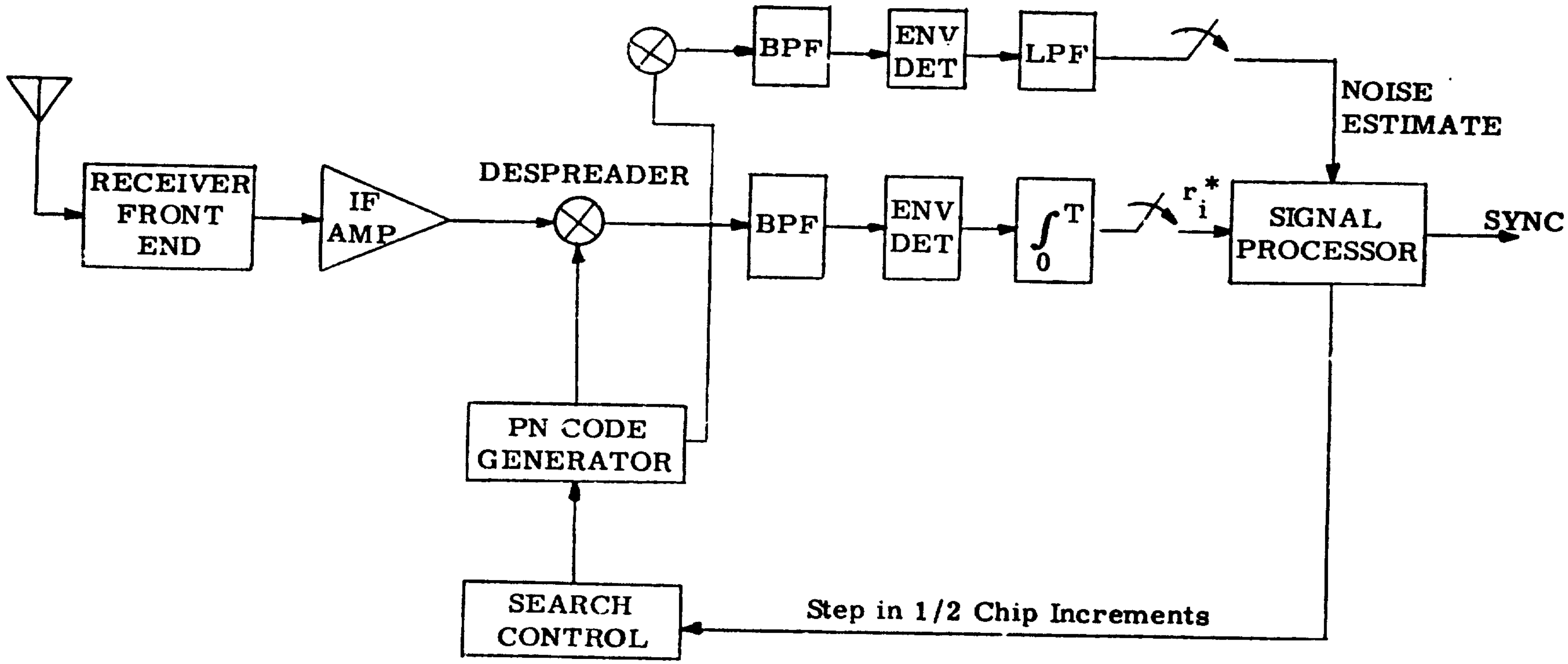

Figure 4. 3-3. Functional Diagram of Sequential Detection Circuit

The basic element within the signal processor is a sequential detection algorithm as developed by Wald.[3]

A sequential probability ratio test can be described as follows. Let $P_m(r|a)$ denote the conditional probability density function of the m data samples $r_1, r_2, \ldots, r_m$ given the signal parameters $a_1, a_2, \ldots, a_j$, and let $P_m(r|0)$ denote the probability density function of the m observed samples given that signal is absent. Then,

$$\ell_m = \frac{P_m(r|a)}{P_m(r|0)} \tag{4.3-12}$$

defines a conditional probability ratio or likelihood ratio for testing the null hypothesis H_0 against hypothesis H_1 that signal plus noise is present. Next, two positive constants A and B $(B < A)$ are selected such that, at each stage of the test, if

$$B < \ell_m(r|a) < A , \tag{4.3-13}$$

the test is continued with an additional observation; if

$$\ell_m(r|a) \le B ,$$

the test terminates with the acceptance of hypothesis H_0 indicating a noise only condition. Similarly, if

$$\ell_m(r|a) \ge A ,$$

the test terminates with the acceptance of hypothesis H_1. The sequential probability ratio test can be summarized as follows:

$$\begin{array}{lll} \text{If} & B < \ell_m(r|a) < A , & \text{continue test.} \\ \text{If} & BP_m(r|0) \ge P_m(r|a) , & \text{accept } H_0 . \\ \text{If} & P_m(r|a) \ge AP_m(r|0) , & \text{accept } H_1 . \end{array} \tag{4.3-14}$$

The thresholds A and B can be related to the false alarm probability α and the probability of detection $1-\beta$ by the following relationships:

$$A \approx \frac{1 - \beta}{\alpha} \tag{4.3-15}$$

and

$$B \approx \frac{\beta}{1 - \alpha} \tag{4.3-16}$$

If we assume that the in-phase and quadrature components of the noise are each white Gaussian random processes of zero mean and variance σ^2, then the received signal plus noise can be represented by

$$y(t) = A d_i(t) \cos \omega_c t + N_c(t) \cos \omega_c t - N_s(t) \sin \omega_c t, \tag{4.3-17}$$

where A is the received signal amplitude and $d_i(t)$ is the ith data bit and can be either ± 1.

Under in-synchronization conditions, the output of the envelope detector is given by

$$r_i(t) = \sqrt{\left[A d_i(t) + N_c(t)\right]^2 + N_s^2(t)} \tag{4.3-18}$$

and, for out-of-synchronization conditions, it is given by

$$r(t) = \sqrt{N_c^2(t) + N_s^2(t)} \tag{4.3-19}$$

Therefore, when the signal is present, the normalized signal plus noise envelope, r_i, is governed by the Rician density function:

$$p(r_i|a) = r_i \exp -\left(\frac{r_i^2 + a^2}{2}\right) I_0(a r_i), \quad r_i > 0, \tag{4.3-20}$$

where a^2 is the peak signal-to-noise ratio and is assumed to be the same for each sample value.

When the signal is absent, the normalized probability density of the envelope is given by the Rayleigh density function:

$$p(r_j|0) = r_i \exp -\left(\frac{r_i^2}{2}\right), \quad r_i > 0. \tag{4.3-21}$$

A simpler technique than computing the likelihood ratio is the computation of the log likelihood ratio. If we let the logarithm of the likelihood ratio defined in equation (4.3-12) be denoted by z_m, then for $a = a_d$,

$$z_m = \ln\left[\frac{P(r_i|a_d)}{P(r_i|0)}\right] \tag{4.3-22}$$

or

$$z_m = \sum_{i=1}^{m} \ln\left[\frac{P(r_i|a_d)}{P(r_i|0)}\right] . \tag{4.3-23}$$

The test procedure in terms of z_m is: (a) continue taking samples when $\ln B < z_m < \ln A$; (b) accept H_0 when $z_m \leq \ln B$; and (c) accept H_1 when $z_m \geq \ln A$. Substituting (4.3.20) and (4.3-21) into (4.3-22), we arrive at the sequential test variate z_i which is given by

$$z_i = -\frac{a_d^2}{2} + \ln I_0(a_d r_i) \tag{4.3-24}$$

or substituting in (4.3-23), we get

$$z_m = -\frac{m a_d^2}{2} + \sum_{i=1}^{m} \ln I_0(a_d r_i) , \tag{4.3-25}$$

where a_d is the design signal-to-noise ratio and is given by

$$a_d^2 = \frac{A^2}{N_0} \tag{4.3-26}$$

where N_0 is the noise spectral density.

The test procedure may be simplified by adding the bias term $-(m a_d^2)/2$ to both sides of the test procedure inequalities, which can then be written as

$$\ln B + \frac{m a_d^2}{2} < \sum_{i=1}^{m} \ln I_0(a_d r_i) < \ln A + \frac{m a_d^2}{2}, \quad \text{continue test}$$

$$\sum_{i=1}^{m} \ln I_0(a_d r_i) \leq \ln B + \frac{m a_d^2}{2}, \quad \text{accept } H_0 \qquad (4.3\text{-}27)$$

$$\sum_{i=1}^{m} \ln I_0(a_d r_i) \geq \ln A + \frac{m a_d^2}{2}, \quad \text{accept } H_1$$

where A and B are given by equations (4.3-15) and (4.3-16).

The sequential test concept is illustrated in Figure 4.3-4. There are two thresholds as shown above, each increasing linearly with the number of samples m. The detector outputs are also accumulated. When the accumulated sum exceeds the upper threshold, synchronization is indicated. When the accumulated sum falls below the lower threshold, it is assumed that no signal is present in that cell position. It is conceivable that the accumulated sum could drift between the two thresholds for a large amount of time; however, Wald has shown that the test is of finite duration. To avoid an excessive drift situation, it is recommended that, at some point, the test be terminated and an in-synchronization condition recognized.

The functional operation of the sequential detector is illustrated in Figure 4.3-5. In this configuration, the output of the envelope detector is integrated for time T. At the end of the integration interval, the output is sampled and quantized with an A/D converter. The quantized output is transformed by the process $\ln I_0(a_d r_i^*)$ and the variate z_i computed. This computation can be made with the use of a ROM lookup table. For a time-bandwidth product of 1, i.e., BT = 1, the integration interval is the inverse of the IF bandwidth. At each sample time, the quantized variate z_i^* is added to the previous sum and compared with two thresholds $Th_1(m)$ and $Th_2(m)$. If the accumulated sum falls below $Th_2(m)$, the signal is not assumed to be present in that cell position and

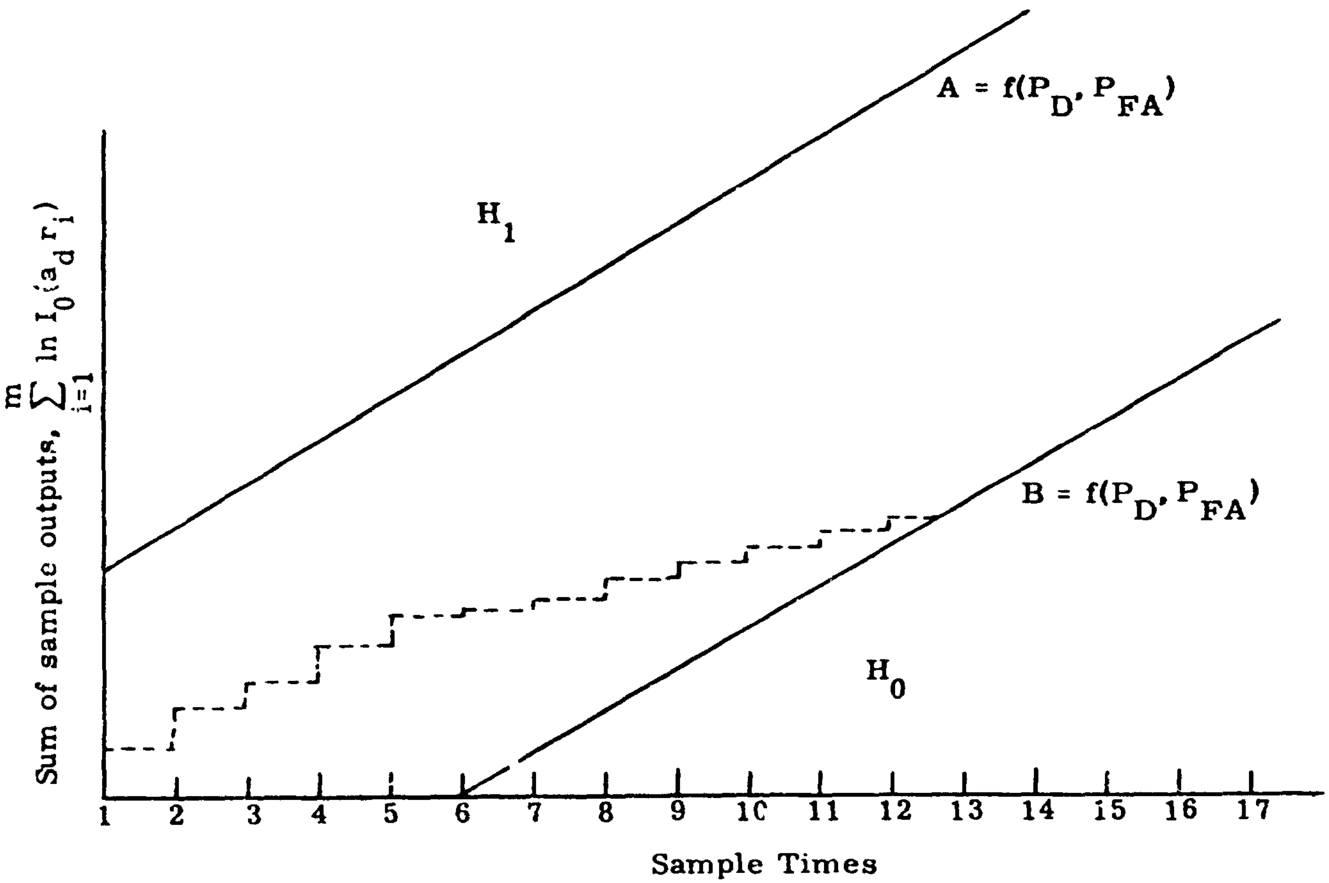

Figure 4.3-4. ILLUSTRATION OF SEQUENTIAL SEARCH STRATEGY

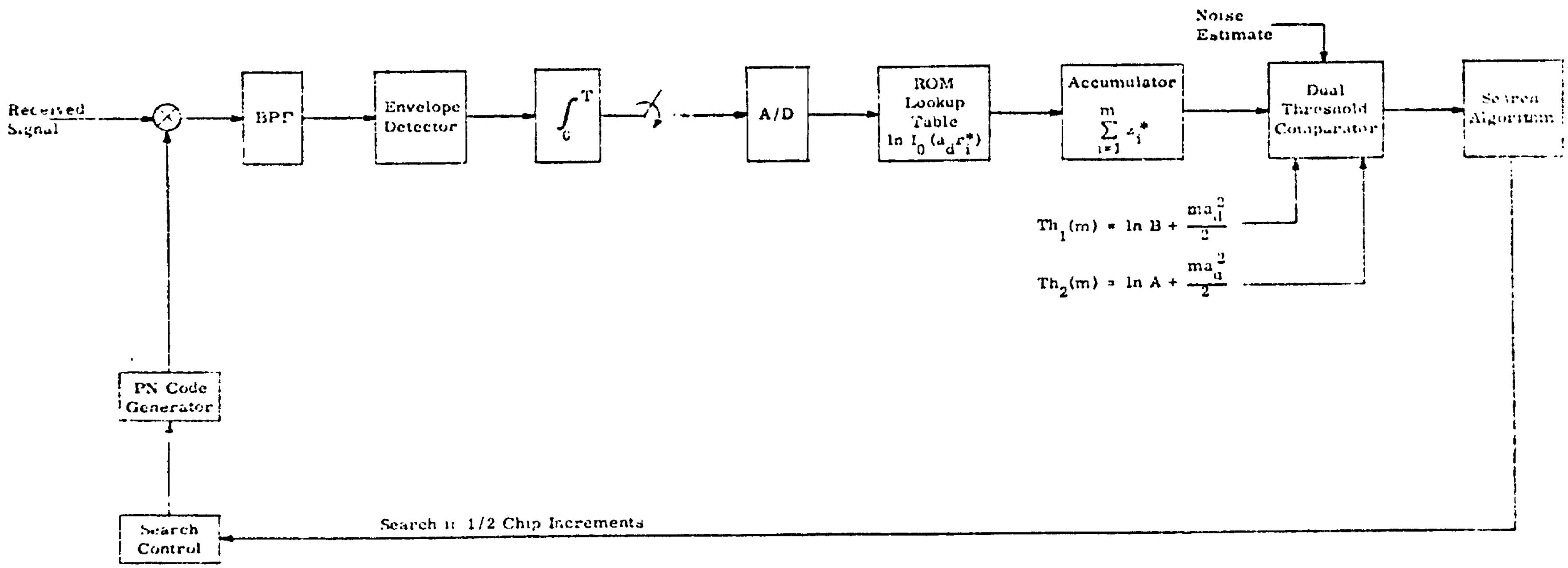

Figure 4.3-5. Functional Diagram of Sequential Acquisition Detector

the search control moves the local PN code one half chip time. If the accumulated value exceeds $Th_1(m)$, signal presence is assumed and is then verified. At this point, the accumulator is reset to zero and the thresholds are reset to their initial conditions. Once signal presence is established, the system falls into a tracking mode, at which time, the delay lock and carrier tracking loops are operating.

Operating Characteristic Function (OCF)

One of the relationships of interest in the sequential search test is the so-called operating characteristic function (OCF), which gives the detection probabilities for signals having amplitudes differing from the design amplitude. The OCF denoted by L(a) is required for the evaluation of the average sample number (ASN). L(a) is the conditional probability of accepting hypothesis H_0 at the end of the test or the probability of a miss. From the definition

$$\begin{aligned} L(0) &= 1 - \alpha \\ L(a) &= \beta(a) \end{aligned} \qquad (4.3\text{-}28)$$

and

$$L(a) = \frac{A^{\left[1 - 2(a/a_d)^2\right]} - 1}{A^{\left[1 - 2(a/a_d)^2\right]} - B^{\left[1 - 2(a/a_d)^2\right]}} \qquad (4.3\text{-}29)$$

where $A = \frac{1-\beta}{\alpha}$ and $B = \frac{\beta}{1-\alpha}$, and α is the probability of false alarm, β is the probability of a missed signal, a^2 is the actual received signal-to-noise ratio, and a_d^2 is the design signal-to-noise ratio.

The OCF can be plotted as is shown in Figure 4.3-6.

Average Sample Number (ASN)

We now let m denote the number of observations or samples required by the test and let $E_a(m)$ be the expected value of m when a^2 is the true value of the signal-to-noise ratio. If we let $\eta = E_a(m)$ denote the average number of observations (ASN) required to terminate the test,

Figure 4.3-6. Operating Characteristic Function

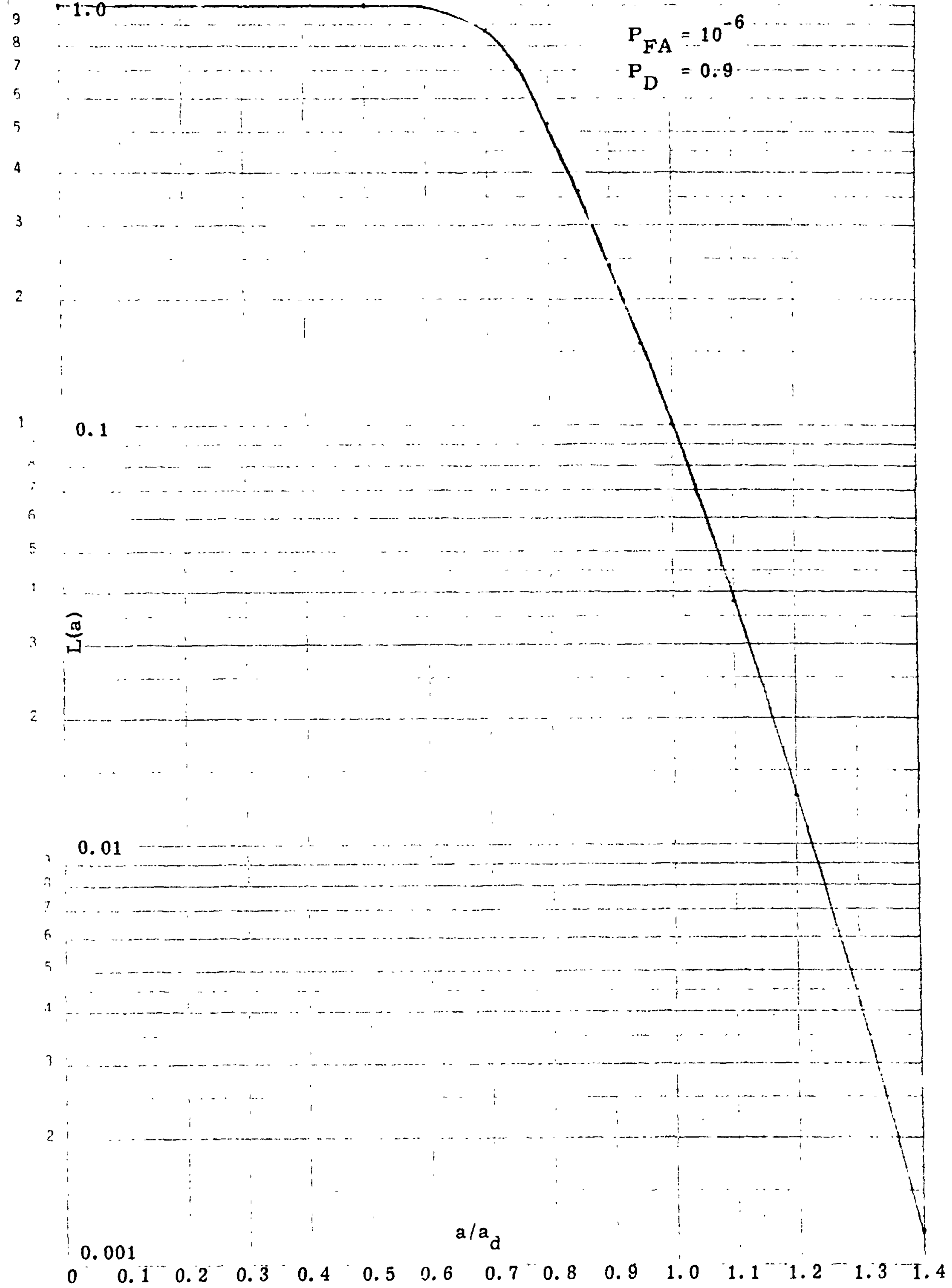

46 5490
K-E SEMI-LOGARITHMIC • 3 CYCLES × 70 DIVISIONS KEUFFEL & ESSER CO. MADE IN U.S.A.

then for independent observations, the average sample number (ASN) is given by

$$\eta = \frac{L(a) \ln B + [1 - L(a)] \ln A}{E(z|a)} \tag{4.3-30}$$

where

$$E(z|a) = -\frac{a_d^4}{8} + \frac{a^2 a_d^2}{4}. \tag{4.3-31}$$

Substituting (4.3-31) into (4.3-30), we get

$$= \frac{L(a) \ln B + [1 - L(a)] \ln A}{-\frac{a_d^4}{4}\left[\frac{1}{2} - \left(\frac{a}{a_d}\right)^2\right]}. \tag{4.3-32}$$

Hence, the ASN is inversely proportional to the square of the design (peak) signal-to-noise ratio.

Average Time to Threshold

At threshold, the peak signal-to-noise ratio is given by

$$a_d^2 = \frac{2C'}{N_0 B_W} \tag{4.3-33}$$

where $2C'/N_0B_W$ is the peak effective design signal-to-noise ratio in the IF filter of bandwidth B_W.

If the output of the envelope detector is sampled at a rate $1/T$, then the mean time to decision can be written as

$$T_d = \eta T$$

$$T \frac{L(a) \ln B + [1 - L(a)] \ln A}{-\left(\frac{C'}{N_0 B_W}\right)_d^2 \left[\frac{1}{2} - k^2\right]}, \tag{4.3-34}$$

where $k = a/a_d$.

The mean time to cell dismissal, T_b, is the case where $a = 0$ in equation (4.3-34). For this case, $L(0) = 1 - \alpha$, and (4.3-34) reduces to

$$T_b = \frac{2T\left[(1-\alpha)\ln B + \alpha \ln A\right]}{-\left(\frac{C'}{N_0 B_W}\right)_d^2} . \tag{4.3-35}$$

The relationship T_b/T versus C'/N_0B_W is plotted in Figure 4.3-7 for several values of the detection probability, $P_D = 1 - \beta$. The curves are almost insensitive to the false alarm probability.

For the low false alarm probabilities which are of interest in the TDRSS application, the greatest reduction in expected dwell time over the fixed length test occurs when noise alone is present or one is in an out-of-synchronization condition. The expected dwell or integration time is only slightly less than that of the fixed length test in the in-synchronization position. Therefore, the benefits of using the sequential detection scheme are greatest when a time uncertainty exists over a large number of chip positions.

4.3.3 Direct Sequence Acquisition Using Dual Mode Detection

Introduction

The purpose of this section is to examine more completely the acquisition technique discussed in sections 4.3.1 and 4.3.2. A more sophisticated model of the acquisition technique will be considered. The model as illustrated in Figure 4.2-3 has both acquisition and verification tests prior to entering the tracking mode. The basic strategy to be employed is to lower the thresholds during acquisition, which thereby increases the miss and false alarm probabilities. When a signal is indicated, the verification mode is entered and a more careful examination of the cell is made (i.e., increased post-detection integration time corresponding to an increase in the threshold levels). The effect is that the

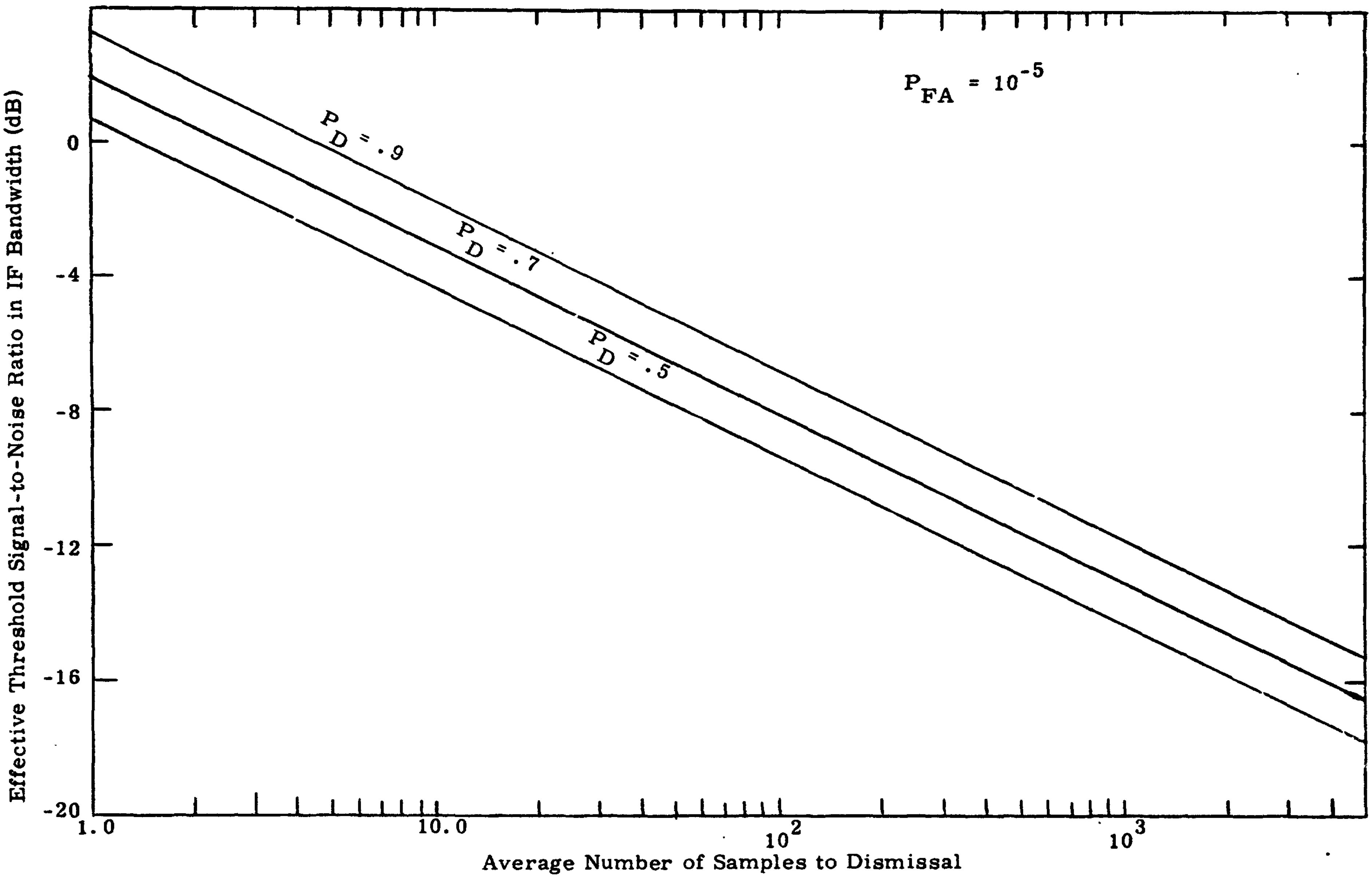

Figure 4.3-7. Average Sample Number Versus Threshold Signal-to-Noise Ratio

local reference may very likely cycle through the uncertainty region, which for initial acquisition is all the cells in the PN sequence, several times before locking onto the desired signal. Once the verification state is entered, the delay lock loop begins operating. Failure to confirm the signal presence during verification causes the code search to continue and the delay lock loop is reset. However, once synchronization is confirmed, the Costas loop sweep begins and the tracking mode is entered.

In the tracking mode, a third set of threshold values are established to insure a very low false alarm rate and miss probability. The delay lock loop bandwidth is gradually narrowed. The thresholds are also set so that it is more difficult to drop out of the tracking mode than either of the other modes. This is to insure that rapid signal fades will not cause the receiver to drop out of lock.

The dual mode synchronizer has greater flexibility than the single mode technique. The thresholds can be optimized and yield acquisition times which, in many cases, are lower than the single mode technique. In addition, the thresholds can be optimized to minimize the probability of locking onto multipath signals.

The optimization of the parameters was not performed during this study. However, an attempt was made to yield results which are considered to be reasonably close to the optimum parameter values.

Theoretical Analysis

When using the sequential synchronization algorithm defined in section 4. 3. 2, the average number of samples required at the output of the envelope detector for dismissal can be calculated from equation (4. 3-34) and is given by

$$\eta = \frac{8\left[L(a) \ln B + \left(1 - L(a)\right) \ln A\right]}{-\left(\frac{2C'}{N_0 B}\right)_d^2}, \qquad (4.3\text{-}36)$$

where $2C'/N_0B$ is the peak effective design signal-to-noise ratio in the IF filter of bandwidth B at threshold. If the output of the envelope detector is integrated for time T and sampled, then the mean time to dismissal can be written as

$$T_b = \eta T = \frac{2T\left[L(a)\ln B + \left(1 - L(a)\right)\ln A\right]}{-\left(\frac{C'}{N_0B}\right)_d^2} . \qquad (4.3\text{-}37)$$

If the length of the code sequence is N chips and the local code reference is stepped in one-half chip increments referred to as cells, then the signal is likely to be in any one of the 2N cell positions. In actuality, it can occur in two and, in some cases, even three half chip positions. This is due to the spread of the delay lock characteristics. The fact that the signal can occur in two cell positions will be accounted for later on in the analysis. The possibility that some of the signal is in a third cell position will be ignored.

We define P(i) as the probability that exactly i steps $(i = 1,2,\ldots,2N)$ are required to reach the signal. Assume each step requires T_α seconds on the average. When N is large, then for all practical purposes, $T_\alpha = T_b$. The average time of first arrival is then

$$T_1 = \sum_{i=1}^{2N} i\,T_\alpha P(i) = \frac{T_\alpha}{2N}\sum_{i=1}^{2N} i = N T_\alpha \qquad (4.3\text{-}38)$$

since $P(i) = 1/2N$.

As above, we define α as the probability of a false acceptance and β as the probability of a false dismissal. Then the probability that the signal is dismissed upon its first arrival but detected upon its first repeat trial is $\beta(1-\beta)$. The probability that the signal will be initially detected on the jth repeat scan is

$$P(j) = \beta^j (1 - \beta) . \tag{4.3-39}$$

The average time required for a repeat scan is $2N\,T_\alpha$. Therefore, the average time lost due to a false dismissal is

$$T_2 = \sum_{j=1}^{\infty} j(2N)\,T_\alpha\,P(j)$$

$$= 2N\,T_\alpha (1 - \beta) \sum_{j=1}^{\infty} j\,\beta^j$$

$$= 2N\,T_\alpha \frac{\beta}{1 - \beta} \tag{4.3-40}$$

Another basic assumption in this analysis is that the signals are assumed to remain uncorrelated in a single cell position throughout the search process. The time required for synchronization, T_{acq}, is then the sum of T_1, the time required to arrive at the correlated cell for the first time, plus T_2, the time lost due to false dismissals, plus T_3, the time required to correctly accept the correlated cell after arriving at it. In all practical cases, T_3 will be negligible compared to T_1 and T_2 for large values of N and will be neglected in the subsequent analysis.

The total average synchronization time, ignoring T_3, is

$$T_{acq} = T_1 + T_2 = N\,T_\alpha + 2N\,T_\alpha \left(\frac{\beta}{1 - \beta}\right)$$

$$= N\,T_\alpha \left(\frac{1 + \beta}{1 - \beta}\right) . \tag{4.3-41}$$

In Figure 4.3-8, the state diagram of the dismissal process of the two-step synchronizer with a tracking loop is illustrated. We define these states as follows:

State 1	Acquisition State
State 2	Verification State
State 3	Tracking State .

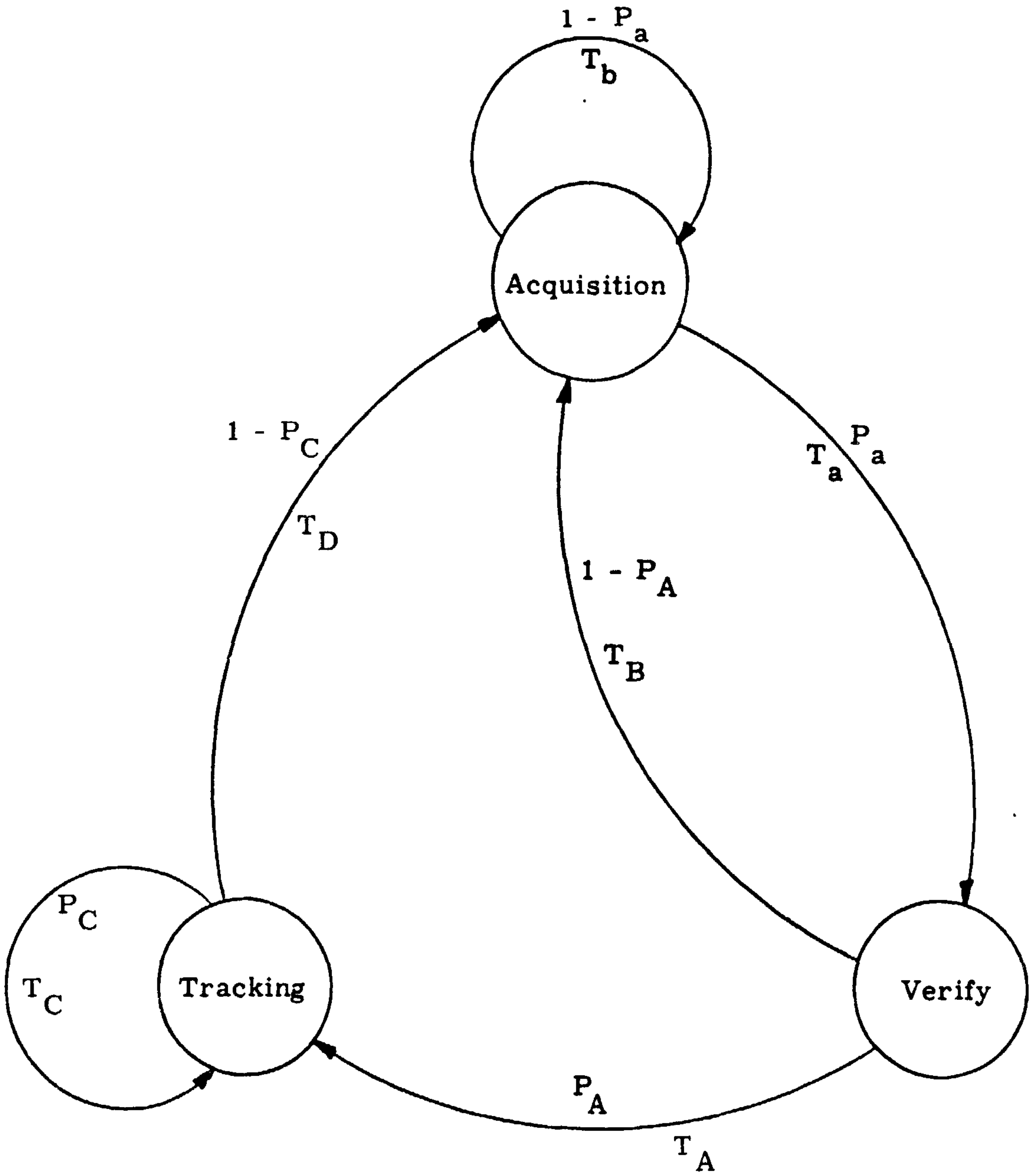

Figure 4.3-8. State Diagram of the Dual Mode Synchronizer

Let us now define the following parameters:

T_a = average time required to perform an acquisition test leading to an accept decision

T_b = average time required to perform an acquisition test leading to a dismiss decisic .

T_A = average time to perform verification test leading to an accept decision

T_B = average time to perform verification test leading to a dismiss decision

T_C = average time required for tracking loop to perform a test leading to an accept decision

T_D = average time required for tracking loop to perform a test leading to a dismiss decision

P_a = probability of false acceptance by acquisition test

P_b = probability of false dismissal by acquisition test

P_A = probability of false acceptance by verification test

P_B = probability of false dismissal by verification test

P_C = probability of false acceptance by tracking loop

P_D = probability of false dismissal by tracking loop

$2N$ - number of cells to be tested .

In Figure 4.3-8, the transition probabilities are shown with the times required to perform the tests leading to a new state. If T_i is the time required for rejection by the ith path and $P(T_i)$ is the probability of traversing that path, then the average dismissal time is given by

$$T = \sum_i T_i P(T_i) . \qquad (4.3\text{-}42)$$

By inspection, the first few terms are

$$
\begin{aligned}
T_\alpha = {} & T_b(1-P_a) + (T_a + T_B) P_a (1-P_A) \\
& + (T_a + T_A + T_D) P_a P_A (1-P_C) \\
& + (T_a + T_A + T_C + T_D) P_a P_A P_C (1-P_C) \\
& + (T_a + T_A + 2T_C + T_D) P_a P_A P_C^2 (1-P_C) . \\
& + \ldots
\end{aligned}
\tag{4.3-43}
$$

This leads to the general expression

$$
\begin{aligned}
T_\alpha = {} & T_b(1-P_a) + (T_a + T_B) P_a (1-P_A) \\
& + P_a P_A (1-P_C) \sum_{j=0}^{\infty} (T_a + T_A + j\,T_C + T_D) P_C^j .
\end{aligned}
\tag{4.3-44}
$$

which can be summed to yield

$$
\begin{aligned}
T_\alpha = {} & T_b(1-P_a) + (T_a + T_B) P_a (1-P_A) \\
& + P_a P_A (1-P_C) \left[\frac{(T_a + T_A + T_D)}{1-P_C} + \frac{T_C P_C}{(1-P_C)^2} \right]
\end{aligned}
\tag{4.3-45}
$$

This can be simplified to yield for the dual mode synchronizer

$$
\begin{aligned}
T_\alpha = {} & T_b + P_a (T_a - T_b + T_B) \\
& + P_a P_A \left(T_A - T_B + T_D + \frac{P_C T_C}{1-P_C} \right) .
\end{aligned}
\tag{4.3-46}
$$

The remaining parameter needed to specify the average synchronization time is β, where for the dual mode synchronization

$$
\beta = P_b + (1-P_b) P_B + (1-P_b)(1-P_B) P_D . \tag{4.3-47}
$$

4.3.4 Code Doppler Analysis

Because of the frequency error between the local reference and the received code, the local code will slide past the incoming signal over the entire integration interval. The code doppler error is given by

$$d_c = \frac{\Delta f \, R_c}{f_c}, \tag{4.3-48}$$

where f_c is the rf carrier frequency
R_c is the chip rate
Δf is the frequency uncertainty .

As an example, in the multiple access forward link,

$$f_c = 2.1064 \times 10^9 \text{ Hz}$$

$$R_c = 3.0778 \times 10^6 \text{ chips/sec}$$

$$\Delta f = \pm 3 \text{ kHz} .$$

Substituting these parameters in equation (4.3-48), we get

$$d_c = \pm 4.38 \text{ chips/sec}$$

as the code drift rate between the local code and the received signal.

During the ith step, the phase change is

$$\Delta\phi_i = d_c T_i - \frac{\Delta T_c}{T_c} , \tag{4.3-49}$$

where $\Delta T_c / T_c$ is the coarse step size, and we assume $\Delta T_c / T_c = 0.5$; that is, we step in one-half chip increments. Therefore, the total change in phase difference between two codes expressed in chips after N steps is

$$\Delta\phi = \sum_{i=1}^{N} \Delta\phi_i = d_c \sum_{i=1}^{N} T_i - 0.5N . \tag{4.3-50}$$

Since N is large, the summation can be expressed in terms of the average dwell time, T_d, where

$$T_d = \frac{1}{N} \sum_{i=1}^{N} T_i \ . \qquad (4.3\text{-}51)$$

Clearly, T_d is mode dependent. Therefore,

$$\Delta\phi = d_c N T_d - 0.5N = N(d_c T_d - 0.5) \ .$$

Hence, the average step size in the worst case direction is

$$\left| 0.5 - d_c T_d \right| \ . \qquad (4.3\text{-}52)$$

On the average, the code drift will aid in the performance, as well as degrade the performance. For the purposes of this analysis, we will assume the worst case condition.

4.3.5 Summary of Acquisition Time Equations

Fixed Length Test - Noncoherent Detection

For the dual mode fixed length test, the mean (average) acquisition time is given by the following equation:

$$\overline{T}_{acq} = N\left[\frac{T}{|1 - 2\, d_c T|} + T_\beta\right]\left(\frac{1 + \beta}{1 - \beta}\right) \qquad (4.3\text{-}53)$$

T is the post-detection integration time or dwell time

$T_\beta = T_\alpha - T_b$, where

T_α is given by equation (4.3-46)

Also, β is given by equation (4.3-47) and N is the number of chips to be searched in the PN sequence.

The degradation due to code doppler is only assumed to occur during initial acquisition. We assume that the code tracking loop is operating during the verification mode.

Sequential Test - Single Mode

Noncoherent Detection

$$\overline{T}_{acq} = \frac{N\,T_b}{|1 - 2\,d_c\,T|} \tag{4.3-54}$$

where

$$T_b = \frac{2\,T\left[L(a)\ln B + \left(1 - L(a)\right)\ln A\right]}{-\left(\frac{C'}{N_0 B}\right)_d^2} \tag{4.3-55}$$

Coherent Detection

$$\overline{T}_{acq} = \frac{N\,T_b}{|1 - 2\,d_c\,T|} \tag{4.3-56}$$

where

$$T_b = \frac{T\left[L(a)\ln B + \left(1 - L(a)\right)\ln A\right]}{-2\left(\frac{C'}{N_0 B}\right)_d} \tag{4.3-57}$$

Sequential Test - Dual Mode

Noncoherent Detection

$$\overline{T}_{acq} = N\left[\frac{T_b}{|1 - 2\,d_c\,T|} + T_\beta\right]\left(\frac{1+\beta}{1-\beta}\right) \tag{4.3-58}$$

where T_β and β are defined above and T_b is given by equation (4.3-55).

Coherent Detection

Coherent detection is the same as in (4.3-58), with T_b given by equation (4.3-57).

4.3.6 Interfering Signal Acquisition Analysis

Introduction

The primary objective of this analysis is to establish the acquisition parameters of the S-band multiple access return link. The baseline system model is developed; this is followed by a discussion of the receiver model. The analysis is then directed to determining the desired signal power, the interfering signal power and the total noise power at the input to the envelope detector. The effective signal-to-noise ratio at the detector input is determined for both the desired signal in its synchronized condition and, similarly, the interfering signal when it is synchronized to a cross-correlation peak.

System Model

The model for the TDRSS S-band multiple access return link is shown in figure 4.3-9. For the purposes of this analysis, the desired signal-to-noise ratio is

$$SNR = \frac{S_0}{\sum_i I_i + N}, \qquad (4.3\text{-}59)$$

where S_0 is the desired signal power

I_i is the i^{th} interfering power level

N is the receiver noise power.

One of the objectives of this study is to compute for the above system model the probability of acquiring one of the interfering signals rather tha~ the desired signal.

Receiver Model

The model of the acquisition detector is shown in figure 4.3-10. The input r(t) is given by

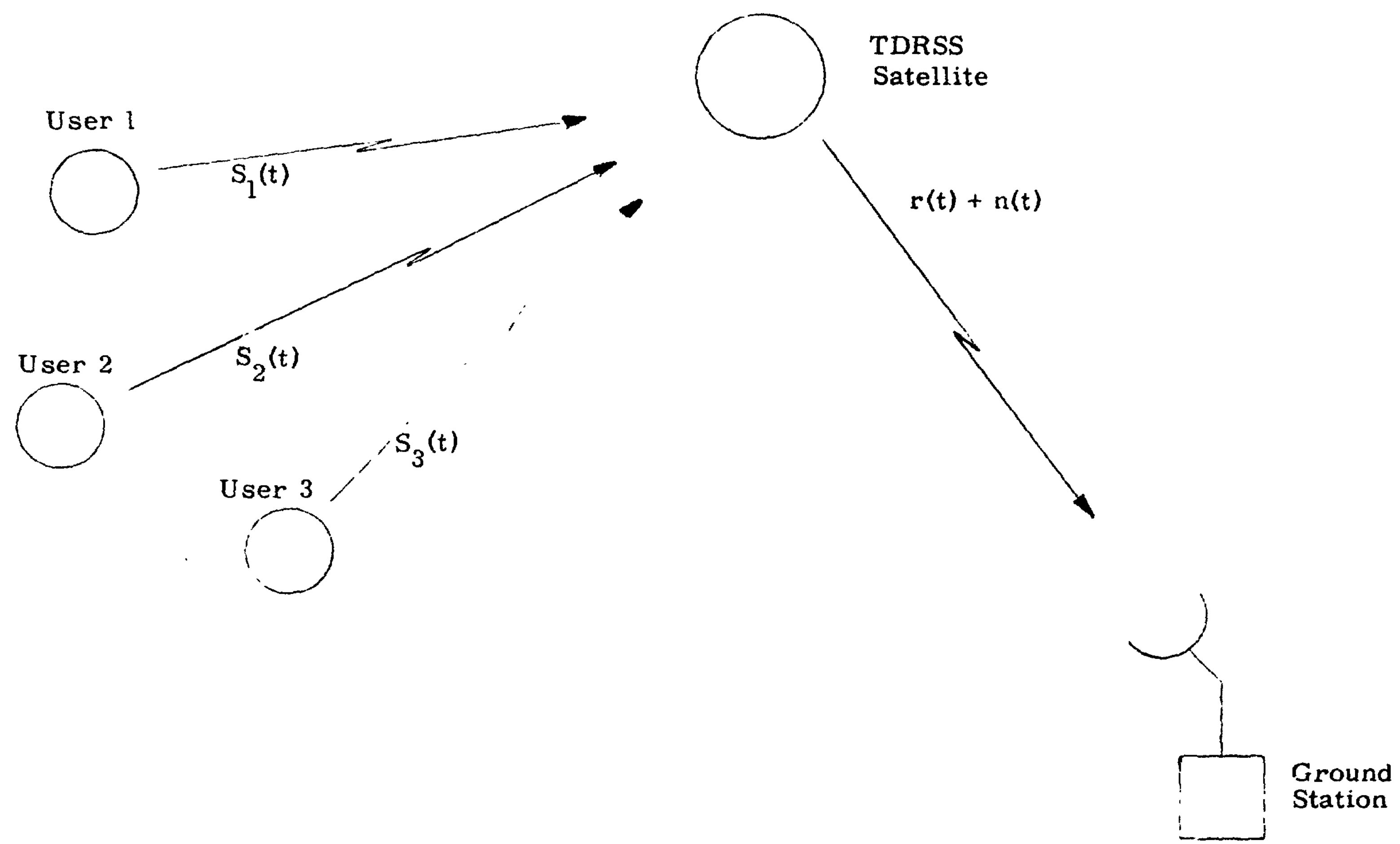

Figure 4.3-9 Model of TDRSS Multiple Access Return Link

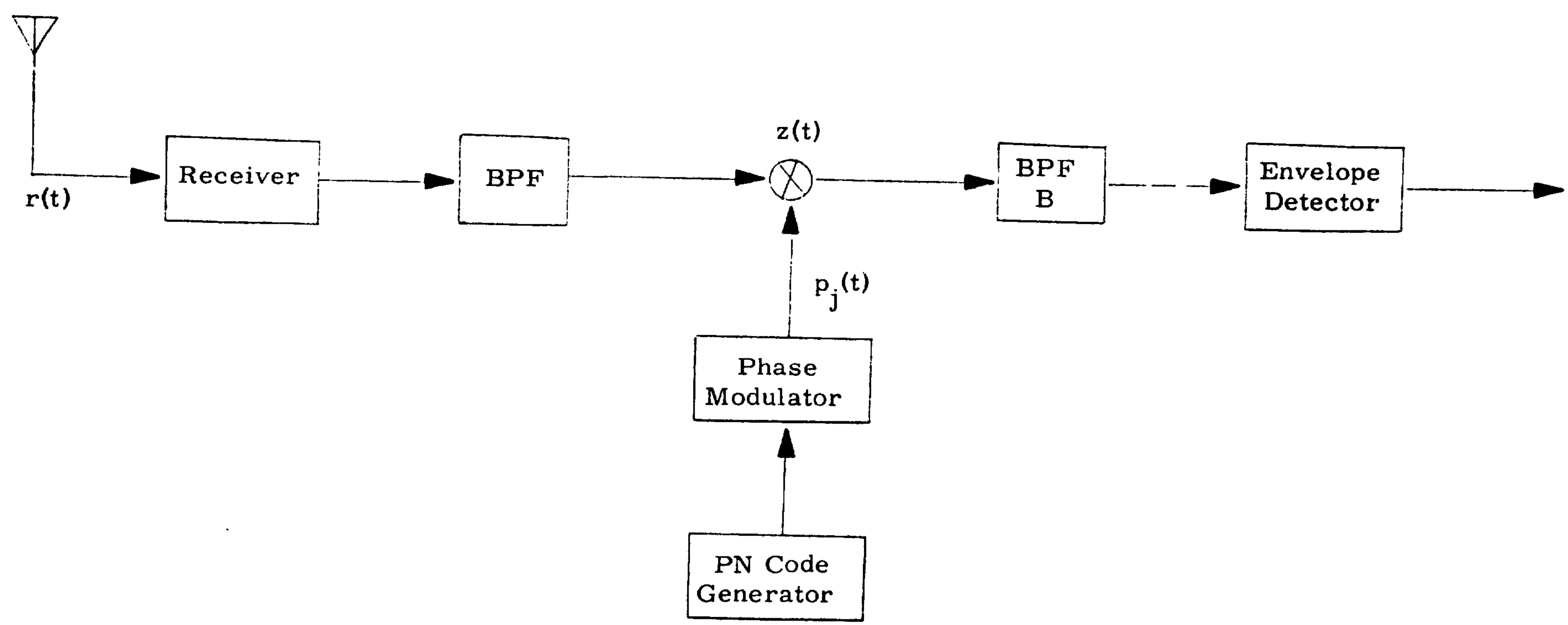

Figure 4.3-10 Model of Receiver Front End and Despreader

$$r(t) = \sum_{i=1}^{3} \sqrt{2 S_i} \; a_i(t) \, X_i(t) \sin[\omega_c t + \theta_i] + n(t) \qquad (4.3\text{-}60)$$

where X_i is the pseudorandom PN code of the i^{th} signal

a_i is the data modulation of the i^{th} signal

θ_i is the relative phase shift of the i^{th} transmitter

n(t) is the thermal noise

S_i is the received power of the i^{th} signal.

The local reference is given by p(t) where

$$p(t) = 2 X_1 (t) \sin(\omega_1 t + \theta_j) \qquad (4.3\text{-}61)$$

and

$$\omega_{IF} = \omega_c - \omega_1 .$$

For the purposes of this analysis, it will be assumed that the local reference is in chip synchronism with the signal transmitted by User 2. We will assume that it is not in chip synchronization with the desired signal $S_1(t)$ and the other interfering signal $S_3(t)$. Clearly, this is the worst-case condition since we maximize the received signal level of $S_2(t)$ and minimize the impact of $S_1(t)$ and $S_3(t)$ which become noise sources. We will also assume that $S_1(t)$ and $S_3(t)$ are both uncorrelated with the local reference.

SIGNAL-TO-NOISE RATIO ANALYSIS

Based on the model developed above, we will compute the probability of acquiring the 50 kbps data rate signal, $S_2(t)$, when the local reference is set to lock onto $S_1(t)$ or the 1 kbps data rate signal. This acquisition probability will be computed for three code sequence lengths and assumes the PN codes for each of the three signals are of equal length and are balanced Gold codes. The cross-correlation code spectrum for the three code lengths assumed in this investigation are summarized in table 4.3-1.

Table 4.3-1. Cross-Correlation Spectrum

n = length of code		Spectrum		
k	$n = 2^k - 1$			
11	2,047	63 (528)	-1 (1023)	-65 (496)
13	3,191	127 (2080)	-1 (4095)	-129 (2016)
15	32,767	255 (8128)	-1 (16383)	-257 (8256)

The value in parentheses associated with the cross-correlation quantity denotes the number of chip positions containing the particular cross-correlation value. However, before we compute the detection probabilities, we will determine the IF signal-to noise ratio.

Signal Power

If the signal power of the received signal $S_2(t)$ is given by S_2, then the spectra at the output of the despreader is given by

$$S_z(\omega) = S_2 T_2 \rho_{1,2} \left[\frac{\sin(\omega - \omega_{IF}) T_2/2}{(\omega - \omega_{IF}) T_2/2}\right]^2 \qquad (4.3\text{-}62)$$

where T_2 is the data baud interval and $1/T_2 = 50$ kbps. The parameter $\rho_{1,2}$ is the cross-correlation coefficient between the local reference, $S_1(t)$ with code i, and the signal $S_2(t)$ with code 2. For the peak sidelobe condition,

$$\rho_{1,2} = \left(\frac{65}{2047}\right)^2 . \qquad (4.3\text{-}63)$$

The signal power at the output of the bandpass filter is given by

$$S_0 = \int_{-\infty}^{\infty} S_z(f) \; |H(f)|^2 \, df \tag{4.3-64}$$

where H(f) is the frequency response of the bandpass filter preceding the envelope detector. If we assume that the filter has at least four poles, then an ideal filter approximation can be made so that

$$S_0 = \frac{1}{2\pi} \int_{\omega_{IF} - B/2}^{\omega_{IF} + B/2} S_z(\omega) \, d\omega \tag{4.3-65}$$

which can be written as

$$S_0 = \frac{S_2}{\pi} \; \rho_{1,2} \int_{-\pi B T_2/2}^{\pi B T_2/2} (\sin x/x)^2 \, dx. \tag{4.3-66}$$

The bandwidth of the bandpass filter is assumed to be 5 kHz since the data rate is 1 kbps and the total frequency uncertainty is $\pm$ 1.5 kHz. Hence,

$$S_0 = \frac{S_2 \; \rho_{1,2}}{\pi} \int_{-0.157}^{0.157} \frac{\sin^2 x}{x^2} \, dx \tag{4.3-67}$$

$$S_0 = \frac{S_2 \; \rho_{1,2}}{\pi} (0.157)\,(2)$$

$$S_0 = (0.1) \, S_2 \; \rho_{1,2} \, . \tag{4.3-68}$$

Interfering Signals as Noise

If we define signals $S_1(t)$ and $S_3(t)$ as interfering signals, where

$$S_1(t) = \sqrt{2 S_1} \; a_1(t) \, X_1(t) \sin \left[\omega_c t + \theta_1 \right] \tag{4.3-69}$$

and

$$S_3(t) = \sqrt{2\,S_3}\; a_3(t)\, X_3(t) \sin[\omega_c t + \theta_3] , \qquad (4.3\text{-}70)$$

then at the output of the despreader, the cross-correlation between the local reference p(t) and $S_i(t)$ is given by

$$R_z(\tau) = \frac{1}{2T}\int_{-T}^{T} X_i(t)\, X_i(t+\tau)\, p(t)\, p(t+\tau)\, dt , \quad i = 1, 3 . \qquad (4.3\text{-}71)$$

Since the signals $S_1(t)$ and $S_3(t)$ are assumed to be uncorrelated with p(t),

$$R_z(\tau) = R_{X_i}(\tau)\, R_p(\tau) \qquad (4.3\text{-}72)$$

or

$$S_z'(\omega) = S_{X_i}(\omega) * S_p(\omega) . \qquad (4.3\text{-}73)$$

Now,

$$R_{X_i}(\tau) = S_i \left\{1 - \left|\frac{\tau}{T_c}\right|\right\} \cos \omega_c \tau , \quad 0 < |\tau| < T_c$$

$$R_p(\tau) = 2\left\{1 - \left|\frac{\tau}{T_c}\right|\right\} \cos \omega_i \tau . \qquad (4.3\text{-}74)$$

Therefore,

$$R_z(\tau) = 2\,S_i\left\{1 - 2\left|\frac{\tau}{T_c}\right| + \left|\frac{\tau}{T_c}\right|^2\right\}\cos\omega_c\tau \quad \cos\omega_1\tau \qquad 0 \le |\tau| < T_c$$

$$= 0 \qquad |\tau| > T_c \tag{4.3-75}$$

where T_c is the chip period.

If we take the Fourier transform in the neighborhood of ω_{IF}, we get (where $\omega_{IF} = \omega_c - \omega_1$),

$$S_z'(\omega) = \frac{2\,S_i}{(\omega - \omega_{IF})^2\,T_c}\left[1 - \frac{\sin(\omega - \omega_{IF})\,T_c}{(\omega - \omega_{IF})\,T_c}\right]. \tag{4.3-76}$$

The resulting interfering signal power at the output of the IF bandpass filter is given by an equation similar to 4.3-65; that is

$$I_i = \frac{1}{2\pi}\int_{\omega_{IF} - B/2}^{\omega_{IF} + B/2} S_z'(\omega)\,d\omega\,. \tag{4.3-77}$$

Clearly, the maximum occurs in the vicinity of $\omega_{IF} = \omega_c - \omega_1$. Since $B \ll 1/T_c$, substituting 4.3-76 into 4.3-77, we get

$$I_i = \frac{2}{3}\,S_i\,T_c\,B\,. \tag{4.3-78}$$

Noise Density Reduction

We will attempt in this section to compute the spreading effect of the receiver noise due to the reference signal p(t). Since the noise is uncorrelated with p(t), the cross-correlation function of the noise with the PN signal is given by

$$R_z(\tau) = R_n(\tau)\ R_p(\tau). \tag{4.3-79}$$

The spectral density at the despreader output is

$$S_1(f) = \int_{-\infty}^{\infty} R_n(\tau)\ R_p(\tau)\, e^{-j\omega\tau}\, d\tau\ . \tag{4.3-80}$$

Since the bandwidth of the received signal is much greater than the bandwidth of the IF filter, the effective spectral height into the IF filter is given by S(0) where

$$S_1(0) = \int_{-\infty}^{\infty} R_n(\tau)\ R_p(\tau)\ d\tau\ . \tag{4.3-81}$$

We can then write the spectral response of the output of the IF filter as

$$S_n(0) = \frac{1}{2\pi}\int_{-\infty}^{\infty} N_0 \left|H(\omega)\right|^2 \quad T_c \left(\frac{\sin\,(\omega - \omega_{IF})\,T_c}{(\omega - \omega_{IF})\,T_c}\right)^2 d\omega\ . \tag{4.3-82}$$

Using the same argument for $\left|H(f)\right|^2$ as given above, we can write

$$S_n(0) = \frac{N_0}{\pi} \int_{-\pi B_1 T_c/2}^{\pi B_1 T_c/2} \left(\frac{\sin x}{x}\right)^2 dx\ . \tag{4.3-83}$$

Therefore, $\quad S_n(0) \approx N_0$

and $$N = N_0 B. \tag{4.3-84}$$

Effective Undesired Signal-to-Noise Ratio

Substituting equations 4.3-68, 4.3-78 and 4.3-84 into 4.3-59, we get the signal-to-noise ratio at the output of the bandpass filter:

$$SNR_2 = \frac{(0.1)\, S_2\, \rho_{1,2}}{\sum_{i=1,3} \frac{2}{3} S_i T_c B + N_0 B T_c}, \qquad (4.3\text{-}85)$$

which can be rewritten as

$$SNR_2 = \frac{0.1\, \rho_{1,2}}{\sum_{i=1,3} \frac{2}{3} \left(\frac{S_i}{S_2}\right) T_c B + \frac{N_0 B}{S_2}} \qquad (4.3\text{-}86)$$

Effective Desired Signal-to-Noise Ratio

The desired signal-to-noise ratio about which the design parameters of the acquisition technique are established is summarized below. With 0 dB design margin, $C/N_0 = 39.9$ dB-Hz.

IF filter bandwidth - 5 kHz	37.0 dB
PN filter loss	0.9 dB
One-half chip offset loss	2.5 dB
Total losses	40.4 dB

Therefore, effective $SNR_1 = C/N_0 - 40.4$ dB

$$SNR_1 = -0.5 \text{ dB}.$$

Now, based on the link analysis given, in section 1.3 for the multiple access return link, the signal-to-noise ratio at the receiver for $S_2(t)$ is

$$\frac{C_2}{N_0} = 33.1 + \text{EIRP} - \text{System losses (dB-Hz)}.$$

If we allow 5 dB for system losses, then with an EIRP of 31.8 dBW, we get

$$\frac{C_2}{N_0} = 59.9 \text{ dB-Hz.}$$

Now, $S_3/S_2 = 1$

and $S_2/N_0B = 59.9 \text{ dB-Hz} - 10 \log 5000$

$= 22.9$ dB.

Therefore, $S_1/S_2 = -23.4$ dB.

Substituting these values into 4.3-86, we get

$$\text{SNR}_2 = \frac{0.1\,(1 \times 10^{-3})}{\frac{2}{3}\,(1.67 \times 10^{-3})\,(1 + 4.57 \times 10^{-3}) + 5.13 \times 10^{-3}}$$

$$= 1.6 \times 10^{-2}$$

or $\text{SNR}_2 = -17.96$ dB.

Therefore, the signal-to-noise ratio at the input to the envelope detector for an interfering signal at a peak cross-correlation condition is approximately 17.5 dB below the design signal-to-noise ratio. If we assume that the signal is encoded with a rate 1/2 code and decoded using a Viterbi decoding algorithm, the transmitters can then operate with 5 dB less output power. For this case $\text{SNR}_1 = -5.5$ dB and $\text{SNR}_2 = -23$ dB.

The results of this analysis for the desired and interfering received signal-to-noise ratios are summarized in table 4.3-2. Two cases were considered for both the acquisition and verification modes. In the first case no error detection and correction coding was assumed on the multiple access return link. In the second case a rate 1/2 Viterbi convolutional decoding algorithm was assumed. By use of this coding technique it is assumed that a 5 dB performance gain can be achieved. The signal-to-noise ratio for the verification mode is 2 dB higher than that for the acquisition mode. This is because code tracking is assumed during verification and the 0.5 dB loss is due to timing jitter.

Table 4.3-2 Baseline IF Signal-to-Noise Ratios

$\frac{S}{N_0 B}$ * (dB) / Link Conditions	Desired Signal		Interfering Signal	
	Acquisition	Verification	Acquisition	Verification
Without Coding	-0.5	1.5	-18.0	-16.0
With Coding R=1/2	-5.5	-3.5	-23.0	-21.0

*B is assumed to be a 5 kHz IF bandwidth.

4.3.7 Multiple Filter Acquisition Approaches

In addition to optimizing the parameters of the acquisition strategies described above, further decreases in acquisition time can be achieved by the use of multiple bandpass filters as shown in figures 4.3-11 and 4.3-12. In these cases a band of contiguous bandpass filters is used to cover the doppler uncertainty range.

A straightforward parallel approach is shown in figure 4.3-11. A set of k bandpass filters cover the frequency uncertainty band. Each filter output is envelope detected and post detection integrated. The outputs are sampled and digitized. Since the sampling rates are relatively slow (less than 6,000 times per second) a single A/D converter can be time shared among the k channels. Each A/D output is then transformed by log $(I_0(a_d r_i))$ which is simply accomplished by a ROM lookup table. The outputs are demultiplexed with each channel being independently accumulated and compared with the thresholds using the sequential search strategy. The same basic technique is also applicable to the fixed length test strategy. The local reference is shifted by one-half chip position only when all of the k frequency cell accumulated outputs fall below the lower threshold. Hence, the dwell time is determined by the longest frequency cell test. If we denote the individual false alarms by α_k and the overall false alarm by α, then the probability of no overall false alarm equals the joint probability of no individual false alarms. Therefore, if $\alpha \ll 1$,

$$1 - \alpha = (1 - \alpha_k)^k \approx 1 - k\,\alpha_k$$

and hence,

$$\alpha \approx k\,\alpha_k \qquad (4.3\text{-}87)$$

Since we are testing for the presence of exactly one signal in one of the k frequency cells, the overall probability of a missed detection, β is equal

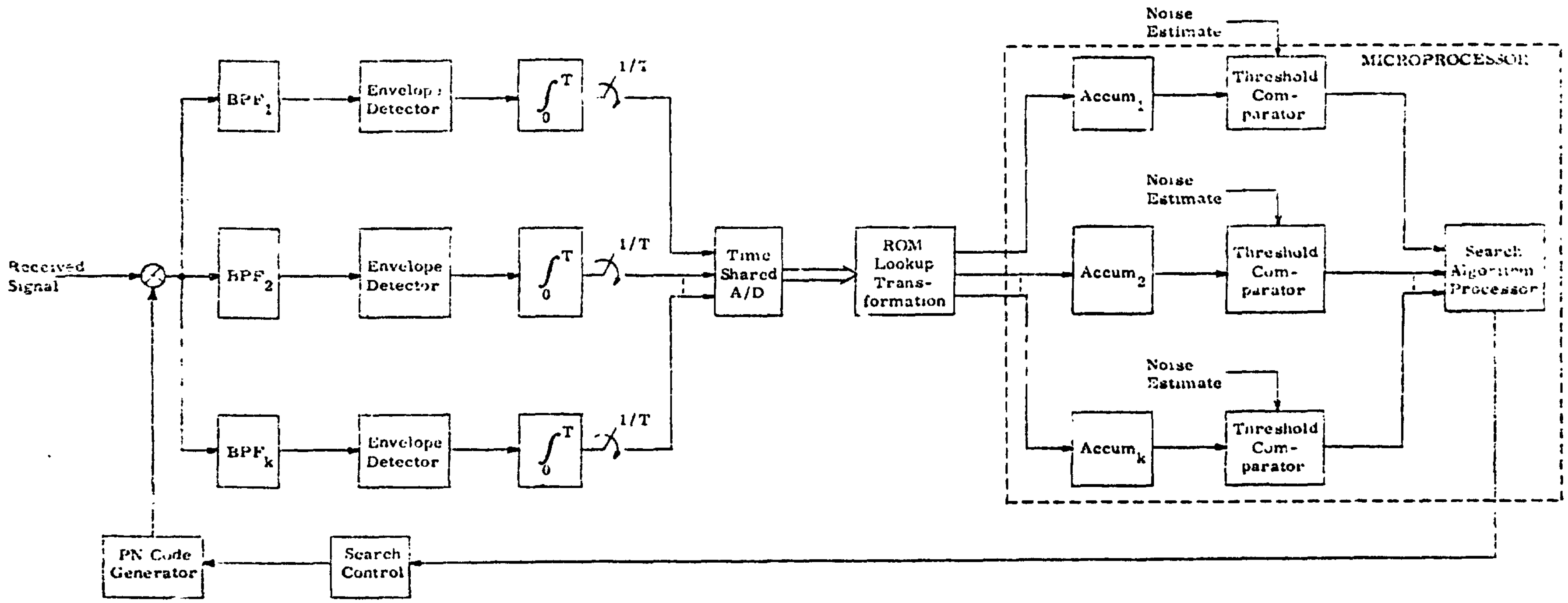

Figure 4.3-11. Parallel and Sequential Analysis Acquisition Circuitry for Frequency Resolution

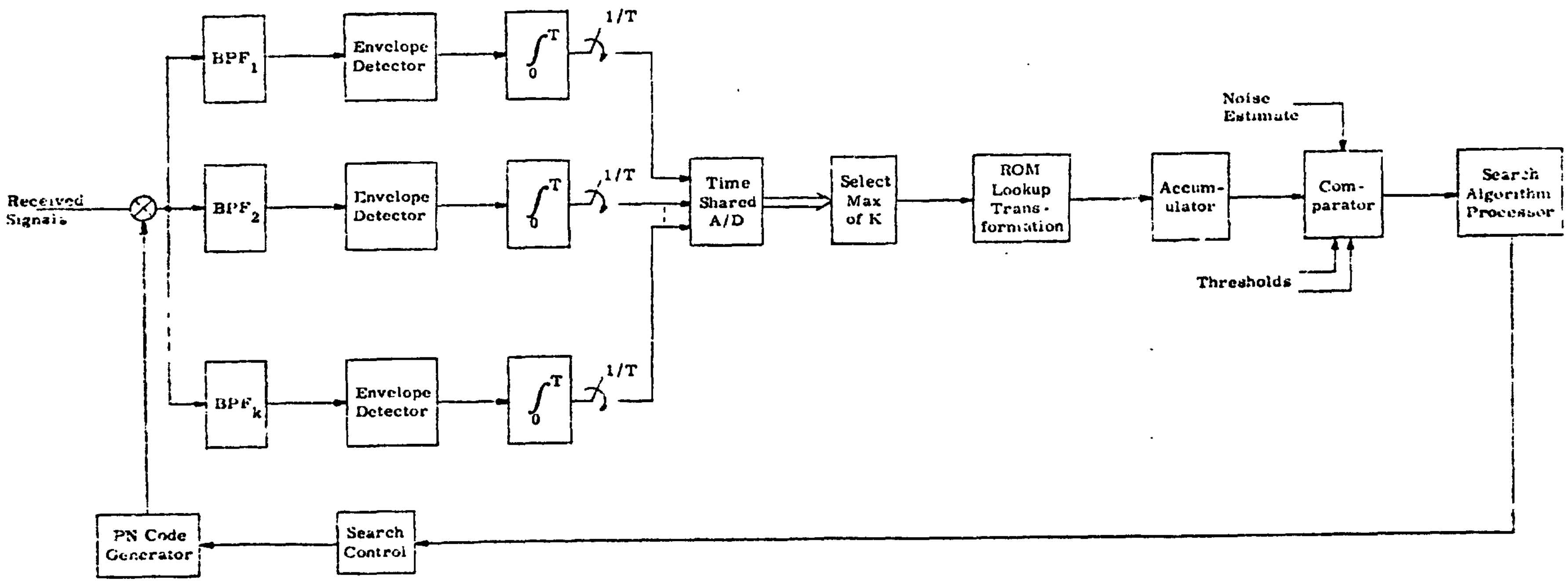

Figure 4.3-12. Parallel Sequential Analysis Acquisition Circuitry for Frequency Resolution with Maximum Detector

to the joint probability that the signal is missed in the ith cell, multiplied by the joint probability of no false alarms in all the other k-1 cells.

Hence,

$$\beta = \beta_k (1 - \alpha_k)^{k-1} = \frac{\beta_k(1-\alpha_k)^k}{1 - \alpha_k}$$

$$= \frac{\beta_k(1 - \alpha)}{1 - \alpha_k} \tag{4.3-88}$$

If $\alpha_k \ll 1$, then $\alpha \ll 1$; hence, the overall probability of missed detection is approximately

$$\beta \approx \beta_k \tag{4.3-89}$$

The average sample number (ASN) when noise alone is present is given by

$$\bar{\eta}_0 = \alpha \; \bar{\eta}_\alpha + (1 - \alpha) \; \bar{\eta}_{1-\alpha} \tag{4.3-90}$$

where $\bar{\eta}_\alpha$ is the average test length when signal presence is falsely declared, $\bar{\eta}_{1-\alpha}$ is the average test length when no signal is correctly indicated. When $\alpha \ll 1$,

$$\bar{\eta}_0 \approx \bar{\eta}_{1-\alpha} \tag{4.3-91}$$

Since the number of cells without a signal greatly exceed the number of cells with a signal, the performance is dominated by the average length to reject a cell position. DiFranco and Rubin[4] derive an expression for the average sample number

$$\bar{\eta}_0 = \sum_{\eta=0}^{\infty} \left[1 - P(\eta)^k \right] \tag{4.3-92}$$

Where $P(\eta) = \frac{1}{\beta} \quad \Phi\left(\frac{-2 \ln\beta}{a_d^2 \sqrt{\eta}} + a_d^2\sqrt{\eta}\right) + \Phi\left(\frac{-2 \ln\beta}{a_d^2 \sqrt{\eta}} - a_d^2\sqrt{\eta}\right)$ (4.3-93)

Where $a_d^2 = \frac{2\, C'}{N_0\, B_k}$ (4.3-94)

Which is the peak signal-to-noise ratio in the IF filter of bandwidth B_k. Typically,

$$B_k = \frac{\text{Total Frequency Uncertainty}}{K}$$

and Φ ( ) is the error function.

Hence, equation (4.3-92) replaces equation (4.3-32) when used to compute the average acquisition time with the multiple filter model given in figure 4.3-11. An alternate multiple filter approach is shown in figure 4.3-12. As above a band of contiguous bandpass filters is used to cover the doppler uncertainty range. At each sample interval the maximum output from a set of filters is selected for processing by the sequential decoding algorithm. A detailed analysis of this technique was not made. However, some simulation results by Marcus and Swerling(5) can be used to estimate the performance gains. In [5], the average sample number (ASN) versus the number of resolution elements is plotted for a noncoherent detector. The number of resolution elements corresponds to the number of contiguous filters utilized. These results only go as low as a 0 dB design signal-to-noise ratio. Extrapolating the results to the threshold SNR pertinent to this study, we can estimate that the ASN is divided by the number of filters and increased by 20 and 50 percent for the 2 and 5 filter cases, respectively. The narrowing of the filter bandwidths increases the signal-to-noise ratio at the filter output with the signal. However, the average time to dismissal is increased over what one might compute for a single filter because one must make a choice between several filter outputs. In a Gaussian noise environment, the best choice is maximum likelihood which was the approach used in the simulation.

4.4 Application of Analysis to User Transponder - Forward Link

4.4.1 Performance Summary

A summary is given in this section of the analysis for the average acquisition time of the recommended signaling technique given in section 2.

Short Code

The short code consists of a 1023 chip sequence which is biphase modulated in quadrature with a similarly modulated 2^{18} chip "long" code sequence. The long code channel is transmitted with a signal power which is 10 dB below that in the short code channel.

At threshold, the received signal power-to-noise spectral density ratio is given by C/N_0 = 32.3 dB-Hz. The total doppler and frequency uncertainties are ±3 kHz. The data modulation rate is 125 bps. The parameters for the short code are as follows:

IF Filter Bandwidth - 6 kHz	37.8 dB
PN Filter Loss	0.9 dB
Power Loss Due to Long Code	0.4 dB
One-Half Chip Offset Loss	2.5 dB
Total Losses	41.6 dB
C/N_0 at Threshold	32.3 dB-Hz
Effective Signal-to-Noise Ratio, C'/N_0B	-9.3 dB

Long Code

Since the acquisition of the long code follows that of the short code, it is possible (if desired) to coherently acquire the long code. This is because it is assumed that, when the long code acquisition begins, code lock and carrier recovery is achieved. It is also assumed that the code doppler is tracked by each of these loops. Hence, the basic timing losses are timing jitter.

The losses associated with the long code are.

IF Filter Bandwidth - 6 kHz	37.8 dB
PN Filter Loss	0.9 dB
Power Loss Due to Short Code	10.5 dB
Timing Jitter Losses	0.3 dB
Total Losses	49.5 dB
C/N_0 at Threshold	32.3 dB-Hz
Effective Signal-to-Noise Ratio, C'/N_0B	-17.2 dB

As seen from equations (4.3-55) and (4.3-58), the average time to dismissal is inversely related to the effective signal-to-noise ratio in the IF bandwidth. Also, the effective SNR in the IF bandwidth is clearly a function of the IF bandwidth. Table 4.4-1 summarizes the relationships between the IF bandwidths and the threshold signal-to-noise ratios. In the case where the IF bandwidth is 1200 Hz or ±600 Hz, the total 6 kHz frequency uncertainty band is divided into 5 frequency cells. Similarly, with an IF bandwidth of ±300 Hz, there are 10 frequency cells.

Table 4.4-1. Threshold SNR Versus IF Bandwidth

IF Bandwidth	C'/N_0B (dB)	
	Short Code	Long Code
6 kHz	-9.3 dB	-17.2 dB
3 kHz	-6.3 dB	-14.2 dB
1.2 kHz	-2.3 dB	-10.2 dB
600 Hz	+0.7 dB	- 7.2 dB

For both the long and short codes, the following detection parameters were assumed for acquisition, verification, and tracking.

Acquisition

The detection probability is based on having two chances during the 2 x 1023 trials for the short code and 1 x 256 trials for the long code.

$$P_{D1} = 0.51 \qquad P_{FA1} = 10^{-3} = P_a$$

Verification

$$P_{D2} = 0.9 \qquad P_{FA2} = 10^{-4} = P_A$$

Tracking

$$P_{D3} \gg 0.9 = 1 - P_D \qquad P_{FA3} = 10^{-6} = P_C$$

For the noncoherent dual state acquisition strategy of the short code, the mean acquisition time is shown to be

$$\overline{T}_{acq} = N\left(\frac{T_i}{|1 - 2d_c T|} + T_\beta\right)\left(\frac{1+\beta}{1-\beta}\right) \tag{4.4-1}$$

where T_i = T for fixed length test
= T_b for sequential test

with the other parameters as defined above. For a good approximation at threshold,

$$T_a \approx T_b \quad \text{and} \quad T_A \approx T_B .$$

Therefore,

$$T_\alpha \approx T_b + P_a T_B + P_a P_A\left(T_D + \frac{F_C T_C}{1 - P_C}\right).$$

$$T_b \gg P_a T_B, \text{ since } P_a = 10^{-3}$$

$$T_b \gg P_a P_A\left(T_D + \frac{P_C T_C}{1 - P_C}\right)$$

since $P_a P_A = 10^{-7}$.

Thus, $T_\alpha \approx T_b$.

Also, from (4.3-47),

$$\beta = P_b + (1 - P_b) P_B + (1 - P_b)(1 - P_B)(1 - P_{D3}) \quad . \qquad (4.4\text{-}2)$$

The last term in (4.4-2) is small compared to the first two terms on the right side of the equation; hence,

$$\beta \approx P_b + (1 - P_b) P_B \ .$$

For the fixed length test, to a good approximation,

$$\overline{T}_{acq} \approx N \left[\frac{T}{|1 - 2 d_c T|} + P_a T_B \right] \left[\frac{1 + P_b + (1 - P_b) P_B}{1 - P_b - (1 - P_b) P_B} \right] . \qquad (4.4\text{-}3)$$

Similarly, for the sequential test,

$$\overline{T}_{acq} \approx \frac{N T_b}{|1 - 2 d_c T|} \left[\frac{1 + P_b + (1 - P_b) P_B}{1 - P_b - (1 - P_b) P_B} \right] \qquad (4.4\text{-}4)$$

where

$$T_b \approx \frac{2 T \ln \beta_1}{-\left(\frac{C'}{N_0 B} \right)_d^2} \ . \qquad (4.4\text{-}5)$$

The parameters used in this analysis for the short code of the multiple access forward link are:

$N = 1023$

$d_c = 4.38$ chips/sec

$\beta_1 = 0.76$

$P_b = 0.49$

$P_B = 0.1$

$T = 1/BW$ for sequential test

T: Variable for fixed length test .

Substituting these parameters into equations (4.4-3), (4.4-4), and (4.4-5), we get the results summarized in table 4.4-2. These results are also plotted in figure 4.4-1. In comparing these two search strategies, one finds that the sequential test strategy is about 50 percent faster than the fixed length strategy for the case where there is only one IF filter. As the IF signal-to-noise ratio increases, the difference in acquisition times increases between the two test approaches. For the case of 10 contiguous IF bandpass filters, the sequential strategy is almost five times as fast as the fixed length strategy. The average acquisition time is given in figure 4.4-2 as a function of the received signal-to-noise ratio. This relationship only holds true if the design signal-to-noise ratio, a_d^2 corresponds to the received signal-to-noise ratio. Therefore, if the input signal-to-noise ratio increases and the thresholds do not track the change in signal-to-noise ratios the effective acquisition time does not change.

The parameters used in this analysis for the long code of the multiple access forward link are similar to those of the short code with the exception of the number of uncertainty cells. The long code is of length $2^{18} - 256$ chips. The relationship of the codes is such that, when the short code is acquired, the uncertainty of the long code is reduced to the number of cells given by

$$\text{Long code uncertainty} = \frac{2^{18} - 256}{1023} = 256 \text{ cells.}$$

Hence, the search for the long code requires selecting one of 256 cell positions.

The acquisition time results for the long code are summarized in table 4.4-3 with the results plotted in figure 4.4-3. The analysis was performed for only the sequential tests, using equations (4.4-4) and (4.4-5) for the noncoherent test and equation (4.4-4) with T_b given by

Table 4.4.2. Comparative Summary of Mean Acquisition Times for the Multiple Access Forward Link Short PN Code

Number of Doppler Cells	IF Bandwidth (Hz)	SNR in IF Bandwidth (dB)	Fixed Length Test Strategy		Sequential Test Strategy	
			$\overline{T}_{acq}$ (sec)	Mean Search Rate (chips/sec)	$\overline{T}_{acq}$ (sec)	Mean Search Rate (chips/sec)
1	6000	-9.3	42.9	23.8	28.6	35.8
2	3000	-6.3	27.5	37.2	14.2	72
5	1200	-2.3	16.5	62.0	5.7	179
10	600	0.7	13.7	74.7	2.9	353

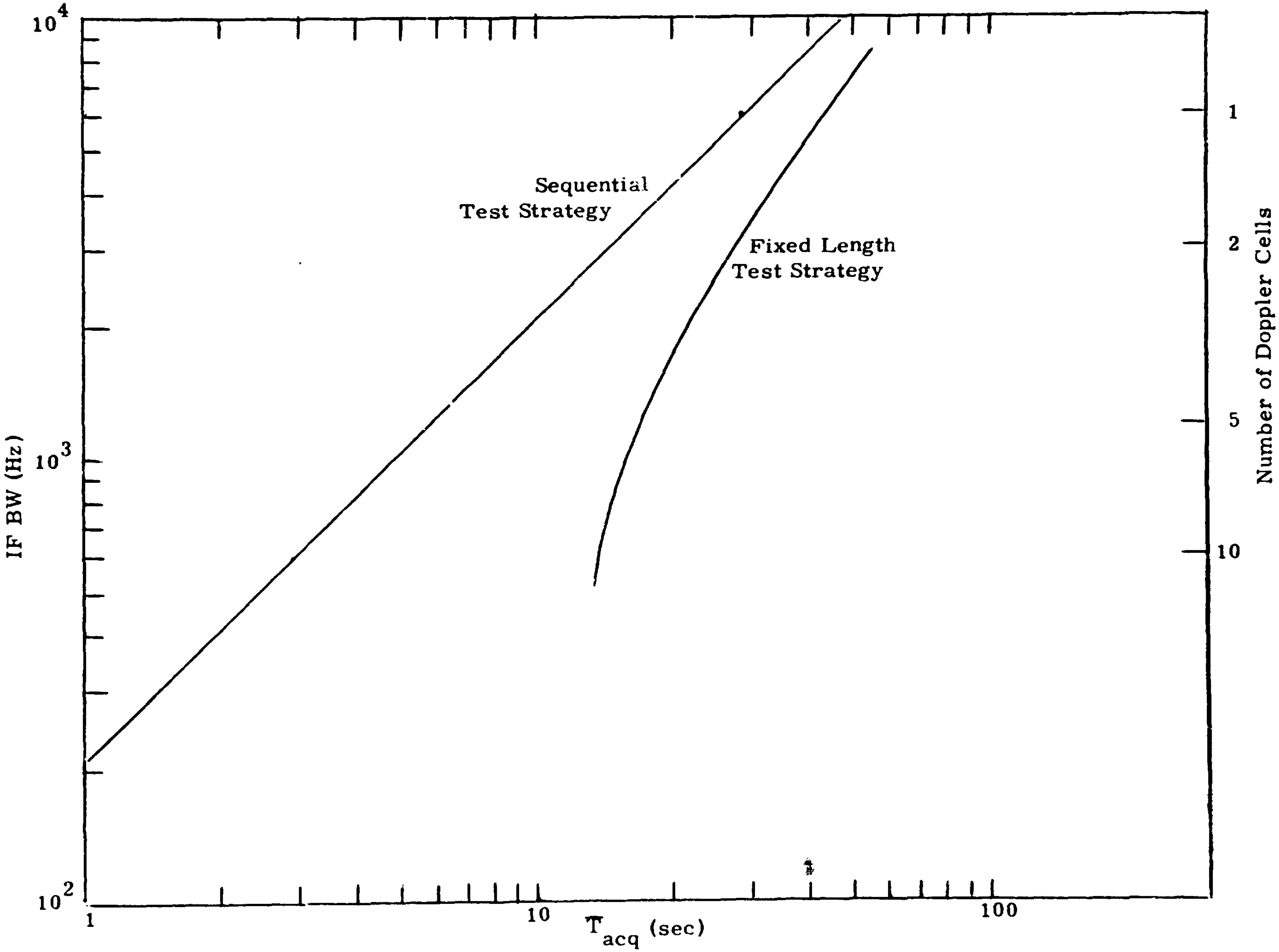

Figure 4.4-1. Mean Acquisition Time vs. IF Bandwidth for MA Forward Link Short Code

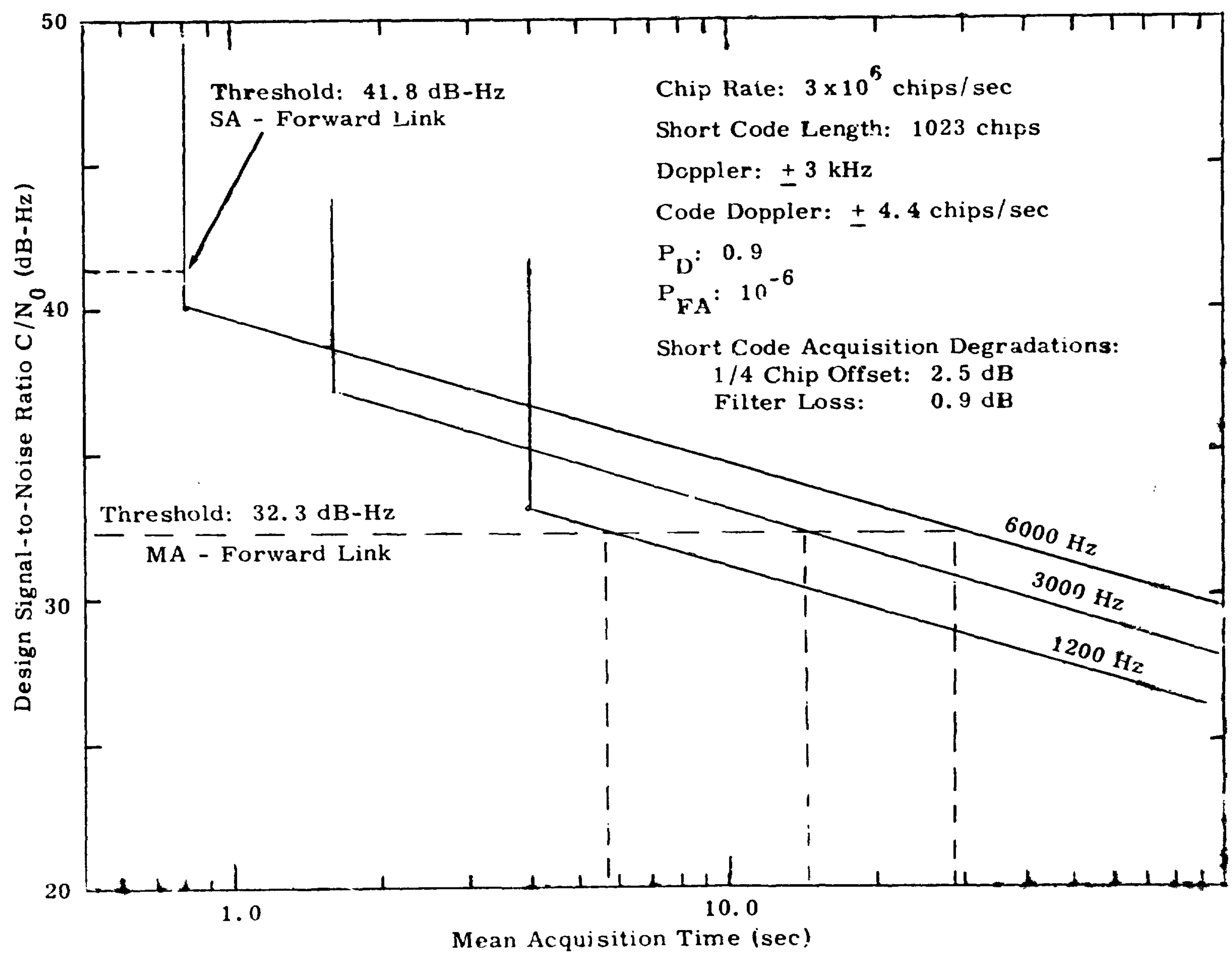

Figure 4.4-2. Average Acquisition Time Versus Design Signal-to-Noise Ratio for Double Step Sequential Acquisition Analysis

Table 4.4.3. Comparative Summary of Mean Acquisition Times for Multiple Access Forward Link Long PN Code

IF Bandwidth (Hz)	SNR in IF Bandwidth (dB)	Sequential Test Strategy Coherent		Sequential Test Strategy Noncoherent	
		$\overline{T}_{acq}$ (sec)	Mean Search Rate (chips/sec)	$\overline{T}_{acq}$ (sec)	Mean Search Rate (chips/sec)
6000	-17.2	1.4	182.9	276	0.93
3000	-14.2	1.35	189.6	138	1.9
1200	-10.2	1.3	196.9	55	4.7
600	-7.2	1.3	196.9	27	9.5

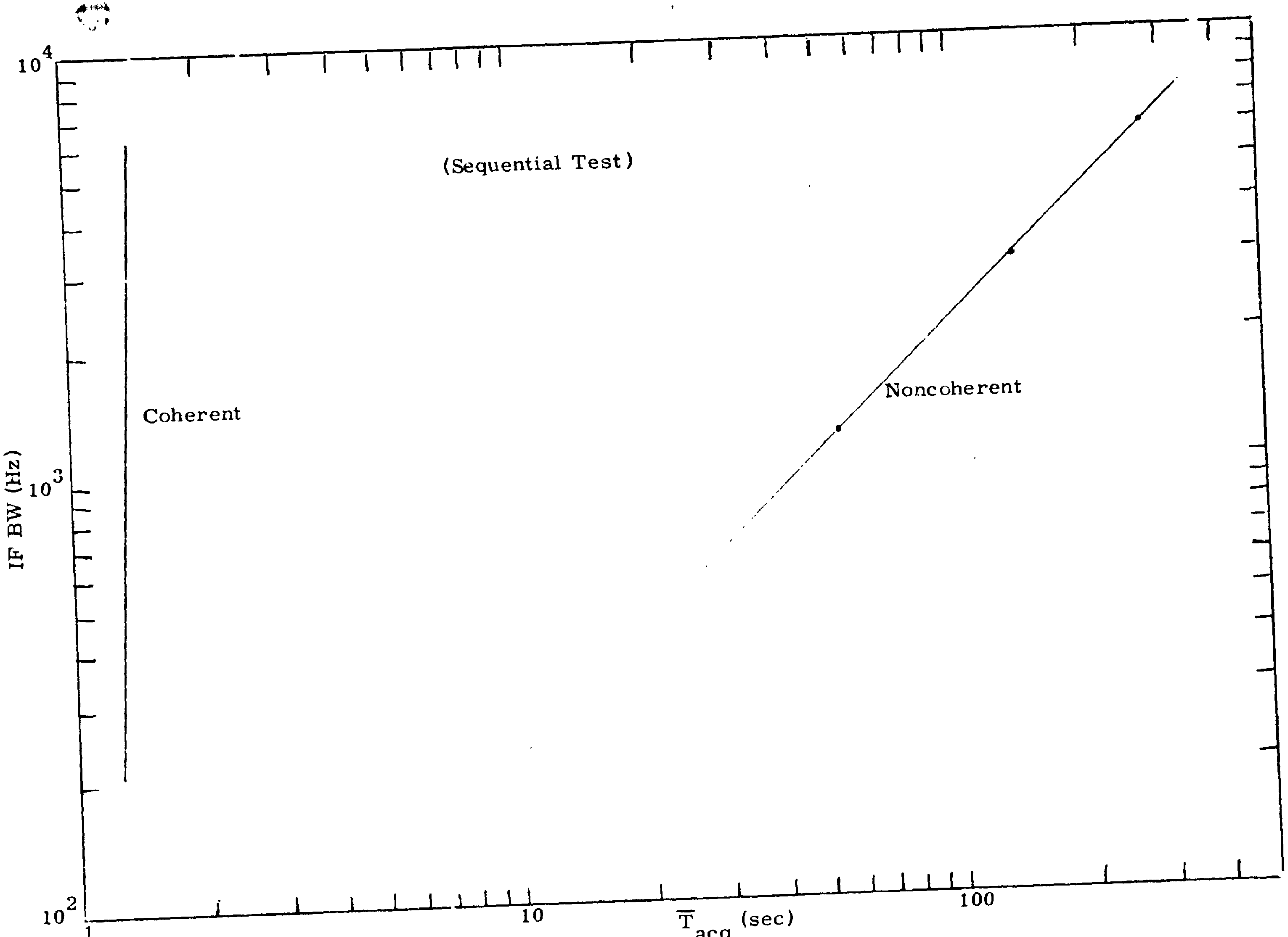

Figure 4.4-3. Mean Acquisition Time vs. IF Bandwidth for Multiple Access Forward Link Long Code

$$T_b \approx \frac{T/2 \ln \beta_1}{-\left(\frac{C'}{N_0 B}\right)_d} \qquad (4.4\text{-}6)$$

for the coherent test and T_b given by equation (4.4-5) for the noncoherent test. For these tests it is assumed that the local reference is stepped in one-half chip increments. Since chip synchronism occurs at the conclusion of the short code acquisition, the long code could be stepped in single chip increments. For this case the average acquisition times are one-half of the values given in table 4.4-3. Another important factor is that carrier lock occurs at the conclusion of short code synchronization. Given carrier lock and the capability for tracking the doppler frequency offsets, the IF bandwidth can be narrowed significantly. Thus, the performance could actually be significantly better than the acquisition times given in table 4.4-3.

4.4.2 Analysis With an Interfering Signal - Forward Link

Introduction

A model of the forward link with two TDRSS satellites in view of the user receiver is shown in figure 4.4-4. The desired signal is $S_1(t)$ and the interfering signal is $S_2(t)$. The objective of this analysis is to determine the probability that the noncoherent acquisition circuitry locks onto the interfering signal rather than the desired signal as a function of their relative signal levels.

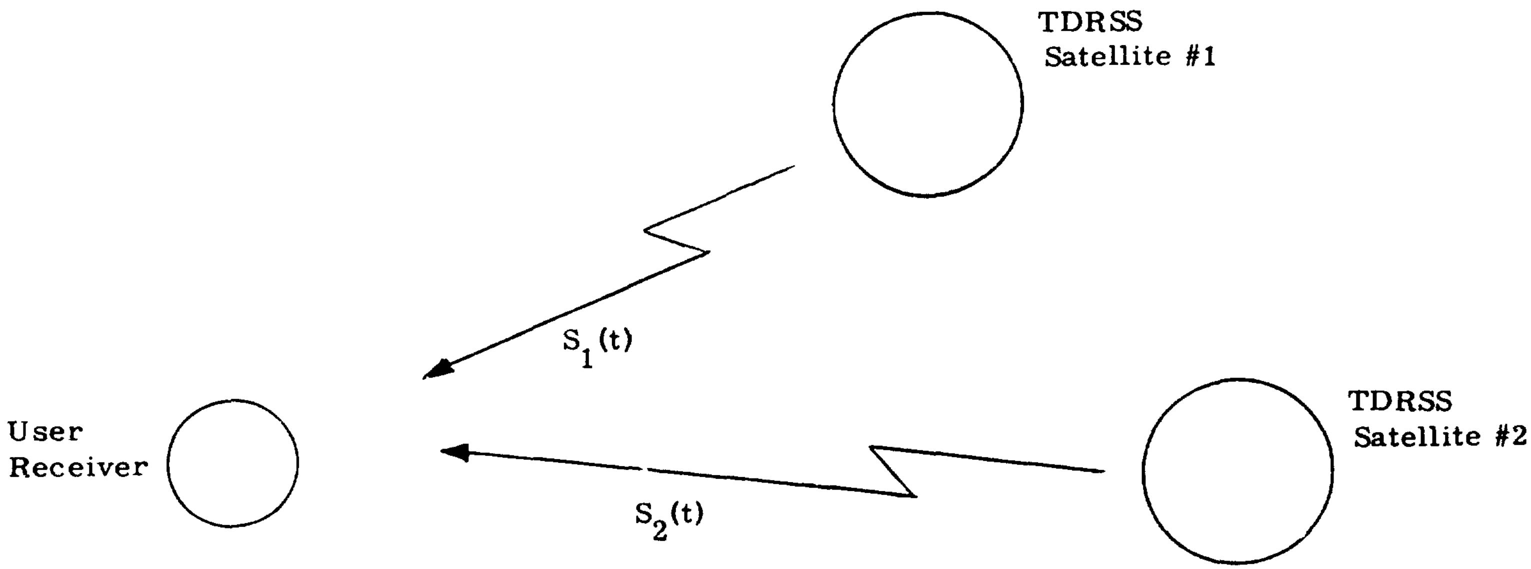

Figure 4.4-4. Model of TDRSS Multiple Access Forward Link

Analysis

Both the desired and interfering signals can be represented in general as

$$S_i(t) = \sqrt{2S_i}\; a_i(t)\, X_i(t) \sin\left[(\omega_c + \Delta_i)t + \theta_i\right] \tag{4.4-7}$$

where X_i = pseudorandom PN Gold code of the ith signal with code length n = 1023 chips

a_i = data modulation of the ith signal

θ_i = relative phase shift of the ith received signal

S_i = received power of the ith signal

Δ_i = sum of the doppler and frequency uncertainties of the ith signal.

The cross-correlation code spectrum for the two codes $a_1(t)$ and $a_2(t)$ is given by

63 (136) -1 (767) -65 (120)

where the value in parentheses associated with the cross-correlation quantity denotes the number of chip positions containing the particular cross-correlation value. That is, out of a total of 1023 chip positions, 136 positions have a cross-correlation value of 63, 767 have a cross-correlation value of -1, and 120 have a cross-correlation value of -65.

In the noncoherent detection analysis, the sign of the cross-correlation value is irrelevant. Since the difference between the cross-correlation values of 63 and 65 is so small, for the purposes of this analysis we will assume that there are 256 positions in which the cross-correlation value is 65. Typical autocorrelation and cross-correlation functions for the 1023 Gold codes are shown in figure 4.4-5.

The frequency spectrum of the interfering signal power at the output of the despreader is given by equation (4.3-62). For the forward link, the data bit rate is assumed to be a nominal 125 bits per second. Hence, T_2 equals 8×10^{-3} seconds. The bandwidth of the bandpass filter is assumed to be 6 kHz since the total frequency uncertainty is $\pm$ 3.0 kHz. Therefore,

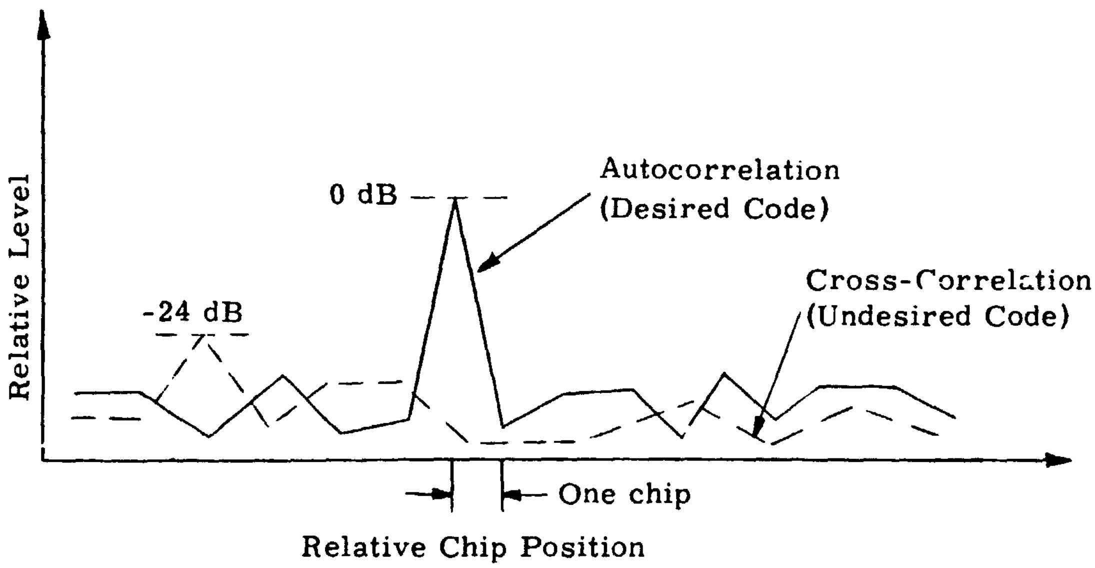

Figure 4.4-5. Typical Auto- and Cross-Correlation Functions for the 1023 Gold Codes

the signal power at the output of the bandpass filter is given by equation (4.3-66) and for the parameters given above, it can be written as

$$S_0 = \frac{S_2 \rho_{1,2}}{\pi} \int_{-94.5}^{94.5} \frac{\sin^2 x}{x^2} dx \tag{4.4-8}$$

$$S_0 \approx \frac{S_2 \rho_{1,2}}{\pi} [\pi] = S_2 \rho_{1,2} . \tag{4.4-9}$$

With the use of equations (4.3-78) and (4.3-84), we can write the following relationship for the signal-to-noise ratio of the interfering signal at the output of the bandpass filter:

$$SNR_2 = \frac{\rho_{1,2}}{\frac{2}{3}\left(\frac{S_1}{S_2}\right) T_c B + \frac{N_0 B}{S_2}} . \tag{4.4-10}$$

In this particular example, the various parameters of (4.4-10) are given by

$$\rho_{1,2} = \left(\frac{65}{1023}\right)^2$$

$$B = 6000 \text{ Hz}$$

$$T_c = 0.333 \times 10^{-6} \text{ sec} . \tag{4.4-11}$$

When the threshold signal-to-noise ratio was computed for the desired signal, a one-half chip offset loss of 2.5 dB was assumed. In comparing the signal-to-noise ratio of the interfering signal, we will take the worst-case position and assume that there is no chip timing loss. From section 4.4.1, we have shown that the threshold signal-to-noise ratio of the desired signal is given by

$$\frac{S_1}{N_0 B} = -9.3 \text{ dB} .$$

Therefore, we can write the relative signal-to-noise ratio of the interfering signal with respect to the desired signal threshold as

$$\frac{S_2}{N_0 B} = \left.\frac{S_1}{N_0 B}\right|_{\substack{\text{at} \\ \text{threshold}}} + 2.5 \text{ dB} + \left.\frac{S_2}{S_1}\right|_{\text{dB}} . \tag{4.4-12}$$

Substituting (4.4-11) and (4.4-12) into (4.4-10), we get the following relationship between the relative ratios of the two signals and the signal-to-noise ratio of the interfering signal:

$$\frac{S_2}{N_0 B} = 0.21\, \rho_{1,2} \frac{S_2}{S_1} \tag{4.4-13}$$

or

$$\frac{S_2}{N_0 B} = -30.8 + \left.\frac{S_2}{S_1}\right|_{\text{dB}} . \tag{4.4-14}$$

The relationship between the interfering signal and the desired signal threshold or operating point of the sequential test can be given as a function of the relative ratios of the interfering signal level and the desired signal level at the user receiver. This is derived from (4.4-14) and is given by

$$\frac{a}{a_d} = -21.5 + \left.\frac{S_2}{S_1}\right|_{\text{dB}} . \tag{4.4-15}$$

The probability of detecting the interfering signal for a given trial is given by $1 - L(a)$ where $L(a)$ is defined by equation (4.3-29). This relationship is plotted in figure 4.4-6 for several sets of false alarm probabilities and detection probabilities at threshold.

During the acquisition mode, the detection probability is set equal to 0.5, whereas for verification, it is set at 0.9.

The probability of detecting the interfering signal as a function of the ratio of the desired signal level to the interfering signal level is given by

Figure 4.4-6. Probability of Detection Versus SNR Relative to Design SNR for Sequential Test Strategy

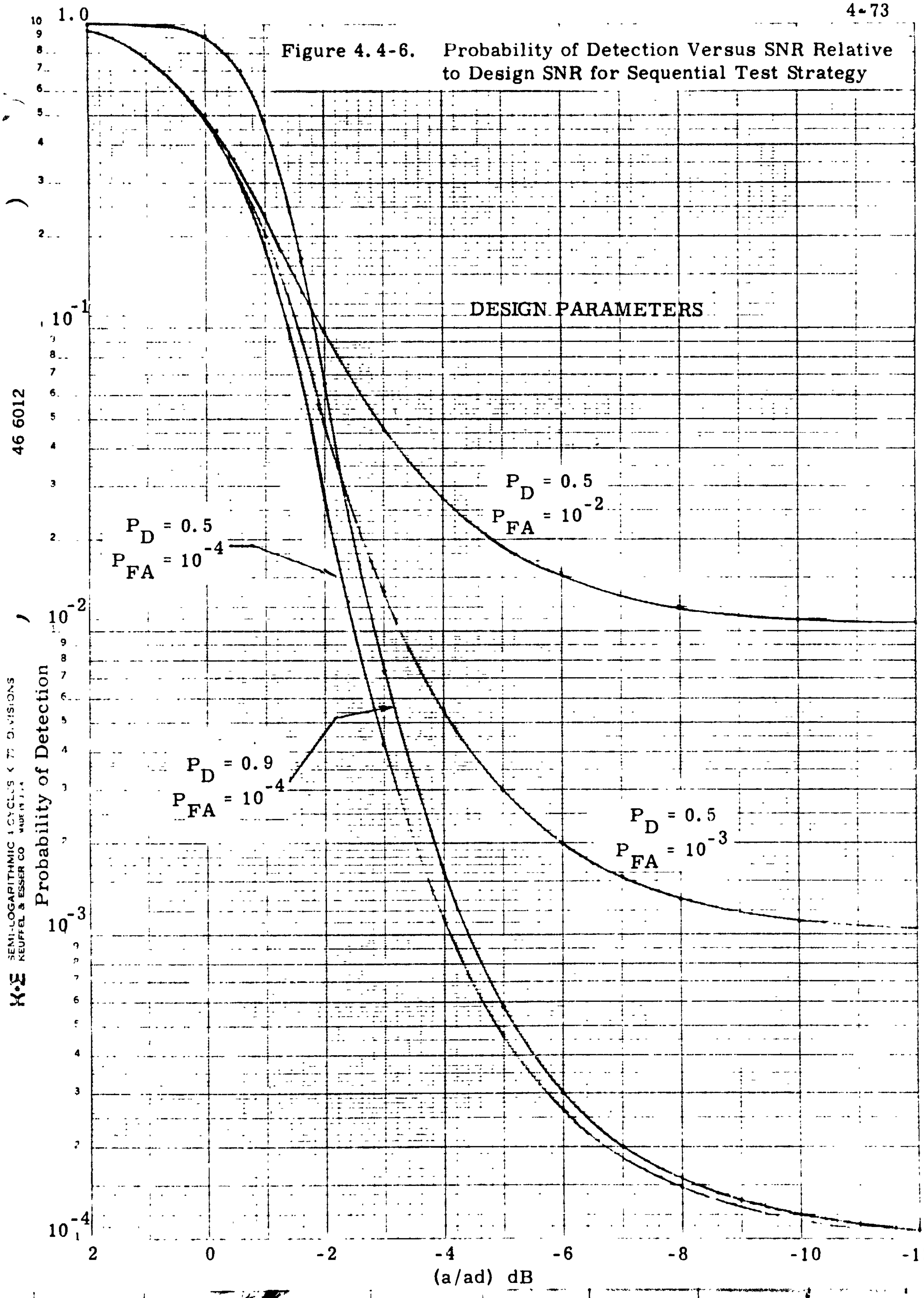

$$P_{DI} = 1 - (1 - P_{DA} \cdot P_{DV})^m \quad (4.4\text{-}16)$$

where m = number of trials or sidelobe peaks = 256

P_{DA} = probability of detecting the interfering signal during acquisition and is plotted in figure 4.4-6 as a function of a/a_d

P_{DV} = probability of detecting the interfering signal during verification and is also plotted in figure 4.4-6 as a function of a/a_d.

The relationship between a/a_d and S_2/S_1 is given by equation (4.4-15).

Analysis Results

The probability of detecting the interfering signal in the process of scanning through each of the cells in the uncertainty range is plotted in figure 4.4-7 as a function of the interfering signal level. This analysis does not consider the probability that the desired signal may be detected prior to detecting the interfering signal and, hence, the results may be slightly pessimistic. The curves in figure 4.4-7 rise rapidly and, as the interfering signal increases to 20 dB above the desired signal, the probability of detecting and verifying the interfering signal in the course of initial acquisition approaches unity.

A nominal worst-case interfering signal level relative to the desired signal level may be 15 dB. This results from a -9 dB user antenna gain in the direction of the desired signal and a +3 dB antenna gain in the direction of the interfering signal. In addition, the desired signal is transmitted with 0 dB design margin, whereas the interfering signal design margin is +3 dB. For this relative ratio of 15 dB, the probability of detecting the interfering signal ranges between 10^{-3} and 10^{-4} depending upon the threshold false alarm probability during acquisition, as seen in figure 4.4-7. This is a very low probability; however, as already noted, the detection probability increases rapidly for a small increase in the relative signal-to-noise ratios and, consequently, means for further reducing the false detection probability should be considered.

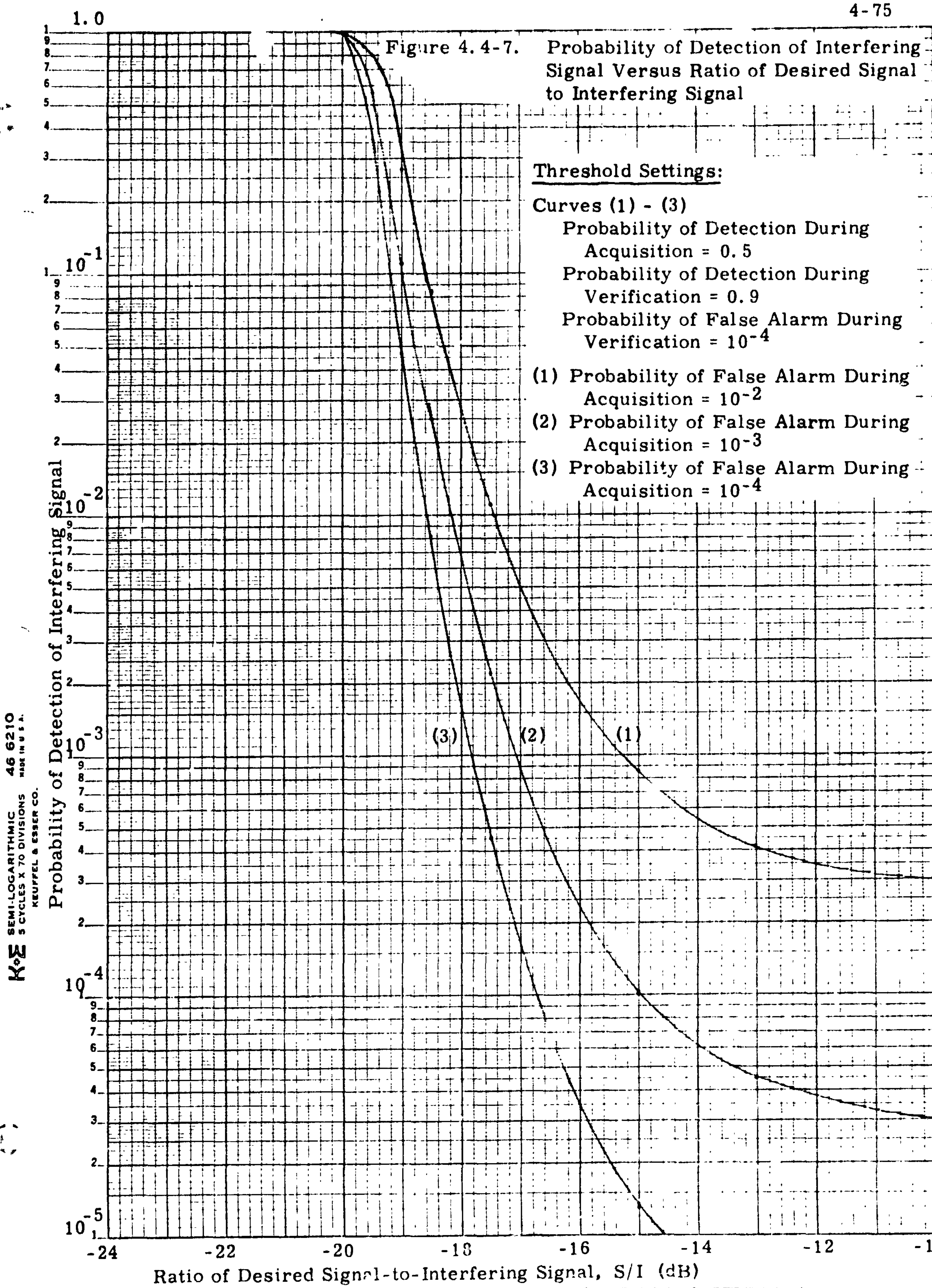

Figure 4.4-7. Probability of Detection of Interfering Signal Versus Ratio of Desired Signal to Interfering Signal

Aids to the Minimization of False Detection

We have seen that, for relatively high interfering signal levels (i.e., greater than 20 dB above the desired signal), the probability of a false lock is high. Once the false lock condition occurs, the local reference is no longer advanced and code tracking begins. One may assume that, by choosing the code loop noise bandwidth B_L such that the interfering signal-to-noise ratio in B_L is below loop threshold, the noise will, with high probability, cause a loss of lock after several time constants. This would probably work if the maximum interfering signal level were 15 dB above the desired signal level. However, if the interfering signal should go to a level 20 dB above the desired signal, then there is insufficient margin to cause the loop to drop lock.

While the delay lock loop is tracking, the carrier tracking circuit is attempting to lock to the carrier of the received signal. The same problem as was indicated above for the delay lock loop may exist with the carrier recovery circuit in discriminating against the interfering signal. However, the quadrature output of the phase recovery circuit or the coherent amplitude detector (CAD) is enabled once carrier lock is accomplished. With the CAD operating, the AGC is thus controlled by the received signal level rather than the receiver noise level. As an example, the signal voltage at the input to the phase detector may be held constant at a 1 v rms level, regardless as to whether the signal is the desired or interfering signal. For this condition, the thresholds associated with the verification mode can be set to a predetermined fixed value independent of the noise. Hence, the mean values of the distributions associated with the interfering and desired signals are separated at their peak by $\rho = (65/1023)^2$ or 24 dB. Thus, even if the interfering signal level is noncoherently acquired and verified, and if the code tracking and phase lock loops lock to the interfering signal, these circuits would be unlocked if the verification test were continued with fixed thresholds that are switched in at the instant the CAD begins functioning.

The probability of unlocking the interfering signal can be made as high as desired by proper selection of the detection threshold. When an interfering signal is detected subsequent to initial acquisition and verification and the acquisition circuitry, code tracking and carrier recovery loops are unlocked, the system should continue searching the cells from the previous point where it had stopped when it had erroneously locked onto an interfering signal.

At the same time the short code is being verified at the conclusion of carrier acquisition, the long code is also in the process of being acquired. Because the thresholds of the long code can be constant values due to the operation of the coherent AGC, it also can be used to unlock the receiver when it falsely locks to an interfering signal. It could in fact be used instead of the short code verification procedure described above. The only drawback is that it would require a longer overall acquisition time. The suggested steps in the synchronization algorithm, with the exception of the multipath test which is discussed in section 4.5, are summarized in the flow diagram given in figure 4.4-8.

Impact on Acquisition Time

When the interfering signal is detected, the effect is one of a false alarm. The difference from a false alarm based on noise is that there is a much greater probability of code lock and carrier lock to the interfering signal (provided, of course, that the level is high enough) than there is to noise alone. This necessitates the continuing verification of the short code subsequent to carrier lock. This additional verification test is one which was not considered in the previous sections of this report. From figure 4.4-6 and equation (4.3-58), we can compute the mean acquisition time as a function of the ratio of the desired signal-to interfering signal. The results for a single doppler cell are shown in figure 4.4-9. The mean acquisition time thresholds sharply as the interfering signal approaches 20 dB above the desired signal. This can be seen by looking at figure 4.4-6. As the signal level, a, approaches the design signal level, a_d, the detection

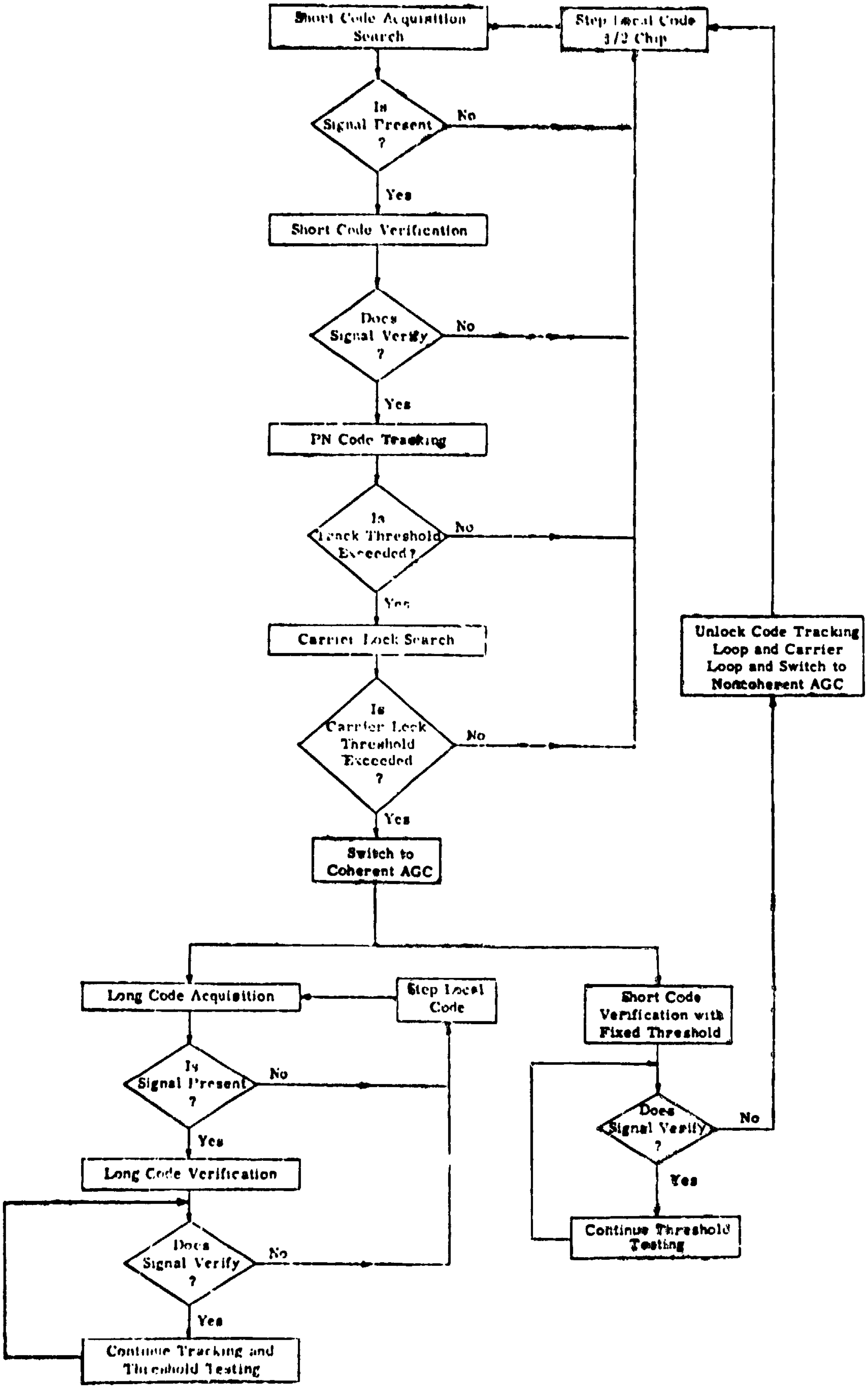

Figure 4.4-8. Simplified Flow Graph of Forward Link Synchronization Algorithm

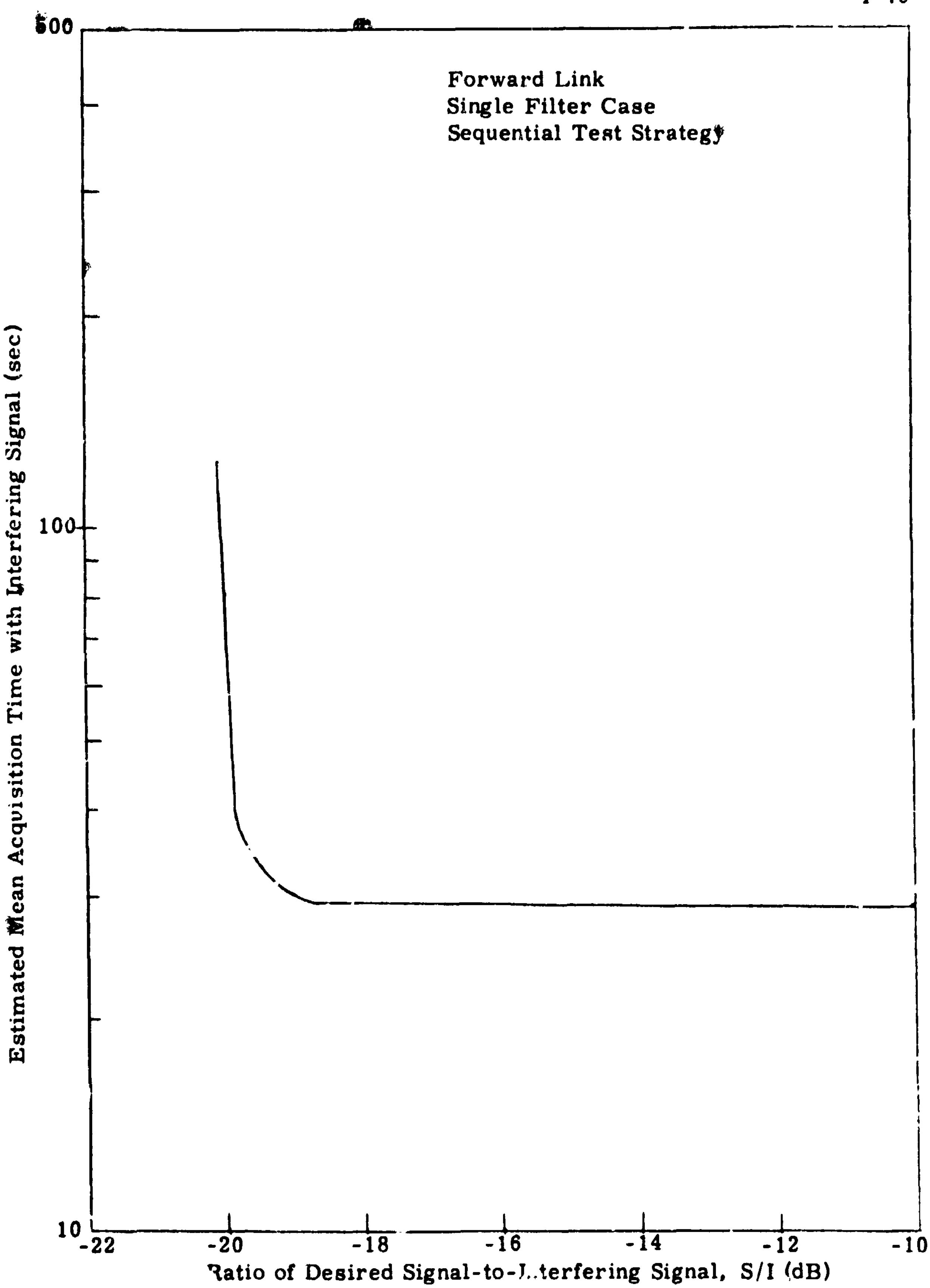

Figure 4.4-9. Estimated Mean Acquisition Time Versus Ratio of Desired Signal-to-Interfering Signal

probabilities in both the acquisition and verification modes approach the design detection probability levels. Since the cross-correlation sidelobes are 24 dB below the autocorrelation peaks, when the interfering signal level approaches 20 dB above the desired signal level, the false alarms due to the cross-correlation peaks approach the design detection proba-bilities. Therefore, as the code search progresses, each time the cross-correlation sidelobe peak occurs (which is about one-fourth of the time), there is a high likelihood of it appearing as a real signal. It then progresses through the various synchronization steps and is finally rejected with the short code verification test with a fixed threshold after the coherent AGC is switched in. The time to PN code lock, carrier lock, and perform the post-lock verification test was estimated to be 0.5 seconds. This accounts for the "estimated" mean acquisition times given in figure 4.4-9.

Impact on Hardware

The impact of the post-lock verification test is very small when microprocessor techniques are employed in processing the synchronization algorithm. It basically involves a few additional instructions and some logic to unlock the code tracking loop, carrier lock loop, and switch back to a noncoherent AGC operation.

4.4.3 Sidelobe False Alarm Analysis

Introduction

The short codes of the forward link are pseudorandom Gold codes of length 1023 with properties enumerated in section 5. The autocorrelation spectra of the Gold codes is similar to the cross correlation spectrum given in section 4.4.2. To simplify this analysis we will assume that there are 256 positions in which the autocorrelation value is 65, one position where it is 1023, and the remaining 766 positions where the autocorrelation value is -1.

The dynamic range of the received signal is assumed to be 35 dB. The objective of this analysis is first to determine the probability of erroneously detecting the sidelobes as in-synchronization positions and then second to consider techniques for either detecting false alarms due to sidelobe detection or reducing the false alarm probability due to sidelobes. A conceptual approach for achieving the former of these objectives is recommended. The impact of this technique on the overall acquisition time is considered, as well as its hardware implications.

The subsequent discussion is primarily conceptual with a level of analysis which is intended to give a first-cut estimate of the system performance. It should be noted that there is room for considerable optimization which could further enhance the overall system performance.

False Sidelobe Detection Probability

The first step in this analysis is to determine the probability of false alarms due to the "self noise" of the received signal (i.e., sidelobe partial correlations) as a function of the received signal level.

The probability of detecting a sidelobe in a given trial for the sequential test algorithm is $1 - L(a)$ where $L(a)$ is defined by equation 4.3-29. The parameter a is the normalized received signal level. The function $L(a)$ is also dependent upon the normalized threshold or design signal level, a_d, which has a preset value.

The probability of false detection on a sidelobe in a given cell position is plotted in figure 4.4-10 as a function of the received signal level above threshold. This is the probability that a sidelobe of the 1023 Gold code passes both the acquisition and verification tests. The sidelobe levels are 24 dB below the peak correlation level. If the signal is 24 dB above threshold, then the sidelobe level is at threshold and, hence, the probability of detecting the sidelobe equals the probability of the product of the detection and verification probabilities, which are 0.45. As the signal level becomes even greater, the detection probability of the sidelobes rapidly

Figure 4.4-10. Probability of Detection of Sidelobe as a Function of Signal Level Above Threshold

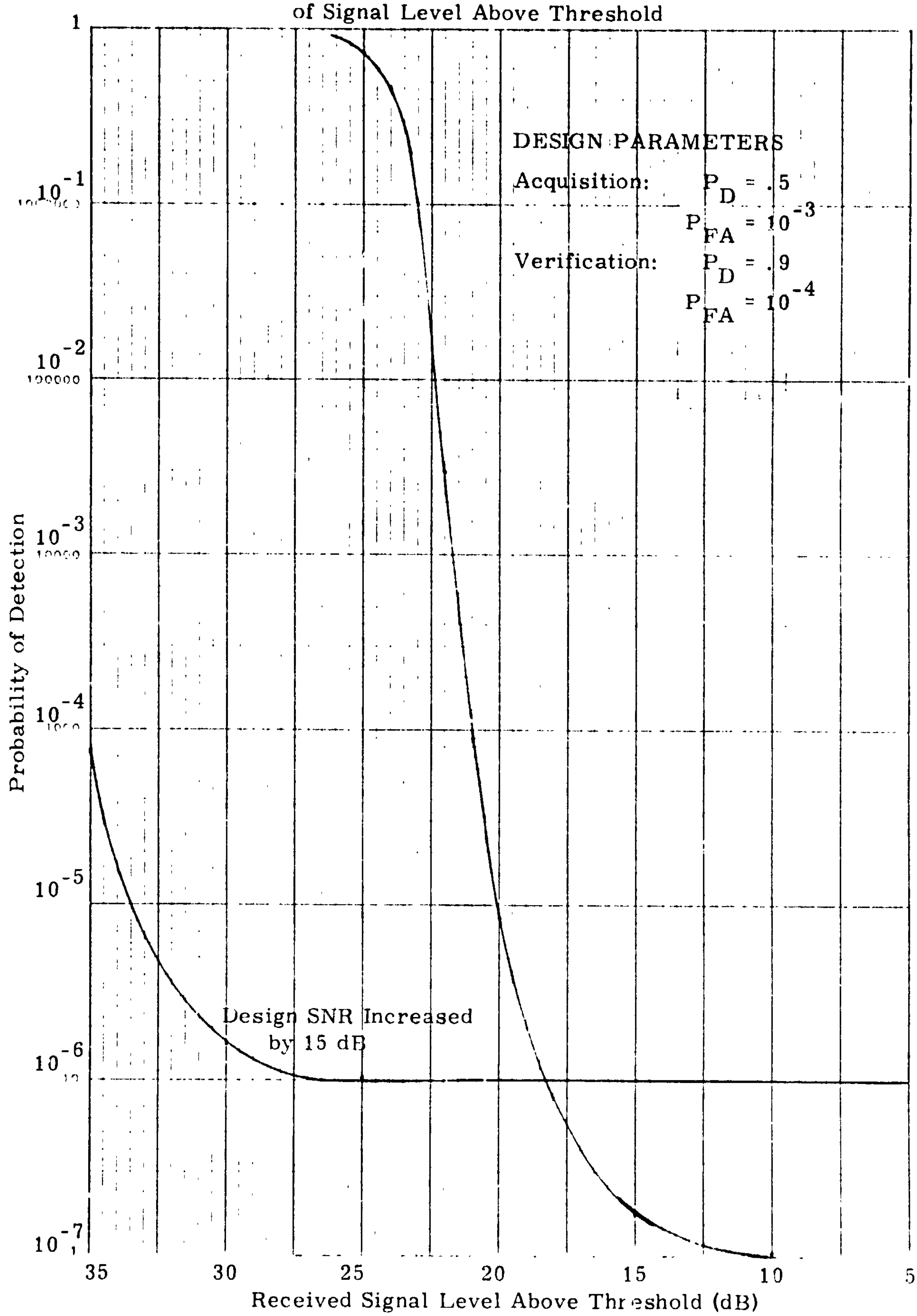

approaches unity. These results do not consider the effect of the "self noise" which contributes more significantly to the total noise as the received signal level increases. The results also assume a perfect noise estimate which is used in normalizing the design and received signal levels. Both of these factors tend to make the sidelobe false alarm probability higher than would actually be the case.

Sidelobe Rejection Algorithm

From figure 4.4-10, we can see that, as the input signal level increases, the partial correlation of a sidelobe is sufficiently high to result in a high probability of false detections. The partially correlated signal level may also be high enough so as to achieve both code and carrier lock. A method must therefore be provided to detect a false synchronization condition, unlock the receiver, and permit it to acquire the correct synchronization position.

There are several ways of detecting a sidelobe lock position. One particularly attractive approach will be considered. The technique takes advantage of the Gold code properties in that the sidelobes with no noise are deterministic and in the case of this code are 24 dB below the peak correlation level. The following discussion presents the case for the sidelobe rejection algorithm.

After initial acquisition, verification, code and carrier lock, a post-detection verification algorithm is employed. This algorithm can be similar to the initial acquisition algorithm with the exception that the threshold is increased by some factor. Two cases are considered. In one case the threshold is increased by 15 dB and in the other it is increased by 20 dB. If the sidelobe rejection algorithm is performed with a sequential test, increasing the threshold corresponds to increasing the design signal level, a_d. For a fixed length test, it implies that the post-detection integration time is such that a pre-established detection and false alarm probability will be achieved for some higher signal-to-noise ratio. Let us first consider the case where the threshold is increased by 15 dB. If the received signal level is so high that it exceeds the first threshold by 35 dB, then it will also exceed the second threshold by 20 dB. The partially correlated sidelobe is 24 dB below the peak. It nominally exceeds the first threshold by 11 dB which results in its high likelihood of being detected. However, it falls below the second threshold by 4 dB on the average; therefore, from figure 4.4-10, its probability of exceeding the second threshold on a per trial basis is 1×10^{-5} for the maximum received signal level case. Since there are 256 sidelobes with close the same average partial correlation level, the probability that any one of them will exceed the threshold in the process of scanning through all 1023 chip positions is

$$1 - (1 - 1\text{x}10^{-5})^{256},$$

which equals 2.5×10^{-3}. However, the probability is almost unity that the mainlobe will exceed the increased threshold given that a partially correlated sidelobe has exceeded the initial thresholds. This assumes that the AGC level is held constant and is controlled by the partial correlation sidelobe level throughout the duration of the sidelobe rejection test. By increasing the sidelobe rejection threshold to 20 dB above its previous level, the probability of the maximum sidelobe level exceeding the new threshold on a per trial basis is decreased to 6×10^{-7}, which yields a probability of 1.5×10^{-4} when scanning through all 1023 cell positions. This reduces the margin between the mainlobe exceeding the increased threshold given that a sidelobe has exceeded the initial synchronization thresholds. However, this margin is still sufficient to yield a detection probability well in excess of 0.9.

The sidelobe rejection test sequence as outlined in the flow chart of figure 4.4-11 can be summarized as follows. After the initial acquisition, verification, code tracking and carrier lock tests are satisfied, the acquisition threshold is increased by 15 dB or 20 dB. The same cell position is checked with the new design parameters. If the new threshold is exceeded, then the position tested is the mainlobe fully correlated cell position. If the threshold is not exceeded, then either the position tested is the mainlobe

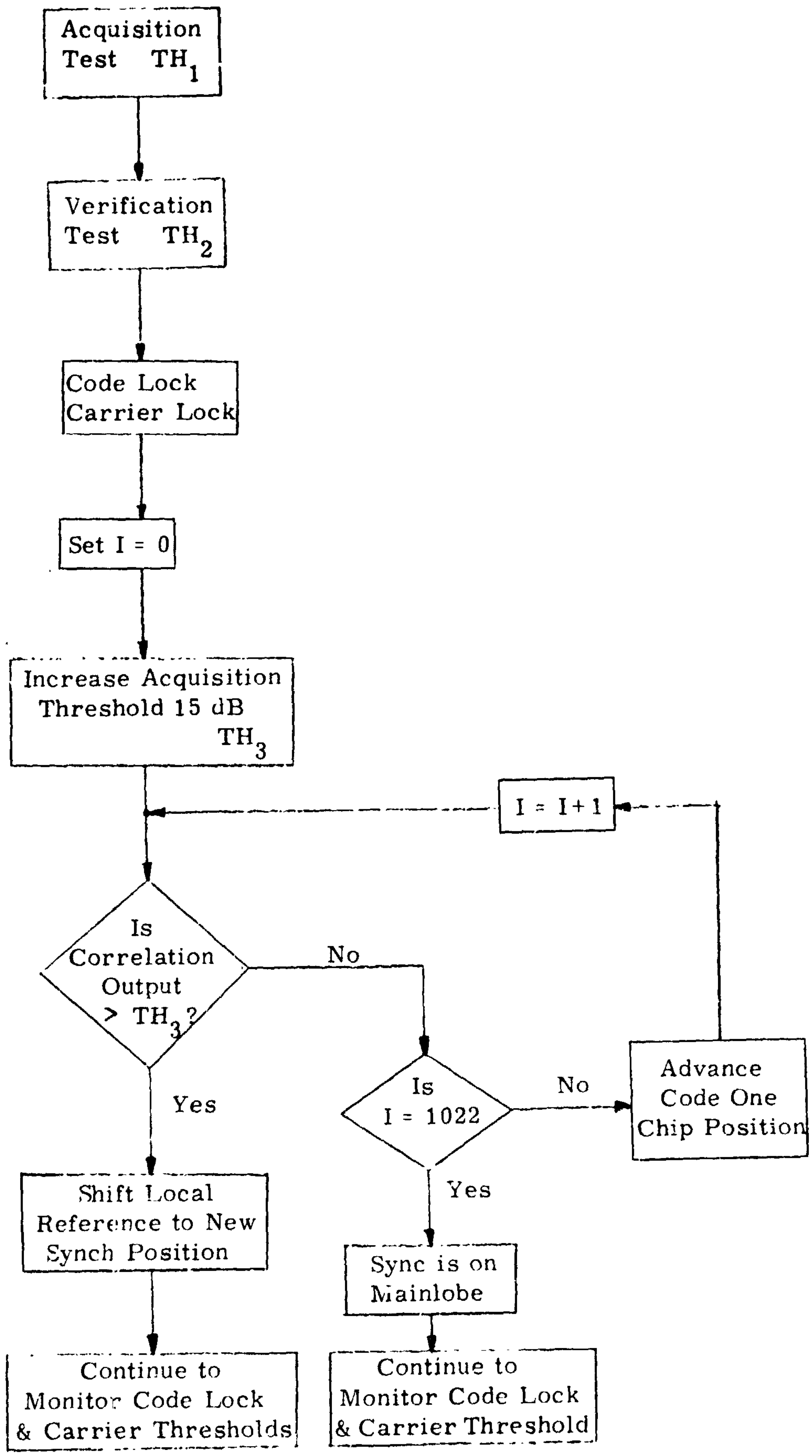

Figure 4.4-11. Sidelobe Rejection Algorithm

cell position or a sidelobe position. The local reference is stepped in successive chip positions and the same test is made at each successive cell position. Because code lock exists, single chip steps are sufficient. If the test indicates a signal in any one of the 1023 positions, that position is assumed to be the mainlobe cell. The local reference is then shifted to the new synchronization position. If the threshold is not exceeded in any one of the 1023 potential synchronization positions, then the original cell position is assumed to be the mainlobe synchronization position. For this case, the received signal level is with high probability above threshold but less than 15 or 20 dB above the original design threshold. This sidelobe rejection test can be either a fixed length or a sequential test. For the sequential test, the probability of detecting a sidelobe for a given trial with the new design signal-to-noise ratio 15 dB above the original design threshold is also plotted in figure 4.4-10.

Impact on Acquisition Time

In this subsection, we will estimate the increase in the overall synchronization time which is due to the sidelobe rejection test. The estimate is made based on a fixed length test for reasons given below. Also, it should be noted that no attempt was made to optimize the synchronization parameters.

The test is to occur after code lock and carrier lock are achieved. When the signal level is near threshold, the probability of false lock to a sidelobe is very small. Since this condition is not known a priori, the sidelobe rejection test must be made. In this case, all 1023 cells will be tested once code and carrier lock are obtained. Thus, in considering the impact on overall acquisition time, we must consider the case where all the cells are tested with the new threshold. Either a coherent or noncoherent test can be made. We will assume the latter. We also assume that the code lock detection probability is high enough that it establishes the overall synchronization detection probability. Therefore, only one scan through the sidelobe rejection test is anticipated per acquisition attempt. Hence, we can just compute the time required to dismiss each position with the threshold SNR set 15 or 20 dB above the threshold for the initial acquisition test. The new threshold 15 dB above the acquisition threshold yields a design SNR greater than 0 dB in the detection bandwidth. The mean time to dismissa omputations given in section 4.3.2 are generally only valid if the design SNR is less than 0 dB. Hence, to simplify the analysis, a fixed length test is assumed. If we draw upon the analysis given in section 4.3.1.1, we obtain the relationship shown in figure 4.4-12, which is a plot of the signal-to-noise ratio at the input to the detector as a function of the time-bandwidth product BT, where $P_{FA} = 10^{-6}$ and $P_D = 0.99$. The design SNR threshold was calculated to be -9.3 dB for the sequential analysis acquisition test with a single doppler cell of 6 kHz (cf. page 4-57). Increasing this threshold by 15 dB yields an SNR of 5.7 dB. To achieve a detection probability of 0.99 with a false alarm probability of 10^{-6} requires, as determined from figure 4.4-12, a BT of 9. Hence, the time to search all 1023 cells with this BT requires approximately 1.5 seconds. These results are slightly optimistic since the sidelobe noise is neglected and does become a significant factor at the higher signal-to-noise ratios. This time can be reduced as shown in table 4.4-4 by increasing the number of doppler cells. The results, however, are only approximate since the analysis for computing the results in figure 4.4-12 are based upon BT products much greater than unity. If one reduces the detection probability to 0.9 and the false alarm probability to 10^{-5}, then with five doppler cells, a BT of 1 is all that is required and this yields a sidelobe rejection test time of 0.85 seconds.

Because of the potential frequency offset between the local reference and the incoming signal, the code doppler shift may be as great as 1 chip per second or more. This shift does not present a problem since the sidelobe rejection test occurs after code lock is attained and consequently the relative code drift is continuously tracked.

The results discussed above are extended to the case where the threshold is increased by 20 dB. These estimated results are summarized

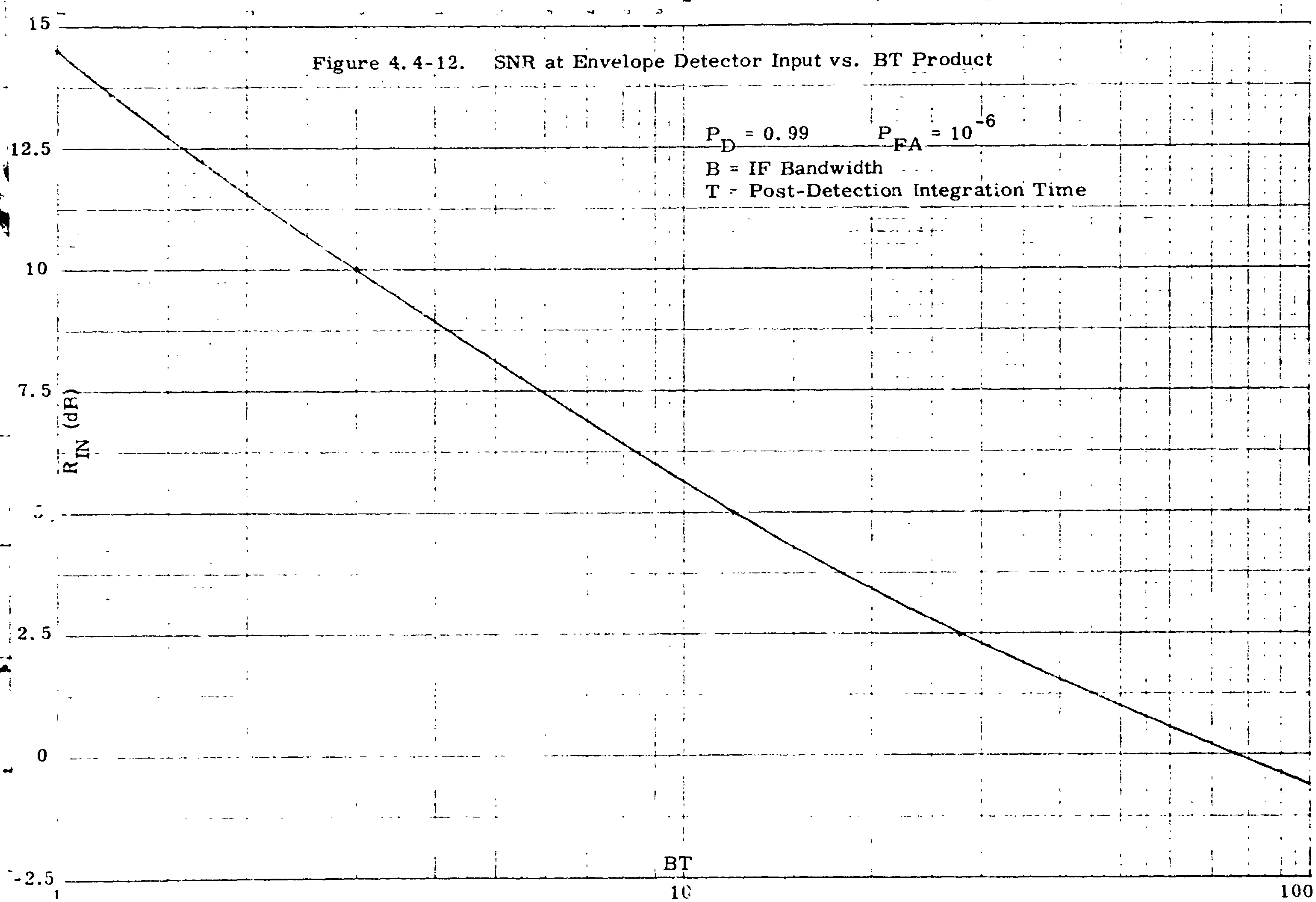

Figure 4.4-12. SNR at Envelope Detector Input vs. BT Product

Table 4.4-4. Maximum Estimated Time for Sidelobe Rejection Test (Fixed Length) With Threshold 15 dB Above Acquisition Threshold

$P_D = 0.99$ $P_{FA} = 10^{-6}$

Number of Doppler Cells	Bandwidth per Cell, B (Hz)	Signal-to-Noise Ratio for Increased Threshold (dB)	Required Time-Bandwidth Product (BT)	Time to Search 1023 Cells (sec)
1	6000	5.7	9	1.5
2	3000	8.7	4	1.4
3	1200	12.7	1.5	1.3

$P_D = 0.9$ $P_{FA} = 10^{-5}$

5 Doppler Cells, BT = 1

Time to Search 1023 Cells = 0.85 seconds in table 4.4-5 and show that the impact on acquisition time of the sidelobe rejection test can be reduced to below 0.5 seconds.

Impact on Hardware Complexity

The additional impact of the sidelobe false alarm detection algorithm to the hardware complexity is small. A separate correlator with a bandpass filter, envelope detector and post-detection integrator as shown in figure 4.3-3 is part of the receiver hardware for the purpose of estimating the receiver noise and the "self noise" level. This hardware can also serve in performing the decorrelator part of the sidelobe rejection test. The other logic, counter and control operations contribute minimally when microprocessor techniques are employed in processing the overall synchronization algorithm.

Table 4.4-5. Maximum Estimated Time for Sidelobe Rejection Test (Fixed Length) With Threshold 20 dB Above Acquisition Threshold

$P_D = 0.99$ $P_{FA} = 10^{-6}$

Number of Doppler Cells	Bandwidth per Cell, B (Hz)	Signal-to-Noise Ratio for Increased Threshold (dB)	Required Time-Bandwidth Product (BT)	Time to Search 1023 Cells (sec)
1	6000	10.7	2.5	0.43
2	3000	13.7	1.2	0.41
5	1200	17.7	0.45	0.4

4.5 Application of Analysis to Ground Receiver

4.5.1 Performance Summary - Multiple Access Return Link

A summary is given in this section of the analysis of the average acquisition time for Mode 2 of the multiple access return link. The modulation technique is staggered QPSK with a recommended chip sequence consisting of $2^{11}-1$ chips.

At threshold, the received signal power-to-noise spectral density ratio without coding is given by C/N_0 = 39.9 dB-Hz and C/N_0 = 34.9 dB-Hz with 1/2 rate Viterbi coding. For the single IF filter configuration, an IF filter bandwidth of 5 kHz is required to accommodate the frequency uncertainties and data modulation. Losses were given in section 4.3.5 with a summary of the IF signal-to-noise ratios in table 4.3-2. The signal-to-noise ratio is assumed to increase by 2 dB in the verification mode because the code tracking loop in operating.

An equation which closely approximates the mean acquisition time was derived above and is given below.

$$T_{ACQ} = N \left[\frac{T}{|1 - 2 d_c T|} + P_a T_B\right] \left(\frac{1+\beta}{1-\beta}\right) \qquad (4.5\text{-}1)$$

where N = number of chips in code length

T = Post Detection Integration Time

T_B = Average time to perform verification test leading to a dismiss decision

P_a = probability of false acceptance by acquisition test

d_c = code doppler error

$\beta \approx P_b + (1 + P_b) P_B$.

Three code lengths were considered: $N = 2^{11} - 1$, $2^{13} - 1$ and $2^{15} - 1$. In order to avoid the problem of partial correlations, the post detection integration interval was selected to correspond to at least as a minimum one complete cycle of the PN code. Since B is assumed to be 5 kHz, for the code length $N = 2^{11} - 1$,

$$BT = \frac{2^{11} - 1}{3 \times 10^6} (5 \times 10^3) = 3.4$$

as a minimum to satisfy the above conditions. If BT is much greater than 3.4, whether or not the integration time is integrally related to the code length period is not all that critical.

No Coding Case

If we consider first the case without coding, we have from table 4.3-2 a signal-to-noise ratio of -0.5 dB during acquisition for the desired signal and 1.5 dB during verification for the desired signal. If we assume a false alarm probability of 0.01 during acquisition, then the detection probability for the desired signal is

$$P_D = 1 - (1 - P_D')^2 \tag{4.5-2}$$

where $$P_D' = \frac{1}{2} \left[1 - \mathrm{erf}\,(.292)\right] = .35$$

from 4.3-11,

and hence, $P_D \approx .58$.

Equation (4.5-2) is used because during acquisition there are at least two chances for detecting the synchronization position when the local reference is stepped in one-half chip increments.

The interfering signal is at - 18.0 dB during acquisition. Since the threshold is set for the desired signal with some minimum false alarm probability, the detection probability of the interfering signal for a given trial is 1.18×10^{-2}, which is very close to the false alarm probability. The total detection probability is a function of the number of trials. For the Gold codes, we will assume that half of the cell positions have sidelobe cross-correlation power corresponding to an $SNR_{IN} = -18$ dB. Therefore, the overall probability of detection is

$$P_D = 1 - (1 - 1.18 \times 10^{-2})^{2047} \approx 1$$

For all practical purposes, if the sidelobe cross-correlation SNR_{IN} is as low as - 18 dB, the undesired signal appears as noise and the probability of detecting the interfering signal is about the same as the false alarm probability. This leads to the verification mode which is designed to reject the acquisition mode false alarms.

During verification, we set the false alarm probability at 10^{-4}. We will also assume a BT = 25. In other words, the post-detection integration interval is set for 5 ms. From table 4.3-2, the SNR_{IN} for the desired signal is 1.5 dB and for the interfering signal is - 16.5 dB. With these parameters, using equations 4.3-8 and 4.3-11, we get

$$P_D \text{ (desired signal)} = 0.95$$

$$P_D \text{ (interfering signal)} = 2 \times 10^{-4}$$

C3

In the verification mode, there is only one cell position in which the interfering signal will be detected and that is the position where acquisition is indicated. From the above results, we see that the probability of detecting the interfering signal for the above conditions is only twice that of the false alarm probability.

We can now substitute the above parameters into (4.5-2) to compute the average acquisition time, T_{ACQ} of the desired signal. A summary of the parameters is:

$$P_b = .42 \qquad d_c = 2.02 \text{ Hz}$$

$$P_B = .05 \qquad T = 6.8 \times 10^{-4} \text{ sec.}$$

$$P_a = 10^{-2} \qquad T_B = 5 \times 10^{-3} \text{ sec.}$$

$$P_A = 10^{-4}$$

Hence, $T_{ACQ} = 3.85$ sec.

If we assume the same time-bandwidth products, for the code lengths $2^{13} - 1$ and $2^{15} - 1$, then the acquisition times for each of these cases is 30.8 sec. and 123 sec., respectively. This is a lower bound since the post detection integration time during acquisition for these two cases results in a partial correlation condition.

Coding Case

Now, if we consider the case with coding we have during acquisition a C/N_0B for the desired signal of -5.5 dB. If we set the threshold for a false alarm probability of 0.1, then the probability of detection is given by (4.3-12) where

$$P_D = \frac{1}{2} \left[1 - \text{erf}(.432)\right]$$

and $$P_D = .47$$

Since the cross-correlation sidelobes with an undesired signal are 17.5 dB below the desired signal, the C/N_0B for this condition is -23 dB. This corresponds to a detection probability per trial of 0.1015, which is essentially the false alarm probability.

If during verification, the time bandwidth product is set at 50 and the false alarm probability is set for 0.01, then the probability of detection is 0.74 for the desired signal. The probability of detection of the undesired signal is 7.25×10^{-2}. If we substitute the following parameters into 4.3-12,

$P_b = .53$	$d_c = 2.02$ Hz
$P_B = .26$	$T = 6.8 \times 10^{-4}$ sec.
$P_a = .1$	$T_B = 10^{-2}$ sec.
$P_A = .01$	Code length $= 2^{11} - 1$

then $T_{ACQ} = 14.65$ sec.

Again, if the code lengths are increased to $2^{13} - 1$ and $2^{15} - 1$, the average acquisition times with the parameters given above are 58.6 seconds and 234.5 seconds, respectively.

The nonoptimized performance results are summarixed in tables 4.5-1 and 4.5-2.

The desired average acquisition time is 15 seconds. Since it is currently planned to use rate 1/2 coding on the multiple access return link, the code length $N = 2^{11}-1$ is the only one which can realistically meet the specified acquisition time requirements. Seven percent of the acquired interfering signals are verified, on the average. The parameters of the code tracking loop need to be such that the likelihood of locking onto the interfering signal is very low. Hence, an interfering signal which triggers a false alarm during verification would be rejected. This subject requires further investigation.

Conclusions

We have shown that, based on an analysis of the acquisition and verification modes, a code length of $2^{11}-1$ is sufficient. This, of course, assumes that the parameters of the code tracking loop are selected to effectively reject interfering signals which pass both the acquisition and verification tests.

Although the sequential testing strategy was not analyzed in this investigation for the return link, it also is a candidate technique for reducing the mean acquisition time. There is only one potential problem with the sequential test in this application: The fixed length test has a threshold set for fixed detection and false alarm probabilities and a fixed integration interval. In the sequential test, the integation (accumulation) interval is variable and the thresholds are set for fixed false alarm and detection probabilities about a design signal-to-noise ratio. The capability of the sequential test to reject an interfering signal and the degree of test truncation required bears more detailed investigation.

There are other possibilities for shortening the acquisition time, some of which were discussed above. One solution is to use parallel correlation, each correlator independently searching separate cells. Two

Table 4.5-1 Detection Performance of Desired and Interfering Signals

Performance / Link Condition	Desired Signal				Undesired Signal			
	Acquisition		Verification		Acquisition		Verification	
	P_{FA}	P_D	P_{FA}	P_D	P_{FA}	P_D	P_{FA}	P_D
Without Coding	10^{-2}	0.58	10^{-4}	0.95	10^{-2}	1.0*	10^{-4}	2×10^{-4}
With Coding	10^{-1}	0.47	10^{-2}	0.74	10^{-1}	1.0*	10^{-2}	7×10^{-2}

*This assumes one searches through all possible cell positions.

Table 4.5-2 Average Acquisition Time vs. Code Length

Code Length N / Link Condition	Average Acquisition Time, T_{ACQ} (sec)		
	$2^{11} - 1$	$2^{13} - 1$	$2^{15} - 1$
Without Coding	3.85	15.4	61.5
With Coding	14.65	58.6	234.5

such correlators would, except for some power losses, approach the possibility of halving the acquisition time. Optimization of the acquisition parameters (i. e., optimum selection of BT products for both acquisition and verification) can be used to shorten the mean acquisition time. Another approach is to use a bank of contiguous doppler resolving filters instead of just one IF filter. At the same time, the maximum output of each filter can be selected for further processing, or each path can be processed independently as discussed above for the forward link.

4.6 Impact of Multipath on Direct Sequence Acquisition Parameters

4.6.1 Introduction

The purpose of this investigation was to assess the impact that multipath may have on the candidate acquisition techniques. The primary acquisition technique of concern is the recommended short code/long code technique described in Section 2. As part of this study, a short subcontract was granted to the Boeing Company to characterize multipath parameters between a low orbiting (200 km altitude) user satellite and the synchronous TDRS satellite. A short summary of these results is presented below. A detailed summary of the results is given in the Interim Report.[1] The impact of these various parameters is discussed relative to acquisition of the 3 Mcps PN signal on the forward link to the user satellite. This is followed by an analysis of the data in an attempt to quantify the multipath impact upon the user receiver. A detailed theoretical analysis, taking into account fading parameters, etc., was not performed.

The Boeing Company has been investigating multipath parameters of satellite-to-aircraft links at L-band for several years. Tests have been run, and computer models have been developed. These models were compared with the test results and a close correlation with the test results was achieved. Thus, the theoretical model is considered to be quite adequate for predicting the results.

4.6.2 Multipath Parameters

The purpose of this section is to define the multipath parameters used in the subsequent discussions.

The multipath channel is a linear system and may be characterized by a time-invariant transfer function which we denote by $T_m(f, t)$. The time-invariant impulse response is denoted by $h_m(t, \zeta)$. If the transmitted signal is denoted by $Z(t)$ with transfer function $Z(f)$, then the input-output relationships corresponding to the use of $T(f, t)$ and $h(t, \zeta)$ are

$$w(t) = \int Z(f)\, T(f,t)\, e^{j2\pi ft}\, df \tag{4.6-1}$$

$$w(t) = \int Z(t-\zeta)\, h(t,\zeta)\, d\zeta \tag{4.6-2}$$

where $w(t)$ is the output signal (complex) and $Z(f)$ is the spectrum of $Z(t)$.

The transfer function $T_m(f,t)$ and the impulse response $h_m(t,\zeta)$ are Fourier transform pairs,

$$T_m(f,t) = \int h_m(t,\zeta)\, e^{j2\pi f\zeta}\, d\zeta \tag{4.6-3}$$

$$h_m(t,\zeta) = \int T_m(f,t)\, e^{j2\pi f\zeta}\, df \tag{4.6-4}$$

The width of the spectrum of a received carrier, i.e., the spectral width of $T_m(f,t)$ with f fixed, is called the Doppler spread of the channel at f_0+f. This doppler spread determines the rate of fading of the channel.

If another carrier is transmitted at a different frequency, $f_0+f+\Omega$, sufficiently close to f_0+f it will be found that the envelopes and phases of the two received carriers essentially fade in step. As the separation frequency Ω is increased, $T_m(f,t)$ and $T_m(f+\Omega,t)$ will begin to depart. The term coherence bandwidth, w_{coh}, will be used to define the frequency interval for which $T_m(f,t)$ and $T_m(f+\Omega,t)$ are 50 percent correlated.

If the spectrum $Z(f)$ of the transmitted signal occupies a bandwidth $w < w_{coh}$, then the output is given approximately by

$$w(t) \approx Z(f)\, T(0,t)\,. \tag{4.6-5}$$

That is, the channel acts as a complex multiplier $T(0,t)$, causing all the frequency components of $Z(t)$ to fluctuate in step. This is referred to as flat fading. If the input signal bandwidths exceed w_{coh}, frequency selective distortion or fading will result, i.e., not all the frequency components will fluctuate in unison.

A complete description of the channel multipath statistics is obtained from the delay Doppler scatter function, $S(\tau, \omega)$, which represents the power spectral density (PSD) of energy returned with a specified delay τ and Doppler ω. Equivalent and lower order multipath parameters are obtained via Fourier and integral operations on $S(\tau, \omega)$.

A summary of the channel parameters pertinent to this study and their mathematical relationships to $S(\tau, \omega)$ is given below.

Delay Spectrum - Power spectral density (PSD) of energy arriving at the receiver with specified delay τ:

$$Q(\tau) = \int_\omega S(\tau, \omega)\, d\omega . \tag{4.6-6}$$

Doppler Spectrum - PSD of energy arriving at the receiver with specified Doppler frequency shift ω:

$$D(\omega) = \int_\tau S(\tau, \omega)\, d\tau . \tag{4.6-7}$$

Frequency Autocorrelation Function - Complex cross-correlation between two received surface modulated carriers transmitted Ω Hz apart:

$$R(0, \Omega) = \int_\tau Q(\tau)\, e^{-j2\pi\tau\Omega}\, d\tau . \tag{4.6-8}$$

Time Autocorrelation Function - Time autocorrelation function of the received surface modulated carrier signals complex amplitude:

$$R(\zeta, 0) = \int_\omega D(\omega)\, e^{-j\omega\zeta}\, d\omega . \tag{4.6-9}$$

Tap-Gain Autocorrelation Function - Autocorrelation function of energy arriving at the receiver with specified delay:

$$Q(\tau, \zeta) = \int_\omega S(\tau, \omega)\, e^{-j\omega\zeta}\, d\omega . \tag{4.6-10}$$

Mean Square Energy - Total mean square multipath signal strength intercepted by the receive antenna:

$$\Gamma = \int_{\tau} \int_{\omega} S(\tau, \omega) \, d\tau \, d\omega \, . \tag{4.6-11}$$

Channel Parameter Spreads - The spread measure provides a compact description of the effective width of a given channel parameter. Figure 4.6-1 illustrates the definitions of the 3 dB and 10 dB measures as they pertain to $Q(\tau)$, $D(\omega)$, $|R(0, \Omega)|$, $|R(\zeta, 0)|$, and $|Q(\tau, \zeta)|$.

4.6.3 Multipath Prediction Model Description

The following section was extracted to a large extent from the Boeing report.[6]

The choice of an appropriate model for the analysis of electromagnetic surface scatter is determined almost exclusively by the roughness characteristics of the reflecting medium. Surfaces are usually classified as slightly rough, very rough, or composite, depending upon the magnitude of the height irregularities. In general, different scatter theories are utilized in each of these situations.

For th se of oceanic scatter at a frequency of 2.1 GHz, the surface will st always appear to be very rough; this implies that the following is approximately satisfied:

$$\frac{2\pi\sigma_H}{\lambda} \cos\theta_i > 1.0 \tag{4.6-12}$$

where λ = electromagnetic wavelength

σ_H = standard deviation of surface height irregularities

θ_i = incident angle of ray upon the surface as measured from the normal .

Analysis of scattering from very rough surfaces is usually developed through the physical optics tangent-plane method. Commonly called the Kirchoff approximation, this model is based upon the assumption of a locally plane surface over the distance of many wavelengths. This constraint is considered to be satisfied if the radius of curvature of the surface undulations (ρ_c) is much greater than λ, i.e.,

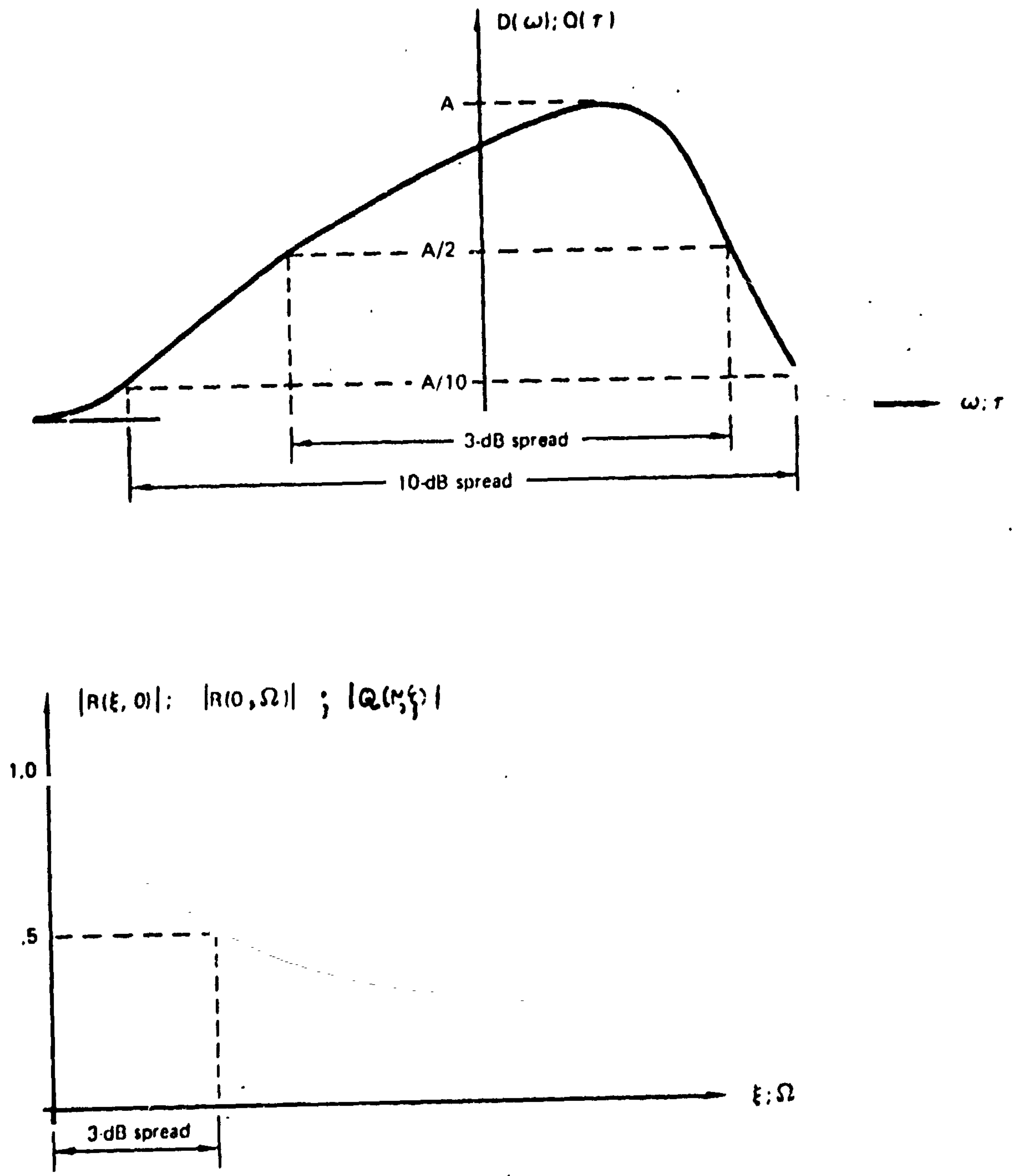

Figure 4.6-1 Spread Parameter Definitions

$$\lambda \ll 4 \rho_c \cos \theta_i . \quad (4.6\text{-}13)$$

For this study, we have employed the vector formulation of the physical optics model and are thus able to properly account for the electromagnetic polarization dependencies of each particular scattering facet on the surface. Due to the complexity of this model, it is not possible to arrive at adequate channel parameter solutions in a closed form. This is circumvented through use of a computerized technique which subdivides the spherical scatter surface into incrementally small areas and then determines the scatter cross-section (including polarization transformation factors), Doppler shift, and time delay associated with each area. The complex vector representation of the scattered signal is coupled to the receiver antenna characteristics, thereby providing an estimation of the received power from the particular surface patch. This allows the channels delay Doppler scatter function, $S(\tau, \omega)$, to be constructed. From $S(\tau, \omega)$, integral and Fourier transform steps identical to those described in Section 4.6.2 are employed to determine the channels delay spectrum, Doppler spectrum, time autocorrelation function, frequency autocorrelation function, total energy content, tap-gain autocorrelation function, and spread values of the unidimensional distributions.

4.6.4 Analysis Parameters

Predictions were generated for the following ensemble of system and sea surface parameters:

Transmitter altitude	Synchronous
Receiver altitude	200,000 meters
Receiver speed	7.8 km/sec
Receiver heading	(a) toward transmitter; great circle path, and (b) broadside to transmitter; great circle path
Transmitter polarization	RHC
Receiver polarization	Vertical, horizontal, RHC, LHC
Antenna directivities	Isotropic
Grazing angles	7°, 30°, 60°, 85°
Surface type	Sea water
Surface total RMS slope	6°

Although all combinations of the above parameters were analyzed, detailed spectra and correlation function prediction were generated only for the circular polarization receiver conditions. A coarser and correspondingly less expensive surface integration procedure was used to predict total RMS scattered energy coefficients for the vertical and horizontal polarizations. In general, one may use the LHC results to provide a relatively close estimation of the linear polarization spectra and correlation function distribution.

4.6.5 Prediction Results

As previously outlined, the multipath channels delay-Doppler scatter function, $S(\tau, \omega)$, is the basic parameter calculated by the computer model. The delay and Doppler coordinates of this function are evaluated with respect to the attributes of the return arriving from a scattering element located at the specular point. For this particular analysis, the delay bins (referred to in the following figures and tables as delay taps) were chosen to be $2\,\mu s$ in width and tap number 2 was selected to have a capture interval beginning with the specular point multipath arrival. Another way of representing the receiver is shown in Figure 4.6-2. The tap spacings are $2\mu s$. Each tap output is multiplied with a locally generated PN sequence and the mixed output is envelope detected. The integrated and sampled tap outputs provide a continuous delay signature of the scattered signal. Taps are aligned side by side with no overlap; hence, tap 1 captures no energy and the n^{th} tap will uniformly capture energy with delays falling between $2(n-1)$ and $2n$ μsec with respect to the specular point return. This τ, ω coordinate reference is related to the delay and Doppler signatures of the direct signal through parameters referred to as the channels differential delay (τ_{diff}) and differential Doppler (f_{diff}).

For the grazing angles considered in this study, we present the differential de'ay and Doppler parameters in table 4.6-1.

Channel Parameter Spread Measures

Spreads of the delay spectra, Doppler spectra, frequency autocorrelation function (coherence bandwidth), and time autocorrelation function (decorrelation time) are given in tables 4.6-2 and 4.6-3 for the RHC and LHC polarization cases, respectively. These parameters refer to the characteristics of the total multipath signal and consequently may be thought of as pertaining to the multipath effects upon a CW signal (or signals).

$Q(\tau, \zeta)$ Spreads and Tap Energy Percent Capture

Tables 4.6-4 and 4.6-5 present the $Q(\tau, \zeta)$ spreads and tap energy percent capture for the RHC and LHC polarization cases, respectively. The spread of $Q(\tau, \zeta)$ represents, in essence, the decorrelation time (0.5 correlation coefficient) of the multipath signal which is captured in tap τ.

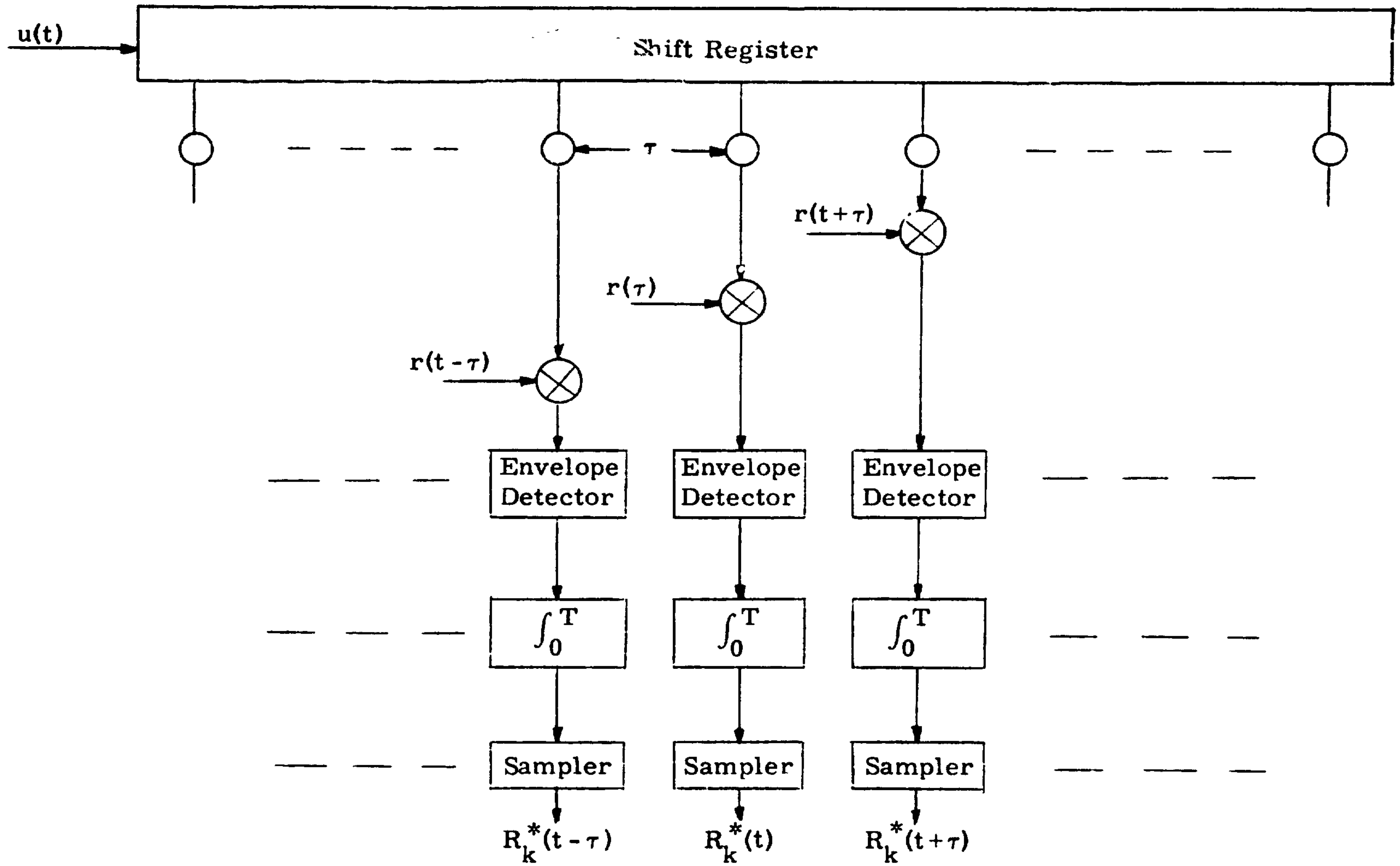

Figure 4. 6-2 Tapped Delay Line Representation of Receiver

Table 4.6-1 Differential Delay and Doppler

Grazing Angle	Differential Delay	Differential Doppler	
		Cross-Plane	In-Plane
7°	98 μs	0 Hz	2.0 kHz
30°	634 μs	0 Hz	2.9 kHz
60°	1150 μs	0 Hz	1.8 kHz
85°	1330 μs	0 Hz	0.3 kHz

Table 4.6-2 Channel Parameter Spread Measures (RHC Polarization)

Spread Measure	Grazing Angle			
	7°	30°	60°	85°
Delay (3dB)	2.1μs	8.0μs	10.0μs	41.8μs
Delay (10dB)	14.6μs	29.7μs	37.8μs	80.2μs
Coherence B.W.	37.1 KHz	18.6 KHz	16.4 KHz	9.3 KHz
Doppler (3dB) In-Plane	.25 KHz	6.1 KHz	13.6 KHz	11.9 KHz
Doppler (10dB) In-Plane	.83 KHz	11.8 KHz	24.6 KHz	26.9 KHz
Doppler (3 dB) X-Plane	2.2 KHz	7.5 KHz	17.0 KHz	30.0 KHz
Doppler (10dB) X-Plane	4.2 KHz	15.3 KHz	28.0 KHz	45.0 KHz
Decorr. Time In-Plane	8.9×10^{-4}s	6.7×10^{-5}s	3.2×10^{-5}s	2.8×10^{-5}s
Decorr. Time X-Plane	1.9×10^{-4}s	5.1×10^{-5}s	2.8×10^{-5}s	1.7×10^{-5}s

Table 4.6-3 Channel Parameter Spread Measures (LHC Polarization)

SPREAD MEASURE	GRAZING ANGLE			
	7^0	30^0	60^0	85^0
DELAY (3dB)	2.36 μs	8.1 μs	8.9 μs	8.84 μs
DELAY(10dB)	18.1 μs	28.8 μs	32.0 μs	32.4 μs
COHERENCE B.W	28.3 KHz	20.4 KHz	19.8 KHz	19.5 KHz
DOPPLER(3dB)	.341 KHz	7.5 KHz	12.5 KHz	15.6 KHz
DOPPLER(10dB)	1.21 KHz	13.7 KHz	26.3 KHz	30.9 KHz
DECORR.TIME	5.7×10^{-4}s	5.9×10^{-5}s	2.9×10^{-5}s	2.5×10^{-5}s

Table 4.6-4 $Q(\tau, \zeta)$ Spreads and Tap Energy Capture (RHC)

Tap Number	% Energy Capture	$Q(\tau,\zeta)$ (In-Plane)	$Q(\tau,\zeta)$ (X-Plane)
2	2%	.12 ms	.093 ms
3	3	.10	.054
4	3	.098	.042
5	4	.085	.035
6	4	.076	.031
7	4	.095	.028
8	5	.094	.026
9	4	.065	.023
10	4	.066	.023

Grazing Angle = 85^{0}

Receiver Polarization = RHC

Table 4.6-4 (continued)

Tap Number	% Energy Capture	$Q(\tau,\xi)$ (In-Plane)	$Q(\tau,\xi)$ (X-Plane)
2	11%	.11 ms	.095 ms
3	10	.063	.052
4	9	.048	.042
5	8	.043	.035
6	7	.039	.031
7	6	.038	.028
8	6	.034	.027
9	5	.034	.025
10	4	.034	.024

Grazing Angle = 60^{o}

Receiver Polarization = RHC

Table 4.6-4 (continued)

Tap Number	% Energy Capture	$Q(\tau,\xi)$ (In-Plane)	$Q(\tau,\xi)$ (X-Plane)
2	14%	.24 ms	.12 ms
3	12	.14	.07
4	9.4	.11	.056
5	7.9	.086	.050
6	7.7	.074	.045
7	6.0	.066	.043
8	4.9	.058	.042
9	4.4	.055	.039
10	3.6	.052	.039

Grazing Angle = 30^{0}

Receiver Polarization = RHC

Table 4.6-4 (continued)

Tap Number	% Energy Capture	$Q(\tau,\zeta)$ (In-Plane)	$Q(\tau,\zeta)$ (X-Plane)
2	32%	2.1 ms	.25 ms
3	17	1.2	.17
4	11	.82	.17
5	8	.72	.17
6	6	.57	.17
7	5	.54	.17
8	4	.45	.17
9	3	.42	.17
10	3	.38	.17

Grazing Angle = 7^{o}

Receiver Polarization = RHC

Table 4.6-5 $Q(\tau, \zeta)$ Spreads and Tap Energy Capture (LHC)

Tap Number	% Energy Capture	$Q(\tau, \zeta)$ (In-Plane)
2	14%	9.6×10^{-5}s
3	11	5.1
4	10	3.9
5	9	3.2
6	8	2.8
7	6	2.5
8	6	2.3
9	5	2.1
10	4	1.8

Grazing Angle = 85^0

Receiver Polarization = LHC

Table 4.6-5 (continued)

Tap Number	% Energy Capture	$Q(\tau,\zeta)$ (In-Plane)
2	13%	.11 ms
3	12	.061
4	10	.045
5	9	.039
6	7	.034
7	6	.030
8	6	.027
9	5	.026
10	4	.024

Grazing Angle = 60°

Receiver Polarization = LHC

Table 4.6-5 (continued)

Tap Number	% Energy Capture	$Q(\tau,\xi)$ (In-Plane)
2	15%	.25 ms
3	12	.14
4	10	.10
5	8	.085
6	8	.073
7	6	.066
8	5	.054
9	5	.053
10	4	.047

Grazing Angle = 30^{0}

Receiver Polarization = LHC

Table 4.6-5 (continued)

Tap Number	% Energy Capture	$Q(\tau,\zeta)$ (In-Plane)
2	28%	2.2 ms
3	15	1.2
4	10	.85
5	8	.80
6	6	.63
7	5	.55
8	4	.52
9	4	.49
10	3	.45

Grazing Angle = 7^{o}

Receiver Polarization = LHC

Total Mean Square Scatter Coefficient (Γ)

The parameter Γ which represents the ratio of the total multipath signal power to the direct line of sight signal level is given in figure 4.6-3. These data are given for horizontal, vertical, RHC, and LHC polarization modes of the receiving antenna. It is noted that for the LHC results, we assume the antenna polarization is RHC towards the synchronous satellite and LHC everywhere else. For the other polarization cases, the antenna is taken to have the same polarization regardless of elevation or azimuth angle.

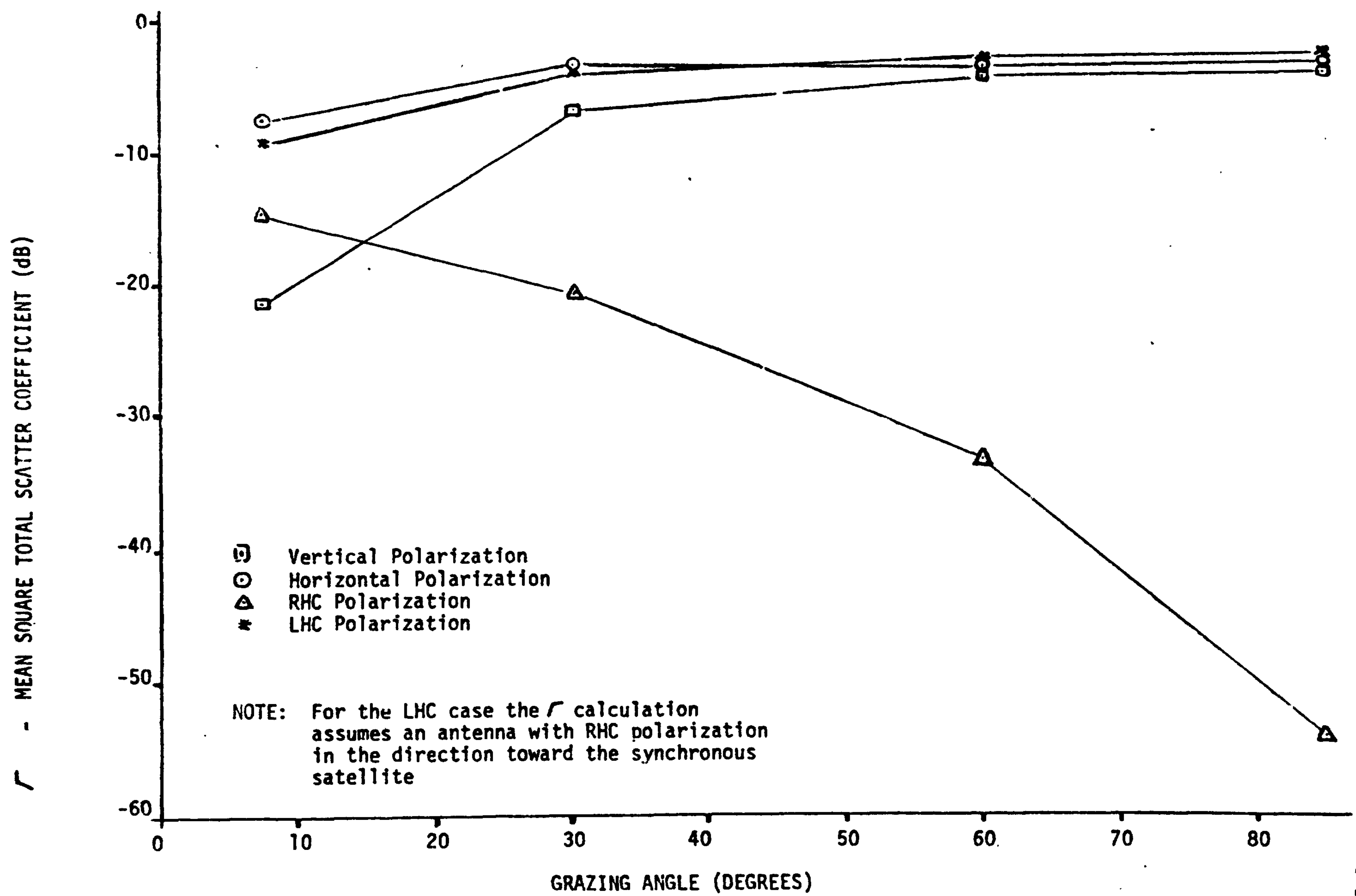

Figure 4.6-3 Relative Mean Square Total Scatter Coefficients

4.6.6 Extension of Model Predictions

The results generated for this study have direct application only to the list of system parameters delineated in Section 4.6.4. Although these parameters were chosen to represent typical TDRSS configurations and operating environments, one may desire to extend the study results to alternate altitudes and velocities of the low orbit satellite and to different sea surface RMS slope conditions. To provide this extension, we make use of: (1) Model predicted results for both the TDRSS channel and for an AEROSAT channel, and (2) Closed form solution to the scatter channel characterization.

Closed form multipath characterizations,[7,8] applicable to "very rough" surface forward scatter, have been generated for a somewhat restrictive set of surface and geometrical conditions which allow one to apply steepest descent integration techniques to the surface integral formulations. Although this procedure has a variety of shortcomings (for example, the steepest descent model predicts no polarization dependence apart from the absolute magnitude of the total scattered energy), it provides a compact description of the altitude, velocity, and surface RMS slope dependencies of the multipath signal. In particular, the dispersion of $S(\tau, \omega)$ in the delay and Doppler variables has the following approximate functional relationship to altitude (h), velocity (v), frequency (f), and RMS slope (η):

Delay Dispersion	$\alpha\ h\ \eta^2$
Doppler Dispersion*	$\alpha\ v\ f\ \eta$

Apart from the effects of f and h on the spherical earth divergence factor and the Fresnel reflection coefficient, respectively, the above parameters are predicted to have only a minor influence upon the total received signal power level. A measure of the applicability of the above

*Doppler dispersion is also very weakly dependent upon altitude.

dispersion relationships is given in table 4.6-6, where we present data pertaining to model predictions for an AEROSAT channel at 1.65 GHz and for the TDRSS channel. For both channels, sea surface and grazing angle conditions were identical (6^{o} RMS slope and 30^{o} grazing angle). The entry under the column titled, "TDRSS EXTRAP," pertains to the results extrapolated from the AEROSAT predictions via the relationship contained under column, "APPROX CLOSED FORM DEPENDENCE." In general, the extrapolated values are seen to be in fairly close accord with the actual TDRSS model predictions. However, it is also noted that the actual predictions tended to lie below the extrapolated results and, as one would expect, the data for the LHC mode provides a somewhat closer fit to the extrapolated results.

Table 4.6-6 Comparison Between Actual TDRSS and AEROSAT Extrapolated Spread Measures

SPREAD PARAMETER[1]	AEROSAT PREDICTION[2]	APPROX CLOSED FORM DEPENDENCE	TDRSS EXTRAP[3]	ACTUAL TDRSS MODEL PREDICTION[4]	ACTUAL TDRSS MODEL PREDICTION[5]
Delay (3dB)	.46 μs	h_s/h_a	9.2 μs	8.0 μs	8.1 μs
Delay(10dB)	1.76 μs	h_s/h_a	35.2 μs	29.7 μs	28.8 μs
Doppler (3dB)	188 Hz	V_s/V_a f_s/f_a	9.3 KHz	6.1 KHz	7.5 KHz
Doppler (10dB)	326 Hz	V_s/V_a f_s/f_a	16.1 KHz	11.8 KHz	13.7 KHz

1 Grazing Angle = 30^0

2 In-plane geometry (horizontal polarization) with aircraft at 10 KM altitude (h_a) flying 200 m/s (V_a); frequency of 1.65 GHz

3 In-plane geometry with low orbit satellite at 200 KM altitude (h_s) traveling at 7800 m/s (V_s); frequency of 2.1 GHz (f_s)

4 From Table 4.6-2 - RHC polarization

5 From Table 4.6-3 - LHC polarization

4.6.7 Analysis Results

The primary purpose of this analysis was to examine the multipath parameters and assess their impact upon the recommended TDRSS signal waveform and, in particular, the acquisition strategy of this waveform. The analysis is preliminary and was intended to try to cover each of the areas to the extent necessary to determine the seriousness of the multipath problem relative to the recommended signal waveform.

As can be observed from the data presented in the tables of Section 4.6.5, the multipath parameters are in most cases greatly dependent upon the antenna configuration and the orientation of the user spacecraft relative to the synchronous satellite.

The period of the 1023 chip short code, as described in Section 2, is 341 μsec. The width of the main lobe of the autocorrelation function at mid-amplitude is about 1 chip period or 334 nsec. The differential delay and differential Doppler between the direct signal and the first tap output of the multipath signal is shown in table 4.6-1 as a function of the grazing angle. The differential delay varies from 98 μsec to greater than 1300 μsec as the grazing angle increases from 7^o to 85^o. Thus, at the low grazing angles, the differential delay is such that the multipath signal falls between the main lobes of the direct signal. Hence, there is no impact to the main lobe of the direct signal and the basic problem is one of false locking to a multipath component. However, as the grazing angle increases, the differential delay increases to a point where the multipath component could overlap the main lobe and therefore result in some fading of the direct signal. The overlap is probabilistic and the intensity is a function of the reflection coefficient and the scatter spreads both in time and frequency.

The differential Doppler is a function of the relative spatial vectors of the user satellite and synchronous satellite. From the data given in table 4.6-1, the differential doppler is small enough so that most of the multipath energy in the majority of the cases will fall within the receiver

IF bandwidth. In this preliminary analysis, all of the multipath energy is assumed to fall within the IF bandwidth.

Tables 4.6-4 and 4.6-5 summarize the tap energy percent capture for the RHC and LHC polarization cases, respectively. The energy spread is given over 9 taps or an 18 μsec interval. The energy for most of the cases is spread beyond these 9 taps as is seen from the 10 dB delay spread given in tables 4.6-2 and 4.6-3. However, except for high grazing angles, most of the energy is concentrated about the first few taps. A cumulative plot of the multipath energy capture as a function of time is given in figures 4.6-4 and 4.6-5 for the RHC and LHC cases, respectively. The results are plotted with elevation angle as a parameter. The mean square scatter coefficient is plotted as a function of grazing angle in figure 4.6-3 for several antenna polarization configurations. The scatter coefficient Γ is a measure of the total reflected energy captured in frequency and time and is given in dB below the direct signal.

Table 4.6-7 summarizes some of this data pertinent to the analysis under consideration. The reflection coefficient is shown versus elevation angle for the RHC and LHC antennas. The percent energy captured in 2 μsec by the tap with the largest energy captured is also shown as a function of elevation angle. For the TDRS application, we are interested in the energy captured within a single tap of its 3 Mcps signal or 0.33 μsec. For each of the cases, this was determined from figures 4.6-4 and 4.6-5 and is also given in table 4.6-7. Thus, knowing the relative total reflected energy and knowing the percentage of that energy which falls within a single chip time window, we can compute the minimum signal-to-interference level, assuming we refer to the multipath as interference. These parameters are also shown in table 4.6-7.

The significance of the signal-to-multipath interference parameter is shown in figure 4.6-6. This figure illustrates the allowable dynamic range of the received signal level above threshold before the possibility exists of locking onto the multipath signal. There are two underlying assumptions. The first assumption is that there is no differential antenna

K•E 10 X 10 TO ½ INCH 7 X 10 INCHES KEUFFEL & ESSER CO. MADE IN U.S.A. 46 1322

Figure 4. 6-4 Cumulative Multipath Energy Capture as a Function of Time

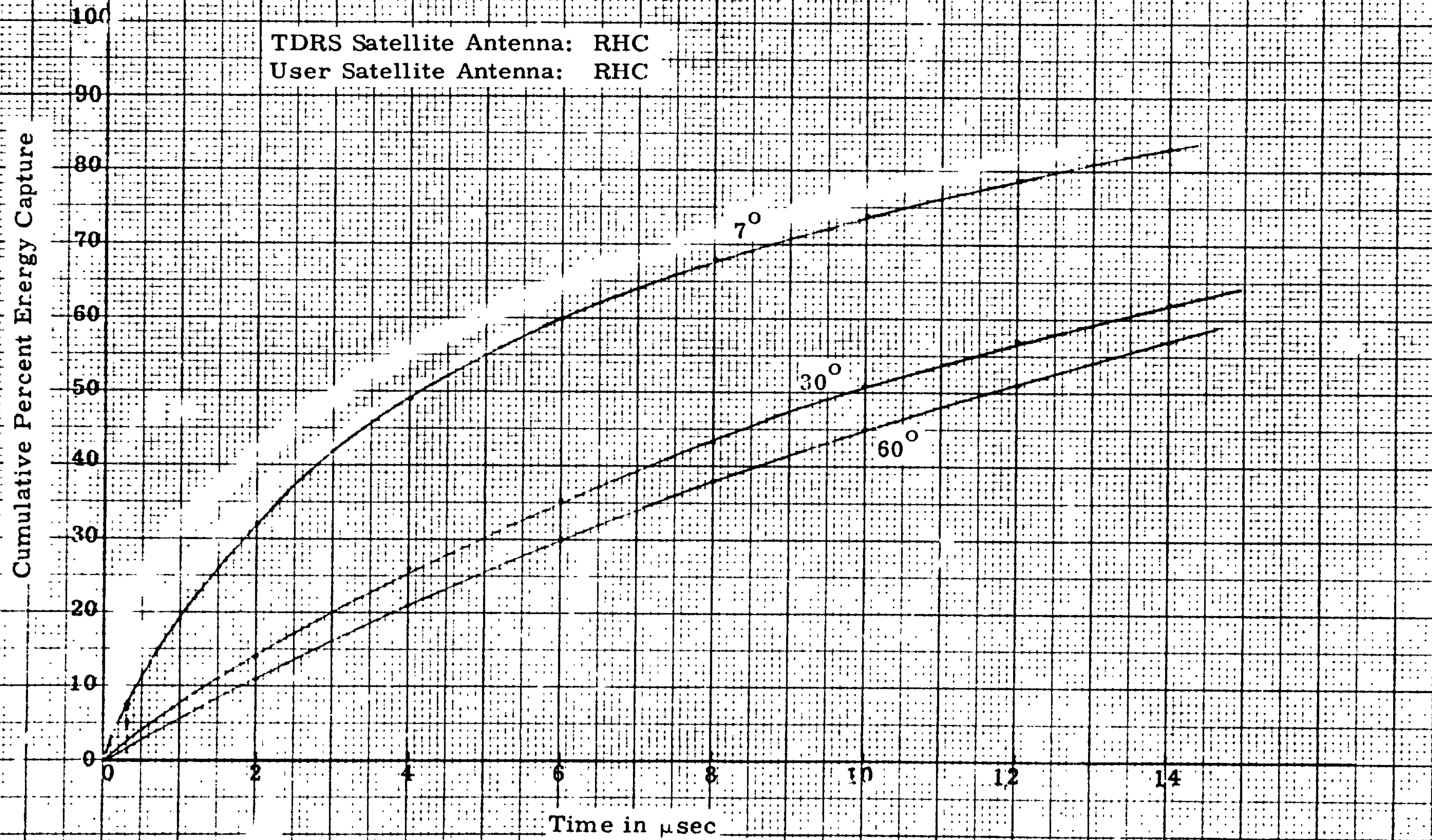

K•E 10 X 10 TO ½ INCH 7 X 10 INCHES KEUFFEL & ESSER CO MADE IN U.S.A. 46 1322

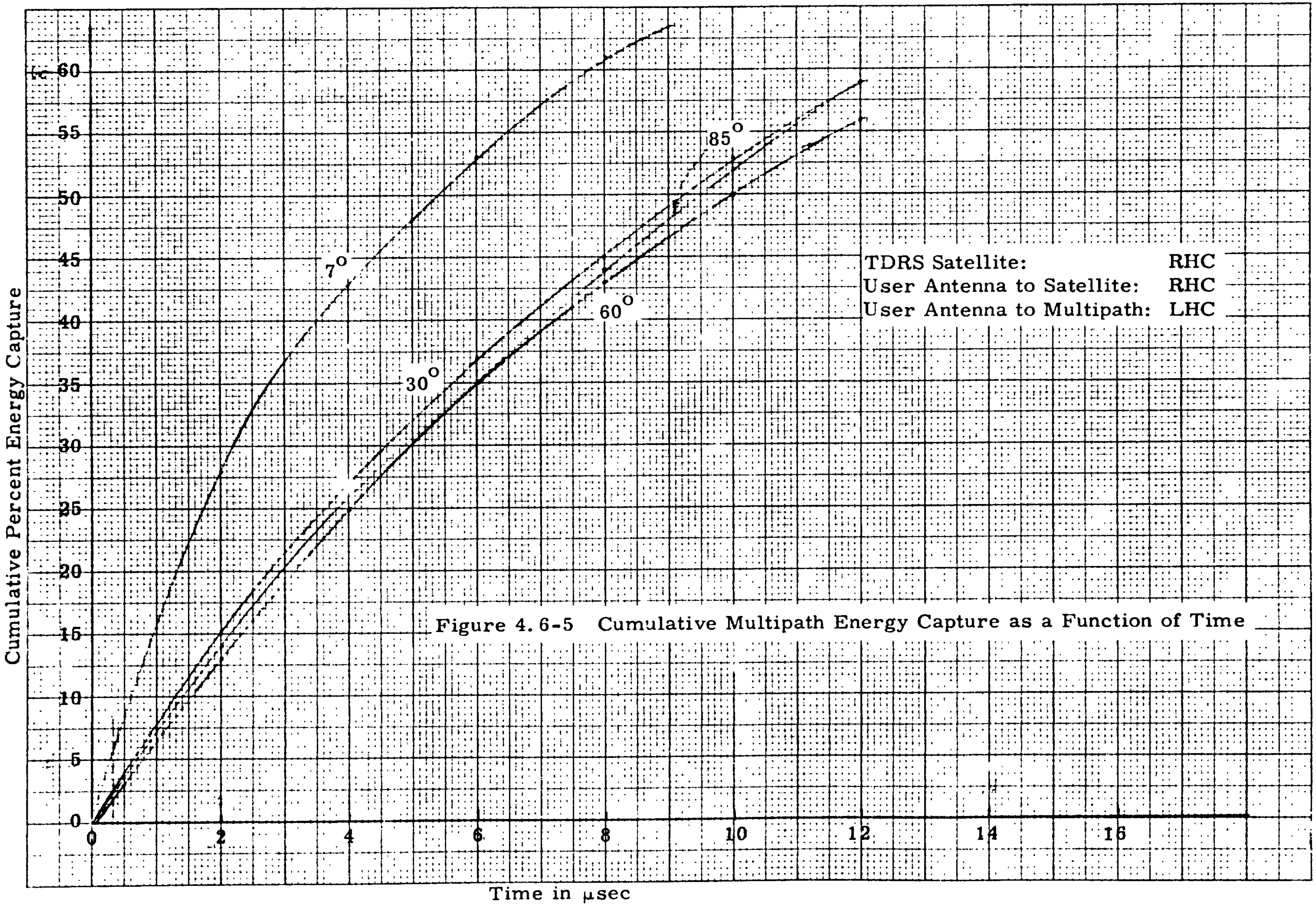

Figure 4.6-5 Cumulative Multipath Energy Capture as a Function of Time

Table 4.6-7 Multipath Interference Parameters (IP) vs. Elevation Angle (EA)

In-Plane/Cross-Plane

IP / EA	RHC				LHC to Multipath, RHC to Satellite			
	Γ (dB)	% Energy in 2 μs Max Tap	% Energy in 0.33 μs Tap	TDRS S/I (dB)	Γ (dB)	% Energy in 2 μs Max Tap	% Energy in 0.33 μs Tap	TDRS S/I (dB)
7^{o}	-14.3	32	7.5	-25.5	-9.1	28	6	-21.3
30^{o}	-20.3	14	3	-35.5	-3.7	15	3	-18.9
60^{o}	-33	11	2	-50	-3.0	13	2	-20
85^{o}	-54	5	0.833	-76.7	-3.0	14	2.5	-19

K•E 10 X 10 TO ½ INCH 7 X 10 INCHES KEUFFEL & ESSER CO. MADE IN U.S.A. 46 1320

Figure 4.6-6 Allowable Dynamic Range of Signal for Various Conditions Versus Elevation Angle (No Differential Antenna Gain Between Multipath and Direct Signal)

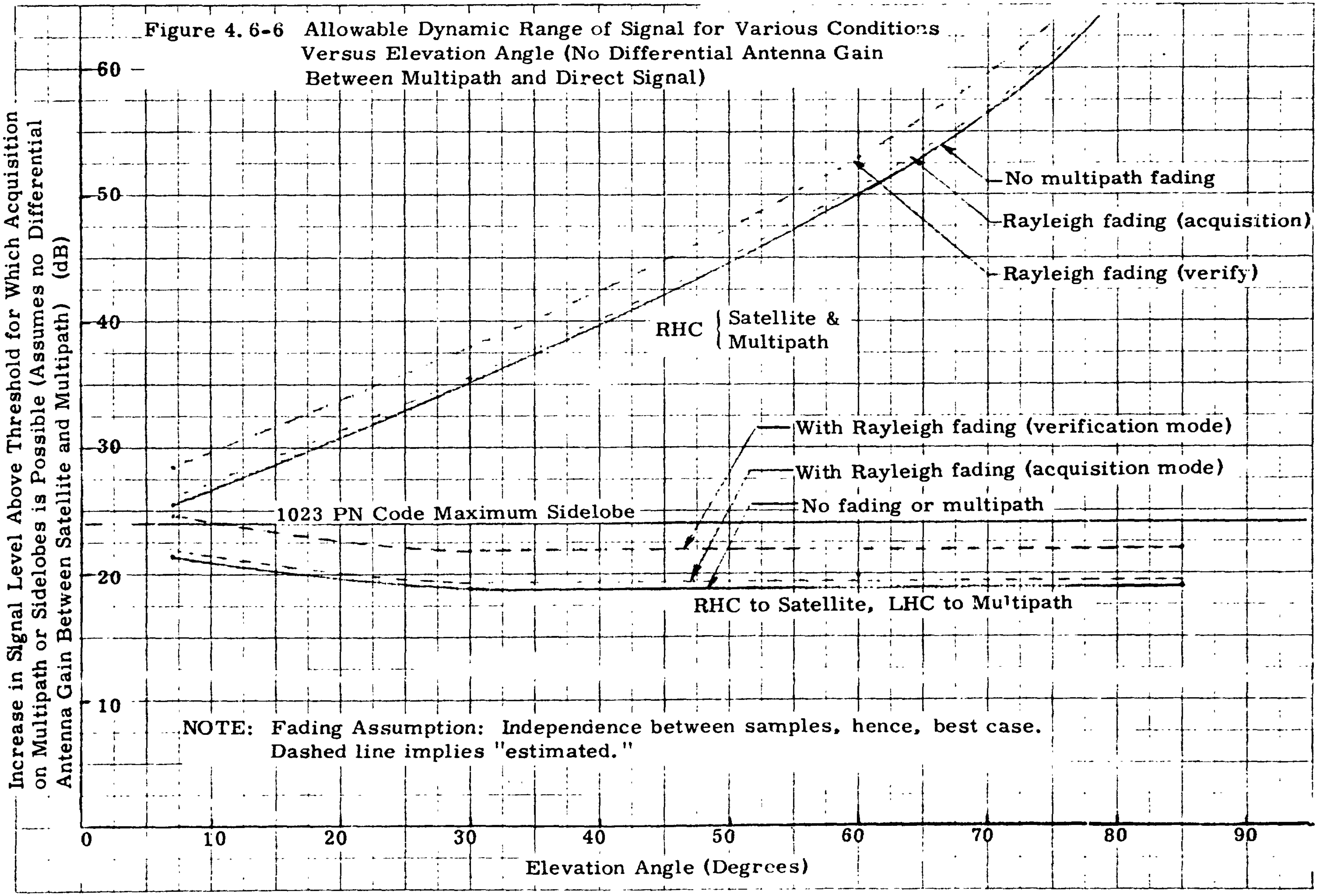

NOTE: Fading Assumption: Independence between samples, hence, best case. Dashed line implies "estimated."

gain between the satellite or direct signal and the multipath signal. The second assumption is that the multipath signal cannot be acquired if its average signal-to-noise ratio is below threshold.

Another factor which impacts this dynamic range analysis relative to the multipath interference is the time spread factor associated with the individual taps. This parameter is denoted by $Q(\tau, \zeta)$ and is given for the various antenna configurations in tables 4.6-4 and 4.6-5. $Q(\tau, \zeta)$ is the time spread for which there is a 0.5 correlation between samples. If we assume a Gaussian shaped Doppler spectra, then the Doppler spread or fading bandwidth associated with a particular individual tap position is given by

$$\sigma\ (\mathrm{Hz}) = \frac{1}{\pi\, Q(\tau, \zeta)} . \qquad (4.6\text{-}14)$$

Using this approach, the estimated fading bandwidth is plotted in figure 4.6-7 for the RHC antenna configuration as a function of elevation angle. The fading bandwidth is seen to vary from 100 Hz at low elevation angles to greater than 3 kHz at high elevation angles. The LHC case was not plotted since it follows very closely the RHC case, which is plotted. The significance of the fading bandwidth is that it determines the degree of correlation between samples taken at the output of the envelope detector during acquisition. Clearly, as the fading rate increases, the successive samples are less correlated and hence a larger signal-to-noise ratio is required to achieve a given detection probability.

From a system point of view, the more difficult it is to acquire a multipath signal, the more desirable the situation. Hence, the best case is when the samples are independent and the effect is as though the multipath component is Rayleigh fading. By making the Rayleigh fading assumption, the increase in the allowable dynamic range is approximately that shown by the dashed lines in figure 4.6-6. The results are plotted for both the acquisition and verify modes in accord with the parameters assumed in Section 4.5.

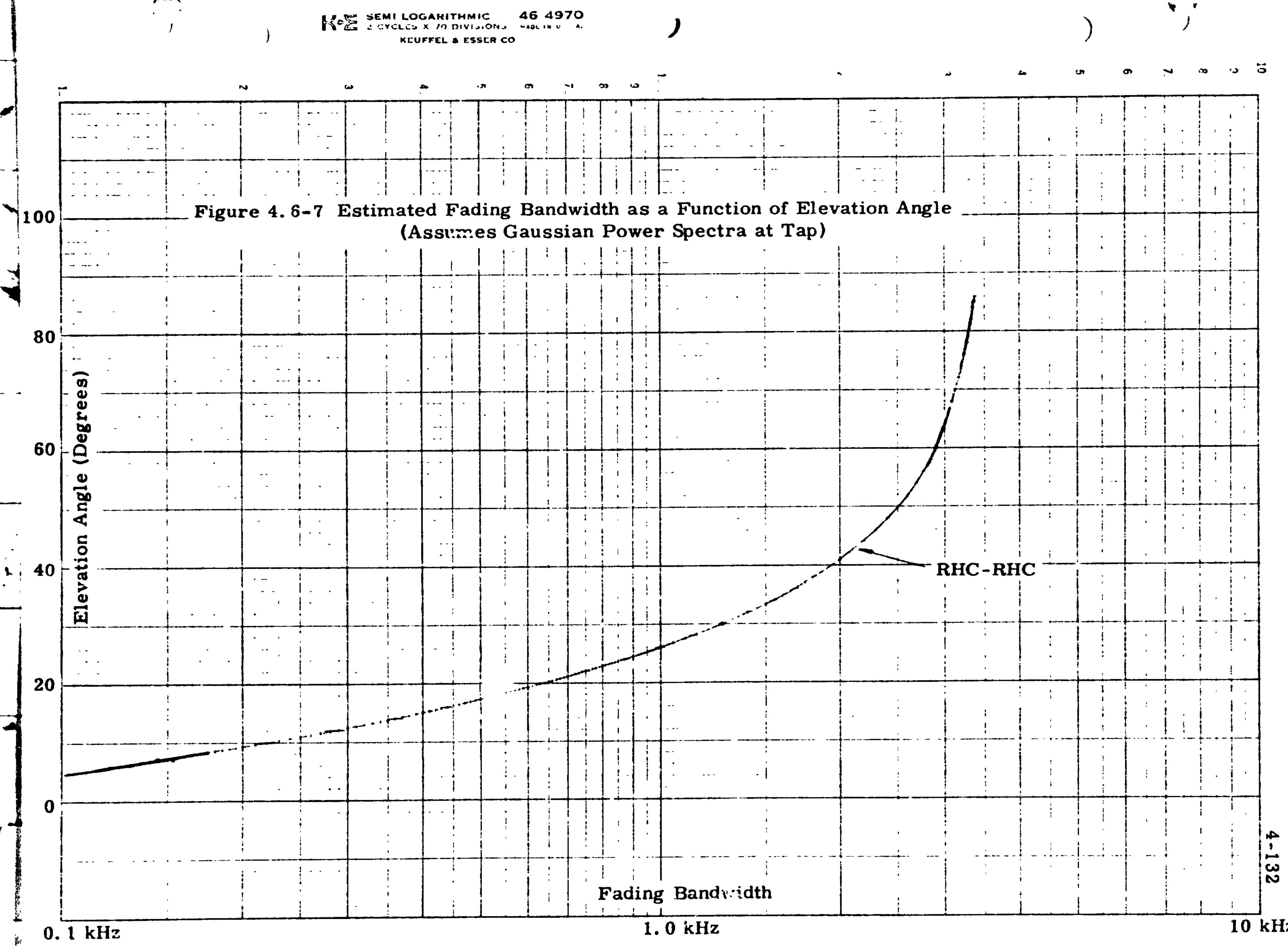

Figure 4.6-7 Estimated Fading Bandwidth as a Function of Elevation Angle
(Assumes Gaussian Power Spectra at Tap)

The dynamic range is least with a minimum value of 18.5 dB when the user receive antenna is RHC toward the satellite and LHC toward the multipath.

A specific case of figure 4.6-6 is shown in figure 4.6-8. In this case, a user antenna gain of -9 dB is assumed in the direction of the TDRS satellite and a +3 dB gain is assumed in the direction of the multipath signal. For this case, with the RHC to the satellite and LHC to the multipath, there is slightly more than 6 dB of margin. For the case when the antenna is RHC toward both the satellite and multipath, the margin is much more favorable.

A summary of maximum signal dynamic range against multipath for several elevation angles and antenna configurations is shown in table 4.6-8. The entries in this table assume the worst case condition in that the multipath signal remains constant throughout the duration of the acquisition test.

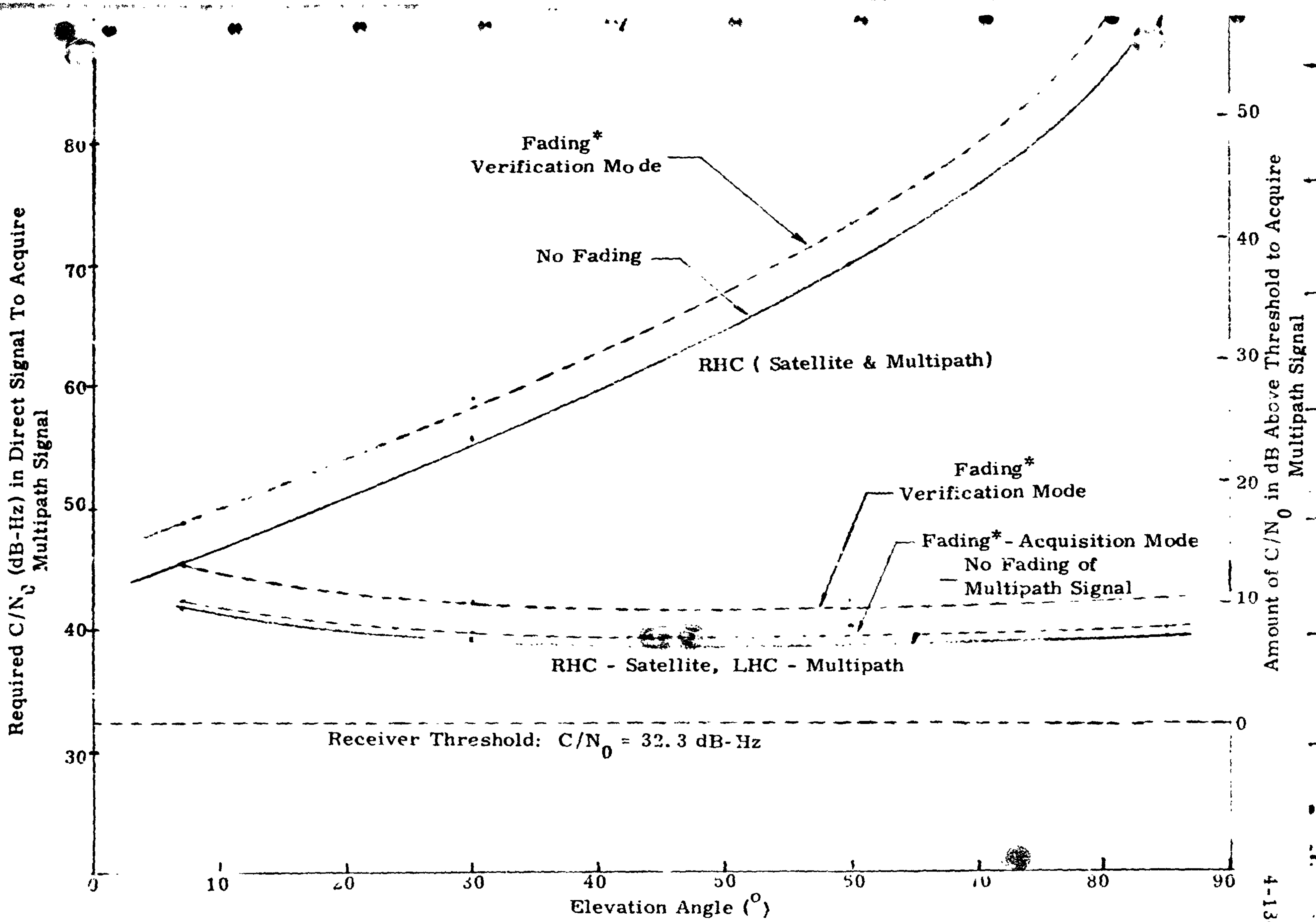

Figure 4.6-8 Required C/N_0 in Direct Signal to Lock Onto Multipath Signal When User Gain is -9 dB to TDRS Satellite and +3 dB to Multipath

Table 4.6-8 Maximum Signal Level Above Threshold to Avoid Multipath Acquisition Versus Elevation Angle for Several Antenna Configurations (assumes no multipath fading)

Maximum Dynamic Range / Elevation Angle	Omni-Directional Antenna*		Maximum Gain of Directional Antenna - Sidelobes Looking at Multipath 10 dB Down		No Differential Antenna Gain Between Direct Signal and Multipath	
	RHC: Satellite Multipath	RHC: Satellite LHC: Multipath	RHC: Satellite Multipath	RHC: Satellite LHC: Multipath	RHC: Satellite Multipath	RHC: Satellite LHC: Multipath
7^{o}	13.5 dB	9.3 dB	35.5 dB	31.3 dB	25.5 dB	21.3 dB
30^{o}	23.5 dB	6.9 dB	45.5 dB	28.9 dB	35.5 dB	18.9 dB
60^{o}	38 dB	8 dB	60 dB	30 dB	50 dB	20 dB
85^{o}	64.7 dB	7 dB	86.7 dB	29 dB	76.7 dB	19 dB

*Omni-Antenna: -9 dB Direct Signal
+3 dB Multipath Signal

4.6.8 Direct Signal Verification

There may well be conditions for which the multipath signal level exceeds the threshold, thereby opening the opportunity for the receiver to lock up to the multipath signal. One potential technique for avoiding locking to a multipath signal is to advance the local clock by an amount exceeding the maximum differential path delay after the first indication of acquisition. Search could then be continued perhaps at a slower rate and the loops enabled when the second indication of acquisition occurs. However, for this approach to work, the PN code period must exceed at least twice the maximum multipath delay. This is not the case for the short code as was shown in Section 4.6.7. The long code in quadrature with the short code could potentially be used to resolve the direct signal from the multipath. The difficulty in this case is that the maximum multipath delay is 13 msec for a 2000 km circular user orbit. At a 3 Mcps PN rate, the receiver must search over 39,000 PN chips to resolve the direct signal. At threshold for the long code using a sequential search strategy, it would require 3 minutes to search through this uncertainty region which is an excessive amount of time.

At the conclusion of short code acquisition the code tracking loop is enabled. When PN lock is indicated carrier acquisition is initiated. Normally carrier lock will occur within some prescribed period of time which is short compared to the short code acquisition time. One of the considerations is whether it is possible to code lock and carrier lock onto a multipath signal. Due to the diffuse nature of the multipath signal the cross-correlation function would tend to be smeared thus precluding the locking onto a stable point. Hence, PN code lock would not be achieved and the algorithm would return to the initial acquisition mode. If code lock is attained by the multipath signal, acquisition of the desired signal is precluded. One possible method of eliminating this problem is through the carrier lock loop. We will just briefly consider this possibility. To achieve carrier lock, a circuit is used to sweep the VCO over the frequency uncertainty range. The bandwidth of the carrier tracking loop is nominally 32 Hz. The primary consideration is whether it is possible to carrier lock onto a multipath signal. The multipath signal as discussed above consists of a large composit of reflected signals phase-shifted and frequency-shifted. The composite waveform is spread in frequency and time.

If we neglect the frequency spreading of the scattered signal, we can write the received multipath signal as

$$r(t) = \sum_{i=1}^{N} a_i(t-\tau_i)\, d(t-\tau_i) \cos(\omega_c t + \theta_i) + n(t) \qquad (4.6\text{-}15)$$

where $a_i(t-\tau_i)$ is the amplitude of the i^{th} reflected signal with relative delay τ_i. The amplitude has Rayleigh statistics. The parameter $d(t-\tau_i)$ represents the chip polarity and takes the value of either plus or minus one. The phase angle θ_i is uniformly distributed between 0 and π. The value n(t) is the additive Gaussian noise.

If we assume that the delay lock loop is noncoherently tracking the chip sequence, then the output of the despreader can be written as

$$Z(t) = a_j(t) \cos(\omega_{IF}(t) + \theta_j) + n(t) + m(t) \qquad (4.6\text{-}16)$$

where the delay lock loop has locked onto the j^{th} reflected multipath signal. Typically, one would anticipate that it would lock onto the largest signal which, for most elevation angles, is the earliest returned signal. The additive noise term m(t) is the cross-correlation of the local PN reference with the N-1 multipath signals that are out of chip synch with the j^{th} signal. Because of the processing gain of the receiver, this term appears as an additional noise factor.

If the carrier loop is to lock cnto the multipath signal, then it must lock to Z(t) above. We will briefly consider the possibility of this occurring. First of all, the amplitude is Rayleigh fading and the phase θ_j which the carrier lock loop must track is uniformly distributed between 0 and 2π. We will consider two effects. The first is the signal-to-noise ratio in the loop bandwidth due to the multipath signal and the other is the fading bandwidth relative to the loop bandwidth.

We will assume that a signal-to-noise ratio of 10 dB is required in the loop bandwidth to give a lock indication. From table 4.6-8, we see that, at an elevation angle of 7°, the average reflected signal is 21 dB below the direct signal in the tap with the largest output. This is then the dynamic range which the direct signal can have so that, under the best conditions, the multipath would be below the carrier loop lock threshold. This dynamic range value changes, of course, as the antenna gain relative to the satellite and multipath varies. The second factor is that the code tracked multipath signal is fluctuating in amplitude and phase. The rate of these fluctuations is a function of the elevation angle (cf. figure 4.6-7). At a 7° elevation angle, this fading banawidth is approximately 150 Hz which is substantially larger than the 32 Hz loop bandwidth. In addition, as the elevation angle increases the fading bandwidth increases. Hence, coupling these two factors together, that is, the fading bandwidth which exceeds the loop bandwidth and the signal-to-noise ratio in the loop bandwidth, one would conclude that only under very unusual circumstances would the carrier loop be able to track the phase of the multipath signal. Therefore, the second check on having acquired a multipath signal is the subsequent inability to achieve carrier lock. To test for carrier lock the output of the coherent amplitude detector (CAD) can be compared with a threshold. If within a predetermined period of time, the threshold is not exceeded, then either a false acquisition or multipath acquisition of the short code is assumed. The receiver will then automatically unlock the short code loop and a new short code search would be initiated. Another multipath rejection technique was suggested by Mr. L. Deerkoski.[9] This technique will probably only work successfully if the long code is noncoherently detected. Coherent detection was recommended above for the long code. This was primarily due to the excessive acquisition time required for noncoherent sequential acquisition of the long code. However, by the use of multiple filters this time could be reduced considerably as shown in table 4.4-2.

The proposed technique takes advantage of the time spread of the multipath signal. Based on the Boeing data, the multipath energy is smeared over a number of chips. The extent to which this is true can be seen from figures 4.6-4 and 4.6-5. The rolloff in energy for most elevation angles is quite slow for 5 or more PN chips. This is in contrast to the PN correlation function which approaches zero when the received and reference codes are out of synchronism by one PN chip.

The suggestion is that this multipath time smear be used to discriminate the multipath from the direct signal. The concept could be implemented in the long code detection strategy by adding a multipath detection test subsequent to initial long code acquisition and verification. The multipath detection test could involve offsetting the long code by 2 PN chips relative to the synch position and determining whether correlation is within 10 dB of the initial long code synch correlation. If it is within the 10 dB or some threshold level to be determined, then the time spread of the arriving signal must be present to identify it as the multipath signal. If this is the case, the receiver would then unlock the short code loop and a new short code search would be initiated. If the multipath detection test fails, then time spread is absent and direct signal acquisition is declared.

With this technique, a direct signal verification step would follow the long code verification. The overall acquisition strategy would then take the following form.

Step 1	Short Code Acquisition
Step 2	Short Code Verification
Step 3	PN Code Tracking with Multipath Test
Step 4	Carrier Lock Search with Coherent Amplitude Detector Multipath Test
Step 5	Long Code Acquisition
Step 6	Long Code Verification
Step 7	Direct Signal Verification

To prevent the possibility of multipath capture of the PN tracking receiver, the PN code tracking circuit should be switched to the long code subsequent to direct signal resolution. Since the long code acquisition mode requires searching 128 PN code cells on the average, the addition of another cell for direct signal verification has a very small impact on the long code acquisition time. The entire acquisition process is summarized in the flow chart of figure 4.6-9.

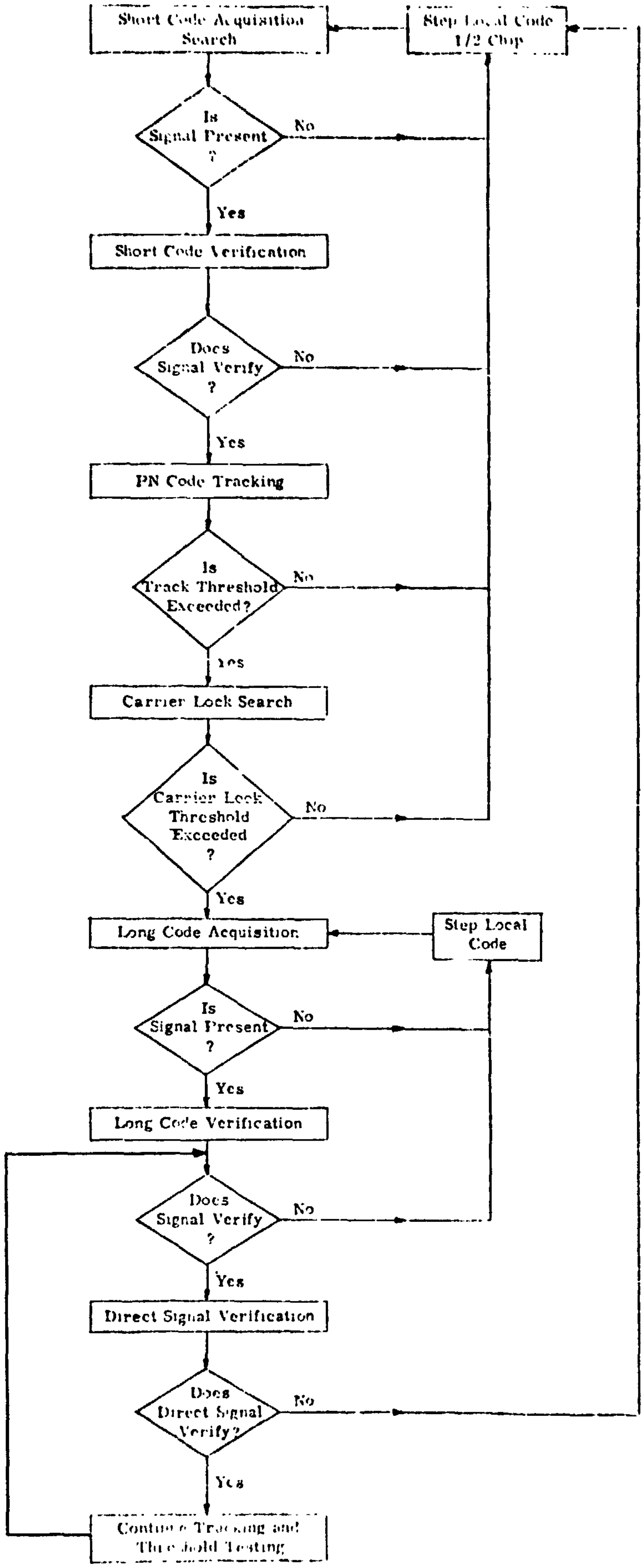

Figure 4.6-9. Summary of Forward Link Acquisition Algorithm

4.7 References

1. R. Dixon, R. Gold, and F. Kaiser, "Interim Report - TDRSS Telecommunications System PN Code Analysis," Contract NAS-22546, Robert Gold Associates, April 30, 1976.

2. A. Wald and J. Wolfowitz, "Optimum Character of the Sequential Probability Ratio Test," Ann. Math. Stat., 19:326, 1948.

3. A. Wald, Sequential Analysis, Wiley, New York, 1947.

4. DiFranco and Rubin, Radar Detection, Prentice-Hall, 1968.

5. M. B. Marcus and P. Swerling, "Sequential Detection in Radar with Multiple Resolution Circuits," IRE Transactions on Information Theory, IT-8 (3), pp. 237-245, April 1962.

6. Allan D. Thompson, "Multipath Characteristics of the Oceanic Tracking and Data Relay Satellite System (TDRSS) Channel," Boeing Commercial Airplane Company, April 15, 1976.

7. S. H. Durrani and H. Staras, "Multipath Problems in Communication Between Spacecraft and Stationary Satellite," RCA Review, March 1968.

8. A. J. Mallincrodt, "Propagation Error," Unpublished UCLA Short Course notes: Satellite Based Navigation, Traffic Control and Communications to Mobile Terminals, October 1969.

9. L. F. Deerkoski, "Direct Signal Resolution for TDRSS Alternate Signal Parameters," Technical Memo, April 16, 1976.

5.0 CODE GENERATION TECHNIQUES FOR TDRS

5.1 Introduction

The purpose of coding transmissions in the TDRSS is to achieve signals which satisfy flux density restrictions imposed by the International Radio Advisory Committee (IRAC), to facilitate rapid signal acquisition, and to achieve multiplexing capability in the multiple access service categories. These objectives are achieved by means of pseudo random codes which, when used to modulate the system waveforms, result in wideband low power density transmissions. The design of special configurations of PN codes facilitates rapid signal acquisition techniques, and the generation of orthogonal or pseudo orthogonal code structures aids in the achievement of system multiplexing capability.

The main source of the binary sequences which are used as the encoding mechanism to implement the coded signals are the linear (shift register) sequences. This class of sequences is easily generated at the required chipping rate with feedback shift register devices; it is amenable to mathematical analysis and it has been shown to have those characteristics which provide the resultant encoded signals with the desired characteristics outlined in the above paragraph.

Other classes of codes, such as primitive root codes and nonlinear binary sequences, may be used as signal encoding devices but, in general, these classes are more difficult to generate and analyze and do not perform as well as the classes of linear binary sequences.

In this section, we present techniques for the generation of encoding sequences which will achieve the TDRSS signal characteristics stated above and employ these techniques to generate code families having the desired properties.

5.2 Some Remarks on Code Tables

A linear shift register code generator is characterized by the number of its shift register stages and its feedback configuration. This information is equivalent to specifying an irreducible polynomial with binary coefficients whose degree is equal to the number of stages in the shift register (Figure 5.2-1). The correspondence between linear feedback shift registers and binary polynomials has been well documented[1,2] and it has been shown that the properties of the sequences generated by the shift register are determined by the algebraic properties of its corresponding binary polynomial.

Many tables of irreducible binary polynomials have been compiled[2-5] and these serve as useful design tools for the configuration of feedback shift registers which will generate linear binary code sequences having specified properties. However useful these tables of irreducible polynomials may be, no one table or even all available tables used together are adequate for the complete design task. In this section, we explain the use of the tables of irreducible polynomials, discuss the advantages and deficiencies of specific tables, and present supplementary techniques which provide the needed information for code generator design which is not available in currently available tables.

The tables by Marsh[3] list all irreducible binary polynomials to degree 19 and the period of the sequences generated by the shift register corresponding to each polynomial. (All phase distinct sequences generated by a linear shift register corresponding to an irreducible polynomial have the same period.) Thus, these tables may be used to generate, for example, maximal linear PN sequences up to period $2^{19}-1$. Since there is no way to determine larger degree irreducible polynomials from those of smaller degree, other tables must be used for PN codes of period exceeding $2^{19}-1$.

A more important deficiency of Marsh's tables concerns the relationship between the different irreducible polynomials of a given degree and hence between the binary coding sequences generated by the corresponding

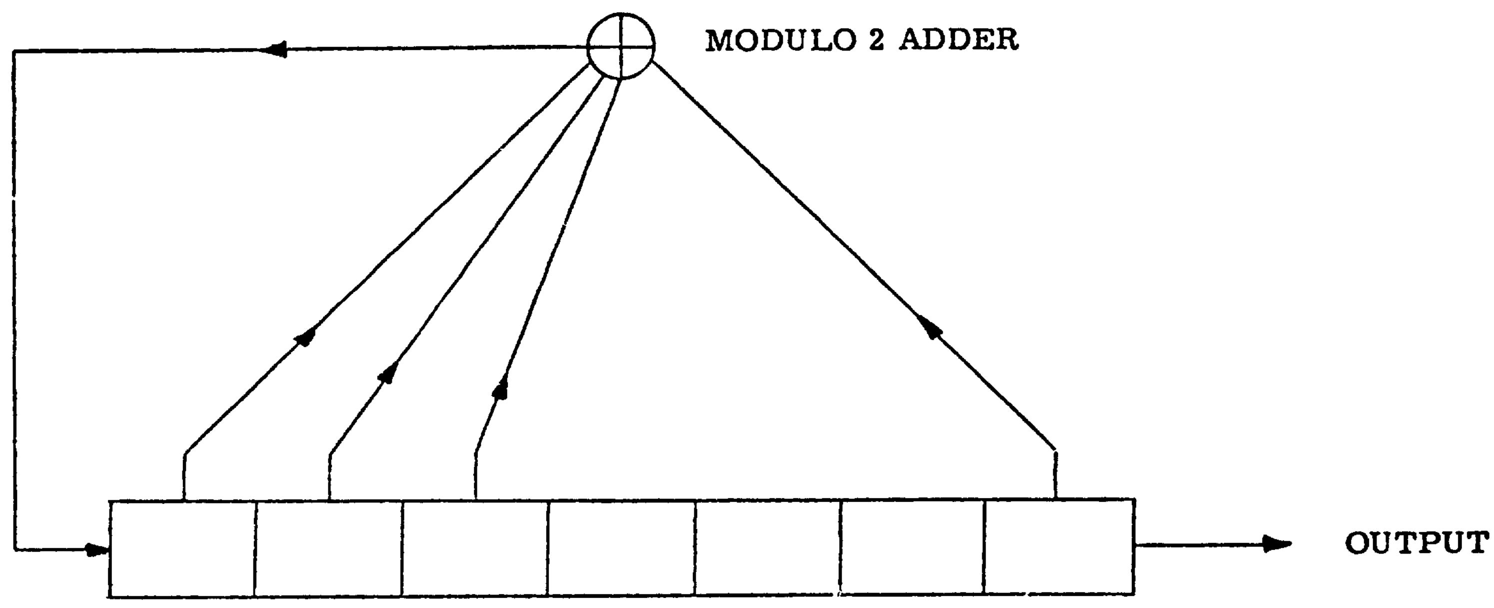

$$1 + 1\cdot X + 1\cdot X^2 + 1\cdot X^3 + 0\cdot X^4 + 0\cdot X^5 + 0\cdot X^6 + 1\cdot X^7$$

$\overbrace{1\ 1\ 1}^{7}\quad \overbrace{1\ 0\ 0}^{1}\quad \overbrace{0\ 1\ 0}^{2}$ BINARY REPRESENTATION

2 1 7 OCTAL TABULAR LISTING

Figure 5.2-1. Linear Feedback Shift Register and its Associated Polynomial shift registers. Taken individually, one maximal linear sequence is indistinguishable from another of the same period with respect to most of its basic properties and thus there is generally no advantage or disadvantage in choosing one such sequence over any other when such a sequence is used by itself in a particular communication system. However, the relationship between two or more maximal linear sequences of the same period is strongly dependent upon the particular set of sequences chosen and the manner in which such sequences interact (e.g., their cross correlation function) may strongly affect the performance of systems in which such sets of codes are employed.

Marsh's tables provide no means of distinguishing between irreducible polynomials which correspond to linear sequences of the same period. This important defect is supplied in part by the tables of irreducible polynomials published by Peterson.(4) In these tables, each irreducible polynomial and the relationship between the polynomials is characterized by identifying the roots of the polynomials. Thus, in later work, when a particular pair of binary polynomials is specified as corresponding to linear feedback shift registers which generate maximal PN sequences having particularly desirable properties with respect to one another, this polynomial pair is described from the table of irreducible polynomials by specifying the roots of each polynomial as listed in the table. A procedure requiring the selection of particular sets of polynomials of a given degree from the tabular listing will, in general, require a complete listing of the irreducible polynomials of that degree. Peterson's tables provide a complete listing of irreducible polynomials and their roots up to degree 16 and partial listings to degree 34. A complete listing of irreducible polynomials of degree 17 and degree 31 would require 7,710 and 69,273,666 entries, respectively. Thus, for example, a pair of 18th degree binary polynomials which generate optimum codes for the TDRSS multiple access service category are specified by their roots 1 and 1025, as listed in Peterson's tables. The first polynomial is present but the latter is not included in the incomplete tabular listing of irreducible polynomials.

Gold[2] has compiled a table of maximal polynomials to degree 13, which also identify the roots of the listed polynomials in the same manner as do Peterson's tables. In addition, Gold's tables list the cross correlation function of the maximal PN sequences generated by the listed polynomials. These tables are thus extremely useful in selecting sets of maximal sequences which are most nearly orthogonal. When one maximal polynomial of a given degree is known, then all irreducible polynomials of this degree may be readily computed by a variety of known techniques,[2] i.e., the table of irreducible polynomials may be compiled and their characterizing roots identified. However, there is no known technique for the direct computation of a maximal polynomial of a given degree and, hence, the production of an initial such polynomial must be largely a matter of trial and error. In this connection, Bradford[5] has published tables which list selected maximal polynomials to degree 58. No identification of these polynomials by means of their roots is provided. Watson[6] has published a list consisting of one maximal polynomial of each degree between 2 and 100 which, for most applications, solves the problem of finding an initial maximal polynomial. A summary of available tables discussed herein is provided in Figure 5.2-2.

	IRREDUCIBLE POLYNOMIALS	NUMBER OF MAXIMALS	DEGREE	POLYNOMIAL ROOTS	CORRELATION FUNCTION OF SEQUENCES
MARSH (1957)	YES	ALL	19	NO	NO
PETERSON (1961)	YES	ALL	16	YES	NO
		PARTIAL	17 - 34		
WATSON (1961)	NO	1	100	NO	NO
GOLD (1964)	NO	ALL	13	YES	YES
BRADFORD (1965)	NO	PARTIAL	58	NO	NO

Figure 5.2-2. Description of Available Tables of Binary Polynomials

5.3 Preferred Pairs of Linear PN Codes

Gold[2] has shown that the relationship between PN codes corresponding to irreducible polynomials of the same degree is not homogeneous and that, for example, a given set of maximal PN codes may be more nearly orthogonal than another set of such codes of the same period. In (7), Gold introduced the notion of a preferred pair of irreducible polynomials and gave the criteria in terms of their roots for specifying such pairs. A preferred pair of irreducible polynomials is one such that the corresponding linear PN sequences have minimal cross-correlation function. Thus, for example, for degree 12 the maximum value for the cross-correlation function for maximal PN sequences corresponding to the pair of polynomials (10123, 10737) is $\theta = 1407$, while the maximum cross-correlation value corresponding to the preferred pair of polynomials (10123, 14501) is $\theta = 127$, the difference between the two cases being 21 dB. A comparison of the cross-correlation function between the maximal PN sequences generated by a preferred pair and the worst case polynomial pair for polynomials to degree 13 is given in Figure 5.3-1.

A preferred pair of polynomials corresponding to a pair of feedback shift registers which generate binary PN sequences with minimal correlation is determined by specifying the roots of each of the polynomials of the pair. If $\alpha^1 \equiv 1$ is a root of any maximal polynomial of degree n, then the other member of the pair is the polynomial $\alpha^{2^k+1} \equiv 2^k+1$ (any k) for polynomials of odd degree and $\alpha^{2^{(n+2)/2}+1} \equiv 2^{(n+2)/2}+1$ for polynomials of even degree. The maximum value of the cross-correlation sidelobes for the sequences corresponding to the preferred pair are then shown to be $2^{(n+1)/2}+1$ for n odd and $2^{(n+2)/2}+1$ for n even.

The TDRSS communication links will use a code pair consisting of two PN codes, one modulating the I channel and one modulating the Q channel of a staggered quadriphase PN modulation technique. In order to achieve maximum isolation between these channels, it is recommended

DEGREE	PERIOD	θ SIDE LOBE WORST CASE	θ SIDE LOBE PREFERRED PAIR	DIFFERENCE (DB)
5	31	11	9	1.7
6	63	23	15	3.7
7	127	41	17	7.6
8	255	95	31	9.7
9	511	113	33	10.7
10	1023	383	63	15.7
11	2047	287	65	12.9
12	4095	1407	127	20.9
13	8191	703	127	14.9

EXAMPLE: DEGREE 12

$$20 \log \frac{1407}{4095} - 20 \log \frac{127}{4095} = 20.9$$

Figure 5.3-1. Performance of Preferred Pairs Compared with Worst Case Polynomial Pairs that the pairs of maximal PN codes chosen for this purpose in single access forward and return links be preferred pairs, or codes generated using preferred pairs.

To find the preferred pair, we select an arbitrary maximal polynomial having root $\alpha^j \equiv j$ from its listing in the table of irreducible polynomials and then find the polynomial having root $(\alpha^j)^t \equiv j \cdot t$ from the same table, where t is as given above. Clearly, only the tables of Peterson and Gold can be used for this procedure, since only these tables assign roots to each polynomial. For preferred pairs of polynomials to degree 16, computational techniques must be used to obtain the polynomial having the specified roots. A computer program for the generation of preferred pairs has been written (Appendix F.5), and a table of the preferred pairs for code lengths as currently described in the TDRSS User's Guide was generated, and is included in Appendix E.5. The code polynomials are listed in octal notation.

5.4 Generation of TDRS Band Spreading Codes

5.4.1 Introduction

The basic bandspreading codes recommended for use in the TDRSS MA service are balanced Gold codes of the appropriate length. In this section, we describe the method for implementing the shift register configuration and determining the register initial conditions which will generate these codes.

The family of 2^n+1 Gold codes of period 2^n-1 is generated by taking the modulo 2 sum of a preferred pair of maximal PN sequences where each of the 2^n-1 relative phases of the two maximal sequences produces one of the 2^n-1 members of the family. It has been shown[8] that the codes of the family fall into one of three categories according to the relative number of ones and zeroes in the code sequence:

	Number of ones in code sequence	Number of codes of family having this number of ones
(a)	2^{n-1}	$2^{n-1}+1$
(b)	$2^{n-1}+2^{(n-1)/2}$	$2^{n-2}-2^{(n-3)/2}$
(c)	$2^{n-1}-2^{(n-1)/2}$	$2^{n-2}+2^{(n-3)/2}$

We note that the $2^{n-1}+1$ codes of category (a) have 2^{n-1} ones and hence (since the code length is 2^n-1) $2^{n-1}-1$ zeroes. The codes of this category are thus balanced in the sense of having only one more one than zeros (this is the best possible balance since the codes have odd period). The codes of categories (b) and (c) have a surplus and deficiency of ones, respectively, and thus have less desirable spectral characteristics. In order to generate balanced code members of the family, we must determine and select the proper relative phases of the two original maximal sequences. In what follows we describe how this is accomplished.

5.4.2 Characteristic Phase of a Maximal PN Sequence

Each maximal PN sequence has a natural "characteristic" phase which is unique to it.[9] The sequence in this phase position has many useful properties. For example, if a maximal PN sequence in its characteristic phase is sampled by every other bit, the result is the same sequence. The required relative phases of the preferred pair of maximal sequences in order to generate balanced members of the code family are described with reference to their characteristic phase and hence it is necessary to show how the characteristic phase and the shift register initial conditions which determine the characteristic phase are determined.

If $f(x)$ is the n^{th} degree binary polynomial corresponding to the maximal PN shift register, than any phase of the maximal sequences generated by the shift register can be represented by the ratio $g(x)/f(x)$, where $g(x)$ is a binary polynomial of degree less than n. Long division of these polynomials results in a formal binary power series whose binary coefficients are the bits of the sequence generated by the shift register. The formula for the polynomial $g(x)$ which results in the characteristic phase for the maximal sequence has been shown[9] to be

$$g(x) = \frac{d\left(x\,f(x)\right)}{dx} \qquad \text{for } f(x) \text{ of odd degree}$$

$$g(x) = f(x) + \frac{d\left(x\,f(x)\right)}{dx} \qquad \text{for } f(x) \text{ of even degree}$$

Here differentiation is carried out in the usual way and then the coefficients are interpreted modulo 2.

For example, the characteristic phase for the maximal PN sequence generated by the 3-stage shift register corresponding to the polynomial $f(x) = 1 + x^2 + x^3$ is found as follows:

$$g(x) = \frac{d\left(x\,f(x)\right)}{dx} = \frac{d(x + x^3 + x^4)}{dx} = 1 + 3x^2 + 4x^3 = 1 + x^2 \; .$$

The characteristic phase for maximal sequences is thus represented by the quotient

$$\frac{1+x^2}{1+x^2+x^3} = 1 + 0 \cdot x + 0 \cdot x^2 + \ldots$$

and the initial conditions of the 3-stage shift register which will result in the characteristic phase are [100].

5.4.3 Relative Phases Required for Balanced Codes

The relative phases in which the preferred pair of maximal PN sequences must be added in order to result in a balanced member of the family may now be described in terms of the characteristic phases of the preferred pair.

Let a and b be the preferred pair of maximal sequences in their characteristic phase. It is easily seen from the polynomial representation that a characteristic maximal sequence generated by a shift register with an odd number of stages has its initial bit equal to one. Any relative phase shifts of the sequences a and b which are obtained by shifting the sequence b until its initial one corresponds to a zero in the sequence a will result in a balanced Gold code when the two sequences are added together. For example, if the two maximal characteristic sequences a and b are given as:

$$a = 1\ 1\ 1\ 0\ 1\ 0\ 0$$
$$b = 1\ 0\ 0\ 1\ 0\ 1\ 1$$

shifting the sequence b cyclically three, five or six positions to the right places the initial one of the characteristic sequence b under a zero of the sequence a. Adding the two sequences in each case produces a balanced code, e.g.,

$$\begin{aligned} a &= 1\ 1\ 1\ 0\ 1\ 0\ 0 \\ b_3 &= \underline{0\ 1\ 1\ 1\ 0\ 0\ 1} \\ a+b_3 &= 1\ 0\ 0\ 1\ 1\ 0\ 1 \end{aligned}$$

$$
\begin{aligned}
a &= 1\ 1\ 1\ 0\ 1\ 0\ 0 \\
b_5 &= 0\ 1\ 0\ 1\ 1\ 1\ 0 \\
\hline
a+b_5 &= 1\ 0\ 1\ 1\ 0\ 1\ 0
\end{aligned}
$$

$$
\begin{aligned}
a &= 1\ 1\ 1\ 0\ 1\ 0\ 0 \\
b_6 &= 0\ 0\ 1\ 0\ 1\ 1\ 1 \\
\hline
a+b_6 &= 1\ 1\ 0\ 0\ 0\ 1\ 1
\end{aligned}
$$

Shifting the sequence b by any other phase and adding the resultant sequences yields an unbalanced code:

$$
\begin{aligned}
a &= 1\ 1\ 1\ 0\ 1\ 0\ 0 \\
b_1 &= 1\ 1\ 0\ 0\ 1\ 0\ 1 \\
\hline
a+b_1 &= 0\ 0\ 1\ 0\ 0\ 0\ 1
\end{aligned}
$$

5.4.4 Determination of Initial Conditions

The initial conditions for the Gold code generator which will result in balanced codes is now readily determined. The required shift register configuration is shown in Figure 5.4-1.

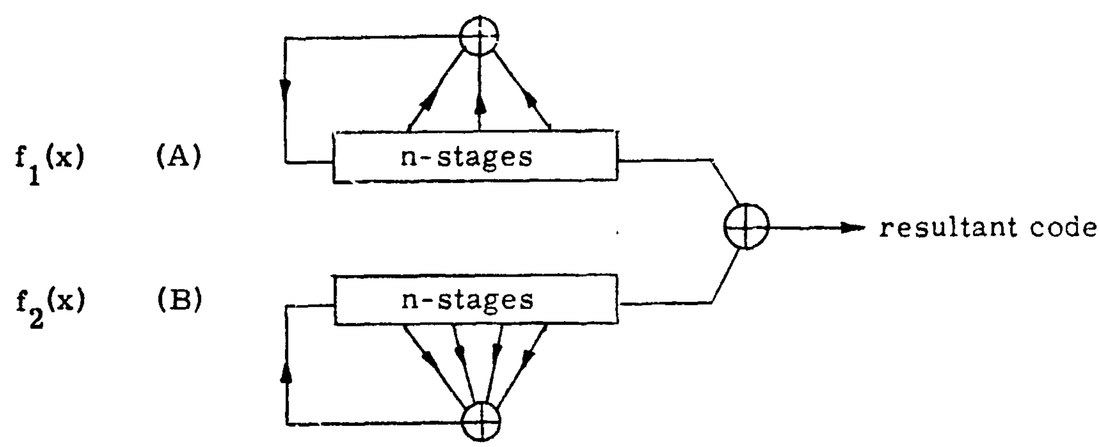

Figure 5.4-1. Code Generator Configuration

The initial conditions for the shift register (B) corresponding to the polynomial $f_2(x)$ are those initial conditions which determine the characteristic phase of the maximal PN sequence generated by shift register (B). These initial conditions are determined from the representation of the characteristic sequence $\left[d\left(x f_2(x)\right)/dx\right]/f_2(x)$ by taking the first n coefficients obtained by performing the indicated long division.

The initial conditions for the shift register (A) corresponding to the polynomial $f_1(x)$ are only subject to the constraint that the first stage contain a zero. This corresponds to a relative phase shift of the characteristic sequences a and b such that sequence a is shifted such that its initial bit corresponds to a zero in the sequence b. We have noted in Section III that the sum of two such relative phase shifts results in a balanced Gold code.

As an example of the above technique, we construct the shift register configuration required to generate balanced Gold codes of period $(2^{19}-1)$. A preferred pair of 19-stage maximal polynomials is found in the table contained in (10).

(A) 2105575 - $1+x^2+x^3+x^4+x^5+x^6+x^8+x^9+x^{11}+x^{15}+x^{19}$

(B) 2000605 - $1+x^2+x^7+x^8+x^{19}$

The characteristic sequence generated by the shift register corresponding to the polynomial (B) is represented by the ratio

$$\frac{g(x)}{1+x^2+x^7+x^8+x^{19}} \qquad \text{where } g(x) = \frac{d}{dx}(x+x^3+x^8+x^9+x^{20}) = 1+x^2+x^8$$

and the initial conditions required for the register (B) are found as the coefficients of the quotient of the two polynomials:

$$\frac{1+x^2+x^8}{1+x^2+x^7+x^8+x^{19}} = 1+x^7+x^9+x^{11}+x^{13}+x^{14}+x^{17}+x^{18}+\ldots$$

Initial condition for (B) register = [1 0 0 0 0 0 0 1 0 1 0 1 0 1 1 0 0 1 1] .

The only constraint on the initial conditions of the (A) register is that the entry in the first stage be zero. Given that 2^k different codes are required, e.g., 32 codes for the TDRS forward link, then a simple configuration for the initial conditions of the A register is to set stages 1 and k+2 through n to zero while each of the remaining 2^k possible initial conditions for the k stages 2 through k+1 determine 2^k distinct balanced Gold codes. The resultant configuration for the generation of balanced Gold codes of period $2^{19}-1$ is shown in Figure 5.4-2.

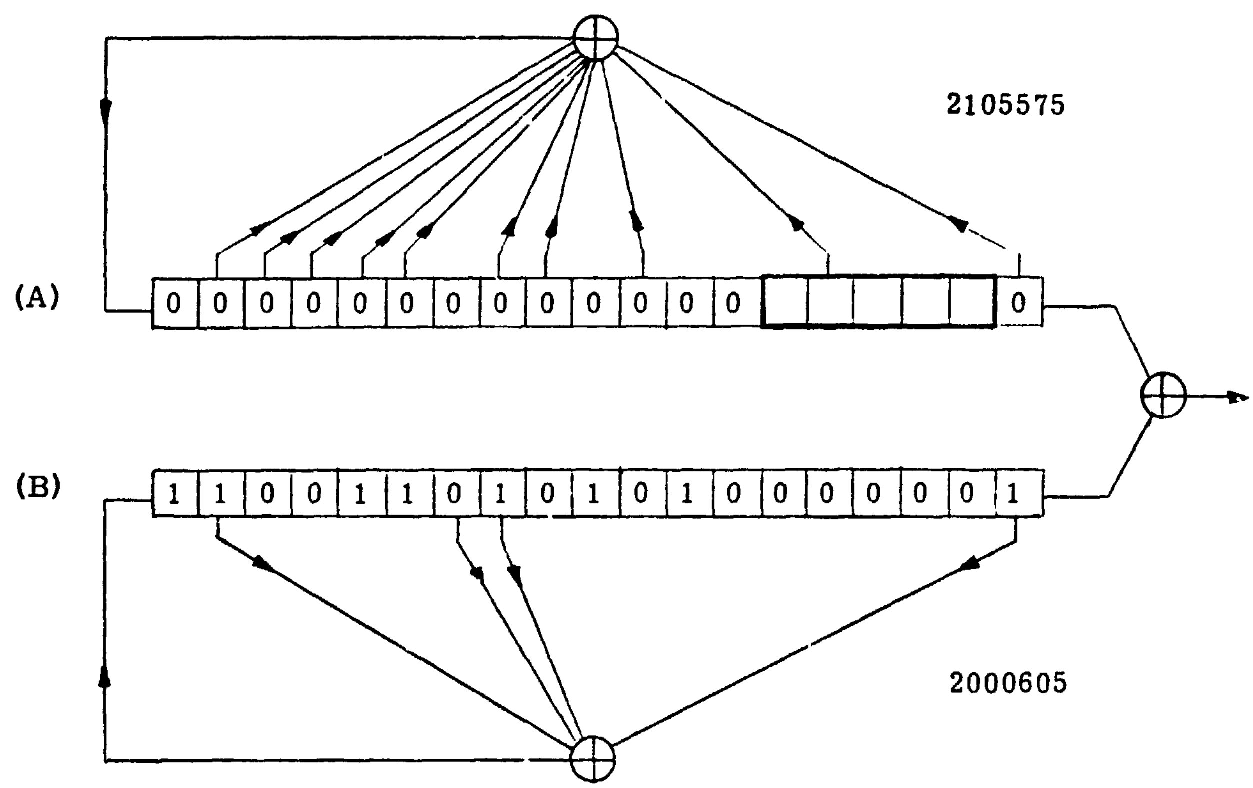

Figure 5.4-2. Generation of Balanced Codes of Period $2^{19}-1$

5.5 The Effect of Clock Error on Acquisition

5.5.1 Introduction

In this section, we consider the effect of clock error on acquisition of a PN signal. We suppose that the chipping rate c of the received signal is in error by one part in n and we compute the acquisition time of the received signal as a function of the error free acquisition time and the ratio $r = n/c$ of clock accuracy to chipping rate. We find that the effect of clock error on the acquisition time increases with increasing error-free acquisition time (no clock error). This is to be expected, since the effect of clock error is to cause the received code to become increasingly decorrelated with time. Specifically, for an error-free acquisition time of not more than 20 seconds, a ratio of clock accuracy to chipping rate of 4×10^2 will add less than 1 second to the acquisition time.

5.5.2 Notation

Let ε = clock error in chips/sec.

Let ρ = code rate in chips/sec.

Then, $\left(\frac{\varepsilon}{\rho}\right) = \frac{1}{n}$ = clock accuracy

$$\Delta = \frac{1}{\rho} = \text{correct chip width}$$

$$\Delta_c = \frac{1}{\rho + \varepsilon} = \text{erroneous chip width}$$

$$\Delta_c = \frac{1}{\rho+\varepsilon} = \frac{1}{\rho}\left(\frac{1}{1+\frac{\varepsilon}{\rho}}\right) \sim \Delta\left(1 - \frac{\varepsilon}{\rho}\right) = \Delta\left(\frac{n-1}{n}\right).$$

5.5.3 Analysis

Suppose the received and reference codes are in sychronism and that the clock is in error by $\left(\frac{\varepsilon}{r}\right) = \frac{1}{n}$. Since the ratio of the correct chip width to the erroneous chip width is $\frac{n-1}{n}$, each successive chip becomes decorrelated by an additional $\frac{1}{n}$ of its width and the codes are completely decorrelated after n chips.

The correlation function between the received and reference codes when the clock is in error by $\frac{1}{n}$ may be written as

$$\theta = \left[a(0)\,a(0)\left(\frac{n-1}{n}\right) + a(0)\,a(1)\frac{1}{n}\right] + \left[a(1)\,a(1)\left(\frac{n-2}{n}\right) + a(1)\,a(2)\frac{2}{n}\right]$$

$$+ \cdots \left[a(i)\,a(i)\ \frac{n-(i+1)}{n} + a(i)\,a(i+1)\left(\frac{i+1}{n}\right)\right] + \cdots$$

$$\theta = \sum_{i=0} a(i)\,a(i)\ \frac{n-(i+1)}{n} \ + \sum_{i=0} a(i)\,a(i+1)\left(\frac{i+1}{n}\right) .$$

Since the out-of-phase terms are uncorrelated, the second sum may be taken as zero, and we have

$$\theta = \frac{1}{n}\sum_{i=1}^{w}(n-i) = w\left[1 - \frac{w+1}{2n}\right] \sim w\left[1 - \frac{w}{2n}\right] ,$$

where w is the number of chips over which we integrate.

The ratio of the correlation function when the clock is correct to the correlation function when the clock is in error is given by $[1 - \frac{w}{2n}]$ and the maximum degradation which is achieved for $w = n$ is seen to be 6 dB. A plot of the degradation of θ as a function of the number of chips integrated is given in figure 5.5-1.

For a 6000 Hz doppler on the S-band carrier, the maximum doppler on the PN clock is approximately $\varepsilon = 10$ chips/sec, which results in a clock accuracy of $n = 3 \times 10^5$. The degradation in the correlation function as a function of the integration interval is shown in figure 5.5-1.

5.5.4 Effect of Clock Accuracy on Integration Time

The starting point of this analysis is the following equation which was derived in Section 4.0, where acquisition time T_a for an accurate clock is given by

$$T_a = \frac{P_i}{\theta^2}\left(\frac{E}{N_0}\right)\left(\frac{N_0}{S}\right) .$$

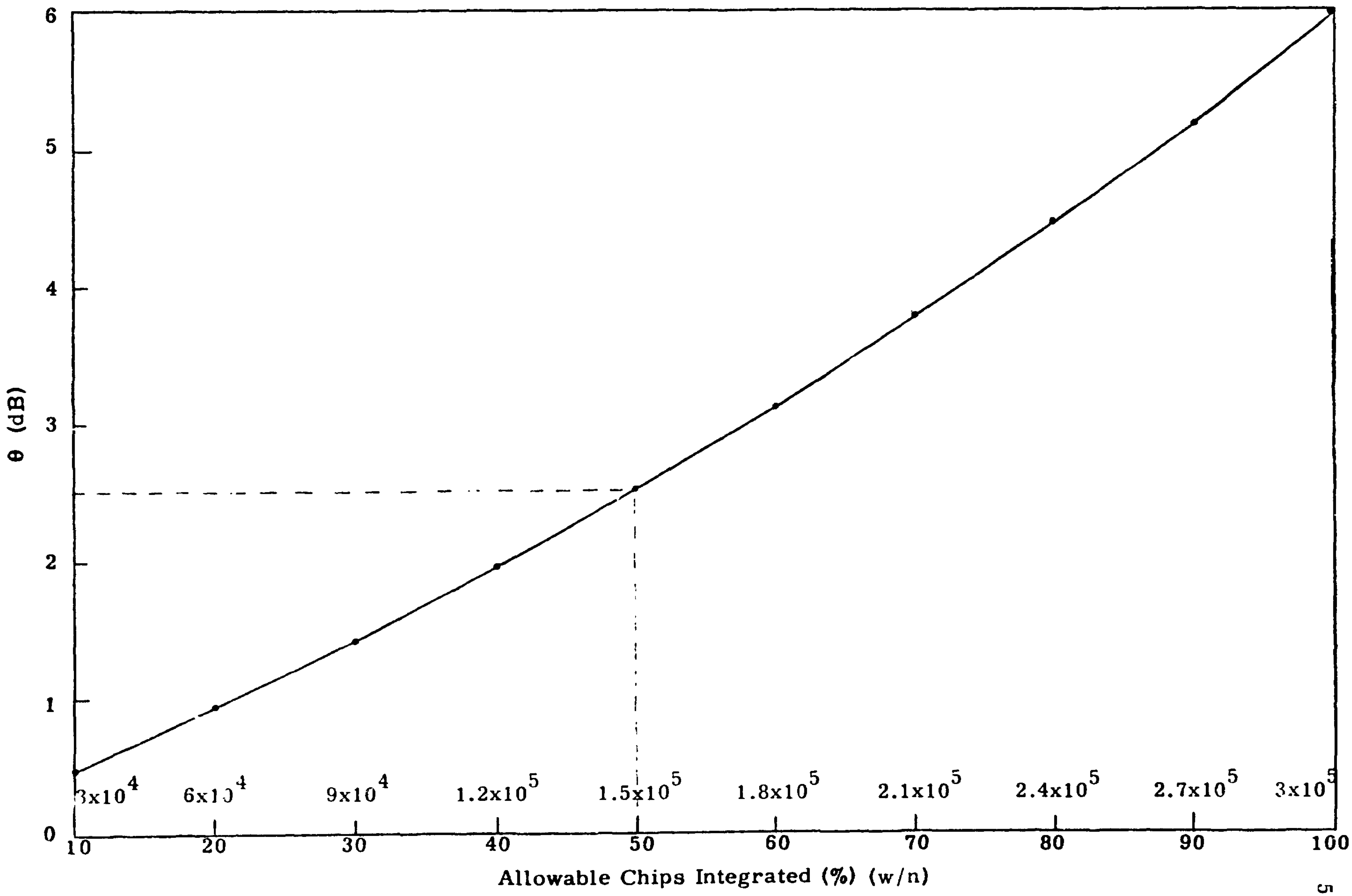

Figure 5.5-1. A Degradation of θ vs. % of Window to Complete Decorrelation

Using the conclusion of the above section, we have

$$\theta' = \theta(1 - \frac{Tc}{2n})$$

where θ' = degraded correlation function

n = clock accuracy (i.e., 1 part in n)

T = new acquisition time

c = chipping rate .

Substituting θ' into the equation for T_a, we have

$$T = \frac{P_i\left(\frac{E}{N_0}\right)\left(\frac{N_0}{S}\right)}{\theta^2\left(1 - \frac{Tc}{2n}\right)^2} = \frac{T_a}{\left(1 - \frac{Tc}{2n}\right)^2} = \frac{T_a}{\left(1 - \frac{T}{2r}\right)^2}$$

where r is the ratio of clock accuracy to chipping rate.

This equation may be used to compute T, the acquisition time with clock error as a function of r, the ratio of clock accuracy to chipping rate with T_a, the acquisition time with an accurate clock as a parameter.

For large r ($\frac{T}{2r} \ll 1$), we have

$$T = \frac{T_a}{(1 - \frac{T}{r})}$$

$$T = \frac{r - \sqrt{r^2 - 4r\,T_a}}{2} .$$

The acquisition times are plotted as a function of r for various error-free acquisition times in Figure 5.5-2.

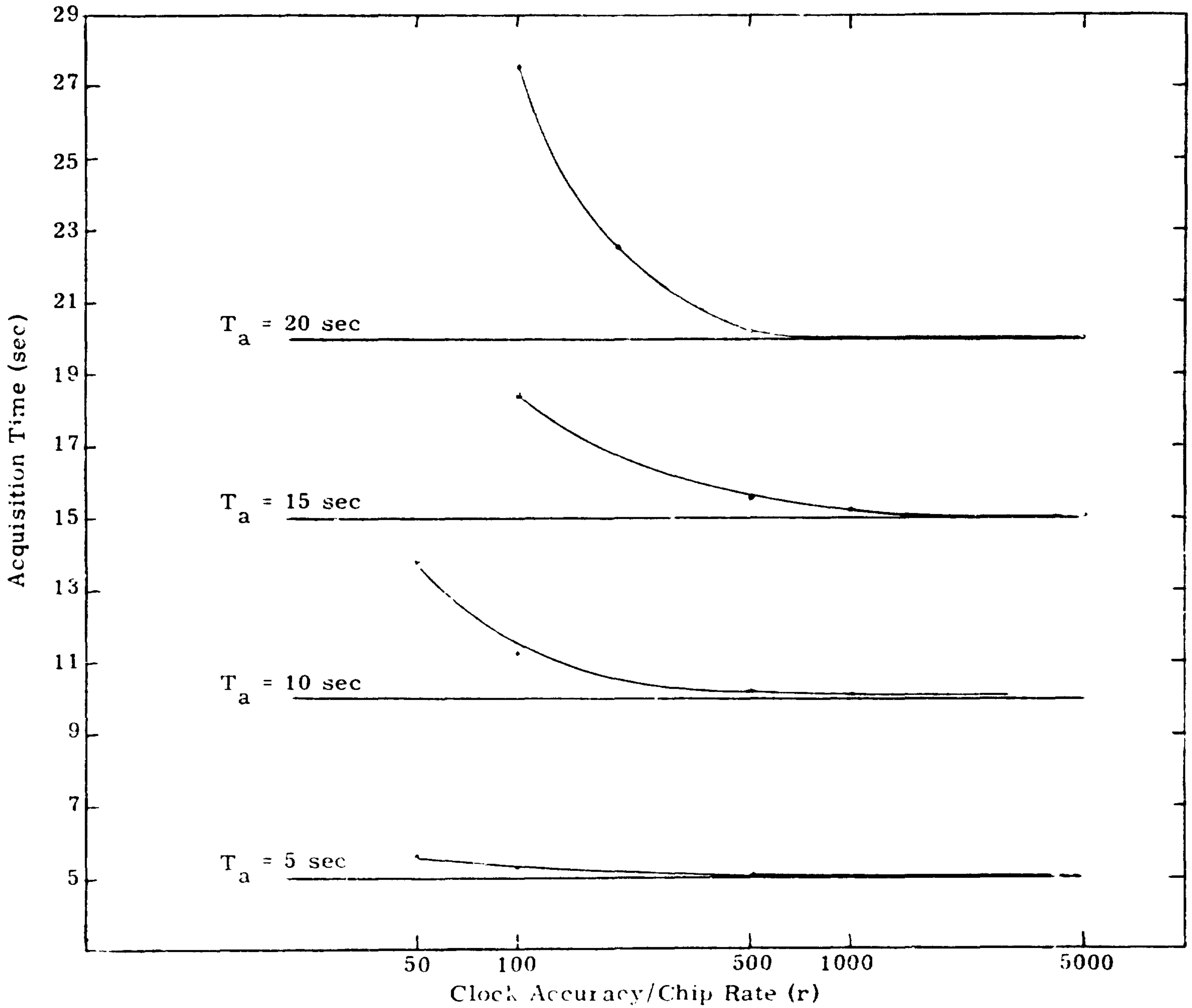

Figure 5.5-2. Acquisition Time vs. Clock Accuracy/Chip Rate

5.6 Code Libraries for TDRS

5.6.1 Forward Link Multiple Access Library

This code library consists of 100 code pairs. The first member of each pair is a code of period $(2^{10}-1) \cdot (256)$ (long code). The second member of each pair is a code of period $(2^{10}-1)$ (short code). The 100 long and short codes are chosen as balanced members of respective Gold families. In what follows, we describe the technique for generating the required library of code pairs.

5.6.1.1 Forward Link Multiple Access Long Code

The code family from which the long code library is selected may be either a set of maximal PN sequences, each of period $2^{18}-1$, or a set of balanced Gold codes generated by a preferred pair of maximal PN sequences. The former approach has the advantage of a simpler implementation (18 shift register stages versus 36 shift register stages) and the code library for this approach consists of the listing of maximal PN codes of period $(2^{18}-1)$ given in Appendix E.5.

In what follows, we describe the shift register configuration to be used for the generation of 127 balanced Gold codes of period $2^{18}-1$.

The preferred pair of maximal PN generators used to generate the desired family is selected from the table of Appendix E.5. The description of one such preferred pair is given in table 5.6-1.

Table 5.6-1. Preferred Pairs for Generation of Code Family of Long Codes

Octal Representations	Polynomial
1000201	$1 + x^7 + x^{18}$
1325427	$1 + x + x^2 + x^4 + x^8 + x^9 + x^{11} + x^{13} + x^{15} + x^{16} + x^{18}$

The shift register configuration which will generate the desired code family is illustrated in figure 5.6-1.

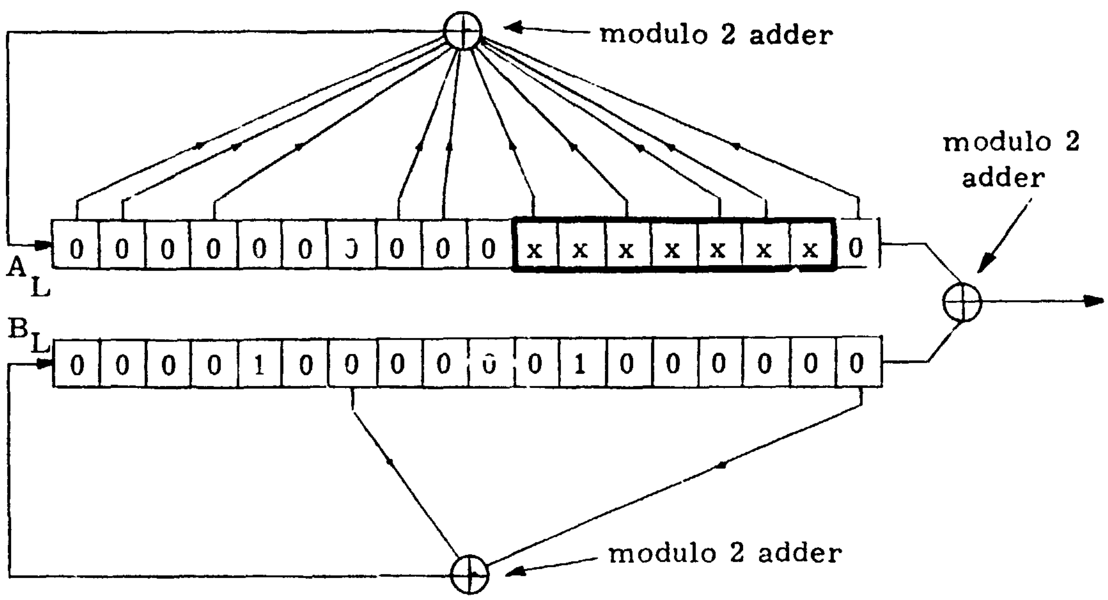

Figure 5.6-1. Long Code Generator Forward Link Multiple Access

In order to generate balanced members of the code family, the relative phases of the two maximal generators must be specified. This is accomplished by requiring that the initial bit of the A_L register be zero and that the initial conditions of the B_L register be as given in figure 5.6-1. The 7 unspecified initial conditions of the A_L register will result in 127 balanced Gold codes whose cross-correlation peaks are -48 dB.

Summary of Parameters for Multiple Access Long Code

(a) A_L register feedback - 1325427 -
$$1 + x + x^2 + x^4 + x^8 + x^9 + x^{11} + x^{13} + x^{15} + x^{16} + x^{18}$$

(b) B_L register feedback - 1000201 - $1 + x^7 + x^{18}$

(c) Initial conditions for A register - 0000000000xxxxxxx0

(d) Initial conditions for B register - 000010000001000000

5.6.1.2 Forward Link Multiple Access Short Code

The code family from which the short code library is selected is generated by the preferred pair of 10-stage maximal generators given in table 5.6-2.

Table 5.6-2. Preferred Pair for Generation of Codes for Forward Link Command Channel

Octal Representation	Polynomial
3515	$1 + x^2 + x^3 + x^6 + x^8 + x^9 + x^{10}$
2011	$1 + x^3 + x^{10}$

The shift register configuration which will generate the desired code family is illustrated in figure 5.6-2.

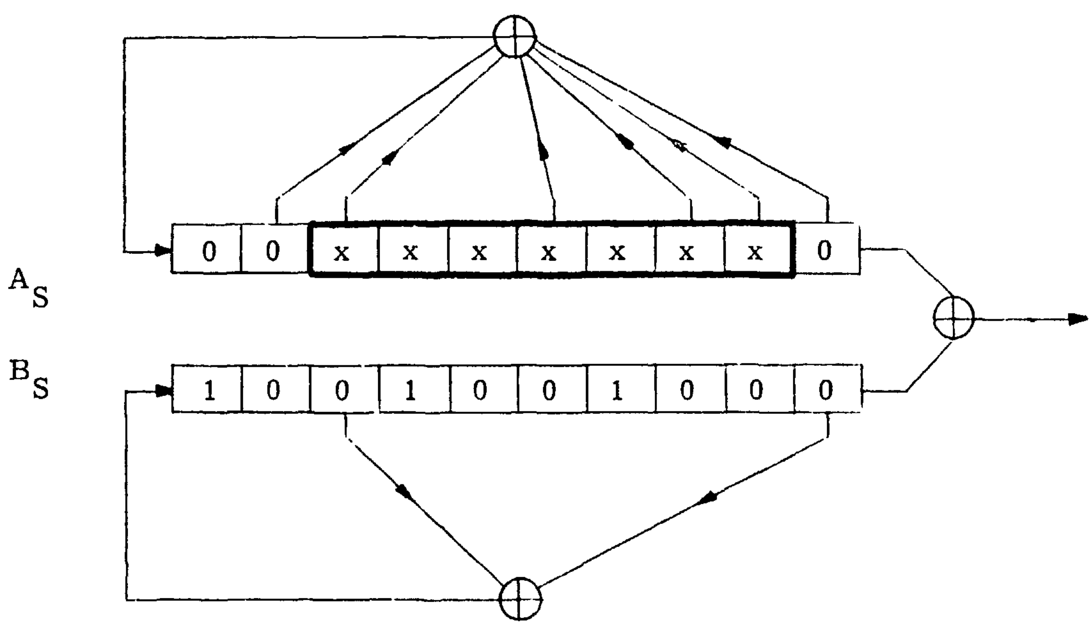

Figure 5.6-2. Short Code Generator Forward Link Multiple Access

As in the case of the generation of the long codes, the relative phases of the two maximal generators must be specified to insure the generation of balanced members of the code family. This is again accomplished by requiring that the initial bit of the A_S register be zero and that the initial conditions of the B_S register be given as in figure 5.6-2. The 7 unspecified initial conditions for the A_S register will result in 127 balanced Gold codes whose cross-correlation peaks are -23.9 dB.

5.6.2 Code Library for Mode 2 Return Link and Its Properties

The code library for the Mode 2 return link consists of 100 code pairs of period $(2^{11}-1)$ selected from the balanced members of a Gold family. The code family from which the code library is selected is generated by the preferred pair of 11-stage maximal generators given in table 5.6-3.

Table 5.6-3. Preferred Pair for Generating Code Library for Mode 2 Return Link

Octal Representation	Polynomial
4445	$1 + x^2 + x^5 + x^8 + x^{11}$
4005	$1 + x^2 + x^{11}$

The shift register configuration which will generate the desired code family is illustrated in figure 5.6-3.

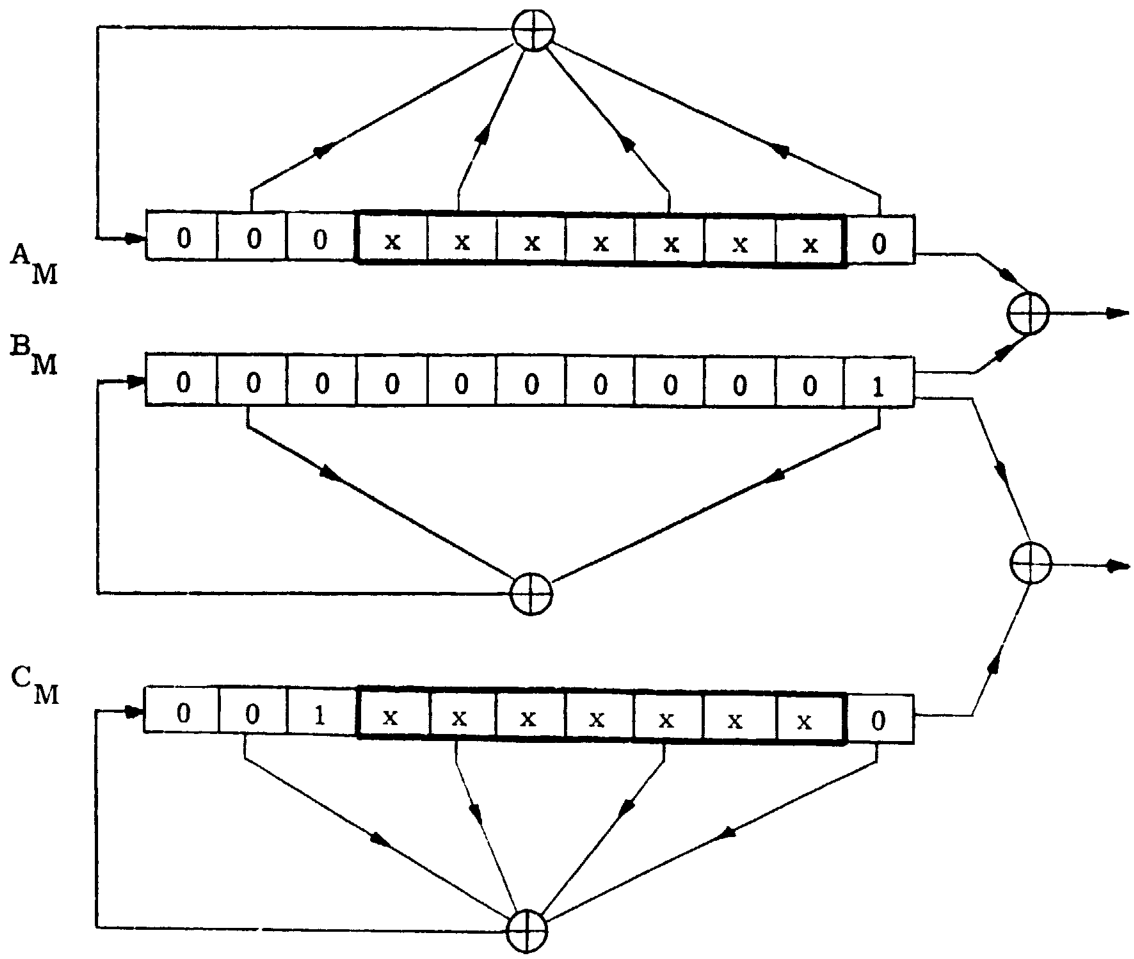

Figure 5.6-3. Generator for Mode 2 Return Link Codes

The requirement that the first bit of the A_M and C_M registers be zero and that the initial conditions of the B_M register be as indicated in figure 5.6-3 guarantees that the code generator will produce balanced codes. Each subset of initial conditions $[x\ x \ldots x]$ of the A_M and C_M registers determines a unique code, while the alternate values of 0 and 1 in the third stage determine the code pair.

Properties of the Code Library for Mod 2 Return Link

The acquisition performance of the Mod 2 return link is dependent upon the distribution of the cross-correlation sidelobes and the RMS value of the cross-correlation function of the code library used for this link. Two algorithms have been developed which make the determination of this distribution feasible; these procedures are documented in the following sections. In this section, we summarize one of these algorithms and the properties of the recommended Mod 2 return link code family whose implementation was described above.

The cross-correlation sidelobes of any two codes of the recommended family have magnitude 65/2047 or 63/2047 , which is approximately 30 dB down from the main correlation peak. The general formula for the number of these sidelobes which occur in the cross-correlation function between two codes a and b of such a family of codes of period 2^n-1 is shown in Appendix A.5 to be

$$x+y = \frac{\sum\theta^2 + 2\sum\theta + (2^n-1)}{2^{n+1}}$$

where

$$\sum\theta^2 = \sum_{\tau=0}^{2^n-2} \theta^2(a,b)(\tau) = \sum_{\tau=0}^{2^n-2} \theta(a,a)(\tau)\,\theta(b,b)(\tau)$$

$$\sum\theta = \sum_{\tau=0}^{2^n-2} \theta(a,b)(\tau) = \theta(a)\cdot\theta(b) .$$

The above formula expresses the number of sidelobes in the cross-correlation function of any pair of codes in terms of the parameters of each of the individual codes. Thus, once the required parameters are computed for each member of the family, the number of sidelobes may be determined using the above formula, rather than by the lengthy process of computing the cross-correlation functions. For a family of n codes, the required computation, using this technique, is reduced by a factor of n.

The sidelobe distribution data for the code family of 100 codes described above is given in table 5.6-4. There are (100)(101)/2 = 5050 code pairs and, hence, 5050 cross-correlation functions. The data in the table presents the cumulative frequency function for the number of sidelobes (of magnitude 65 or 63) which occur in each of the 5050 cross-correlation functions. Thus, for example, 104 of the 5050 cross-correlation functions have 1070 sidelobes or more. This cumulative frequency function is plotted in figure 5.6-4.

Table 5.6-4. Probability Distribution of Sidelobes in Mode 2 Codes of Period $2^{11}-1$

NO. OF SIDE LOBES	CUM. FREQ.	PROBABILITY DISTRIBUTION
1115	2	.000
1110	3	.001
1105	4	.001
1100	6	.001
1095	7	.001
1090	12	.002
1085	20	.004
1080	39	.008
1075	68	.013
1070	104	.021
1065	166	.033
1060	265	.052
1055	413	.082
1050	594	.118
1045	869	.172
1040	1209	.239
1035	1557	.308
1030	1991	.394
1025	2400	.475
1020	2862	.567
1015	3282	.650
1010	3675	.728
1005	4039	.800
1000	4348	.861
995	4564	.904
990	4755	.942
985	4852	.961
980	4909	.972
975	4974	.985
970	4999	.990
965	5028	.996
960	5034	.997
955	5047	.999
950	5049	1.000
945	5050	1.000

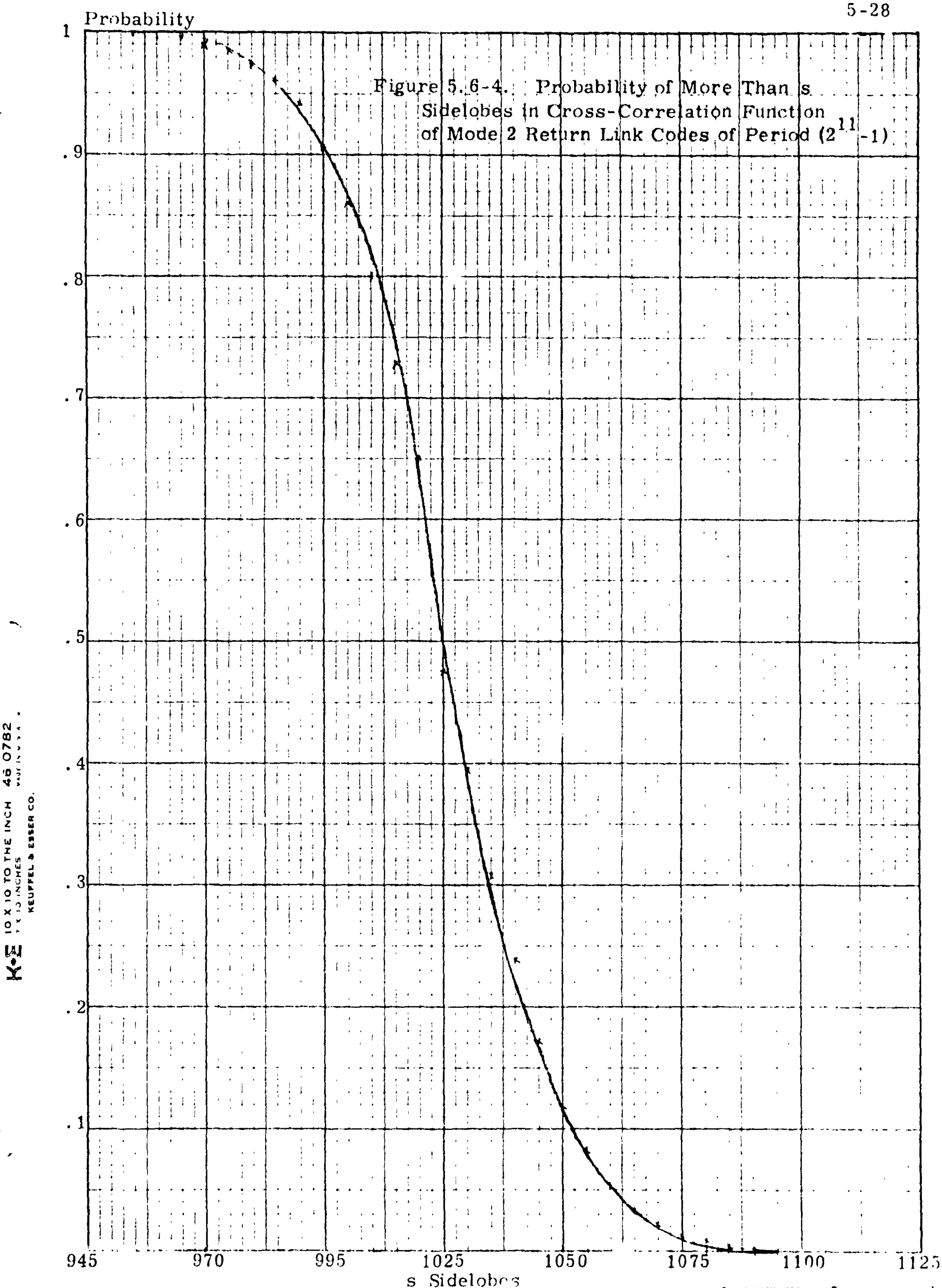

Figure 5.6-4. Probability of More Than s Sidelobes in Cross-Correlation Function of Mode 2 Return Link Codes of Period $(2^{11}-1)$

5.6.3 Dedicated Return Link Mode 1 Code

In this section, we describe a library of code pairs, each consisting of a maximal PN shift register code and a proper phase shift of this code which can be obtained from it via the shift-and-add property discussed in Appendix A.5. The phase difference between the PN codes of each pair is required to be at least 5000 chips. Any prespecified phase shift of a maximal PN code may be generated by taking an appropriate modulo 2 linear combination of the outputs of the taps of the shift register generating the code, as indicated in figure 5.6-5.

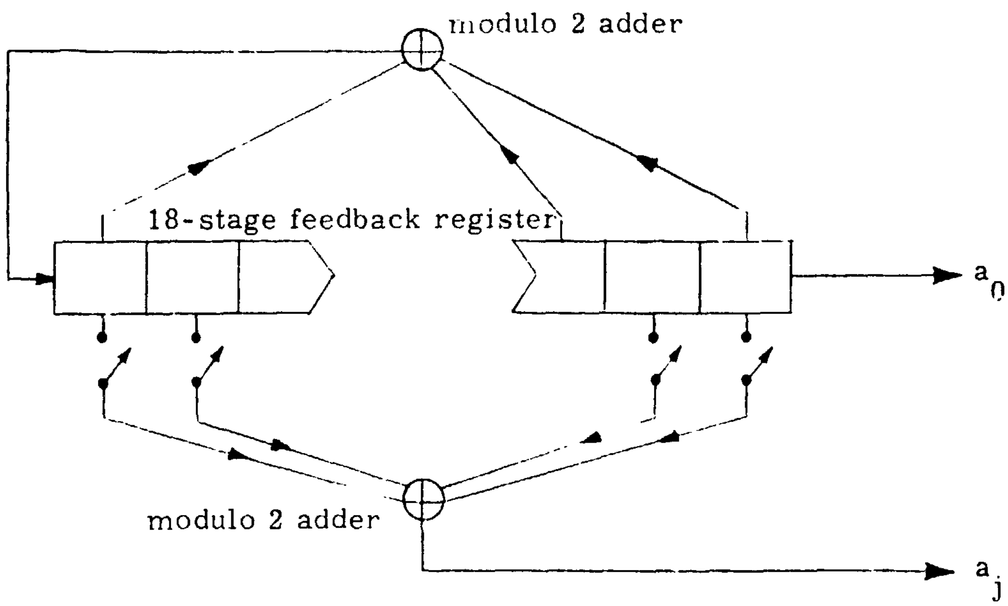

Figure 5.6-5. Generation of Phase Shifts of Maximal PN Sequences

There are $2^{18}-1$ settings of the indicated switches, each corresponding to a phase shift a_j ($j = 0, 1, \ldots, 2^{18}-1$) of the maximal PN sequence a_0. Thus, any prespecified phase shift a_k may be obtained by the proper switch settings. We may, however, obtain phase shifts in excess of 5000 chips by adding the sequence a_0 to the output sequence obtained from closing one of the switches as indicated in figure 5.6-6.

This is to be expected, since the probability of a phase shift generated at random being less than 5000 chips is less than 2×10^{-2}. The code library given in Appendix B.5 lists the phase shift a_j obtained when the output sequence is added modulo 2 to the output sequence obtained from the kth tap of the shift register. The computer program used for obtaining this data is included in Appendix C.5.

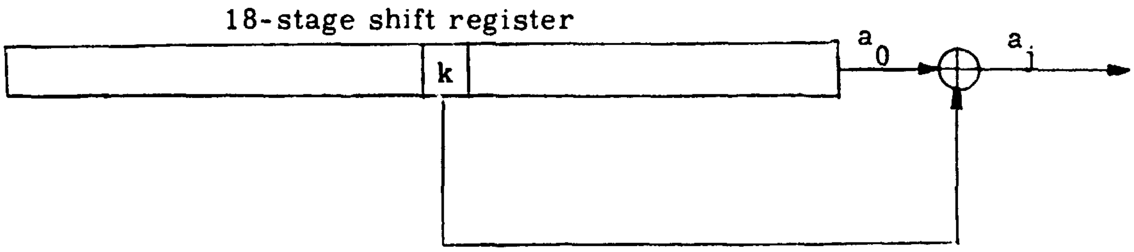

Figure 5.6-6. Generation of Phase-Shifted Version of Maximal PN Code

5.7 Listing of TDRSS User Code Libraries

A listing of the TDRSS user code libraries is contained in table 5.7-1. In what follows, we give a brief description of the contents of this table and reference the appropriate sections of this report for further details.

Column 2 contains the user-unique initial conditions for the seven stages of the 10-stage A register used to generate the 1023 bit code for the forward link command channel, as illustrated in figure 5.6-2. The code generator configuration and the remaining initial conditions for the A and B registers are chosen so that the user-unique initial conditions can consist of the binary representation of the user number.

Column 3 contains the octal representation of the feedback taps for maximal PN generators of period $2^{18}-1$ to be used for the forward link range channel. Each feedback configuration requires no more than six feedback taps.

Column 4 contains the octal representation of the feedback taps for maximal PN generators of period $2^{18}-1$ to be used for the Mode 1 return link. These feedback configurations each have the property that, if the output of the first stage is added modulo-2 to the output of the tenth stage, the resultant code differs in phase from the code at the first stage by at least 20,000 chips. The exact phase difference between the two codes is given in Column 5. The numbering of the shift register stages is further described in Appendix B.5. Each feedback configuration of this code library will use no more than eight feedback taps.

Column 6 contains initial conditions for the seven stages of the A and C registers of the configurations generating Mode 2 return link codes, as described in 5.6.2. As in the case of the forward link range channel, these initial conditions may be taken to be the binary representation of the user number.

Column 7 contains the octal representation of the feedback taps for maximal PN generators of period $2^{18}-1$ to be used as Alternate Mode 1 return link codes. No more than six feedback taps are used for any configuration of this library.

Table 5.7-1. Summary of TDRSS Code Libraries

1	2	3	4	5	6	7
User Number	Forward Link Command Channel Initial Conditions Register A	Forward Link Range Channel Feedback Taps	Mode 1 Return Link Feedback Taps	Mode 1 Return Link Channel Phase Difference in Chips	Mode 2 Return Link Initial Conditions Registers A & C	Alternate Mode 1 Return Link Feedback Taps
1	1000000	1022005	1000047	94672	1000000	1000115
2	0100000	1022027	1431503	35529	0100000	1000743
3	1100000	1022055	1012633	100097	1100000	1000751
4	0010000	1022131	1012715	37927	0010000	1001013
5	1010000	1022145	1010551	20125	1010000	1002031
6	0110000	1022225	1101063	127909	0110000	1002061
7	1110000	1022311	1010463	124686	1110000	1002075
8	0001000	1022443	1011267	48528	0001000	1002133
9	1001000	1022461	1010313	122601	1001000	1002171
10	0101000	1022621	1125611	130803	0101000	1002211
11	1101000	1023045	1010211	42628	1101000	1002241
12	0011000	1023103	1011333	121824	0011000	1002441
13	1011000	1023111	1010163	81188	1011000	1002623
14	0111000	1023221	1011533	61209	0111000	1002705
15	1111000	1023405	1010133	36812	1111000	1002741
16	0000100	1024017	1011553	66194	0000100	1003011
17	1000100	1024027	1011347	53036	1000100	1003035
18	0100100	1024063	1116115	74458	0100100	1003053
19	1100100	1024065	1011261	104408	1100100	1003215
20	0010100	1024305	1011571	102103	0010100	1003451
21	1010100	1025105	1012527	97306	1010100	1003461
22	0110100	1025141	1012547	82029	0110100	1003521
23	1110100	1026023	1007705	88320	1110100	1004073
24	0001100	1026043	1012363	106369	0001100	1004163
25	1001100	1026061	1013525	43037	1001100	1004205

Table 5.7-1 (continued)

1	2	3	4	5	6	7
User Number	Forward Link Command Channel Initial Conditions Register A	Forward Link Range Channel Feedback Taps	Mode 1 Return Link Feedback Taps	Mode 1 Return Link Channel Phase Difference in Chips	Mode 2 Return Link Initial Conditions Registers A & C	Alternate Mode 1 Return Link Feedback Taps
26	0101100	1030145	1201011	38185	0101100	1004313
27	1101100	1030161	1007543	117247	1101100	1004405
28	0011100	1030215	1013625	98985	0011100	1004447
29	1011100	1030303	1007501	46045	1011100	1004455
30	0111100	1030311	1014555	49892	0111100	1004545
31	1111100	1030321	1007417	91623	1111100	1004623
32	0000010	1030341	1716201	124677	0000010	1004643
33	1000010	1030407	1007315	124514	1000010	1004645
34	0100010	1034013	1015037	25407	0100010	1004711
35	1100010	1034051	1007263	79938	1100010	1005035
36	0010010	1034105	1230121	53510	0010010	1005213
37	1010010	1035021	1014365	38428	1010010	1005225
38	0110010	1040043	1014475	33738	0110010	1005305
39	1110010	1040051	1007165	45941	1110010	1005341
40	0001010	1040117	1141703	30125	0001010	1005431
41	1001010	1040205	1007121	57531	1001010	1005451
42	0101010	1040247	1021553	26391	0101010	1005521
43	1101010	1040361	1001705	83753	1101010	1006113
44	0011010	1040463	1020277	22264	0011010	1006161
45	1011010	1040465	1001661	59945	1011010	1006605
46	0111010	1040545	1017611	113772	0111010	1007031
47	1111010	1040645	1001651	106789	1111010	1010045
48	0000110	1040721	1017511	103124	0000110	1010051
49	1000110	1041011	1001631	65712	1000110	1010463
50	0100110	1041035	1017311	58281	0100110	1010551

Table 5.7-1 (continued)

1	2	3	4	5	6	7
User Number	Forward Link Command Channel Initial Conditions Register A	Forward Link Range Channel Feedback Taps	Mode 1 Return Link Feedback Taps	Mode 1 Return Link Channel Phase Difference in Chips	Mode 2 Return Link Initial Conditions Registers A & C	Alternate Mode 1 Return Link Feedback Taps
51	1100110	1041207	1001625	112199	1100110	1010613
52	0010110	1041225	1017161	123092	0010110	1010615
53	1010110	1041423	1001607	77447	1010110	1010741
54	0110110	1041445	1017071	25412	0110110	1011041
55	1110110	1041451	1001567	130143	1110110	1011245
56	0001110	1041505	1016705	95333	0001110	1310001
57	1001110	1200441	1021473	95661	1001110	1436001
58	0101110	1640441	1021475	111502	0101110	1136001
59	1101110	1320441	1001453	62504	1101110	1501001
60	0011110	1150441	1133015	74581	0011110	1140401
61	1011110	1230441	1001427	130092	1011110	1060401
62	0111110	1244441	1101533	91020	0111110	1360401
63	1111110	1114441	1001361	94465	1111110	1550401
64	0000001	1422441	1402335	92879	0000001	1170401
65	1000001	1062441	1001253	30646	1000001	1104401
66	0100001	1046441	1301323	25494	0100001	1024401
67	1100001	1221441	1001165	128965	1100001	1022401
68	0010001	1411441	1015631	115634	0010001	1446401
69	1010001	1111441	1001141	25409	1010001	1216401
70	0110001	1045441	1025051	78323	0110001	1036401
71	1110001	1203441	1001023	103808	1110001	1101401
72	0001001	1700241	1021355	42612	0001001	1341401
73	1001001	1640241	1010615	98036	1001001	1521401
74	0101001	1460241	1021363	27778	0101001	1305401
75	1101001	1260241	1000757	77032	1101001	1123401

Table 5.7-1 (continued)

1	2	3	4	5	6	7
User Number	Forward Link Command Channel Initial Conditions Register A	Forward Link Range Channel Feedback Taps	Mode 1 Return Link Feedback Taps	Mode 1 Return Link Channel Phase Difference in Chips	Mode 2 Return Link Initial Conditions Registers A & C	Alternate Mode 1 Return Link Feedback Taps
76	0011001	1214241	1060065	110203	0011001	1063401
77	1011001	1211241	1010741	75695	1011001	1053401
78	0111001	1031241	1205651	98275	0111001	1560201
79	1111001	1440641	1000743	39070	1111001	1470201
80	0000101	1420641	1021237	25929	0000101	1204201
81	1000101	1060641	1000621	67745	1000101	1514201
82	0100101	1230141	1530521	125022	0100101	1202201
83	1100101	1070141	1000517	121793	1100101	1622201
84	0010101	1334141	1021273	69616	0010101	1322201
85	1010101	1414141	1000407	61200	1010101	1232201
86	0110101	1114141	1324243	80039	0110101	1446201
87	1110101	1054141	1000355	86513	1110101	1426201
88	0001101	1034141	1020753	60361	0001101	1226201
89	1001101	1602141	1000347	56667	1001101	1116201
90	0101101	1500341	1020771	105837	0101101	1341201
91	1101101	1120341	1000333	47180	1101101	1505201
92	0011101	1210341	1032067	25351	0011101	1245201
93	1011101	1041341	1000201	131066	1011101	1215201
94	0111101	1420021	1017243	55015	0111101	1035201
95	1111101	1120021	1000173	44889	1111101	1143201
96	0000011	1710021	1017261	27451	0000011	1123201
97	1000011	1204021	1011055	122484	1000011	1053201
98	0100011	1624021	1016435	111283	0100011	1510601
99	1100011	1074021	1000077	50633	1100011	1070501
100	0010011	1462021	1016561	74848	0010011	1206601

5.8 Modular Implementation of Shift Register Code Generators

In this section, we discuss the modular configuration for shift register generators. The output of these shift registers is equivalent to the simple shift registers; however, the modular configuration has some advantages in its hardware implementation. The general n-stage linear shift register and the equivalent n-stage modular register are illustrated below in figure 5.8-1.

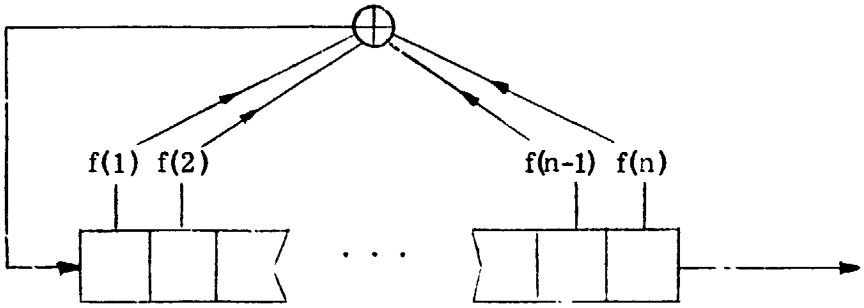

(a) n-Stage Simple Feedback Shift Register

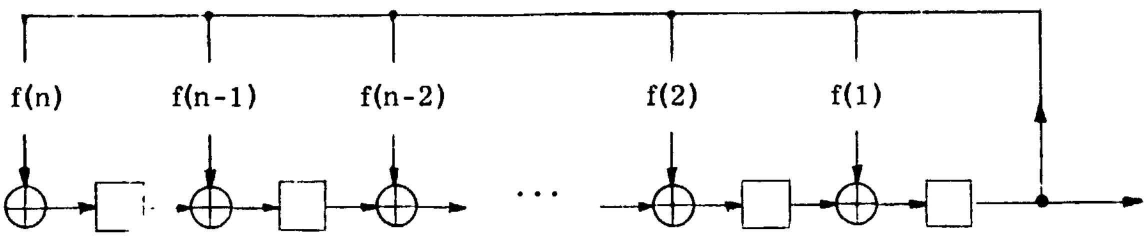

(b) n-Stage Modular Shift Register

Figure 5.8-1. Equivalent n-Stage Shift Registers

In figure 5.8-2 below, we illustrate the equivalence between the simple and modular form of the shift register using the A_S short code generator of figure 5.6-2. The polynomial corresponding to this shift register generator is

$$f(x) = 1 + x^2 + x^3 + x^6 + x^8 + x^9 + x^{10}$$

and hence

$$f(0) = f(2) = f(3) = f(6) = f(8) = f(9) = f(10) = 1$$

and

$$f(1) = f(4) = f(5) = f(7) = 0 .$$

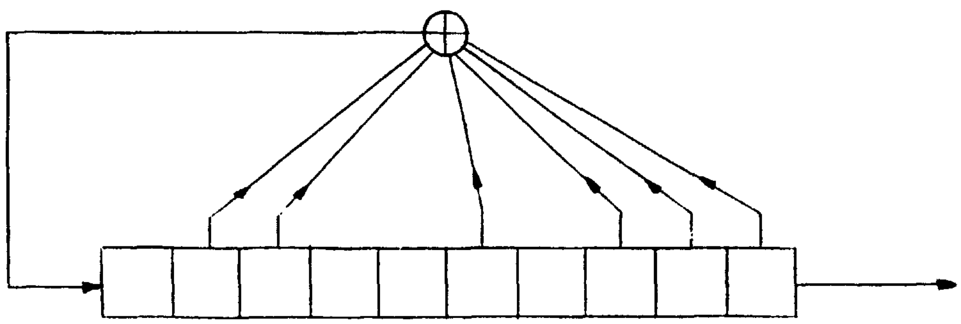

(a) Simple Feedback Shift Register

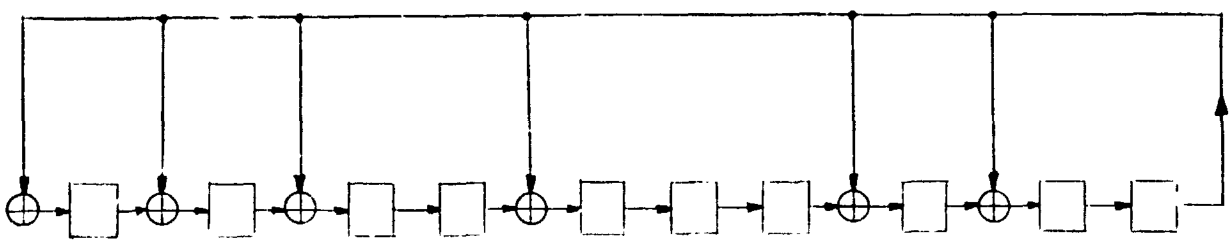

(b) Equivalent Modular Shift Register

Figure 5.8-2. Equivalent 10-Stage Simple and Modular Shift Registers

We note that the general rule for constructing the n-stage modular register from the shift register polynomial is that the output of the last stage on the right of the modular register feeds back to the kth stage (counting from left to right) if and only if $f(n-k+1) = 1$. Thus, in the above example, the output of the tenth stage is fed back to stage $k = 3$ since $f(10-3+1) = f(8) = 1$.

5.9 References

1. N. Zierler, "Linear Recurring Sequences," J. Soc. Indust. Appl. Math., Vol. 7, No. 1, March 1959, 31-48.

2. Robert Gold Associates, "Properties of Linear Binary Encoding Sequences," November 1973.

3. R. W. Marsh, "Tables of Irreducible Polynomials Over GF(2) Through Degree 19," Clearinghouse of Federal Scientific and Technical Information, U. S. Department of Commerce, October 24, 1957.

4. W. W. Peterson, Error-Correcting Codes, The MIT Press and John Wiley & Sons, Inc., 1961.

5. M. Bradford, "Some Further Generating Polynomials for Binary M-Sequences (U)," DRTE Report No. 1144, Defence Research Telecommunications Establishment, Canada, June 1965.

6. E. J. Watson, "Primitive Polynomials (Mod 2)," J. Soc. Indust. Appl. Math., Vol. 10, No. 1, March 1962, 368-369.

7. R. Gold, "Optimal Binary Sequences for Spread Spectrum Multiplexing," IEEE Transactions on Information Theory, IT-13, No. 4, October 1967, 619-621.

8. R. Gold, "Maximal Recursive Sequences with 3-Valued Recursive Cross-Correlation Functions," IEEE Transactions on Information Theory, Vol. IT-14, No. 1, January, 1968, 154-156.

9. R. Gold, "Characteristic Linear Sequences and Their Coset Functions," J. SIAM Appl. Math., Vol. 14, No. 5, September 1966, 980-985.

10. W. W. Peterson, Error Correcting Codes, The MIT Press and John Wiley & Sons, Inc., 1961

11. Magnavox Co., "TDRSS Telecommunications Study, Phase I - Final Report," MRL Report R-4953, September 15, 1974.

APPENDIX A.5

CORRELATION PROPERTIES OF GOLD CODES

A.5.1 INTRODUCTION

In this appendix, we give a detailed description and derivation of the two algorithms which may be used to determine the data presented in section 5.6.2.

Let G(a, b) be the family of Gold codes generated by taking all linear combinations of the maximal PN sequences a and b. The cross-correlation function of any two members of the family G(a, b) takes on values which are selected from the values of the cross-correlation function of the maximal sequences a and b. Thus, once a bound on the cross-correlation function of the sequences a and b has been determined, the same bound holds for the correlation function of any two sequences of the family G(a, b).

The distribution of the cross-correlation values and the rms value of the cross-correlation function for any pair of Gold codes are of interest in the calculation of the acquisition performance of these codes. However, although this distribution and rms value have been determined for preferred pairs of maximal sequences and have been used as an approximation to the distribution and rms value for the corresponding family of codes generated by the pair of maximal PN sequences, the precise distribution of correlation values and the rms value for the codes of the family have not been determined. In what follows, we present two algorithms for the determination of the distribution of the cross-correlation values of any pair of Gold codes.

A.5.2 RESULTS FOR MAXIMAL PN SEQUENCES

We first note the distribution function of the cross-correlation values of a preferred pair of maximal PN sequences and the rms value of the cross-correlation function of any two maximal PN sequences.

A.5.2.1 Distribution of Correlation Values

The following result holds for the distribution of the 2^n-1 correlation values of a preferred pair of maximal PN sequences of period 2^n-1 (n odd).

$\theta(a,b)$	Frequency of occurrence
$-(2^{(n+1)/2}+1)$	$2^{n-2} - 2^{(n-3)/2}$
$(2^{(n+1)/2}-1)$	$2^{n-2} + 2^{(n-3)/2}$
-1	$2^{n-1} - 1$
	$\Sigma = 2^n - 1$

We thus note that the cross-correlation sidelobes occur at 2^{n-1} of the 2^n-1 correlation values.

A.5.2.2 RMS Value of Correlation Function of Maximal Sequences

The sum of the squares of the correlation values of any two maximal sequences of period $p = 2^n - 1$ is given by $p^2 + p - 1$ from which the rms value of the distribution of the correlation function is readily computed to be $\sqrt{p+1-(1/p)} \sim \sqrt{p}$ for large periods p. To see this, we use the following relationship between the cross- and autocorrelation function of binary sequences, which is proved in sec. A.5.3.4.3.

$$\sum_{\tau=0}^{p-1} \theta^2(a,b)(\tau) = \sum_{\tau=0}^{p-1} \theta(a,a)(\tau)\,\theta(b,b)(\tau)\,.$$

Since for maximal linear sequences we have:

$$\begin{aligned}\theta(a,a)(\tau) = \theta(b,b)(\tau) &= p \quad \text{for } \tau = 0\\ &= -1 \text{ for } \tau \neq 0\,,\end{aligned}$$

$$\sum_{\tau=0}^{p-1} \theta^2(a,b)(\tau) = p^2 + p - 1\,,$$ and the result follows.

For $p = 15$, we have

$$\sum_{\tau=0}^{15} \theta^2(a,b)(\tau) = 239\,.$$

However, we note from Table 2 that, in fact, the sum of the squares of the correlation function for the Gold codes of this example vary from 79 to 623 and, hence, a more precise estimate of their performance than that derived from the cross-correlation function of the maximal PN sequences which generate the family is desirable. An algorithm to obtain more precise estimates of code performance is discussed in the following section.

A.5.3 DERIVATION OF ALGORITHM

In this section, we derive an algorithm for the computation of the precise correlation functions of the Gold codes. The resultant expression will give the cross-correlation values of any two codes of the family in terms of the cross-correlation values and the shift-and-add function of the maximal PN codes which generate the family. In sec. A.5.3.1, we define the shift-and-add function of maximal linear PN sequences and indicate how these functions may be computed efficiently. In sec. A.5.3.2, we describe further properties of Gold codes which are required, and in sec. A.5.3.3, we detail the algorithm for the efficient computation of the cross-correlation function of these codes.

A.5.3.1 Shift-and-Add Function of a Maximal Linear Sequence

Let a_0 be a maximal PN sequence and let a_i denote the sequence obtained from a_0 by cyclically shifting this sequence i positions to the right. Since the modulo-2 sum of a maximal sequence with a proper phase shift of itself is another phase shift of the original sequence (i.e., the shift-and-add property of maximal linear sequences), we have:

$$a_k + a_{k+i} = a_{\phi_a(i)+k} ,$$

where ϕ_a is the shift-and-add function of the sequence a. Thus, $\phi_a(i)$ is the shift of the sequence a_k obtained when the sequence a_k is added modulo-2 to an i^{th} cyclic shift of itself. The shift-and-add function of a maximal linear sequence of period 2^n-1 is a permutation of the integers $1, 2, \ldots, 2^n-2$. This permutation may be determined from a reduced number of values since it is the product of transpositions and, if (i, j) is one of the transpositions, so is $(2i, 2j)$.

Thus, for example, for the maximal PN sequence given by $a = 1110100$:

$$\phi_a = \begin{pmatrix} 1 & 2 & 3 & 4 & 5 & 6 \\ 3 & 6 & 1 & 5 & 4 & 2 \end{pmatrix}$$

$$= (13)(26)(45)$$

$$(2,6) = 2(1,3)$$

$$(4,5) = 2(2,6)\ .$$

Thus, once we have determined that $\phi_a(1) = 3$, the permutation ϕ_a is readily determined.

A. 5. 3. 2 Properties of Gold Family of Codes

The members of the family of codes $G(a_0, b_0)$ consisting of the linear combinations of the maximal PN sequences a_0 and b_0 and all phase shifts of these linear combinations may be represented by all phase shifts of the set of sequences given by

$$g_i = a_0 + b_i \qquad\qquad i = 0, 1, 2, \ldots$$

where b_i denotes the i^{th} cyclic shift of the sequence b_0. The codes $\{g_i\}_{i=0}^{2^n-2}$ and their proper phase shifts are all distinct, since $(g_i)_{\tau_1} = (g_j)_{\tau_2}$ implies $(a_0 + b_i)_{\tau_1} = (a_0 + b_j)_{\tau_2}$ implies $a_{\tau_1} + b_{i+\tau_1} = a_{\tau_2} + b_{j+\tau_2}$ implies

$$a_{\tau_1 + \phi_a(\tau_2 - \tau_1)} = b_{(i+\tau_1)+\phi_b((\tau_2 - \tau_1)+(j-i))}\ .$$

This latter equation implies that phase shifts of two different maximal PN sequences are equal, which is impossible.

We also note that the family of codes $G(a, b)$ is closed with respect to modulo-2 addition, i.e., the modulo-2 sum of any two codes of the family $G(a, b)$ is another member of the family:

$$(g_i)_{\tau_1} + (g_j)_{\tau_2}$$

$$(a_0 + b_i)_{\tau_1} + (a_0 + b_j)_{\tau_2}$$

$$a_{\tau_1} + b_{i+\tau_1} + a_{\tau_2} + b_{j+\tau_2}$$

$$a_{\tau_1+\phi_a(\tau_2-\tau_1)} + b_{i+\tau_1+\phi_b((\tau_2-\tau_1)+(j-i))}$$

$$(a_0+b_k)_{\tau_3} = (g_k)_{\tau_3}$$

where $\qquad k = i+\phi_b((\tau_2-\tau_1)+j-i)-\phi_a(\tau_2-\tau_1)$

and $\qquad \tau_3 = \tau_1+\phi_a(\tau_2-\tau_1)$.

A.5.3.3 Correlation Function of Gold Codes

To compute the cross-correlation function $\theta(a,b)$ of codes a and b of period 2^n-1, we add the codes in each of their relative phase shifts and count the number of zeroes minus the number of ones in their modulo-2 sum, i.e.,

$$\theta(a,b)(i) = (n_0-n_1)(a+b_i) = (n_0-n_1)(g_i) \qquad i = 0,1,2,\ldots,2^n-2.$$

Since the family of codes G(a, b) is closed with respect to modulo-2 addition, the cross-correlation function of any two members g_i, g_j of the family takes correlation values from the set of values $\{\theta(a,b)(i)\}$, i.e.,

$$\theta(g_i,g_j)(t) = (n_0-n_1)(g_i+g_{j+t}) = (n_0-n_1)(g_k) = \theta(a,b)(k)$$

for some integer k. Unfortunately, as t varies from 0 to 2^n-2, k does not cover all integers from 0 to 2^n-2 (the mapping from t to k is not one-to-one) and, hence, the distribution of the values of $\theta(g_i,g_j)$ is not the same as the known distribution of the values of $\theta(a,b)$. In what follows, we present an algorithm for the computation of the cross-correlation function $\theta(g_i,g_j)$ of any two members of the family G(a, b) in terms of the cross-correlation function of the maximal PN codes a and b which generate the family.

Theorem: Let g_s and g_t be any two codes of the family $G(a_0, b_0)$ where $g_s = a_0+b_s$ and $g_t = a_0+b_t$. Then,

$$\theta(g_s,g_t)(\tau) = \theta(a,b)(s+\phi_b(t-s+\tau)-\phi_a(\tau)), \qquad \tau \neq 0,\ t-s+\tau \neq 0$$

$$= -1, \text{ otherwise.}$$

ϕ_a and ϕ_b are the shift-and-add functions of the sequences a and b, respectively.

Proof: Case 1 -- $\tau \neq 0$, $t - s + \tau \neq 0$

$\theta(g_s, g_t)(\tau)$

$(n_0 - n_1)(g_s + (g_t)_\tau)$ Number of zeroes - number of ones in $g_s + g_{t+\tau}$

$(n_0 - n_1)(a_0 + b_s + (a_0 + b_t)_\tau)$

$(n_0 - n_1)((a_0 + a_\tau) + (b_s + b_{t+\tau}))$

$(n_0 - n_1)(a_{\phi_a(\tau)} + b_{s+\phi_b(t-s+\tau)})$

$(n_0 - n_1)(a_0 + b_{s+\phi_b(t-s+\tau)-\phi_a(\tau)})$

$\theta(a_0, b_0)(s + \phi_b(t-s+\tau) - \phi_a(\tau))$

Case 2 -- $\tau = 0$

$\theta(g_s, g_t)(0)$

$(n_0 - n_1)(g_s + g_t)$

$(n_0 - n_1)(a_0 + b_s + a_0 + b_t)$

$(n_0 - n_1)(b_s + b_t) = -1$ since b is a maximal linear PN sequence.

The proof for the case $t - s + \tau = 0$ is similar.

A.5.3.4 Computational Example of Algorithm

A.5.3.4.1 G generated by any two maximal PN sequences

In this section, we illustrate the application of the above theorem in an algorithm for the computation of the cross-correlation function of any two members of the family G(a, b). The required inputs to the algorithm are the cross-correlation function of the maximal sequences a and b and the shift-and-add functions of these sequences. In the following example, we consider the two maximal linear sequences of period 15 and the family $G(a_0, b_0)$ of Gold codes generated therefrom. The shift-and-add functions ϕ_a and ϕ_b and the cross-correlation function of these sequences have been computed and are listed below. The data in Table 1 illustrates the computations required for the determination of the cross-correlation function $\theta(g_2, g_3)$.

Computation of $\theta(g_2, g_3)$

$$\theta(g_s, g_t)(\tau) = \theta(a, b)(s + \phi_b(t - s + \tau) - \phi_a(\tau)) \qquad \tau \neq 0, \; t - s + \tau \neq 0$$

$$= -1, \quad \text{otherwise}.$$

$$\theta(g_2, g_3)(\tau) = \theta(a, b)(2 + \phi_b(1 + \tau) - \phi_a(\tau)) \qquad \tau \neq 0, \tau \neq 14$$

$$= -1, \quad \text{otherwise}.$$

Let $\tau' = (2 + \phi_b(1 + \tau) - \phi_a(\tau))$.

τ	τ'	$\theta(a, b)(\tau')$	$\theta(g_2, g_3)(\tau)$
0	--	--	-1
1	7	-1	-1
2	13	-1	-1
3	6	3	3
4	11	-1	-1
5	0	-1	-1
6	2	-5	-5
7	14	-1	-1
8	2	-5	-5
9	0	-1	-1
10	11	-1	-1
11	6	3	3
12	13	-1	-1
13	7	-1	-1
14	--	--	--

Table 1. Input Data for Algorithm

		0	1	2	3	4	5	6	7	8	9	10	11	12	13	14		
a_0	=	0	1	1	1	1	0	1	0	1	1	0	0	1	0	0		
b_0	=	0	0	0	1	0	0	1	1	0	1	0	1	1	1	1		
g_0	=	0	1	1	0	1	0	0	1	1	0	0	1	0	1	1	$\theta(g_0)$	= -1
g_1	=	1	1	1	1	0	0	1	1	0	1	1	0	0	1	1	$\theta(g_1)$	= -5
g_2	=	1	0	1	1	1	1	1	0	0	0	0	1	1	1	1	$\theta(g_2)$	= -5
g_3	=	1	0	0	1	1	0	0	0	1	0	1	0	0	0	1	$\theta(g_3)$	= 3
g_4	=	1	0	0	0	1	0	1	1	1	1	1	1	1	1	0	$\theta(g_4)$	= -5
g_5	=	0	0	0	0	0	0	1	0	0	1	0	1	0	0	1	$\theta(g_5)$	= 7
g_6	=	1	1	0	0	0	1	1	0	1	0	0	0	0	1	0	$\theta(g_6)$	= 3
g_7	=	0	0	1	0	0	1	0	0	1	1	1	0	1	1	1	$\theta(g_7)$	= -1
g_8	=	1	1	0	1	0	1	0	1	1	1	0	1	1	0	1	$\theta(g_8)$	= -5
g_9	=	1	0	1	0	1	1	0	1	0	1	0	0	0	0	0	$\theta(g_9)$	= 3
g_{10}	=	0	0	0	1	0	0	0	1	0	0	0	0	1	1	0	$\theta(g_{10})$	= 7
g_{11}	=	0	1	0	0	1	1	1	1	0	0	1	0	1	0	1	$\theta(g_{11})$	= -1
g_{12}	=	1	1	1	0	0	0	0	0	0	0	1	1	1	0	0	$\theta(g_{12})$	= 3
g_{13}	=	0	0	1	1	0	1	1	1	1	0	1	1	0	0	0	$\theta(g_{13})$	= -1
g_{14}	=	0	1	0	1	1	1	0	0	0	1	1	1	0	1	0	$\theta(g_{14})$	= -1

$\theta(g_i)$ = number of zeroes - number of ones in g_i

	0	1	2	3	4	5	6	7	8	9	10	11	12	13	14
ϕ_a	-	4	8	14	1	10	13	9	2	7	5	12	11	6	3
ϕ_b	-	12	9	4	3	10	8	13	6	2	5	14	1	7	11
$\theta(a,b)$	-1	-5	-5	3	-5	7	3	-1	-5	3	7	-1	3	-1	-1

As an example of the above computation, we have (see Table 1):

$$\theta(g_2, g_3)(6)$$

$$\theta(a, b)(2 + \phi_b(7) - \phi_a(6))$$

$$\theta(a, b)(2 + 13 - 13)$$

$$\theta(a, b)(2) = -5 .$$

A.5.3.4.2 Case for a and b reverse sequences

The formula for the correlation of members of the code family which was presented in sec. A.5.3.4.1 may be simplified in the case where the pair of maximal PN sequences generating the code family consists of sequences which are the reverse of one another. In this case, the formula for the correlation of any pair g_s, g_t of codes of the family becomes

$$\theta(g_s, g_t)(\tau) = \theta(a, b)(s + \phi_b(t - s + \tau) - \phi_b(\tau)) \qquad \tau \neq 0,\ \tau + t - s \neq 0$$

$$= -1 , \quad \text{otherwise} .$$

This simplification follows from the fact that, in this case, we have $\phi_a(\tau) = [illegible] \cdot \phi_b(\tau)$ and in any case we have $\phi_b(\tau) - \phi_b(-\tau) =$ [illegible]. Using these two formulas results in the above expression for $\theta(g_s, g_t)(\tau)$.

It is also useful to note that, in the present case, the cross-correlation function $\theta(g_s, g_t)$ is symmetric about some value of τ. To see this, we note that $t - s + \tau_0 = -\tau_0$ for τ_0 a solution of the congruence $2\tau \equiv s - t$ modulo $2^n - 1$. Then $\theta(g_s, g_t)$ is symmetric about τ_0 and hence we need only compute the values of $\theta(g_s, g_t)$ at $\tau_0, \tau_0+1, \tau_0+2, \ldots, \tau_0+2^{n-2}-1$. As an example, we again consider the family of Gold codes of period 15 given in sec. A.5.3.4.1. We note from the data of that section.

	0	1	2	3	4	5	6	7	8	9	10	11	12	13	14
$\theta(g_0, g_1) =$	-1	7	-1	-5	3	-1	-1	3	-1	-1	3	-5	-1	7	-1

Solving the congruence $2\tau = -1$ modulo 15, we find $\tau_0 = 7$ and note that $\theta(g_0, g_1)$ is in fact symmetric about $\tau_0 = 7$.

A. 5. 3. 4. 3 Proof of basic formulas

In this section, we present the proofs of the basic formulas used in the previous sections.

<u>Theorem</u>: Let a and b be any two binary sequences of period p.

Then: $$\sum_{\tau=0}^{p-1} \theta(a,b)(\tau) = \theta(a)\cdot\theta(b),$$ where

$\theta(a)$ = number of zeroes - number of ones in a period of the sequence a

<u>Proof</u>:

$$\sum_{\tau=0}^{p-1} \theta(a,b)(\tau)$$

$$\sum_{\tau=0}^{p-1}\sum_{i=0}^{p-1} a(i)\, b(i-\tau)$$

$$\sum_{i=0}^{p-1} a(i) \sum_{\tau=0}^{p-1} b(i-\tau)$$

$$\left(\sum_{i=0}^{p-1} a(i)\right)\theta(b)$$

$$\theta(a)\ \theta(b)$$

<u>Theorem</u>: Let a and b be any two binary ($\underline{+}$) sequences of period p.

Let $$\theta(a,b)(\tau) = \sum_{i=0}^{p-1} a(i)\, b(i-\tau)$$

Then: $$\sum_{\tau=0}^{p-1}\left[\theta(a,b)(\tau)\right]^2 = \sum_{\tau=0}^{p-1}\theta(a,a)(\tau)\ \theta(b,b)(\tau)$$

<u>Proof</u>:

$$\sum_{\tau=0}^{p-1}\left[\theta(a,b)(\tau)\right]^2$$

$$\sum_{\tau=0}^{p-1}\left[\sum_{i=0}^{p-1} a(i)\, b(i-\tau)\right]^2$$

$$\sum_{\tau=0}^{p-1}\sum_{i=0}^{p-1}\sum_{j=0}^{p-1} a(i)\, a(j)\, b(i-\tau)\, b(j-\tau)$$

$$\sum_{i=0}^{p-1}\sum_{j=0}^{p-1} a(i)\, a(j) \sum_{\tau=0}^{p-1} b(i-\tau)\, b(j-\tau)$$

$$\sum_{i=0}^{p-1}\sum_{j=0}^{p-1} a(i)\, a(j)\; \theta(b,b)(j-i)$$

Letting $\ell = j-i$, we have

$$\sum_{\tau=0}^{p-1}\sum_{j=0}^{p-1} a(j)\, a(j-\ell)\;\theta(b,b)(\ell)$$

$$\sum_{\tau=0}^{p-1} \theta(a,a)(\ell)\;\theta(b,b)(\ell)$$

<u>Theorem:</u> Let F be any family of binary sequences of period p. For any two sequences $a, b \epsilon F$, we have:

$$\sum_{\tau=0}^{p-1} \theta^2(a,b)(\tau) \le \max_{c\epsilon F} \sum_{\tau=0}^{p-1} \theta^2(c,c)(\tau)$$

<u>Proof:</u>

$$\sum_{\tau=0}^{p-1} \theta^2(a,b)(\tau)$$

$$\sum_{\tau=0}^{p-1} \theta(a,a)(\tau)\;\theta(b,b)(\tau) \qquad \text{by previous theorem}$$

$$\le \sqrt{\sum_{\tau=0}^{p-1} \theta^2(a,a)(\tau)}\;\sqrt{\sum_{\tau=0}^{p-1} \theta^2(b,b)(\tau)}$$

$$\leq \max_{c \in F} \sum_{\tau=0}^{p-1} \theta^2(c,c)(\tau)$$

The following example shows that, in general, this bound cannot be improved. Let $F = \{a, b\}$ where a and b are maximal PN sequences. Then,

$$\sum_{\tau=0}^{p-1} \theta^2(a,b)(\tau) = \sum_{\tau=0}^{p-1} \theta(a,a)(\tau)\ \theta(b,b)(\tau) = p^2 + p - 1 .$$

The significance of this result is that it provides a bound for the rms value of the cross-correlation function of members of a family of sequences F from an examination of the rms values of the autocorrelation function of the members of the family.

Example: Let G be the family of 15 binary PN sequences of the example of sec. A.5.3.4.1 (Table 1). The sum of the squares of the cross-correlation function

$$\sum_{\tau=0}^{p-1} \theta^2(g_i, g_j)(\tau)$$

are listed in Table 2. We note that

$$\sum_{\tau=0}^{p-1} \theta^2(g_i, g_j)(\tau) \leq \max \sum_{\tau=0}^{p-1} \theta^2(g_i, g_j)(\tau) = 623 \quad \text{for all } i, j.$$

This bound may be reduced to 497 by omitting the sequence g_1 from the family; however, this will not in fact improve the overall cross-correlation bound.

A.5.4 ALTERNATE TECHNIQUES FOR THE DETERMINATION OF CROSS-CORRELATION FUNCTION OF GOLD CODES

In what follows, we present formulas for the number of times each of the possible three correlation values appears in the cross-correlation function of any two Gold codes. The input data for these formulas depends on the autocorrelation function of the codes being correlated and hence, while some preliminary calculations are required, the determination of

Table 2. Sum of Squares of Cross-Correlation Values of Gold Codes of Period 15

$\theta(g_i, g_j)$	0	1	2	3	4	5	6	7	8	9	10	11	12	13	14
0	623	183	183	135	183	255	135	239	183	135	255	239	135	239	239
1		479	287	239	191	199	271	311	287	79	167	119	143	215	215
2			479	79	287	167	239	119	191	143	199	215	271	215	311
3				447	143	151	191	295	271	191	311	231	287	199	199
4					479	199	79	215	287	271	167	215	239	311	119
5						463	311	223	167	311	271	159	151	223	159
6							447	231	143	287	151	199	191	199	295
7								367	215	199	159	143	199	303	143
8									479	239	199	311	79	119	215
9										447	151	295	191	231	199
10											463	223	311	159	223
11												367	199	143	303
12													447	295	231
13														367	143
14															367

the distribution function of the sidelobes of the cross-correlation values of a family of Gold codes is reduced by means of these formulas to a feasible computational problem.

A. 5. 4. 1 Statement of Formulas

Theorem: Let g_1 and g_2 be any two Gold codes of period 2^n-1 (n odd). The cross-correlation function $\theta(g_1, g_2)$ is known to assume the three values:

$$\theta_1 = -(2^{(n+1)/2}+1); \quad \theta_2 = 2^{(n+1)/2}-1; \quad \theta_3 = -1 .$$

The number of times each of these values is assumed is given by

$$N(\theta_1) = \frac{(\sum\theta^2) - (\sum\theta)(2^{(n+1)/2} - 2) - (2^n - 1)(2^{(n+1)/2} - 1)}{2^{n+2}}$$

$$N(\theta_2) = \frac{(\sum\theta^2) + (\sum\theta)(2^{(n+1)/2} + 2) - (2^n - 1)(2^{(n+1)/2} + 1)}{2^{n+2}}$$

$$N(\theta_3) = \frac{(2^n - 1)(2^{n+1} - 1) - \sum\theta^2 - 2\sum\theta}{2^{n+1}}$$

where

$$\sum\theta^2 = \sum_{\tau=0}^{2^n-2} \theta^2(g_1, g_2)(\tau) \quad \sum_{\tau=0}^{2^n-1} \theta(g_1, g_2)(\tau)$$

The autocorrelation function of any such Gold code assumes the same three values. The number of times each of these values is assumed in the autocorrelation function is given by

$$N(\theta_1) = \frac{\sum\theta^2 - (\sum\theta)(2^{(n+1)/2} - 2) - (2^{2n} - 2^n - 2^{(n+1)/2} + 1)}{2^{n+2}}$$

$$N(\theta_2) = \frac{\sum\theta^2 + (\sum\theta)(2^{(n+1)/2} + 2) - (2^{2n} - 2^n + 2^{(n+1)/2} + 1)}{2^{n+2}}$$

$$N(\theta_3) = \frac{(3 \cdot 2^{2n} - 2^{n+2} + 2^n + 1) - \sum \theta^2 - 2\sum \theta}{2^{n+1}}$$

Since $\displaystyle\sum_{\tau=0}^{2^n-2} \theta^2(g_1, g_2)(\tau) = \sum_{\tau=0}^{2^n-2} \theta(g_1, g_1)(\tau)\, \theta(g_2, g_2)(\tau)$

and $\displaystyle\sum_{\tau=0}^{2^n-2} \theta(g_1, g_2)(\tau) = \theta(g_1) \cdot \theta(g_2)$,

where $\theta(g_i)$ = number of zeroes - number of ones in the sequence g_i, the number of sidelobes in the cross-correlation function of any two Gold codes may be determined in terms of the parameters of each of the codes itself.

A. 5. 4. 2 Example

Let $n = 3$. We consider the following family of Gold codes:

g_0 = 0 1 1 1 1 1 1 $\quad \theta(g_0) = -5$

g_1 = 0 0 1 0 0 0 1 $\quad \theta(g_1) = 3$

g_2 = 0 0 0 0 1 1 0 $\quad \theta(g_2) = 3$

g_3 = 1 0 0 1 1 0 1 $\quad \theta(g_3) = -1$

g_4 = 0 1 0 1 0 0 0 $\quad \theta(g_4) = 3$

g_5 = 1 0 1 1 0 1 0 $\quad \theta(g_5) = -1$

g_6 = 1 1 0 0 0 1 1 $\quad \theta(g_6) = -1$

τ =	0	1	2	3	4	5	6
$\theta(g_0, g_0)$	7	3	3	3	3	3	3
$\theta(g_1, g_1)$	7	-1	-1	3	3	-1	-1
$\theta(g_2, g_2)$	7	3	-1	-1	-1	-1	3
$\theta(g_3, g_3)$	7	-1	-5	3	3	-5	-1
$\theta(g_4, g_4)$	7	-1	3	-1	-1	3	-1
$\theta(g_5, g_5)$	7	-5	3	-1	-1	3	-5
$\theta(g_6, g_6)$	7	3	-1	-5	-5	[illegible]	3

The product $\sum_{\tau=0}^{2^n-2} \theta^2(g_i, g_j)(\tau) = \sum_{\tau=0}^{2^n-2} \theta(g_i, g_i)(\tau) \cdot \theta(g_j, g_j)(\tau)$

$$= \theta(g_i, g_i) \cdot \theta(g_j, g_j)$$

is given as follows:

$\theta(g_i, g_i) \cdot \theta(g_j, g_j)$

	0	1	2	3	4	5	6
0	103	55	55	31	55	31	31
1		71	39	79	39	47	15
2			71	47	39	15	79
3				119	15	23	23
4					71	79	47
5						119	23
6							119

The products $\theta(g_i) \cdot \theta(g_j)$ are given as follows:

	0	1	2	3	4	5	6
0	25	-15	-15	5	-15	5	5
1		9	9	-3	9	-3	-3
2			9	-3	9	-3	-3
3				1	-3	1	1
4					9	-3	-3
5						1	1
6							1

The data in the previous two tables represents the required inputs to the formulas for determining the distribution of sidelobes in the correlation function of any two Gold codes. In this example, the general formulas become:

Cross-Correlation

$$N(\theta_1) = \frac{\sum\theta^2 - 2\sum\theta - 21}{32}$$

$$N(\theta_2) = \frac{\sum\theta^2 + 6\sum\theta + 35}{32}$$

$$N(\theta_3) = \frac{105 - 2\sum\theta - \sum\theta^2}{16}$$

Autocorrelation

$$N(\theta_1) = \frac{\sum\theta^2 - 2(\sum\theta) - 53}{32}$$

$$N(\theta_2) = \frac{\sum\theta^2 + 6(\sum\theta) - 61}{32}$$

$$N(\theta_3) = \frac{153 - 2\sum\theta - \sum\theta^2}{16}$$

We note that the distribution of the sidelobes in the case of autocorrelation could be obtained during the computation of

$$\sum_{\tau=0}^{2^n-1} \theta(g_i, g_i)(\tau) ;$$

however, the given formulas are useful with respect to unifying the required computer programming.

Using the above formulas, we may compute the following table of sidelobe distributions, $N(\theta_1, \theta_2, \theta_3)$:

	0	1	2	3	4	5	6
0	(0,6,0)	(2,0,5)	(2,0,5)	(0,3,4)	(2,0,5)	(0,3,4)	(0,3,4)
1		(0,2,4)	(0,4,3)	(2,3,2)	(0,4,3)	(1,2,4)	(0,1,6)
2			(0,2,4)	(1,2,4)	(0,4,3)	(0,1,6)	(2,3,2)
3				(2,2,2)	(0,1,6)	(0,2,5)	(0,2,5)
4					(0,2,4)	(2,3,2)	(1,2,4)
5						(2,2,2)	(0,2,5)
6							(2,2,2)

A.5.4.3 Proof of Formulas

Let x, y, z be the number of times the values $-(2^{(n+1)/2}+1)$, $(2^{(n+1)/2}-1)$, -1, respectively, occur in the cross-correlation function of two Gold codes, g_1 and g_2, of period (2^n-1). We then have the system of equations:

$$x\,(2^{(n+1)/2}+1)^2 + y\,(2^{(n+1)/2}-1)^2 + z = \sum_{\tau=0}^{2^n-2} \theta^2(g_1,g_2)(\tau) = \sum\theta^2$$

$$x + y + z = 2^n - 1$$

$$x\,{-(2^{(n+1)/2}+1)} + y\,(2^{(n+1)/2}-1) - z = \sum_{\tau=0}^{2^n-2} \theta(g_1,g_2)(\tau) = \sum\theta$$

Solving this system of equations, we have

$$x = \frac{\sum\theta^2 - \sum\theta(2^{(n+1)/2}-2) - (2^n-1)(2^{(n+1)/2}-1)}{2^{n+2}}$$

$$y = \frac{\sum\theta^2 + \sum\theta(2^{(n+1)/2}+2) + (2^n-1)(2^{(n+1)/2}+1)}{2^{n+2}}$$

$$z = \frac{(2^n-1)(2^{n+1}-1) - \sum\theta^2 - 2\sum\theta}{2^{n+1}}$$

The number of sidelobes in the cross-correlation function of two Gold codes, x+y, may be obtained more directly using the following argument.

The possible values for $\theta(a,b)(\tau)$ are $-2^{(n+1)/2}-1,\ 2^{(n+1)/2}-1,\ -1,$ and hence the values for $[\theta(a,b)(\tau)+1]^2$ are 2^{n+1} when there is a sidelobe and 0 when there is no sidelobe. Thus,

$$\sum_{\tau=0}^{2^n-2} [\theta(a,b)(\tau)+1]^2 = (x+y)\cdot 2^{n+1}$$

or

$$(x+y) = \frac{\sum_{\tau=0}^{2^n-2} [\theta(a,b)(\tau)+1]^2}{2^{n+1}} = \frac{\sum\theta^2 + 2\sum\theta + (2^n-1)}{2^{n+1}}$$

Autocorrelation

In this case, our system of equations is:

$$x\ (2^{(\text{[illegible]}}+1)^2 + y\,(2^{(n+1)/2}-1)^2 + z = \sum_{\tau=0}^{2^n-2} \theta^2(g,g)(\tau) - (2^n-1)^2$$

$$x + y + z = 2^n - 2$$

$$x\,-(2^{(n+1)/2}+1) + y\,(2^{(n+1)/2}-1) - z = \sum_{\tau=0}^{2^n-2} \theta(g,g)(\tau) - (2^n-1)$$

Solving this system of equations, we obtain:

$$x = \frac{\sum\theta^2 - (\sum\theta)\,(2^{(n+1)/2}-2) - (2^{2n} - 2^n - 2^{(n+1)/2} + 1)}{2^{n+2}}$$

$$y = \frac{\sum\theta^2 + (\sum\theta)\,(2^{(n+1)/2}+2) - (2^{2n} - 2^n + 2^{(n+1)/2} + 1)}{2^{n+2}}$$

$$z = \frac{(3 \cdot 2^{2n} - 2^{n+2} - 2^n + 1) - \sum\theta^2 - 2\sum\theta}{2^{n+1}}$$

As in the case of the cross-correlation function, the number of sidelobes in the autocorrelation function of a Gold code, x+y, may be obtained more directly.

The possible values for $\theta(a,b)(\tau)$ are $-2^{(n+1)/2}-1$, $2^{(n+1)/2}-1$, -1, 2^n-1 ($\tau = 0$), and hence the values for $[\theta(a,b)(\tau)+1]^2$ are 2^{n+1} when there is a sidelobe, 0 when there is no sidelobe, and 2^{2n} (for $\tau = 0$). Thus, we have

$$\sum_{\tau=0}^{2^n-2} [\theta(a,b)(\tau)+1]^2 = 2^{2n} + (x+y)\,2^{n+1}$$

or

$$(x+y) = \frac{\sum\theta^2 + 2\sum\theta - (2^{2n} - 2^n + 1)}{2^{n+1}}$$

The required computation to obtain the sidelobe distribution in the cross-correlation of Gold codes may be reduced by noting that the sidelobe structure is the same for the pair of codes g_t, g_s and $g_{2^k t}, g_{2^k s}$ for any k. This follows from the fact that

$$\sum_{\tau=0}^{2^n-2} \theta^2(g_t, g_s)(\tau) = \sum_{\tau=0}^{2^n-2} \theta^2(g_{2^k t}, g_{2^k s})(\tau)$$

and

$$\sum_{\tau=0}^{2^n-2} \theta(g_t, g_s)(\tau) = \sum_{\tau=0}^{2^n-2} \theta(g_{2^k t}, g_{2^k s})(\tau)$$

and the number of sidelobes of each kind is seen from the previously derived formulas to depend only upon these quantities. Thus, in the example given for $n = 3$, the tables of input data may be reduced to:

$\theta(g_i, g_i) \cdot \theta(g_j, g_j)$

	0	1	2	3	4	5	6
0	103	55		31			
1		71	39	79	39	47	15
3				119	15	23	23

$\theta(g_i) \cdot \theta(g_j)$

	0	1	2	3	4	5	6
0	25	-15		5			
1		9	9	-3	9	-3	-3
3				1	-3	1	1

The table of sidelobe distributions becomes:

	0	1	2	3	4	5	6
0	(0, 6, 0)	(2, 0, 5)		(0, 3, 4)			
1		(0, 2, 4)	(0, 4, 3)	(2, 3, 2)	(0, 4, 3)	(1, 2, 4)	(0, 1, 6)
3				(2, 2, 2)	(0, 1, 6)	(0, 2, 5)	(0, 2, 5)

A.5.5 FURTHER PROPERTIES OF GOLD CODES

Result: Let $G(a, b)$ be a family of Gold codes of period 2^n-1 generated by the characteristic maximal linear sequences a_0, b_0. Denote $g_i = a_0 + b_i$. Let Ta be the sequence obtained from a by sampling every other term. Then, $T^k(g_i) = g_{i \cdot 2^{n-k}}$.

Proof:

$$T^k(g_i)$$

$$T^k(a_0 + b_i)$$

$$T^k a_0 + T^k b_i$$

$a_0 + b_{i \cdot 2^{n-k}}$ by sampling property of characteristic maximal sequences

$g_{i \cdot 2^{n-k}}$

<u>Example:</u> A Gold family of codes of period $2^4-1 = 15$ is given below.

	0	1	2	3	4	5	6	7	8	9	10	11	12	13	14
g_0	0	1	1	0	1	0	0	1	1	0	0	1	1	0	0
g_1	1	1	1	0	0	1	1	0	1	1	0	0	1	1	1
g_2	1	1	1	1	1	0	0	0	0	1	1	1	1	1	0
g_3	1	1	0	0	0	1	0	1	0	0	0	1	1	0	0
g_4	1	0	1	1	1	1	1	1	1	1	[illegible]	1	0	0	0
g_5	0	1	0	0	1	0	1	0	0	1	0	0	0	0	0
g_6	1	0	1	0	0	0	0	1	0	1	1	0	0	0	1
g_7	0	1	1	1	0	1	1	1	0	0	1	0	0	1	0
g_8	1	1	0	1	1	0	1	1	1	0	1	0	1	0	1
g_9	1	0	0	0	0	0	1	0	1	0	1	1	0	1	0
g_{10}	0	0	1	1	0	0	0	0	1	0	0	0	1	0	0
g_{11}	0	1	0	1	0	1	0	0	1	1	1	1	0	0	1
g_{12}	1	0	0	1	1	1	0	0	0	0	0	0	0	1	1
g_{13}	0	0	0	0	1	1	0	1	1	1	1	0	1	1	0
g_{14}	0	0	1	0	1	1	1	0	0	0	1	1	1	0	1

We note that

$$Tg_1 = T(111001101\ldots) = 11011\ldots$$

$$= g_8 = g_{1 \cdot 2^{4-1}}$$

<u>Result:</u> Let G(a, b) be a family of Gold codes of period [illegible]-1 generated by the characteristic maximal linear sequences a_0, b_0. Denote $g_i = a_0 + b_i$. Then,

$$\{\theta(g_s, g_t)(\tau) \mid \tau = 0,1,\ldots,2^n-1\} = \{\theta(g_{2^k s}, g_{2^k t})(\tau) \mid \tau = 0,1,\ldots,2^n-1\}$$

for any k.

$$\theta(g_s, g_t)(\tau)$$

$$(n_0 - n_1)(g_s + (g_t)_\tau)$$

$$(n_0 - n_1)(a_0 + b_s + a_\tau + b_{t+\tau})$$

$$(n_0 - n_1)\, T^{n-k}(a_0 + b_s + a_\tau + b_{t+\tau})$$ since $n_0 - n_1$ in sampled sequence $= n_0 - n_1$ in original sequence

$$(n_0 - n_1)(a_0 + b_{s \cdot 2^k} + a_{\tau \cdot 2^k} + b_{t \cdot 2^k + \tau \cdot 2^k})$$

$$(n_0 - n_1)(g_{s \cdot 2^k} + (g_{t \cdot 2^k})_{\tau \cdot 2^k})$$

$$\theta(g_{s \cdot 2^k}, g_{t \cdot 2^k})(\tau \cdot 2^k)$$

As τ goes through the numbers $0, 1, \ldots, 2^n-1$, so does $\tau \cdot 2^k$, although in a different order. Thus, the result follows.

This latter result shows that the set of correlation values for g_s and g_t is the same as the set of correlation values for $g_{2^k s}$ and $g_{2^k t}$, and hence the equations:

$$\sum_{\tau=0}^{2^n-2} \theta^2(g_s, g_t)(\tau) = \sum_{\tau=0}^{2^n-2} \theta^2(g_{2^k s}, g_{2^k t})(\tau)$$

and

$$\sum_{\tau=0}^{2^n-2} \theta(g_s, g_t)(\tau) = \sum_{\tau=0}^{2^n-2} \theta(g_{2^k s}, g_{2^k t})(\tau)$$

Using the above results, the data of Table 2 may be reduced to that of the following table.

Table 3. Reduced Listing of Cross-Correlation Values

	0	1	2	3	4	5	6	7	8	9	10	11	12	13	14
0	623	183	183	135	183	255	135	239	183	135	255	239	135	239	239
1		479	287	239	191	199	271	311	287	79	167	119	143	215	215
3				447	143	151	191	295	271	191	311	231	287	199	199
5						463	311	223	167	311	271	159	151	223	159
7								367	215	199	159	143	199	303	143

APPENDIX B. 5

PHASE SHIFT OBTAINED BY ADDITION MODULO 2 OF OUTPUT SEQUENCE AND OUTPUT OF Kth TAP

The following table contains the phase shift obtained when the maximal sequence of period $2^{18}-1$ generated by the shift register corresponding to the listed maximal polynomial is added modulo-2 to the phase-shifted version of the same sequence available at each of the stages of the shift register.

The shift register configuration is illustrated below.

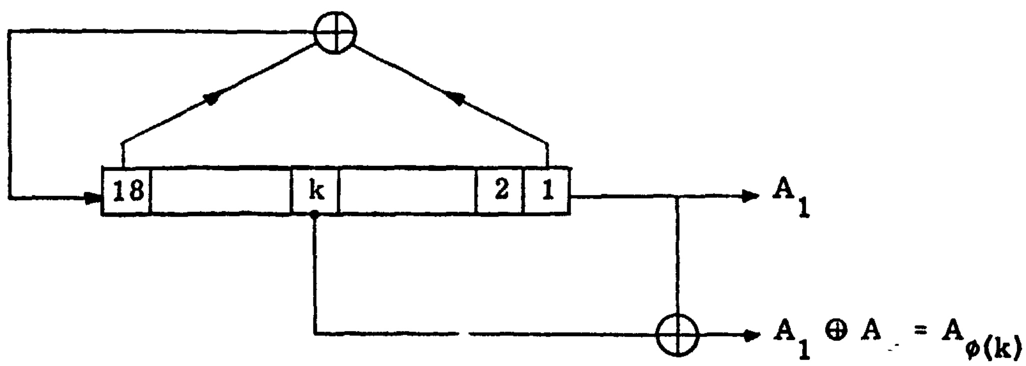

The table lists the phase shift $\phi(k)$ obtained when the sequence A_1 is added to the sequence A_k obtained at the kth stage of the shift register.

For the 100 maximal codes listed, the tap k=10 will yield a maximum phase shift of more than 20,000 chips. The maximum number of feedback taps required for any of the 112 listed generators is 8.

SHIFT REGISTER TAP CONNECTIONS	POSITION OF SECOND TAP K	PHASE SHIFT OF SUM SEQUENCE PHI(K)
1000047	2	125989
1000047	3	10165
1000047	4	112241
1000047	5	20330
1000047	6	96872
1000047	7	37661
1000047	8	30947
1000047	9	40660
1000047	10	94672
1000047	11	68399
1000047	12	28005
1000047	13	75322
1000047	14	23897
1000047	15	61894
1000047	16	16045
1000047	17	81320
1000047	18	21624

SHIFT REGISTER TAP CONNECTIONS	POSITION OF SECOND TAP K	PHASE SHIFT OF SUM SEQUENCE PHI(K)
1431503	2	96930
1431503	3	68283
1431503	4	113163
1431503	5	125577
1431503	6	116535
1431503	7	35817
1431503	8	116062
1431503	9	10989
1431503	10	35529
1431503	11	29073
1431503	12	74626
1431503	13	71634
1431503	14	91302
1431503	15	30019
1431503	16	107836
1431503	17	21978
1431503	18	45909

SHIFT REGISTER TAP CONNECTIONS	POSITION OF SECOND TAP K	PHASE SHIFT OF SUM SEQUENCE PHI(K)
1012633	2	43572
1012633	3	87144
1012633	4	127381
1012633	5	87855
1012633	6	45227
1012633	7	7381
1012633	8	13863
1012633	9	86433
1012633	10	100097
1012633	11	90454
1012633	12	102506
1012633	13	14762
1012633	14	118450
1012633	15	27726
1012633	16	58664
1012633	17	89277
1012633	18	31935

SHIFT REGISTER TAP CONNECTIONS	POSITION OF SECOND TAP K	PHASE SHIFT OF SUM SEQUENCE PHI(K)
1012715	2	45391
1012715	3	90782
1012715	4	126062
1012715	5	80579
1012715	6	20544
1012715	7	10019
1012715	8	3954
1012715	9	100985
1012715	10	37927
1012715	11	41088
1012715	12	58801
1012715	13	20038
1012715	14	122582
1012715	15	7908
1012715	16	97624
1012715	17	60173
1012715	18	56405

SHIFT REGISTER TAP CONNECTIONS	POSITION OF SECOND TAP K	PHASE SHIFT OF SUM SEQUENCE PHI(K)
1010551	2	62969
1010551	3	125938
1010551	4	82800
1010551	5	10267
1010551	6	26517
1010551	7	96543
1010551	8	631
1010551	9	20534
1010551	10	20125
1010551	11	53034
1010551	12	76220
1010551	13	69057
1010551	14	127531
1010551	15	1662
1010551	16	65374
1010551	17	41068
1010551	18	26830

SHIFT REGISTER TAP CONNECTIONS	POSITION OF SECOND TAP K	PHASE SHIFT OF SUM SEQUENCE PHI(K)
1101063	2	37843
1101063	3	75686
1101063	4	98881
1101063	5	110771
1101063	6	130085
1101063	7	64381
1101063	8	47534
1101063	9	40601
1101063	10	127909
1101063	11	1973
1101063	12	26414
1101063	13	128762
1101063	14	18943
1101063	15	95068
1101063	16	109918
1101063	17	81202
1101063	18	69798

SHIFT REGISTER TAP CONNECTIONS	POSITION OF SECOND TAP K	PHASE SHIFT OF SUM SEQUENCE PHI(K)
1010463	2	28668
1010463	3	57336
1010463	4	119485
1010463	5	114672
1010463	6	104310
1010463	7	23173
1010463	8	102626
1010463	9	32799
1010463	10	124686
1010463	11	53523
1010463	12	71542
1010463	13	46346
1010463	14	115389
1010463	15	56891
1010463	16	65488
1010463	17	65598
1010463	18	115013

SHIFT REGISTER TAP CONNECTIONS	POSITION OF SECOND TAP K	PHASE SHIFT OF SUM SEQUENCE PHI(K)
1011267	2	65808
1011267	3	130527
1011267	4	5684
1011267	5	1089
1011267	6	39749
1011267	7	11368
1011267	8	52355
1011267	9	2178
1011267	10	48528
1011267	11	79498
1011267	12	43678
1011267	13	22736
1011267	14	44129
1011267	15	104710
1011267	16	73446
1011267	17	4356
1011267	18	129074

SHIFT REGISTER TAP CONNECTIONS	POSITION OF SECOND TAP K	PHASE SHIFT OF SUM SEQUENCE PHI(K)
1010313	2	69277
1010313	3	123589
1010313	4	64382
1010313	5	14965
1010313	6	123891
1010313	7	128764
1010313	8	2663
1010313	9	29930
1010313	10	122601
1010313	11	14361
1010313	12	53592
1010313	13	4615
1010313	14	40054
1010313	15	5326
1010313	16	5594
1010313	17	59860
1010313	18	77369

SHIFT REGISTER TAP CONNECTIONS	POSITION OF SECOND TAP K	PHASE SHIFT OF SUM SEQUENCE PHI(K)
1125611	2	110099
1125611	3	41945
1125611	4	1533
1125611	5	83890
1125611	6	82283
1125611	7	3066
1125611	8	39706
1125611	9	94363
1125611	10	130803
1125611	11	97577
1125611	12	129371
1125611	13	6132
1125611	14	123547
1125611	15	79412
1125611	16	123310
1125611	17	73417
1125611	18	22468

SHIFT REGISTER TAP CONNECTIONS	POSITION OF SECOND TAP K	PHASE SHIFT OF SUM SEQUENCE PHI(K)
1010211	2	127056
1010211	3	8031
1010211	4	52599
1010211	5	16062
1010211	6	107711
1010211	7	105198
1010211	8	17771
1010211	9	32124
1010211	10	42628
1010211	11	46721
1010211	12	47123
1010211	13	51747
1010211	14	98726
1010211	15	35542
1010211	16	121897
1010211	17	64248
1010211	18	2180

SHIFT REGISTER TAP CONNECTIONS	POSITION OF SECOND TAP K	PHASE SHIFT OF SUM SEQUENCE PHI(K)
1011333	2	125793
1011333	3	10557
1011333	4	108058
1011333	5	21114
1011333	6	2463
1011333	7	46027
1011333	8	81832
1011333	9	42228
1011333	10	121824
1011333	11	4926
1011333	12	70058
1011333	13	92054
1011333	14	116935
1011333	15	98479
1011333	16	38478
1011333	17	84456
1011333	18	103740

SHIFT REGISTER TAP CONNECTIONS	POSITION OF SECOND TAP K	PHASE SHIFT OF SUM SEQUENCE PHI(K)
1010163	2	108919
1010163	3	44305
1010163	4	71027
1010163	5	88610
1010163	6	15978
1010163	7	120089
1010163	8	63469
1010163	9	84923
1010163	10	81188
1010163	11	31956
1010163	12	6569
1010163	13	21965
1010163	14	70101
1010163	15	126938
1010163	16	24856
1010163	17	92297
1010163	18	71392

SHIFT REGISTER TAP CONNECTIONS	POSITION OF SECOND TAP K	PHASE SHIFT OF SUM SEQUENCE PHI(K)
1011533	2	109089
1011533	3	43965
1011533	4	85850
1011533	5	87930
1011533	6	40236
1011533	7	90443
1011533	8	62483
1011533	9	86283
1011533	10	61209
1011533	11	80472
1011533	12	68904
1011533	13	81257
1011533	14	36828
1011533	15	124966
1011533	16	82924
1011533	17	89577
1011533	18	116317

SHIFT REGISTER TAP CONNECTIONS	POSITION OF SECOND TAP K	PHASE SHIFT OF SUM SEQUENCE PHI(K)
1010133	2	104694
1010133	3	52755
1010133	4	77029
1010133	5	105510
1010133	6	101908
1010133	7	108085
1010133	8	108824
1010133	9	51123
1010133	10	36812
1010133	11	58327
1010133	12	46132
1010133	13	45973
1010133	14	10648
1010133	15	44495
1010133	16	102832
1010133	17	102246
1010133	18	11420

SHIFT REGISTER TAP CONNECTIONS	POSITION OF SECOND TAP K	PHASE SHIFT OF SUM SEQUENCE PHI(K)
1011553	2	101729
1011553	3	58685
1011553	4	37512
1011553	5	117370
1011553	6	122981
1011553	7	75024
1011553	8	33214
1011553	9	27403
1011553	10	66194
1011553	11	16181
1011553	12	72743
1011553	13	112095
1011553	14	44233
1011553	15	66428
1011553	16	50628
1011553	17	54806
1011553	18	85278

SHIFT REGISTER TAP CONNECTIONS	POSITION OF SECOND TAP K	PHASE SHIFT OF SUM SEQUENCE PHI(K)
1011347	2	26633
1011347	3	53266
1011347	4	34128
1011347	5	106532
1011347	6	90465
1011347	7	68256
1011347	8	130139
1011347	9	49079
1011347	10	53036
1011347	11	81213
1011347	12	109728
1011347	13	125631
1011347	14	103457
1011347	15	1865
1011347	16	102654
1011347	17	98158
1011347	18	30199

SHIFT REGISTER TAP CONNECTIONS	POSITION OF SECOND TAP K	PHASE SHIFT OF SUM SEQUENCE PHI(K)
1116115	2	49146
1116115	3	98292
1116115	4	79151
1116115	5	65559
1116115	6	109802
1116115	7	103841
1116115	8	41796
1116115	9	131025
1116115	10	74458
1116115	11	42539
1116115	12	73403
1116115	13	54461
1116115	14	109218
1116115	15	83592
1116115	16	92552
1116115	17	93
1116115	18	115775

SHIFT REGISTER TAP CONNECTIONS	POSITION OF SECOND TAP K	PHASE SHIFT OF SUM SEQUENCE PHI(K)
1011261	2	65170
1011261	3	130340
1011261	4	103440
1011261	5	1463
1011261	6	6539
1011261	7	55263
1011261	8	40815
1011261	9	2926
1011261	10	104408
1011261	11	13078
1011261	12	110441
1011261	13	110526
1011261	14	79925
1011261	15	81630
1011261	16	17499
1011261	17	5852
1011261	18	46245

SHIFT REGISTER TAP CONNECTIONS	POSITION OF SECOND TAP K	PHASE SHIFT OF SUM SEQUENCE PHI(K)
1011571	2	120780
1011571	3	20583
1011571	4	121799
1011571	5	41166
1011571	6	123121
1011571	7	18545
1011571	8	33727
1011571	9	82332
1011571	10	102103
1011571	11	15901
1011571	12	25502
1011571	13	37090
1011571	14	28367
1011571	15	67454
1011571	16	56481
1011571	17	97479
1011571	18	8166

SHIFT REGISTER TAP CONNECTIONS	POSITION OF SECOND TAP K	PHASE SHIFT OF SUM SEQUENCE PHI(K)
1012527	2	107643
1012527	3	46857
1012527	4	112118
1012527	5	93714
1012527	6	85834
1012527	7	37907
1012527	8	62
1012527	9	74715
1012527	10	97306
1012527	11	90475
1012527	12	31364
1012527	13	75814
1012527	14	72472
1012527	15	124
1012527	16	122007
1012527	17	112713
1012527	18	46975

SHIFT REGISTER TAP CONNECTIONS	POSITION OF SECOND TAP K	PHASE SHIFT OF SUM SEQUENCE PHI(K)
1012547	2	3973
1012547	3	7946
1012547	4	80251
1012547	5	15892
1012547	6	25576
1012547	7	101641
1012547	8	79868
1012547	9	31784
1012547	10	82029
1012547	11	51152
1012547	12	94429
1012547	13	58861
1012547	14	89109
1012547	15	102407
1012547	16	128621
1012547	17	63568
1012547	18	9903

SHIFT REGISTER TAP CONNECTIONS	POSITION OF SECOND TAP K	PHASE SHIFT OF SUM SEQUENCE PHI(K)
1007705	2	119517
1007705	3	23109
1007705	4	67235
1007705	5	46218
1007705	6	19445
1007705	7	127673
1007705	8	62063
1007705	9	92436
1007705	10	88320
1007705	11	38890
1007705	12	75428
1007705	13	6797
1007705	14	8860
1007705	15	124126
1007705	16	30767
1007705	17	77271
1007705	18	130631

SHIFT REGISTER TAP CONNECTIONS	POSITION OF SECOND TAP K	PHASE SHIFT OF SUM SEQUENCE PHI(K)
1012363	2	79592
1012363	3	102959
1012363	4	116388
1012363	5	56225
1012363	6	39135
1012363	7	29367
1012363	8	129619
1012363	9	112450
1012363	10	106369
1012363	11	78270
1012363	12	33952
1012363	13	58734
1012363	14	69808
1012363	15	2905
1012363	16	91035
1012363	17	37243
1012363	18	57988

SHIFT REGISTER TAP CONNECTIONS	POSITION OF SECOND TAP K	PHASE SHIFT OF SUM SEQUENCE PHI(K)
1013525	2	54440
1013525	3	108880
1013525	4	86343
1013525	5	44383
1013525	6	56316
1013525	7	89457
1013525	8	98147
1013525	9	88766
1013525	10	43037
1013525	11	112632
1013525	12	1348
1013525	13	83229
1013525	14	45498
1013525	15	65849
1013525	16	68680
1013525	17	84611
1013525	18	29623

SHIFT REGISTER TAP CONNECTIONS	POSITION OF SECOND TAP K	PHASE SHIFT OF SUM SEQUENCE PHI(K)
1201011	2	89998
1201011	3	82147
1201011	4	19196
1201011	5	97849
1201011	6	75595
1201011	7	38392
1201011	8	125173
1201011	9	66445
1201011	10	38185
1201011	11	110953
1201011	12	2333
1201011	13	76784
1201011	14	92305
1201011	15	11797
1201011	16	114324
1201011	17	129253
1201011	18	68333

SHIFT REGISTER TAP CONNECTIONS	POSITION OF SECOND TAP K	PHASE SHIFT OF SUM SEQUENCE PHI(K)
1007543	2	124152
1007543	3	13839
1007543	4	101302
1007543	5	27678
1007543	6	16408
1007543	7	59539
1007543	8	28526
1007543	9	55356
1007543	10	117247
1007543	11	32816
1007543	12	56175
1007543	13	119078
1007543	14	16287
1007543	15	57052
1007543	16	128516
1007543	17	110712
1007543	18	34854

SHIFT REGISTER TAP CONNECTIONS	POSITION OF SECOND TAP K	PHASE SHIFT OF SUM SEQUENCE PHI(K)
1013625	2	33103
1013625	3	66206
1013625	4	37898
1013625	5	129731
1013625	6	50960
1013625	7	75796
1013625	8	11097
1013625	9	2681
1013625	10	98985
1013625	11	101920
1013625	12	111316
1013625	13	110551
1013625	14	30138
1013625	15	22194
1013625	16	90110
1013625	17	5362
1013625	18	116167

SHIFT REGISTER TAP CONNECTIONS	POSITION OF SECOND TAP K	PHASE SHIFT OF SUM SEQUENCE PHI(K)
1007501	2	8995
1007501	3	17990
1007501	4	126325
1007501	5	35980
1007501	6	37480
1007501	7	9493
1007501	8	97298
1007501	9	71960
1007501	10	46045
1007501	11	74960
1007501	12	125775
1007501	13	18986
1007501	14	118694
1007501	15	67547
1007501	16	30116
1007501	17	118223
1007501	18	121642

SHIFT REGISTER TAP CONNECTIONS	POSITION OF SECOND TAP K	PHASE SHIFT OF SUM SEQUENCE PHI(K)
1014555	2	120780
1014555	3	20583
1014555	4	99265
1014555	5	41166
1014555	6	1139
1014555	7	63613
1014555	8	26800
1014555	9	82332
1014555	10	49892
1014555	11	2278
1014555	12	120376
1014555	13	127226
1014555	14	9609
1014555	15	53600
1014555	16	104233
1014555	17	97479
1014555	18	95955

SHIFT REGISTER TAP CONNECTIONS	POSITION OF SECOND TAP K	PHASE SHIFT OF SUM SECUENCE PHI(K)
1007417	2	47663
1007417	3	95326
1007417	4	4784
1007417	5	71491
1007417	6	116069
1007417	7	9568
1007417	8	44697
1007417	9	119161
1007417	10	91623
1007417	11	30005
1007417	12	95394
1007417	13	19136
1007417	14	111168
1007417	15	89394
1007417	16	47278
1007417	17	23821
1007417	18	18781

SHIFT REGISTER TAP CONNECTIONS	POSITION OF SECOND TAP K	PHASE SHIFT OF SUM SEQUENCE PHI(K)
1716201	2	111722
1716201	3	38699
1716201	4	115196
1716201	5	77398
1716201	6	122836
1716201	7	31751
1716201	8	3357
1716201	9	107347
1716201	10	124677
1716201	11	16471
1716201	12	82084
1716201	13	63502
1716201	14	28953
1716201	15	6714
1716201	16	90728
1716201	17	47449
1716201	18	76794

SHIFT REGISTER TAP CONNECTIONS	POSITION OF SECOND TAP K	PHASE SHIFT OF SUM SEQUENCE PHI(K)
1007315	2	20641
1007315	3	41282
1007315	4	43663
1007315	5	82564
1007315	6	24679
1007315	7	87326
1007315	8	67491
1007315	9	97015
1007315	10	124514
1007315	11	49358
1007315	12	20716
1007315	13	87491
1007315	14	78725
1007315	15	127161
1007315	16	31200
1007315	17	68113
1007315	18	2810

SHIFT REGISTER TAP CONNECTIONS	POSITION OF SECOND TAP K	PHASE SHIFT OF SUM SEQUENCE PHI(K)
1015037	2	123111
1015037	3	15921
1015037	4	29670
1015037	5	31842
1015037	6	61993
1015037	7	59340
1015037	8	110272
1015037	9	63684
1015037	10	25407
1015037	11	123986
1015037	12	38778
1015037	13	118680
1015037	14	23157
1015037	15	41599
1015037	16	116340
1015037	17	127368
1015037	18	16787

SHIFT REGISTER TAP CONNECTIONS	POSITION OF SECOND TAP K	PHASE SHIFT OF SUM SEQUENCE PHI(K)
1007263	2	49910
1007263	3	99820
1007263	4	7386
1007263	5	62503
1007263	6	128667
1007263	7	14772
1007263	8	60767
1007263	9	125006
1007263	10	79938
1007263	11	4809
1007263	12	113194
1007263	13	29544
1007263	14	34789
1007263	15	121534
1007263	16	74419
1007263	17	12131
1007263	18	112531

SHIFT REGISTER TAP CONNECTIONS	POSITION OF SECOND TAP K	PHASE SHIFT OF SUM SEQUENCE PHI(K)
1230121	2	55144
1230121	3	110288
1230121	4	111085
1230121	5	41567
1230121	6	99045
1230121	7	39973
1230121	8	67113
1230121	9	83134
1230121	10	53510
1230121	11	64053
1230121	12	107694
1230121	13	79946
1230121	14	6656
1230121	15	127917
1230121	16	84263
1230121	17	95875
1230121	18	58527

SHIFT REGISTER TAP CONNECTIONS	POSITION OF SECOND TAP K	PHASE SHIFT OF SUM SEQUENCE PHI(K)
1014365	2	29048
1014365	3	58096
1014365	4	17471
1014365	5	116192
1014365	6	13645
1014365	7	34942
1014365	8	10503
1014365	9	29759
1014365	10	38428
1014365	11	27290
1014365	12	103669
1014365	13	69884
1014365	14	24555
1014365	15	21006
1014365	16	15851
1014365	17	59518
1014365	18	127041

SHIFT REGISTER TAP CONNECTIONS	POSITION OF SECOND TAP K	PHASE SHIFT OF SUM SEQUENCE PHI(K)
1014475	2	56737
1014475	3	113474
1014475	4	101120
1014475	5	35195
1014475	6	10464
1014475	7	59903
1014475	8	60239
1014475	9	70390
1014475	10	33738
1014475	11	20928
1014475	12	31333
1014475	13	119806
1014475	14	56454
1014475	15	120478
1014475	16	85344
1014475	17	121363
1014475	18	118672

SHIFT REGISTER TAP CONNECTIONS	POSITION OF SECOND TAP K	PHASE SHIFT OF SUM SEQUENCE PHI(K)
1007165	2	18934
1007165	3	37868
1007165	4	21299
1007165	5	75736
1007165	6	45044
1007165	7	42598
1007165	8	78255
1007165	9	110671
1007165	10	45941
1007165	11	90088
1007165	12	36499
1007165	13	85196
1007165	14	114847
1007165	15	105633
1007165	16	7680
1007165	17	40801
1007165	18	7949

SHIFT REGISTER TAP CONNECTIONS	POSITION OF SECOND TAP K	PHASE SHIFT OF SUM SEQUENCE PHI(K)
1141703	2	11448
1141703	3	22896
1141703	4	79557
1141703	5	45792
1141703	6	17201
1141703	7	103029
1141703	8	3143
1141703	9	91584
1141703	10	30125
1141703	11	34402
1141703	12	46846
1141703	13	56085
1141703	14	4865
1141703	15	6286
1141703	16	50153
1141703	17	78975
1141703	18	122016

SHIFT REGISTER TAP CONNECTIONS	POSITION OF SECOND TAP K	PHASE SHIFT OF SUM SEQUENCE PHI(K)
1007121	2	25635
1007121	3	51270
1007121	4	127449
1007121	5	102540
1007121	6	82629
1007121	7	7245
1007121	8	103140
1007121	9	57063
1007121	10	57531
1007121	11	96885
1007121	12	55203
1007121	13	14490
1007121	14	92893
1007121	15	55863
1007121	16	19152
1007121	17	114126
1007121	18	114621

SHIFT REGISTER TAP CONNECTIONS	POSITION OF SECOND TAP K	PHASE SHIFT OF SUM SEQUENCE PHI(K)
1021553	2	47405
1021553	3	94810
1021553	4	22061
1021553	5	72523
1021553	6	43913
1021553	7	44122
1021553	8	6934
1021553	9	117097
1021553	10	26391
1021553	11	87826
1021553	12	103968
1021553	13	88244
1021553	14	32423
1021553	15	13868
1021553	16	72642
1021553	17	27949
1021553	18	85283

SHIFT REGISTER TAP CONNECTIONS	POSITION OF SECOND TAP K	PHASE SHIFT OF SUM SEQUENCE PHI(K)
1001705	2	32336
1001705	3	64672
1001705	4	83291
1001705	5	129344
1001705	6	117483
1001705	7	95561
1001705	8	130516
1001705	9	3455
1001705	10	83753
1001705	11	27177
1001705	12	49645
1001705	13	71021
1001705	14	10146
1001705	15	1111
1001705	16	127090
1001705	17	6910
1001705	18	129001

SHIFT REGISTER TAP CONNECTIONS	POSITION OF SECOND TAP K	PHASE SHIFT OF SUM SEQUENCE PHI(K)
1020277	2	46819
1020277	3	93638
1020277	4	1270
1020277	5	74867
1020277	6	80681
1020277	7	2540
1020277	8	124474
1020277	9	112409
1020277	10	22264
1020277	11	100781
1020277	12	119810
1020277	13	5080
1020277	14	80814
1020277	15	13195
1020277	16	99783
1020277	17	37325
1020277	18	116410

SHIFT REGISTER TAP CONNECTIONS	POSITION OF SECOND TAP K	PHASE SHIFT OF SUM SEQUENCE PHI(K)
1001661	2	36517
1001661	3	73034
1001661	4	74422
1001661	5	116075
1001661	6	80742
1001661	7	113299
1001661	8	128084
1001661	9	29993
1001661	10	59945
1001661	11	100659
1001661	12	30346
1001661	13	35545
1001661	14	22633
1001661	15	5975
1001661	16	19777
1001661	17	59986
1001661	18	31680

SHIFT REGISTER TAP CONNECTIONS	POSITION OF SECOND TAP K	PHASE SHIFT OF SUM SEQUENCE PHI(K)
1017611	2	6338
1017611	3	12676
1017611	4	16649
1017611	5	25352
1017611	6	39888
1017611	7	33298
1017611	8	29767
1017611	9	50704
1017611	10	113772
1017611	11	79776
1017611	12	14667
1017611	13	66596
1017611	14	16536
1017611	15	59534
1017611	16	32361
1017611	17	101408
1017611	18	35877

SHIFT REGISTER TAP CONNECTIONS	POSITION OF SECOND TAP K	PHASE SHIFT OF SUM SEQUENCE PHI(K)
1001651	2	69796
1001651	3	122551
1001651	4	86167
1001651	5	17041
1001651	6	117179
1001651	7	89809
1001651	8	127190
1001651	9	34082
1001651	10	106789
1001651	11	27785
1001651	12	396
1001651	13	82525
1001651	14	34309
1001651	15	7763
1001651	16	107267
1001651	17	68164
1001651	18	55203

SHIFT REGISTER TAP CONNECTIONS	POSITION OF SECOND TAP K	PHASE SHIFT OF SUM SEQUENCE PHI(K)
1017511	2	11550
1017511	3	23100
1017511	4	92066
1017511	5	46200
1017511	6	40153
1017511	7	78011
1017511	8	119271
1017511	9	92400
1017511	10	103124
1017511	11	80306
1017511	12	67560
1017511	13	106121
1017511	14	66481
1017511	15	23601
1017511	16	107278
1017511	17	77343
1017511	18	85645

SHIFT REGISTER TAP CONNECTIONS	POSITION OF SECOND TAP K	PHASE SHIFT OF SUM SEQUENCE PHI(K)
1001631	2	47121
1001631	3	94242
1001631	4	85047
1001631	5	73659
1001631	6	105792
1001631	7	92049
1001631	8	71959
1001631	9	114825
1001631	10	65712
1001631	11	50559
1001631	12	94826
1001631	13	78045
1001631	14	55843
1001631	15	118225
1001631	16	80839
1001631	17	32493
1001631	18	106827

SHIFT REGISTER TAP CONNECTIONS	POSITION OF SECOND TAP K	PHASE SHIFT OF SUM SEQUENCE PHI(K)
1017311	2	80078
1017311	3	101987
1017311	4	105979
1017311	5	58169
1017311	6	107136
1017311	7	50185
1017311	8	52205
1017311	9	116338
1017311	10	58281
1017311	11	47871
1017311	12	111209
1017311	13	100370
1017311	14	59368
1017311	15	104410
1017311	16	46116
1017311	17	29367
1017311	18	67189

SHIFT REGISTER TAP CONNECTIONS	POSITION OF SECOND TAP K	PHASE SHIFT OF SUM SEQUENCE PHI(K)
1001625	2	16096
1001625	3	32192
1001625	4	62795
1001625	5	64384
1001625	6	76569
1001625	7	125590
1001625	8	32458
1001625	9	128768
1001625	10	112199
1001625	11	109005
1001625	12	71923
1001625	13	10963
1001625	14	90666
1001625	15	64916
1001625	16	119862
1001625	17	4607
1001625	18	123

SHIFT REGISTER TAP CONNECTIONS	POSITION OF SECOND TAP K	PHASE SHIFT OF SUM SEQUENCE PHI(K)
1017161	2	20270
1017161	3	40540
1017161	4	100996
1017161	5	81080
1017161	6	1170
1017161	7	60151
1017161	8	98141
1017161	9	99983
1017161	10	123092
1017161	11	2340
1017161	12	25295
1017161	13	120302
1017161	14	14841
1017161	15	65861
1017161	16	39012
1017161	17	62177
1017161	18	43349

SHIFT REGISTER TAP CONNECTIONS	POSITION OF SECOND TAP K	PHASE SHIFT OF SUM SEQUENCE PHI(K)
1001607	2	41857
1001607	3	83714
1001607	4	24734
1001607	5	94715
1001607	6	76652
1001607	7	49468
1001607	8	17132
1001607	9	72713
1001607	10	77447
1001607	11	108839
1001607	12	68362
1001607	13	98936
1001607	14	120869
1001607	15	34264
1001607	16	121992
1001607	17	116717
1001607	18	93803

SHIFT REGISTER TAP CONNECTIONS	POSITION OF SECOND TAP K	PHASE SHIFT OF SUM SEQUENCE PHI(K)
1017071	2	104867
1017071	3	52403
1017071	4	35443
1017071	5	104818
1017071	6	121608
1017071	7	70886
1017071	8	80471
1017071	9	52507
1017071	10	25412
1017071	11	18927
1017071	12	24920
1017071	13	120371
1017071	14	15524
1017071	15	101201
1017071	16	18779
1017071	17	105014
1017071	18	12674

SHIFT REGISTER TAP CONNECTIONS	POSITION OF SECOND TAP K	PHASE SHIFT OF SUM SEQUENCE PHI(K)
1001567	2	103393
1001567	3	55357
1001567	4	59109
1001567	5	110714
1001567	6	113709
1001567	7	118218
1001567	8	1800
1001567	9	40715
1001567	10	130143
1001567	11	34725
1001567	12	108128
1001567	13	25707
1001567	14	123389
1001567	15	3600
1001567	16	67577
1001567	17	81430
1001567	18	87968

SHIFT REGISTER TAP CONNECTIONS	POSITION OF SECOND TAP K	PHASE SHIFT OF SUM SEQUENCE PHI(K)
1016705	2	65052
1016705	3	130104
1016705	4	107853
1016705	5	1935
1016705	6	111638
1016705	7	46437
1016705	8	57146
1016705	9	3870
1016705	10	95338
1016705	11	38867
1016705	12	96974
1016705	13	92874
1016705	14	74671
1016705	15	114292
1016705	16	107239
1016705	17	7740
1016705	18	36549

SHIFT REGISTER TAP CONNECTIONS	POSITION OF SECOND TAP K	PHASE SHIFT OF SUM SEQUENCE PHI(K)
1021473	2	67392
1021473	3	127359
1021473	4	90960
1021473	5	7425
1021473	6	18208
1021473	7	80223
1021473	8	83430
1021473	9	14850
1021473	10	95661
1021473	11	36416
1021473	12	13695
1021473	13	101697
1021473	14	42897
1021473	15	95283
1021473	16	48768
1021473	17	29700
1021473	18	32705

SHIFT REGISTER TAP CONNECTIONS	POSITION OF SECOND TAP K	PHASE SHIFT OF SUM SEQUENCE PHI(K)
1021475	2	56372
1021475	3	112744
1021475	4	108654
1021475	5	36655
1021475	6	18502
1021475	7	44835
1021475	8	68180
1021475	9	73310
1021475	10	111502
1021475	11	37004
1021475	12	23028
1021475	13	89670
1021475	14	81196
1021475	15	125783
1021475	16	112648
1021475	17	115523
1021475	18	16332

SHIFT REGISTER TAP CONNECTIONS	POSITION OF SECOND TAP K	PHASE SHIFT OF SUM SEQUENCE PHI(K)
1001453	2	25624
1001453	3	51248
1001453	4	114933
1001453	5	102496
1001453	6	71640
1001453	7	32277
1001453	8	77703
1001453	9	57151
1001453	10	62504
1001453	11	118863
1001453	12	87493
1001453	13	64554
1001453	14	18903
1001453	15	106737
1001453	16	63748
1001453	17	114302
1001453	18	83404

SHIFT REGISTER TAP CONNECTIONS	POSITION OF SECOND TAP K	PHASE SHIFT OF SUM SEQUENCE PHI(K)
1133015	2	28277
1133015	3	56554
1133015	4	67044
1133015	5	113108
1133015	6	56421
1133015	7	128055
1133015	8	74148
1133015	9	35927
1133015	10	74581
1133015	11	112842
1133015	12	112659
1133015	13	6033
1133015	14	12677
1133015	15	113847
1133015	16	112120
1133015	17	71854
1133015	18	12630

SHIFT REGISTER TAP CONNECTIONS	POSITION OF SECOND TAP K	PHASE SHIFT OF SUM SEQUENCE PHI(K)
1001427	2	52744
1001427	3	105488
1001427	4	108582
1001427	5	51167
1001427	6	91126
1001427	7	44979
1001427	8	53263
1001427	9	102334
1001427	10	130092
1001427	11	79891
1001427	12	54116
1001427	13	89958
1001427	14	41060
1001427	15	106526
1001427	16	69839
1001427	17	57475
1001427	18	34141

SHIFT REGISTER TAP CONNECTIONS	POSITION OF SECOND TAP K	PHASE SHIFT OF SUM SEQUENCE PHI(K)
1101533	2	5685
1101533	3	11370
1101533	4	33792
1101533	5	22740
1101533	6	9596
1101533	7	67584
1101533	8	41333
1101533	9	45480
1101533	10	91020
1101533	11	19192
1101533	12	36154
1101533	13	126975
1101533	14	128420
1101533	15	82666
1101533	16	12424
1101533	17	90960
1101533	18	8268

SHIFT REGISTER TAP CONNECTIONS	POSITION OF SECOND TAP K	PHASE SHIFT OF SUM SEQUENCE PHI(K)
1001361	2	8790
1001361	3	17580
1001361	4	18210
1001361	5	35160
1001361	6	18158
1001361	7	36420
1001361	8	42786
1001361	9	70320
1001361	10	94465
1001361	11	36316
1001361	12	48857
1001361	13	72840
1001361	14	120952
1001361	15	85572
1001361	16	69945
1001361	17	121503
1001361	18	8591

SHIFT REGISTER TAP CONNECTIONS	POSITION OF SECOND TAP K	PHASE SHIFT OF SUM SEQUENCE PHI(K)
1402335	2	97889
1402335	3	66365
1402335	4	35344
1402335	5	129413
1402335	6	2884
1402335	7	70688
1402335	8	40059
1402335	9	3317
1402335	10	92879
1402335	11	5768
1402335	12	129880
1402335	13	120767
1402335	14	50377
1402335	15	80118
1402335	16	33787
1402335	17	6634
1402335	18	84390

SHIFT REGISTER TAP CONNECTIONS	POSITION OF SECOND TAP K	PHASE SHIFT OF SUM SEQUENCE PHI(K)
1001253	2	74810
1001253	3	112523
1001253	4	69711
1001253	5	37097
1001253	6	16611
1001253	7	122721
1001253	8	76258
1001253	9	74194
1001253	10	39646
1001253	11	33222
1001253	12	92197
1001253	13	16701
1001253	14	99034
1001253	15	109627
1001253	16	7262
1001253	17	113755
1001253	18	19513

SHIFT REGISTER TAP CONNECTIONS	POSITION OF SECOND TAP K	PHASE SHIFT OF SUM SEQUENCE PHI(K)
1301323	2	43456
1301323	3	86912
1301323	4	97346
1301323	5	88319
1301323	6	128775
1301323	7	67451
1301323	8	17183
1301323	9	85505
1301323	10	25494
1301323	11	4593
1301323	12	80615
1301323	13	127241
1301323	14	90867
1301323	15	34366
1301323	16	80014
1301323	17	91133
1301323	18	72790

SHIFT REGISTER TAP CONNECTIONS	POSITION OF SECOND TAP K	PHASE SHIFT OF SUM SEQUENCE PHI(K)
1001165	2	61729
1001165	3	123458
1001165	4	69281
1001165	5	15227
1001165	6	85582
1001165	7	123581
1001165	8	73098
1001165	9	30454
1001165	10	128965
1001165	11	90979
1001165	12	4480
1001165	13	14981
1001165	14	93604
1001165	15	115947
1001165	16	126834
1001165	17	60908
1001165	18	127726

SHIFT REGISTER TAP CONNECTIONS	POSITION OF SECOND TAP K	PHASE SHIFT OF SUM SEQUENCE PHI(K)
1015631	2	94174
1015631	3	73795
1015631	4	29044
1015631	5	114553
1015631	6	60382
1015631	7	58088
1015631	8	60036
1015631	9	33037
1015631	10	115634
1015631	11	120764
1015631	12	104679
1015631	13	116176
1015631	14	31417
1015631	15	120072
1015631	16	93673
1015631	17	66074
1015631	18	37258

SHIFT REGISTER TAP CONNECTIONS	POSITION OF SECOND TAP K	PHASE SHIFT OF SUM SEQUENCE PHI(K)
1001141	2	85505
1001141	3	91133
1001141	4	110402
1001141	5	79877
1001141	6	34226
1001141	7	41339
1001141	8	14992
1001141	9	102389
1001141	10	25409
1001141	11	68452
1001141	12	23309
1001141	13	82678
1001141	14	18414
1001141	15	29984
1001141	16	30916
1001141	17	57365
1001141	18	1695

SHIFT REGISTER TAP CONNECTIONS	POSITION OF SECOND TAP K	PHASE SHIFT OF SUM SEQUENCE PHI(K)
1025051	2	55834
1025051	3	111668
1025051	4	52553
1025051	5	38807
1025051	6	83433
1025051	7	105106
1025051	8	33388
1025051	9	77614
1025051	10	78323
1025051	11	95277
1025051	12	778
1025051	13	51931
1025051	14	110554
1025051	15	66776
1025051	16	117317
1025051	17	106915
1025051	18	125806

SHIFT REGISTER TAP CONNECTIONS	POSITION OF SECOND TAP K	PHASE SHIFT OF SUM SEQUENCE PHI(K)
1001023	2	63208
1001023	3	126416
1001023	4	47311
1001023	5	9311
1001023	6	90307
1001023	7	94622
1001023	8	124474
1001023	9	18622
1001023	10	103808
1001023	11	81529
1001023	12	92537
1001023	13	72899
1001023	14	88243
1001023	15	13195
1001023	16	80481
1001023	17	37244
1001023	18	2954

SHIFT REGISTER TAP CONNECTIONS	POSITION OF SECOND TAP K	PHASE SHIFT OF SUM SEQUENCE PHI(K)
1021355	2	84968
1021355	3	92207
1021355	4	121075
1021355	5	77729
1021355	6	126397
1021355	7	19993
1021355	8	110171
1021355	9	106685
1021355	10	42612
1021355	11	9349
1021355	12	101246
1021355	13	39986
1021355	14	65972
1021355	15	41801
1021355	16	15001
1021355	17	48773
1021355	18	65038

SHIFT REGISTER TAP CONNECTIONS	POSITION OF SECOND TAP K	PHASE SHIFT OF SUM SEQUENCE PHI(K)
1010615	2	114760
1010615	3	32623
1010615	4	43589
1010615	5	65246
1010615	6	97291
1010615	7	87178
1010615	8	73503
1010615	9	130492
1010615	10	98036
1010615	11	67561
1010615	12	42818
1010615	13	87787
1010615	14	48025
1010615	15	115137
1010615	16	97401
1010615	17	1159
1010615	18	79179

SHIFT REGISTER TAP CONNECTIONS	POSITION OF SECOND TAP K	PHASE SHIFT OF SUM SEQUENCE PHI(K)
1021363	2	116502
1021363	3	29139
1021363	4	53247
1021363	5	58278
1021363	6	32940
1021363	7	106494
1021363	8	21595
1021363	9	116556
1021363	10	27778
1021363	11	65880
1021363	12	73781
1021363	13	49155
1021363	14	29795
1021363	15	43190
1021363	16	41519
1021363	17	29031
1021363	18	115446

SHIFT REGISTER TAP CONNECTIONS	POSITION OF SECOND TAP K	PHASE SHIFT OF SUM SEQUENCE PHI(K)
1000757	2	3265
1000757	3	6530
1000757	4	73075
1000757	5	13060
1000757	6	9785
1000757	7	115993
1000757	8	94193
1000757	9	26120
1000757	10	77032
1000757	11	19570
1000757	12	30886
1000757	13	30157
1000757	14	127370
1000757	15	73757
1000757	16	89729
1000757	17	52240
1000757	18	98580

SHIFT REGISTER TAP CONNECTIONS	POSITION OF SECOND TAP K	PHASE SHIFT OF SUM SEQUENCE PHI(K)
1060065	2	7311
1060065	3	14622
1060065	4	46381
1060065	5	29244
1060065	6	80975
1060065	7	92762
1060065	8	41684
1060065	9	58488
1060065	10	110203
1060065	11	100193
1060065	12	112367
1060065	13	76619
1060065	14	29049
1060065	15	83368
1060065	16	121710
1060065	17	116976
1060065	18	30453

SHIFT REGISTER TAP CONNECTIONS	POSITION OF SECOND TAP K	PHASE SHIFT OF SUM SEQUENCE PHI(K)
1010741	2	127874
1010741	3	6395
1010741	4	63516
1010741	5	12790
1010741	6	62184
1010741	7	127032
1010741	8	78180
1010741	9	25580
1010741	10	75695
1010741	11	124368
1010741	12	39336
1010741	13	8079
1010741	14	52160
1010741	15	105783
1010741	16	10583
1010741	17	51160
1010741	18	111061

SHIFT REGISTER TAP CONNECTIONS	POSITION OF SECOND TAP K	PHASE SHIFT OF SUM SEQUENCE PHI(K)
1205651	2	84556
1205651	3	93031
1205651	4	105166
1205651	5	76081
1205651	6	38963
1205651	7	51811
1205651	8	110487
1205651	9	105981
1205651	10	98275
1205651	11	77926
1205651	12	30692
1205651	13	103622
1205651	14	113547
1205651	15	23169
1205651	16	119270
1205651	17	42181
1205651	18	93526

SHIFT REGISTER TAP CONNECTIONS	POSITION OF SECOND TAP K	PHASE SHIFT OF SUM SEQUENCE PHI(K)
1000743	2	19416
1000743	3	38832
1000743	4	16811
1000743	5	77664
1000743	6	24907
1000743	7	33622
1000743	8	96058
1000743	9	106815
1000743	10	39070
1000743	11	49814
1000743	12	6717
1000743	13	67244
1000743	14	58030
1000743	15	70027
1000743	16	55555
1000743	17	48513
1000743	18	27895

SHIFT REGISTER TAP CONNECTIONS	POSITION OF SECOND TAP K	PHASE SHIFT OF SUM SEQUENCE PHI(K)
1021237	2	32161
1021237	3	64322
1021237	4	106583
1021237	5	128644
1021237	6	21691
1021237	7	48977
1021237	8	107756
1021237	9	4855
1021237	10	25929
1021237	11	43382
1021237	12	95597
1021237	13	97954
1021237	14	79342
1021237	15	46631
1021237	16	114995
1021237	17	9710
1021237	18	90728

SHIFT REGISTER TAP CONNECTIONS	POSITION OF SECOND TAP K	PHASE SHIFT OF SUM SEQUENCE PHI(K)
1000621	2	70490
1000621	3	121163
1000621	4	88761
1000621	5	19817
1000621	6	20329
1000621	7	84621
1000621	8	113728
1000621	9	39634
1000621	10	87745
1000621	11	40658
1000621	12	73074
1000621	13	92901
1000621	14	16357
1000621	15	34687
1000621	16	95029
1000621	17	79268
1000621	18	54287

SHIFT REGISTER TAP CONNECTIONS	POSITION OF SECOND TAP K	PHASE SHIFT OF SUM SEQUENCE PHI(K)
1530521	2	124009
1530521	3	14125
1530521	4	105939
1530521	5	28250
1530521	6	11297
1530521	7	50265
1530521	8	74916
1530521	9	56500
1530521	10	125022
1530521	11	22594
1530521	12	672
1530521	13	100530
1530521	14	23110
1530521	15	112311
1530521	16	103461
1530521	17	113000
1530521	18	19067

SHIFT REGISTER TAP CONNECTIONS	POSITION OF SECOND TAP K	PHASE SHIFT OF SUM SEQUENCE PHI(K)
1000517	2	37444
1000517	3	74888
1000517	4	42803
1000517	5	112367
1000517	6	83784
1000517	7	85606
1000517	8	113742
1000517	9	37409
1000517	10	121793
1000517	11	94575
1000517	12	125387
1000517	13	90931
1000517	14	106447
1000517	15	34659
1000517	16	106396
1000517	17	74818
1000517	18	51470

SHIFT REGISTER TAP CONNECTIONS	POSITION OF SECOND TAP K	PHASE SHIFT OF SUM SEQUENCE PHI(K)
1021273	2	110124
1021273	3	41895
1021273	4	60706
1021273	5	83790
1021273	6	6183
1021273	7	121412
1021273	8	37551
1021273	9	94563
1021273	10	69616
1021273	11	12366
1021273	12	100630
1021273	13	19319
1021273	14	57707
1021273	15	75102
1021273	16	2393
1021273	17	73017
1021273	18	46888

SHIFT REGISTER TAP CONNECTIONS	POSITION OF SECOND TAP K	PHASE SHIFT OF SUM SEQUENCE PHI(K)
1000407	2	49350
1000407	3	98700
1000407	4	19403
1000407	5	64743
1000407	6	116090
1000407	7	38806
1000407	8	56729
1000407	9	129486
1000407	10	61200
1000407	11	29963
1000407	12	75745
1000407	13	77612
1000407	14	55780
1000407	15	113458
1000407	16	25159
1000407	17	3171
1000407	18	124381

SHIFT REGISTER TAP CONNECTIONS	POSITION OF SECOND TAP K	PHASE SHIFT OF SUM SEQUENCE PHI(K)
1324243	2	98331
1324243	3	65481
1324243	4	15974
1324243	5	130962
1324243	6	119625
1324243	7	31948
1324243	8	66716
1324243	9	219
1324243	10	80039
1324243	11	22893
1324243	12	7845
1324243	13	63896
1324243	14	20033
1324243	15	128711
1324243	16	72882
1324243	17	438
1324243	18	85765

SHIFT REGISTER TAP CONNECTIONS	POSITION OF SECOND TAP K	PHASE SHIFT OF SUM SEQUENCE PHI(K)
1000355	2	3923
1000355	3	7846
1000355	4	110343
1000355	5	15692
1000355	6	30094
1000355	7	41457
1000355	8	124439
1000355	9	31384
1000355	10	86513
1000355	11	60188
1000355	12	15525
1000355	13	82914
1000355	14	10309
1000355	15	13265
1000355	16	79337
1000355	17	62768
1000355	18	95230

SHIFT REGISTER TAP CONNECTIONS	POSITION OF SECOND TAP K	PHASE SHIFT OF SUM SEQUENCE PHI(K)
1020753	2	18925
1020753	3	37850
1020753	4	114296
1020753	5	75700
1020753	6	129427
1020753	7	33551
1020753	8	42170
1020753	9	110743
1020753	10	60361
1020753	11	3289
1020753	12	50317
1020753	13	67102
1020753	14	10065
1020753	15	84340
1020753	16	73295
1020753	17	40657
1020753	18	65856

SHIFT REGISTER TAP CONNECTIONS	POSITION OF SECOND TAP K	PHASE SHIFT OF SUM SEQUENCE PHI(K)
1000347	2	41418
1000347	3	82836
1000347	4	11047
1000347	5	96471
1000347	6	30382
1000347	7	22094
1000347	8	73939
1000347	9	69201
1000347	10	56667
1000347	11	60764
1000347	12	105487
1000347	13	44188
1000347	14	8729
1000347	15	114265
1000347	16	378
1000347	17	123741
1000347	18	80962

SHIFT REGISTER TAP CONNECTIONS	POSITION OF SECOND TAP K	PHASE SHIFT OF SUM SEQUENCE PHI(K)
1020771	2	121382
1020771	3	19379
1020771	4	56262
1020771	5	38758
1020771	6	116539
1020771	7	112524
1020771	8	124481
1020771	9	77516
1020771	10	105837
1020771	11	29065
1020771	12	15770
1020771	13	37095
1020771	14	55190
1020771	15	13181
1020771	16	92539
1020771	17	107111
1020771	18	85278

SHIFT REGISTER TAP CONNECTIONS	POSITION OF SECOND TAP K	PHASE SHIFT OF SUM SEQUENCE PHI(K)
1000333	2	19273
1000333	3	38546
1000333	4	27896
1000333	5	77092
1000333	6	43690
1000333	7	55792
1000333	8	81602
1000333	9	107959
1000333	10	47180
1000333	11	87380
1000333	12	67198
1000333	13	111584
1000333	14	66887
1000333	15	98939
1000333	16	57643
1000333	17	46225
1000333	18	48009

SHIFT REGISTER TAP CONNECTIONS	POSITION OF SECOND TAP K	PHASE SHIFT OF SUM SEQUENCE PHI(K)
1032067	2	109793
1032067	3	42557
1032067	4	6240
1032067	5	85114
1032067	6	16939
1032067	7	12480
1032067	8	90341
1032067	9	91915
1032067	10	25351
1032067	11	33878
1032067	12	10443
1032067	13	24960
1032067	14	122556
1032067	15	81461
1032067	16	14015
1032067	17	78313
1032067	18	118872

SHIFT REGISTER TAP CONNECTIONS	POSITION OF SECOND TAP K	PHASE SHIFT OF SUM SEQUENCE PHI(K)
1000201	2	52379
1000201	3	104758
1000201	4	126258
1000201	5	52627
1000201	6	114090
1000201	7	9627
1000201	8	11
1000201	9	105254
1000201	10	131066
1000201	11	33963
1000201	12	18
1000201	13	19254
1000201	14	28738
1000201	15	22
1000201	16	103274
1000201	17	51635
1000201	18	50628

SHIFT REGISTER TAP CONNECTIONS	POSITION OF SECOND TAP K	PHASE SHIFT OF SUM SEQUENCE PHI(K)
1017243	2	47380
1017243	3	94760
1017243	4	17348
1017243	5	72623
1017243	6	34675
1017243	7	34696
1017243	8	71413
1017243	9	116897
1017243	10	55015
1017243	11	69350
1017243	12	6342
1017243	13	69392
1017243	14	115368
1017243	15	119317
1017243	16	13875
1017243	17	28349
1017243	18	84744

SHIFT REGISTER TAP CONNECTIONS	POSITION OF SECOND TAP K	PHASE SHIFT OF SUM SEQUENCE PHI(K)
1000173	2	111420
1000173	3	39303
1000173	4	23904
1000173	5	78606
1000173	6	23819
1000173	7	47808
1000173	8	59151
1000173	9	104931
1000173	10	44889
1000173	11	47638
1000173	12	8630
1000173	13	95616
1000173	14	128885
1000173	15	118302
1000173	16	89105
1000173	17	52281
1000173	18	21461

SHIFT REGISTER TAP CONNECTIONS	POSITION OF SECOND TAP K	PHASE SHIFT OF SUM SEQUENCE PHI(K)
1017261	2	57114
1017261	3	114228
1017261	4	33002
1017261	5	33687
1017261	6	75527
1017261	7	66004
1017261	8	101252
1017261	9	67374
1017261	10	27451
1017261	11	111089
1017261	12	68666
1017261	13	130135
1017261	14	124968
1017261	15	59639
1017261	16	127054
1017261	17	127395
1017261	18	33291

SHIFT REGISTER TAP CONNECTIONS	POSITION OF SECOND TAP K	PHASE SHIFT OF SUM SEQUENCE PHI(K)
1011055	2	1956
1011055	3	3912
1011055	4	122800
1011055	5	7824
1011055	6	69199
1011055	7	16543
1011055	8	45547
1011055	9	15648
1011055	10	122484
1011055	11	123745
1011055	12	38728
1011055	13	33086
1011055	14	9889
1011055	15	91094
1011055	16	14283
1011055	17	31296
1011055	18	27351

SHIFT REGISTER TAP CONNECTIONS	POSITION OF SECOND TAP K	PHASE SHIFT OF SUM SEQUENCE PHI(K)
1016435	2	53810
1016435	3	107620
1016435	4	69218
1016435	5	46903
1016435	6	114963
1016435	7	123707
1016435	8	10645
1016435	9	93806
1016435	10	111283
1016435	11	32217
1016435	12	66098
1016435	13	14729
1016435	14	24942
1016435	15	21290
1016435	16	35636
1016435	17	74531
1016435	18	61443

SHIFT REGISTER TAP CONNECTIONS	POSITION OF SECOND TAP K	PHASE SHIFT OF SUM SEQUENCE PHI(K)
1000077	2	66335
1000077	3	129473
1000077	4	33161
1000077	5	3197
1000077	6	94555
1000077	7	66322
1000077	8	63176
1000077	9	6394
1000077	10	50633
1000077	11	73033
1000077	12	127109
1000077	13	129499
1000077	14	101267
1000077	15	126352
1000077	16	899
1000077	17	12788
1000077	18	104092

SHIFT REGISTER TAP CONNECTIONS	POSITION OF SECOND TAP K	PHASE SHIFT OF SUM SEQUENCE PHI(K)
1016561	2	99988
1016561	3	62167
1016561	4	85923
1016561	5	124334
1016561	6	21358
1016561	7	90297
1016561	8	116509
1016561	9	13475
1016561	10	74848
1016561	11	42716
1016561	12	41023
1016561	13	81549
1016561	14	61074
1016561	15	29125
1016561	16	21750
1016561	17	26950
1016561	18	59156

SHIFT REGISTER TAP CONNECTIONS	POSITION OF SECOND TAP K	PHASE SHIFT OF SUM SEQUENCE PHI(K)
1013227	2	106962
1013227	3	48219
1013227	4	17509
1013227	5	96438
1013227	6	116241
1013227	7	35018
1013227	8	94698
1013227	9	69267
1013227	10	112817
1013227	11	29661
1013227	12	38299
1013227	13	70036
1013227	14	119902
1013227	15	72747
1013227	16	113296
1013227	17	123609
1013227	18	64876

SHIFT REGISTER TAP CONNECTIONS	POSITION OF SECOND TAP K	PHASE SHIFT OF SUM SEQUENCE PHI(K)
1013263	2	9315
1013263	3	18630
1013263	4	56725
1013263	5	37260
1013263	6	120691
1013263	7	113450
1013263	8	89070
1013263	9	74520
1013263	10	114937
1013263	11	20761
1013263	12	92104
1013263	13	35243
1013263	14	76365
1013263	15	84003
1013263	16	109756
1013263	17	113103
1013263	18	126373

SHIFT REGISTER TAP CONNECTIONS	POSITION OF SECOND TAP K	PHASE SHIFT OF SUM SEQUENCE PHI(K)
1013323	2	122983
1013323	3	16177
1013323	4	80100
1013323	5	32354
1013323	6	78104
1013323	7	101943
1013323	8	62546
1013323	9	64708
1013323	10	48320
1013323	11	105935
1013323	12	72654
1013323	13	58257
1013323	14	99335
1013323	15	125092
1013323	16	75458
1013323	17	129416
1013323	18	115767

SHIFT REGISTER TAP CONNECTIONS	POSITION OF SECOND TAP K	PHASE SHIFT OF SUM SEQUENCE PHI(K)
1013331	2	81802
1013331	3	98539
1013331	4	89998
1013331	5	65065
1013331	6	56632
1013331	7	82147
1013331	8	21153
1013331	9	130130
1013331	10	96803
1013331	11	113264
1013331	12	38646
1013331	13	97849
1013331	14	105292
1013331	15	42306
1013331	16	78633
1013331	17	1883
1013331	18	39511

SHIFT REGISTER TAP CONNECTIONS	POSITION OF SECOND TAP K	PHASE SHIFT OF SUM SEQUENCE PHI(K)
1013561	2	29481
1013561	3	58962
1013561	4	170
1013561	5	117924
1013561	6	51441
1013561	7	340
1013561	8	94438
1013561	9	26295
1013561	10	42598
1013561	11	102882
1013561	12	95620
1013561	13	680
1013561	14	65979
1013561	15	73267
1013561	16	71510
1013561	17	52590
1013561	18	118526

SHIFT REGISTER TAP CONNECTIONS	POSITION OF SECOND TAP K	PHASE SHIFT OF SUM SEQUENCE PHI(K)
1013607	2	61117
1013607	3	122234
1013607	4	87434
1013607	5	17675
1013607	6	24786
1013607	7	87275
1013607	8	119135
1013607	9	35350
1013607	10	97900
1013607	11	49572
1013607	12	106740
1013607	13	87593
1013607	14	47514
1013607	15	23873
1013607	[illegible]	15003
1013607	[illegible]	70700
1013607	18	40072

SHIFT REGISTER TAP CONNECTIONS	POSITION OF SECOND TAP K	PHASE SHIFT OF SUM SEQUENCE PHI(K)
1015155	2	84157
1015155	3	93829
1015155	4	80057
1015155	5	74485
1015155	6	121733
1015155	7	102029
1015155	8	41730
1015155	9	113173
1015155	10	130006
1015155	11	18677
1015155	12	27877
1015155	13	58085
1015155	14	100083
1015155	15	83460
1015155	16	21301
1015155	17	35797
1015155	18	122794

SHIFT REGISTER TAP CONNECTIONS	POSITION OF SECOND TAP K	PHASE SHIFT OF SUM SEQUENCE PHI(K)
1015253	2	130336
1015253	3	1471
1015253	4	130629
1015253	5	2942
1015253	6	5690
1015253	7	885
1015253	8	1557
1015253	9	5884
1015253	10	93131
1015253	11	11380
1015253	12	122935
1015253	13	1770
1015253	14	65102
1015253	15	3114
1015253	16	21200
1015253	17	11768
1015253	18	114622

SHIFT REGISTER TAP CONNECTIONS	POSITION OF SECOND TAP K	PHASE SHIFT OF SUM SEQUENCE PHI(K)
1015271	2	71803
1015271	3	118537
1015271	4	3209
1015271	5	25069
1015271	6	71722
1015271	7	6418
1015271	8	104437
1015271	9	50138
1015271	10	115895
1015271	11	118699
1015271	12	56755
1015271	13	12836
1015271	14	34295
1015271	15	53269
1015271	16	35374
1015271	17	100276
1015271	18	78517

SHIFT REGISTER TAP CONNECTIONS	POSITION OF SECOND TAP K	PHASE SHIFT OF SUM SEQUENCE PHI(K)
1015325	2	60672
1015325	3	121344
1015325	4	17874
1015325	5	19455
1015325	6	5186
1015325	7	35748
1015325	8	66361
1015325	9	38910
1015325	10	63236
1015325	11	10372
1015325	12	68148
1015325	13	71496
1015325	14	121562
1015325	15	129421
1015325	16	116454
1015325	17	77820
1015325	18	55416

APPENDIX C. 5

COMPUTER PROGRAM LISTING FOR GENERATION OF PHASE SHIFTS OF 18-STAGE MAXIMAL CODES

The following is the computer program listing used for the generation of phase shifts of maximal PN sequences of period $2^{18}-1$ as described in Appendix B. 5.

The program sets up an 18-stage register with a specified initial condition vector $a = [a_0, a_1, \ldots a_{17}]$. The shift register is then clocked -k times to obtain the initial condition vector $b = [b_0, b_1, \ldots b_{17}]$ of the sequence obtained at the kth tap of the shift register. The sequence which is generated by the shift register with initial conditions a is then searched for the state vector A+b. The position of this state vector gives the phase shift obtained when the output sequence of the shift register is added modulo 2 to the sequence obtained at the kth stage of the shift register.

```
RUNX COMPILER (VER.2.3M)                 07/01/76. 21.04.05.

              PROGRAM RGA12(TAPE5,TAPE6)
        *
        *
        *  FULL 18 STAGE CODE LIBRARY--7505
        *
        *     FORMAT TAILORED TO 2 18 STAGE RESULTS/PAGE
        *     ALIGN PAPER 3 SPACES ABOVE TEAR STRIP BEFORE PRINTING
        *
        *  AUTHORS--IRA GREEN AND ROBERT GOLD
        *
        *     MAXIMUM SIZE OF SHIFT REGISTER IS 20 STAGES.
        *
        *
000004        DIMENSION IFA(21)
000004        REWIND 5
000006        REWIND 6
        C     WRITE(6,105)
000010   105  FORMAT(/* FILE *7H*TAPE5** SHOULD CONTAIN*/
000010     1          *  ORDER OF POLYNOMIAL*/
000010     2          *  OCTAL REPRESENTATION OF INITIAL CONDITIONS OF *
000010     3          *SHIFT REGISTER*/
000010     4          *     FOLLOWED BY A B*/)
000010   111  ACCEPT(5) IORDER,INH
000017        IF (IORDER.GE.1 .AND. IORDER.LE.20) GO TO 115
000030        WRITE(6,112)
000033   112  FORMAT(/* 1 TO 20 STAGES, RE-ENTER DATA*/)
000033        GO TO 111
000034   115  CONTINUE
        C     WRITE(6,110)
000034   110  FORMAT(/* FILE *7H*TAPE5** SHOULD CONTAIN A LIST OF*/
000034     1          *  ASSOCIATED POLYNOMIALS (OCTAL REPRESENTATION *
000034     2          *FOLLOWED BY      */
000034     3          *  TERMINATE. . . A 0*/)
        *
        *  SET UP BIT CONFIGURATION IN SHIFT REGISTER FOR INITIAL CONDITIONS
        *
000034        CALL INITPI(INH,ISR,IORDER,IFA)
```

```
000037            IFIRST = ISR
000041            CALL MIRROR(ISR,IFIRSTM,IORDER,IFA)
           *
           *  LOOP TO GENERATE LIBRARY OF ACCEPTED CONNECTIONS
           *
000044     125    ISR = IFIRST
000045            ACCEPT(5) INF
000053            WRITE(6,150)
000057     150    FORMAT(9(/) 25X *POSITION   PHASE SHIFT OF*/
000057       1           18X *SHIFT      OF        SUM SEQUENCE*/
000057       2           15X *REGISTER   SECOND*/
000057       3           7X * TAP CONNECTIONS     TAP*/
000057       4           28X *K* 10X *PHI(K)*//)
000057            IF (INF.EQ.0) STOP
           *
           *  SET UP MASKS FOR PIN HOOKUP OF SHIFT REGISTER AND ITS REVERSE
           *
000062            CALL CONNECT(INF,IPINL,IPINR,IORDER,IFA)
           *
           *  IORDER-1 IS THE NUMBER OF POSSIBLE TAP CONNECTIONS
           *
000066            DO 300 I=2,IORDER
           *
           *  CLOCK SHIFT REGISTER AND ADD TO FIRST VALUE TO OBTAIN THE NEXT
           *    TEST SEQUENCE AND ITS MIRROR IMAGE FOR THE REVERSE SEQUENCE
           *
000070            CALL PULSR(ISR,IPINL,IORDER)
000072            CALL ADDSK(IFIRST,ISR,IT)
000075            CALL MIRROR(IT,ITT,IORDER,IFA)
           *
           *  TEST CONNECTION
           *
000100            ITL = IFIRST
000101            ITR = IFIRSTM
000103            II = 0
000104     200    CONTINUE
000104            IF (ITT.EQ.ITR .OR. IT.EQ.ITL) GO TO 280
000114            II = II + 1
```

```
          *
          *  ITR =RIGHT SHIFTED= TO AN EARLIER TIME
          *    BUT IT IS A MIRROR IMAGE OF THE ORIGINAL SHIFT REGISTER
          *
000115          CALL PULSR(ITR,IPINR,IORDER)
          *
          *  ITL =LEFT SHIFTED= TO A LATER TIME
          *
000120          CALL PULSR(ITL,IFINL,IORDER)
000123          GO TO 200
          *
          *  PHASE SHIFT OF SUM SEQUENCE DETERMINED FOR TAP CONNECTIONS
          *
000124    280   CONTINUE
000124          WRITE(6,290) INF,I,II
000136    290   FORMAT(16X O7, I6, I15)
000136    300   CONTINUE
000141          GO TO 125
000141          END
```

RUNX COMPILER (VER.2.3M)   07/01/76. 21.04.05.   RGA12

PROGRAM LENGTH
000357

STATEMENT FUNCTION REFERENCES

LOCATION	GEN TAG	SYM TAG	REFERENCES

STATEMENT NUMBER REFERENCES

LOCATION	GEN TAG	SYM TAG	REFERENCES
000153	C00010	105	NONE
000216	C00053	110	NONE
000010	L00007	111	000033
000211	C00046	112	000027
000034	L00022	115	000027
000044	L00027	125	000140
000246	C00103	150	000053
000104	L00057	200	000123
000124	L00071	280	000113
000305	C00142	290	000124

BLOCK NAMES AND LENGTHS
FIOBUF$- 002050

VARIABLE REFERENCES

LOCATION	GEN TAG	SYM TAG	REFERENCES					
000351	V00012	I	000067	000131	000136			
000314	A00001	IEA	000035	000042	000064	000076		
000344	V00005	IFIRST	000040	000044	000072	000100		
000345	V00006	IFIRSTM	000041	000101				
000356	V00017	II	000103	000113	000133			
000346	V00007	INF	000050	000057	000062	000127		
000342	V00003	INH	000014	000034				
000341	V00002	IORDER	000012	000017	000035	000041	000063	000070
			000076	000116	000121	000136		
000347	V00010	IPINL	000062	000070	000120			
000350	V00011	IPINR	000063	000115				

```
RUNX COMPILER (VER.2.3M)              07/01/76. 21.04.05.          RGA12

        000343   V00004   ISR   000034   000037   000040   000045   000067   000072
        000352   V00013   IT    000073   000075   000107
        000354   V00015   ITL   000101   000110   000120
        000355   V00016   ITR   000102   000104   000115
        000353   V00014   ITT   000075   000104

START OF CONSTANTS
000143

START OF TEMPORARIES
000310

START OF INDIRECTS
000314

EXTERNAL REFERENCES
        QENTRY   REWINM   INPUTE   OUTPTC   INITPT   MIRROR   STOP   CONNECT
        PULSR    ADDSR    END

COMPILER SPACE
UNUSED -  007700    USED  -  040100
```

```
RUNX COMPILER (VER.2.3M)                    07/01/76. 21.04.05.

                SUBROUTINE CONNECT(INF,IPINL,IPINR,IORDER,IFA)
          *
          *  SET UP MASKS FOR PIN HOOKUP OF SHIFT REGISTER AND ITS REVERSE
          *
          *
          *  IPINL IS NORMAL REGISTER WHICH IS CLOCKED TO THE LEFT
          *    OR A LATER TIME
          *
          *  IPINR IS THE REVERSED REGISTER WHICH IS CLOCKED TO THE RIGHT
          *    OR AN EARLIER TIME
000010          DIMENSION IFA(1)
000010          CALL BINCOEF(INF,IFA,IORDER+1)
000014          IPINR = IPINL = 0
000021          DO 150 I=1,IORDER
000022          CALL SBYT(I,1,IPINL,IFA(IORDER+2-I))
000030          CALL SBYT(I,1,IPINR,IFA(I))
00004C     150  CONTINUE
000046          RETURN
000046          END
```

```
RUNX COMPILER (VER.2.3M)                    07/01/76. 21.04.05.          CONNECT

SUBPROGRAM LENGTH
000057

STATEMENT FUNCTION REFERENCES

          LOCATION   GEN TAG   SYM TAG   REFERENCES

STATEMENT NUMBER REFERENCES

          LOCATION   GEN TAG   SYM TAG   REFERENCES

BLOCK NAMES AND LENGTHS

VARIABLE REFERENCES

          LOCATION   GEN TAG   SYM TAG   REFERENCES
          000056     V00006    I         000021    000024    000033    000035    000043

START OF CONSTANTS
000050

START OF TEMPORARIES
000052

START OF INDIRECTS
000055

EXTERNAL REFERENCES
          BINCOEF    SBYT      END

COMPILER SPACE
UNUSED -  010400    USED   -   037400
```

```
RUNX COMPILER (VER.2.3M)                 07/01/76. 21.04.05.

                SUBROUTINE INITPT(INH,ISR,IORDER,IFA)
          *
          *  SET UP BIT CONFIGURATION IN SHIFT REGISTER FOR INITIAL CONDITIONS
          *
          *
          *  SHIFT REGISTER IS REPRESENTED WITH THE COEFFICIENT OF THE
          *    CONSTANT TERM ON THE RIGHT OR IN BIT 0
          *
000007          DIMENSION IFA(1)
000007          CALL BINCOEF(INH,IFA,IORDER)
000010          ISR = 0
000013          DO 150 I = 1,IORDER
000015          CALL SBYT(I,1,ISR,IFA(I))
000023    150   CONTINUE
000030          RETURN
000030          END
```

```
RUNX COMPILER (VER.2.3M)                    07/01/76. 21.04.05.          INITPT

SUBPROGRAM LENGTH
000040

STATEMENT FUNCTION REFERENCES

         LOCATION  GEN TAG   SYM TAG   REFERENCES

STATEMENT NUMBER REFERENCES

         LOCATION  GEN TAG   SYM TAG   REFERENCES

BLOCK NAMES AND LENGTHS

VARIABLE REFERENCES

         LOCATION  GEN TAG   SYM TAG   REFERENCES
         000037    V00005    I         000014    000016    000025

START OF CONSTANTS
000032

START OF TEMPORARIES
000034

START OF INDIRECTS
000036

EXTERNAL REFERENCES
         BINCOEF   SBYT      END

COMPILER SPACE
UNUSED -  010500   USED   -  037300
```

```
RUNX COMPILER (VER.2.3M)                    07/01/76. 21.04.05.

                SUBROUTINE MIRROR(IT,ITT,IORDER,IFA)
          *
          *  GENERATE THE MIRROR IMAGE OF SHIFT REGISTER IT AND
          *    PUT IT IN ITT FOR A SHIFT REGISTER OF IORDER STAGES
          *
000007          DIMENSION IFA(1)
000007          CALL BINCOEF(IT,IFA,IORDER)
000010          ITT = 0
000013          DO 200 I=1,IORDER
000015          CALL SBYT(1,1,ITT,IFA(IORDER+1-I))
000023    200   CONTINUE
000030          RETURN
000030          END
```

```
RUN COMPILER (VER.2.3M)                 07/01/76. 21.04.05.          MIRROR

SUBPROGRAM LENGTH
000040

STATEMENT FUNCTION REFERENCES

          LOCATION   GEN TAG    SYM TAG    REFERENCES

STATEMENT NUMBER REFERENCES

          LOCATION   GEN TAG    SYM TAG    REFERENCES

BLOCK NAMES AND LENGTHS

VARIABLE REFERENCES

          LOCATION   GEN TAG    SYM TAG    REFERENCES
          000037     V00005     I          000014    000016    000025

START OF CONSTANTS
000032

START OF TEMPORARIES
000034

START OF INDIRECTS
000036

EXTERNAL REFERENCES
          BINCOFF    SBYT       END

COMPILER SPACE
UNUSED -  010500    USED   -  037300
```

```
RUN COMPILER (VER.2.3M)                07/01/76. 21.04.05.

                 SUBROUTINE BINCOFF(IP,IPA,NA)
000006           DIMENSION IPA(1)
            *
000006           IH = IP
            *
            *
000007           DO 10 I=1,NA
000010           IPA(I) = IH
000012           IH = IH/2
000013      10   CONTINUE
            *
000015           DO 20 I=1,NA
000016           IZ = IPA(I)
000017           IH = IZ/2
000021           IPA(I) = IZ - 2*IH
000024      20   CONTINUE
            *
000024           RETURN
000026           END
```

```
RUNX COMPILER (VER.2.3M)                07/01/76. 21.04.05.          BINCOEF

SUBPROGRAM LENGTH
000040

STATEMENT FUNCTION REFERENCES

          LOCATION   GEN TAG   SYM TAG   REFERENCES

STATEMENT NUMBER REFERENCES

          LOCATION   GEN TAG   SYM TAG   REFERENCES

BLOCK NAMES AND LENGTHS

VARIABLE REFERENCES

          LOCATION   GEN TAG   SYM TAG   REFERENCES
          000036     V00005    I         000007    000015
          000035     V00004    IH        000006    000011    000020    000022
          000037     V00006    IZ        000017    000022

START OF CONSTANTS
000030

START OF TEMPORARIES
000031

START OF INDIRECTS
000033

EXTERNAL REFERENCES
          END

COMPILER SPACE
UNUSED -  010500    USED    -   037300
```

```
STORAGE ALLOCATION.

        ADDRESS   LENGTH            BINARY CONTROL CARDS.

              0        6            IDENT   PULSR
              6                     END

                         ENTRY POINTS.

                         PULSR    -     1
```

```
                                          IDENT   PULSR
                                          ENTRY   PULSR
                               ***
                               *
                               *  CALL PULSR(ISR,IPINS,IORDER)
                               *
                               *    ISR = CONDITION OF SHIFT REGISTER
                               *
                               *    IPINS = MASK OF PIN CONNECTIONS
                               *
                               *    IORDER = ORDER OR NUMBER OF BITS IN SHIFT REGISTER
                               *
                               ***
0 20251423220000000002                    VFD     42/CLPULSR,18/2
1                              PULSR      BSS     1                 ENTRY/EXIT LINE
2 56110                                   SA1     B1                FETCH CONDITION OF SHIFT REGISTER
       56220                              SA2     B2                FETCH PIN CONNECTIONS
            56530                         SA5     B3                FETCH ORDER
3 6255777776                              SB5     X5-1              B5 IS SHIFT TO HIGH ORDER
            11312                         BX3     X1*X2             TRANSMIT PIN CONNECTIONS TO X3
                 47433                    CX4     X3                ADD RESULTS
4 43073                                   MX0     -1                 BY MOD 2
       15440                              BX4     -X0*X4               IN X4
            22454                         LX4     B5,X4             LEFT SHIFT TO HIGH ORDER
                 21101                    AX1     1                 SHIFT REGISTER RIGHT SHIFTED END OFF
5 12614                                   BX6     X1+X4             OR IN NEW HIGH ORDER BIT
       56610                              SA6     B1                STORE NEW CONDITION
            0400000001+                   EQ      PULSR             RETURN
6                                         END

     42760 STORAGE USED        29 STATEMENTS        1 SYMBOLS
```

```
SYMBOLIC REFERENCE TABLE.

 PULSR            1  PROGRAM*     1/09       2/15 L     2/28
```

```
STORAGE ALLOCATION.

     ADDRESS   LENGTH              BINARY CONTROL CARDS.

          0         4              IDENT   ADDSP
          4                        END

                         ENTRY POINTS.

                         ADDSR    -     1
```

```
                                     IDENT  ADDSR
                                     ENTRY  ADDSR
                            ***
                            *
                            *  CALL ADDSR(ISRA,ISRB,ISRS)
                            *
                            *    WHERE ISRS = ISRA (+) ISRB
                            *
                            *    AND (+) MEANS MOD 2 BIT BY BIT ADDITION OR EXCLUSIVE OR
                            *
                            ***
0 01040423220000000003             VFD    42/0LADDSR,18/3
1                          ADDSR   BSS    1               ENTRY/EXIT LINE
2 56110                            SA1    B1              FETCH SHIFT REGISTER A
       56220                       SA2    B2              FETCH SHIFT REGISTER B
             13612                 BX6    X1-X2           MOD 2 SR ADDITION
                   56630           SA6    B3              STORE SUM
3 0400000001+                      EQ     ADDSR           RETURN
4                                  END

    41161 STORAGE USED      19 STATEMENTS      1 SYMBOLS
```

SYMBOLIC REFERENCE TABLE.

```
 ADDSR          1  PROGRAM*     1/09      2/13 L    2/18
```

APPENDIX D. 5

COMPUTER PROGRAM LISTING FOR DETERMINATION OF SIDELOBE DISTRIBUTION OF GOLD CODES

The following listing is the computer program used for the generation of the sidelobe distribution of Gold codes of period $2^{11}-1$. The program computes the number of sidelobes in the cross-correlation function θ of any Gold codes of period 2^n-1 by making use of the formula for the number S of cross-correlation sidelobes given in A. 5. 4, i.e.,

$$S = \frac{\sum\theta^2 + 2\sum\theta + 2^n-1}{2^{n+1}} .$$

For each code, the program first computes its unbalance and its autocorrelation function. For each pair of codes to be correlated, the program then computes the product of the unbalances which yields the quantity $\sum\theta$ and the dot product of the autocorrelation function, which yields the quantity $\sum\theta^2$. The above formula then is used to compute the number of sidelobes for given cross-correlation and the distribution of code pairs with a given number of sidelobes.

```
RUNX COMPILER (VER.2.3M)                    07/06/76. 20.59.06.

                  PROGRAM PGA13(TAPE6,TAPE7)
            *
            *  CROSSCORRELATION FOR SIDE LOBE DISTRIBUTION OF GOLD CODES--7505
            *
            *  AUTHORS--IRA GREEN AND ROBERT GOLD
            *
            *  ACCEPTS OUTPUT FROM RGA10 ON *TAPE7* FOR SHIFT REGISTERS
            *    UP TO 11 STAGES AND GENERATES SOME CROSS CORRELATION
            *    DISTRIBUTIONS.
            *
            *  G1(J) = G2I(J) IS NOT USED.
            *
            *  ITHETAI IS THE ITH CORRELATION SEQUENCE
            *  ITHETAJ IS THE JTH CORRELATION SEQUENCE
            *  NTHETA IS THE CORRELATION COUNT
            *
000004            COMMON ITHETAI(2047),ITHETAJ(2047),NTHETAZ,NTHETA(2047),
000004           1       NCLR(4),ICDR(4)
            *
            *  INITIALIZE CORRELATION COUNT MATRIX
            *
000004            NTHETAZ = 0
000005            DO 101 I = 1,2047
000007            NTHETA(I) = 0
000010      101   CONTINUE
000012            REWIND 6
000014            REWIND 7
000016            READ(7) IHA,IFA,NA,ICODE1,IFB,NB,IPERIOD,JTHETAI,NCODES
000043            IF (NA.LE.11) GO TO 110
000046            WRITE(6,105) NA
000053      105   FORMAT(// I5 * STAGE SHIFT REGISTER EXCEEDS MAXIMUM OF*
000053           1       * 11 STAGES*/)
000053            STOP 1
000055      110   CONTINUE
000055            I1FACT = (2**NA - 1) * ((2**(NA+1)) - 1)
000071            I2FACT = 2**(NA+1)
000076            FSUM = NCODES * (NCODES+1) / 2.0
```

```
       *
       *  PROCESS MATRIX BY ROWS FROM THE DIAGONAL
       *
000103          IIM2 = NCODES - 1
000104          DO 500 II=1,IIM2
000104          IF (II.EQ.1) GO TO 120
000110          REWIND 7
000112          NRECBLK = IPERIOD/500
000115          IF (MOD(IPERIOD,500).NE.0) NRECBLK = NRECBLK + 1
000122          M2 = (II-1) * (2+NRECBLK)
000127          DO 115 I=1,M2
000127          READ(7)
000133    115   CONTINUE
000136          READ(7) IHA,IFA,NA,ICODEI,IFB,NB,IPERIOD,JTHETAI,NCODES
000163    120   CONTINUE
000163          CALL RTHETA(ITHETAI,IPERIOD)
000165          READ(7) NCOR,ICOR
       *
       *  COUNT AUTOCORRELATION OR DIAGONAL TERM
       *
000174          NMICOR = NCOR(I)
000175          NTHETA(NMICOR) = NTHETA(NMICOR) + 1
       *
       *  PROCESS THE IITH ROW FROM THE DIAGONAL
       *
000200          IJM1 = II + 1
000202          DO 300 IJ=IJM1,NCODES
000202          READ(7) IHA,IFA,NA,ICODEJ,IFB,NB,IPERIOD,JTHETAJ,NCODES
000230          CALL RTHETA(ITHETAJ,IPERIOD)
000232          READ(7) NCOR,ICOR
       *
       *  CALCULATE SUM OF THETA**2 FROM FORMULA
       *
       *  SUM OF THETA**2 = SUM OVER SEQUENCE OF THETA(GI,GI)*THETA(GJ,GJ)
       *
000241          ISUMT2 = 0
000242          DO 200 I=1,IPERIOD
000242          ISUMT2 = ISUMT2 + ITHETAI(I)*ITHETAJ(I)
```

```
CC0247     200  CONTINUE
              *
              *  CALCULATE NUMBER OF OCCURANCES FOR CORRELATION -1 FOR THE
              *     IJTH TERM FROM AN EXPRESSION
              *
CC0252              NM1COR = (IIFACT - ISUMT2 - 2*JTHETAI*JTHETAJ) / I2FACT
              *
              *  COUNT CROSSCORRELATION OF OFF DIAGONAL TERM
              *
CC0260              NTHETA(NM1COR) = NTHETA(NM1COR) + 1
CC0262     300  CONTINUE
CC0265     500  CONTINUE
              *
              *  ADD REMAINING AUTOCORRELATION OF LAST DIAGONAL TERM
              *
CC0270              NM1COR = NCOR(1)
CC0271              NTHETA(NM1COR) = NTHETA(NM1COR) + 1
              CCCCC
              C     WRITE(6,600)
              C600  FORMAT(////* STATISTICS FOR ALL I AND J ON AND ABOVE THE*
              C     1          * DIAGONAL*//
              C     2          * NUMBER OF TIMES CORRELATION (THETA) OF -1 OCCURS*
              C     3          * FOR EACH ELEMENT*/
              C     4          * VS*/
              C     5          * NUMBER OF ELEMENTS IN WHICH THE FREQUENCY OCCURS*//)
              C      I = 0
              C     IF (NTHETAZ.NE.0) WRITE(6,620) I,NTHETAZ
              C620  FORMAT(I15,I7)
              C     DO 630 I=1,IPERIOD
              C     IF (NTHETA(I).NE.0) WRITE(6,620) I,NTHETA(I)
              C630  CONTINUE
              CCCCC
CC0273              WRITE(6,635)
CC0277     635  FORMAT(////*                     OF     CUM.    PROBABILITY*/
CC0277          1          *                   LOBES  FREQ.   DISTRIBUTION*//)
              *
              *  CALCULATE CUMULA       FREQUENCY DISTRIBUTION
              *
```

```
RUNX COMPILER (VER.2.3M)                C7/C8/76. 20.59.06.          RGA13

000277          NTHETA(1) = NTHETA(1) + NTHETAZ
000301          DO 640 I=2,IPERIOD
000302          NTHETA(I) = NTHETA(I) + NTHETA(I-1)
000304    640   CONTINUE
          *
          *   PICK OUT CUMMULATIVE FREQUENCIES FOR NUMBER OF SIDE LOBES
          *     WHICH ARE A MULTIPLE OF 5
          *
000306          NLOBES = (IPERIOD/5) * 5
000311          IFREQ = 0
000313    645   ILFREQ = IFREQ
000314          I = IPERIOD - NLOBES
000316          IF (I.NE.0) GO TO 650
000320          IFREQ = NTHETAZ
000321          GO TO 660
000321    650   IFREQ = NTHETA(I)
000323    660   CONTINUE
000323          IF (IFREQ.EQ.0 .OR. IFREQ.EQ.ILFREQ) GO TO 750
000332          PDIST = IFREQ/FSUM
000334          WRITE(6,710) NLOBES,IFREQ,PDIST
000345    710   FORMAT(I16,I9,F11.3)
000345    750   NLOBES = NLOBES - 5
000347          IF (NLOBES.GE.0) GO TO 645
000350          STOP
000352          END
```

RLNX COMPILER (VER.2.3M)   07/06/76. 20.59.06.   RGA13

PROGRAM LENGTH
000501

STATEMENT FUNCTION REFERENCES

LOCATION	GEN TAG	SYM TAG	REFERENCES

STATEMENT NUMBER REFERENCES

LOCATION	GEN TAG	SYM TAG	REFERENCES	
000344	C00010	105	000045	
000035	L00026	110	000044	000045
000163	L00061	120	000107	
000401	C00025	635	000273	
000313	L00130	645	000347	
000321	L00126	650	000317	
000323	L00137	660	000320	
000416	C00042	710	000333	
000345	L00147	750	000331	

BLOCK NAMES AND LENGTHS
FIEBUF$- 002050 - 014006

VARIABLE REFERENCES

LOCATION	GEN TAG	SYM TAG	REFERENCES					
000462	V00025	FSUM	000102	000332				
000446	V00007	I	000006	000127	000133	000243	000301	000316
			000321					
000452	V00013	ICODEI	000026	000145				
000472	V00033	ICODEJ	000213					
014002002	A00005	ICER	000172	000237				
000450	V00011	IFA	000022	000142	000207			
000453	V00014	IFB	000030	000150	000215			
000476	V00037	IFREQ	000312	000313	000322	000323	000340	
000447	V00010	IHA	000020	000140	000205			
000464	V00025	II	000105	000123	000200	000265		
000463	V00024	IIM2	000103	000265				

RLNX COMPILER (VER.2.3M)   07/06/76. 20.59.06.   RCA13

```
        000471    V00032    IJ        000202    000262
        000470    V00031    IJM1      000201
        000477    V00040    ILFREQ    000315    000325
        000455    V00016    IPERIOD   000034    000112    000154    000163    000221    000230
                                      000247    000304    000314
        000474    V00035    ISUMT2    000241    000245    000252
        000000002 A00001    ITHETAI   000163
        003777002 A00002    ITHETAJ   000230
        000460    V00021    I1FACT    000071    000251
        000461    V00022    I2FACT    000076    000255
        000456    V00017    JTHETAI   000036    000156    000252
        000473    V00034    JTHETAJ   000223    000253
        000466    V00027    N2        000126    000133
        000451    V00012    NA        000024    000043    000050    000055    000064    000070
                                      000144    000211
        000454    V00015    NB        000032    000152    000217
        000457    V00020    NCODES    000040    000075    000160    000225    000263
        013776002 A00004    NCOR      000170    000174    000235    000267
        000475    V00036    NLOBES    000311    000314    000336    000345
        000467    V00030    NMICOR    000175    000257    000260
        000465    V00026    NRECBLK   000115    000120    000122
        007777002 A00003    NTHETA    000277
        007776002 V00006    NTHETAZ   000004    000277    000317
        000500    V00041    PDIST     000333    000342
```

START OF CONSTANTS
000354

START OF TEMPORARIES
000422

START OF INDIRECTS
000442

EXTERNAL REFERENCES
```
        CENTRY    REWINM    INPUTB    OUTPTC    STOP      IEAIEX    RTHETA    END
```

COMPILER SPACE

```
RUNX COMPILER (VER.2.3M)                 07/08/76. 20.59.06.        RGA13

UNUSED -  007300    USED   -  040500
```

```
RUNX COMPILER (VER.2.3M)                    07/08/76. 20.59.06.

                SUBROUTINE RTHETA(ITHETA,IPERIOD)
          *
          *  INPUT BLOCKED SET OF CORRELATIONS FOR THE DIAGONAL TERM
          *
          *     BLOCKING IS 500 WORDS/RECORD
          *
000005          DIMENSION ITHETA(1)
000005          ILEFT = IPERIOD
000005          IM2 = 0
000007     125  ILEFT = ILEFT - 500
000011          IM1 = IM2 + 1
000012          IM2 = IM2 + 500
000013          IF (ILEFT.GE.0) GO TO 135
000015          IF (ILEFT.LT.-499) GO TO 140
000017          IM2 = IM2 + ILEFT
000020     135  READ(7) (ITHETA(I),I=IM1,IM2)
000033          GO TO 125
000035     140  CONTINUE
000035          RETURN
000036          END
```

RUNX COMPILER (VER.2.3M)   07/08/76. 20.59.06.   RTHETA

SUBPROGRAM LENGTH
000051

STATEMENT FUNCTION REFERENCES

LOCATION	GEN TAG	SYM TAG	REFERENCES

STATEMENT NUMBER REFERENCES

LOCATION	GEN TAG	SYM TAG	REFERENCES	
000007	L00007	125	000034	
000020	L00017	135	000013	000014
000035	L00025	140	000016	

BLOCK NAMES AND LENGTHS

VARIABLE REFERENCES

LOCATION	GEN TAG	SYM TAG	REFERENCES		
000050	V00006	I	NONE		
000045	V00003	ILEFT	000005	000007	
000047	V00005	IM1	000012	000022	
000046	V00004	IM2	000006	000010	000027

START OF CONSTANTS
000040

START OF TEMPORARIES
000042

START OF INDIRECTS
000045

EXTERNAL REFERENCES
INPUTB   END

COMPILER SPACE
UNUSED - 010500   USED - 037300

```
              PROGRAM RGA10(TAPE5,TAPE6,TAPE7)
         *
         *   AUTOCORRELATION FOR SIDE LOBE DISTRIBUTION OF GOLD CODES--7505
         *
         *   AUTHORS--IRA GREEN AND ROBERT GOLD
         *
         *   A AND B SHIFT REGISTERS MUST BE THE SAME SIZE AND
         *     THEIR MAXIMUM IS 15.
         *
         *     H IS INITIAL CONDITION SHIFT REGISTER CONFIGURATION
         *     G IS INITIAL CONDITION POLYNOMIAL
         *     F IS ASSOCIATED POLYNOMIAL
         *
         *   OUTPUTS ON A SEPARATE FILE *TAPE7* IN BINARY THE INITIAL
         *     CONFIGURATION OF THE A AND B REGISTERS, THE PERIOD, N(0)-N(1)
         *     OF THE BASIC CODE, THE NUMBER OF CODES IN THIS RUN,
         *     AND THE SEQUENCE OF ALL THETAS
         *     FOLLOWED BY THEIR DISTRIBUTION.
         *
         *   THE SEQUENCE OF ALL THETAS IS GENERATED BY CORRELATING THE
         *     SEQUENCE WITH ITSELF AND SHIFTING.
         *
         *
000004        COMMON IH1(16),IG1(16),IF1(16),
000004       1        IH2(16),IG2(16),IF2(16),
000004       1        IF12(32),IT(32),ITS(32),ITP1(32),ITP2(32),
000004       1        IG(32),ITHETA(500),ICOR(4),NCOR(4)
000004        DIMENSION IHB(3)
000004        DATA IHB/2,2,2/
000004        NAMELIST/NLIST/ IHA,IFA,NA,IHB,IFB,NB,IPERIOD,ICOR
         *
         *   IHA, IFA, AND IFB ARE TO BE INPUT IN OCTAL AND THEREFORE MUST
         *     BE FOLLOWED BY A B.
         *
         *
         *   IHB IS THE BEGINNING, FINAL, AND INCREMENT FOR THE INITIAL
         *     CONDITION OF SHIFT REGISTER B IN OCTAL AND MUST BE
```

```
          *    FOLLOWED BY A B ON INPUT.
          *
          *  NA AND NB ARE THE ORDERS OF THE A AND B SHIFT REGISTERS.
          *
          *  IPERIOD IS THE PERIOD OF THE A AND B SHIFT REGISTERS.
          *
          *
000004          REWIND 5
000006          REWIND 6
000010          REWIND 7
000012          READ(5,NLIST)
000015          IPERIOD = 2**NA-1
          *
          *  CALCULATE NUMBER OF TERMS FROM THE ORDER
          *
000021          N1 = NA + 1
000023          N2 = NB + 1
          *
          *  CALCULATE NUMBER OF TERMS IN THE CORRELATION PRODUCT POLYNOMIAL
          *
000024          NTCOR = NA*2 + 1
          *
          *  CALCULATE THE POSSIBLE VALUES OF THE AUTOCORRELATION FUNCTION.
          *
000025          ICOR(1) = -1
000026          ICOR(2) = - (2 ** ((NA+1)/2)  +  1)
000035          ICOR(3) = 2 ** ((NA+1)/2)  -  1
000043          ICOR(4) = IPERIOD
000045          WRITE(6,NLIST)
          *
          *  INITIALIZE OUTPUT ON *TAPE6* FOR THE SEQUENCE OF CODES
          *
000050          WRITE(6,180) NA,IFA,IHA,NB,IFB,IPERIOD,ICOR
000072     180  FORMAT(///* A REGISTER* I3 * STAGES*/
000072       1          1H  O10 * ASSOCIATED POLYNOMIAL*/
000072       2          * INITIAL CONDITION*/ 13X O5//
000072       3          * B REGISTER* I3 * STAGES*/
000072       4          1H O10 * ASSOCIATED POLYNOMIAL*10X*MAXIMAL PERIOD * I10//
```

```
000072        5       * INITIAL CONDITION N(C)-N(1)* 4I10//)
000072          IF (NA.EQ.NE) GO TO 200
000074          PRINT 190
000100   190    FORMAT(* SHORT SHIFT REGISTERS MUST BE OF SAME LENGTH*)
000100          STOP 1
000102   200    CONTINUE
         *
         *  INPUT OCTAL REPRESENTATION IS CONVERTED TO A BINARY COEFFICIENT
         *    TABLE WITH THE FIRST ELEMENT BEING THE CONSTANT TERM.
         *     1ST ARG = OCTAL REPRESENTATION
         *     2ND ARG = OUTPUT TABLE OF BINARY COEFFICIENTS
         *     3RD ARG = NUMBER OF TERMS
         *
000102          CALL BINCOEF(IHA,IH1,N1)
000105          CALL BINCOEF(IFA,IF1,N1)
000110          CALL BINCOEF(IFB,IF2,N2)
000113          CALL PMPY(IF1,IF2,IF12,N1)
         *  ZERO TERM ADDED AT THE END OF IF12
         *    MAKING THE NUMBER OF TERMS = 2 * N1
         *
         *  IF12 MUST HAVE A CONSTANT TERM
         *
         *
         *  COMPACT IF12 POLYNOMIAL INTO ONE WORD
000116          CALL CPACT(IF12,IFF,NTCOR)
         *  IFF MUST HAVE A CONSTANT TERM
         *    IFF = F1 * F2
         *
         *
         *  INITIAL CONDITION POLYNOMIAL IS OBTAINED FROM INITIAL CONDITIONS
         *    FOR SHIFT REGISTER A AND THEN MULTIPLIED BY THE ASSOCIATED
         *    POLYNOMIAL FOR B.  THIS TERM DOES NOT CHANGE.
         *
000121          CALL INITIAL(IG1,IF1,IH1,N1)
000124          CALL PMPY(IG1,IF2,ITP1,N2)
000127          M1 = IHB(1)
000130          M2 = IHB(2)
000132          M3 = IHB(3)
```

```
000133           ITEMP = M2 - M1 + 1
000136           NCODES = ITEMP/M3
000141           IF (MOD(ITEMP,M3) .NE. 0) NCODES=NCODES+1
000147           DO 610 ICODE=M1,M2,M3
000151           CALL BINCOEF(ICODE,IH2,N2)
        *
        *  INITIAL CONDITION POLYNOMIAL IS OBTAINED FROM INITIAL CONDITIONS
        *    OF SHIFT REGISTER FOR THE SET OF GOLD CODES AS DETERMINED BY ICODE.
        *
000153           CALL INITIAL(IG2,IF2,IH2,N2)
000156           CALL PMPY(IG2,IF1,ITP2,N1)
000161           CALL PADD(ITP1,ITP2,IT,NTCOR)
        *  ZERO TERM ADDED AT THE END OF IT
        *    MAKING THE NUMBER OF TERMS = NTCOR + 1
        *
        *
        *  CALCULATE N(0)-N(1) IN THE BASIC CODE
        *
000164           CALL CPACT(IT,IGG,NTCOR)
000167           CALL COR(IGG,IFF,IPERIOD,IRHO,C)
000173           JTHETA = IPERIOD - 2*IRHO
        *
        *  INITIALIZE OUTPUT ON *TAPE7* FOR EACH CODE
        *
000176           WRITE(7) IHA,IFA,NA,ICODE,IFB,NB,IPERIOD,JTHETA,NCODES
000223           NCOR(1) = NCOR(2) = NCOR(3) = NCOR(4) = 0
000230           DO 260 I=1,NTCOR
000230           ITS(I) = IT(I)
000234     260   CONTINUE
000236           ITS(NTCOR+1) = 0
000237           ILEFT = IPERIOD
000240           IM2 = 500
000241     450   ILEFT = ILEFT - 500
000243           IF (ILEFT.GE.0) GO TO 460
000244           IF (ILEFT.LT.-499) GO TO 600
000246           IM2 = ILEFT + 500
000247     460   DO 500 I=1,IM2
000247           CALL PADD(IT,ITS,IG,NTCOR)
```

```
        *
        *  IG = (IG1*IF2+IG2*IF1)  +  (IG1*IF2+IG2*IF1)SHIFTED
        *
        *  CALCULATE IRHO = THE NUMBER OF DISAGREEMENTS OR N(1) IN THE
        *    CORRELATION PRODUCT POLYNOMIAL
        *
000254        CALL CPACT(IG,IGG,NTCOR)
000257        CALL COR(IGG,IFF,IPERIOD,IRHO,0)
        *
        *  THETA = N(0) - N(1)
        *
000263        ITHETA(I) = IPERIOD - 2*IRHO
        *
        *  DETERMINE THETA DISTRIBUTION
        *
000266        DO 490 II=1,4
000270        IF (ITHETA(I).EQ.ICOR(II)) GO TO 495
000273   490  CONTINUE
000275        WRITE(6,492) ITHETA(I)
000302   492  FORMAT(// * THETA =* I10, 10X *IS NOT A VALID ANALYTIC RESULT*)
000302        STOP 2
000304   495  NCOR(II) = NCOR(II) + 1
        *
        *  SHIFT PRODUCT OF THE A AND B POLYNOMIALS BY 1
        *
000307        CALL XSHIFT(ITS,IF12,NTCOR)
000311   500  CONTINUE
000314        WRITE(7) (ITHETA(1),I=1,IM2)
000326        GO TO 450
000327   600  CONTINUE
000327        WRITE(7) NCOR,ICOR
000336        WRITE(6,605) ICODE,JTHETA,NCOR
000350   605  FORMAT(13X O5, 5I10)
000350   610  CONTINUE
        *
000353        STOP
000355        END
```

RUNX COMPILER (VER.2.3M) 07/01/76. 20.57.03. RGA10

PROGRAM LENGTH
000576

STATEMENT FUNCTION REFERENCES

LOCATION	GEN TAG	SYM TAG	REFERENCES

STATEMENT NUMBER REFERENCES

LOCATION	GEN TAG	SYM TAG	REFERENCES
000424	C00013	180	000050
000474	C00063	190	000074
000102	L00044	200	000073
000241	L00125	450	000326
000247	L00133	460	000243
000506	C00075	492	000274
000304	L00156	495	000272
000327	L00170	600	000245
000516	C00105	605	000336

BLOCK NAMES AND LENGTHS
FIOBUFS- 003074 - 001434

VARIABLE REFERENCES

LOCATION	GEN TAG	SYM TAG	REFERENCES					
000572	V00044	I	000231	000250	000263	000267	000277	000311
000566	V00040	ICODE	000150	000206	000341	000350		
001424C02	A00016	ICPR	000026	000070	000334	000466		
000550	V00022	IFA	000055	000105	000202	000364		
000552	V00024	IFB	000063	000110	000210	000375		
000560	V00032	IFF	000116	000167	000257			
000040C02	A00003	IF1	000105	000113	000121	000156		
000140C02	A00007	IF12	000114	000116	000307			
000120C02	A00006	IF2	000110	000113	000124	000153		
000400C02	A00014	IG	000251	000254				
000567	V00041	IGG	000164	000167	000254	000257		
000020C02	A00002	IG1	000121	000124				

```
RUNX COMPILER (VER.2.3M)                07/01/76. 20.57.03.          RGA10

          000100C02 A00005   IG2      000153   000156
          000547    V00021   IHA      000057   000102   000200   000361
          000544    A00020   IHB      000127   000372
          000000C02 A00001   IH1      000102   000122
          000060C02 A00004   IH2      000151   000154
          000575    V00047   II       000267   000304
          000573    V00045   ILEFT    000237   000241
          000574    V00046   IM2      000240   000246   000311   000322
          000554    V00026   IPERIOD  000021   000043   000065   000170   000173   000214
                                      000236   000260   000264   000403
          000570    V00042   IRHO     000170   000173   000260   000264
          000200C02 A00010   IT       000162   000164   000250
          000564    V00036   ITEMP    000136   000141
          000440C02 A00015   ITHETA   NONE
          000300C02 A00012   ITP1     000125   000161
          000340C02 A00013   ITP2     000157   000161
          000240C02 A00011   ITS      000235   000251   000306
          000571    V00043   JTHETA   000175   000216   000343
          000561    V00033   M1       000130   000133   000147
          000562    V00034   M2       000132   000133   000351
          000563    V00035   M3       000134   000136   000350
          000551    V00023   NA       000015   000021   000034   000053   000072   000204
                                      000367
          000553    V00025   NB       000022   000061   000072   000212   000400
          000565    V00037   NCODES   000142   000145   000220
          001430C02 A00017   NCOR     000226   000332   000346
          000557    V00031   NTCOP    000025   000117   000162   000165   000233   000252
                                      000255   000307
          000555    V00027   N1       000023   000103   000106   000114   000122   000157
          000556    V00030   N2       000024   000111   000125   000151   000154

START OF CONSTANTS
000411

START OF TEMPORARIES
000522

START OF INDIRECTS
```

```
RUNX COMPILER (VER.2.3M)                  07/01/76. 20.57.03.           RGA10

C00541

EXTERNAL REFERENCES
        QBNTRY    REWINM    INPUTN    IBAIEX    OUTPTN    OUTPTC    STOP      BINCOEF
        PMPY      CPACT     INITIAL   PADD      COR       OUTPTB    XSHIFT    END

COMPILER SPACE
UNUSED -  C36700    USED   -  C41100
```

```
RUNX COMPILER (VER.2.3M)                     07/01/76. 20.57.03.

                 SUBROUTINE CPACT(IP,IPC,NN)
         *
         *  COMPACT IP POLYNOMIAL WITH NN TERMS INTO ONE WORD IPC
         *
         *    SIGN BIT IS LOW ORDER TERM OF POLYNOMIAL
         *
000006           DIMENSION IP(1)
000006           IPC = 0
000006           DO 100 I=1,NN
000010           CALL SBYT(61-I,1,IPC,IP(I))
000017   100     CONTINUE
000024           RETURN
000024           END
```

```
RUNX COMPILER (VER.2.3M)                 07/01/76. 20.57.03.        CRACT

SUBPROGRAM LENGTH
000035

STATEMENT FUNCTION REFERENCES

         LOCATION   GEN TAG    SYM TAG    REFERENCES

STATEMENT NUMBER REFERENCES

         LOCATION   GEN TAG    SYM TAG    REFERENCES

BLOCK NAMES AND LENGTHS

VARIABLE REFERENCES

         LOCATION   GEN TAG    SYM TAG    REFERENCES
         000034     V00004     I          000C07     000021

START OF CONSTANTS
000026

START OF TEMPORARIES
000030

START OF INDIRECTS
000033

EXTERNAL REFERENCES
         SBYT       END

COMPILER SPACE
UNUSED -  010500    USED    -   037300
```

```
X COMPILER (VER.2.3M)                         07/01/76. 20.57.03.

                 SUBROUTINE XSHIFT(IG,IP,N)
           *
           *  CLOCK TO LEFT OR ADVANCE IN TIME
           *
           *  N IS THE ORDER+1
           *
000006           DIMENSION IG(1),IP(1)
000006           IF (IG(1).EQ.0) GO TO 30
000007           DO 20 I=1,N
000010           IG(I) = IG(I) + IP(I) - 2*IG(I)*IP(I)
000015     20    CONTINUE
000020     30    CONTINUE
000020           DO 40 I=1,N
000022           IG(I) = IG(I+1)
           *  N+1 ELEMENT OF IG MUST CONTAIN A 0
           *
000024     40    CONTINUE
000026           RETURN
000026           END
```

```
RUNX COMPILER (VER.2.3M)                    07/01/76. 20.57.03.          XSHIFT

SUBPROGRAM LENGTH
000036

STATEMENT FUNCTION REFERENCES

         LOCATION  GEN TAG   SYM TAG   REFERENCES

STATEMENT NUMBER REFERENCES

         LOCATION  GEN TAG   SYM TAG   REFERENCES
         00002C    L00014    30        000006

BLOCK NAMES AND LENGTHS

VARIABLE REFERENCES

         LOCATION  GEN TAG   SYM TAG   REFERENCES
         000035    V00004    I         000007    000015    000021

START OF CONSTANTS
000030

START OF TEMPORARIES
000031

START OF INDIRECTS
000033

EXTERNAL REFERENCES
         END

COMPILER SPACE
UNUSED - 010500   USED   - 037300
```

```
                     SUBROUTINE PADD(IA,IB,IC,NN)
              *
              *   IC = IA (+) IB WITH ZERO TERM ADDED AT THE END MAKING
              *                 THE NUMBER OF TERMS = NN+1
              *
000007               DIMENSION IA(1),IB(1),IC(1)
000007               DO 100 I=1,NN
000010               IC(I) = IA(I) + IB(I) -IA(I)*IB(I)*2
000017        100    CONTINUE
000022               IC(NN+1) = 0
000023               RETURN
000023               END
```

```
RUNX COMPILER (VER.2.3M)                07/01/76. 20.57.03.          PAGD

SUBPROGRAM LENGTH
000035

STATEMENT FUNCTION REFERENCES

         LOCATION  GEN TAG   SYM TAG   REFERENCES

STATEMENT NUMBER REFERENCES

         LOCATION  GEN TAG   SYM TAG   REFERENCES

BLOCK NAMES AND LENGTHS

VARIABLE REFERENCES

         LOCATION  GEN TAG   SYM TAG   REFERENCES
         000034    V00005    I         000007    000017

START OF CONSTANTS
000025

START OF TEMPORARIES
000026

START OF INDIRECTS
000030

EXTERNAL REFERENCES
         END

COMPILER SPACE
UNUSED - 010500    USED  -  037300
```

```
RUNX COMPILER (VER.2.3M)                    07/01/76. 20.57.03.

                  SUBROUTINE INITIAL(IG,IF,IH,NN)
           *
           *   CALCULATE INITIAL CONDITION POLYNOMIAL IG FROM
           *     INITIAL CONDITIONS OF SHIFT REGISTER IH AND
           *     ASSOCIATED POLYNOMIAL IF
           *   NN IS THE ORDER+1
           *
000007            DIMENSION IG(1),IF(1),IH(1)
000007            DO 200 I=1,NN
000010            IG(I) = 0
000011     200    CONTINUE
000013            NNM1 = NN - 1
000015            DO 500 IO=1,NNM1
000015            DO 400 II=1,IO
000016            IJ = IO - II + 1
000021            IT = IH(II) * IF(IJ)
000025            IG(IO) = IG(IO) + IT - IG(IO)*IT*2
000032     400    CONTINUE
000035     500    CONTINUE
000037            RETURN
000040            END
```

```
FUNX COMPILER (VER.2.3M)                07/01/76. 20.57.03.          INITIAL

SUBPROGRAM LENGTH
000056

STATEMENT FUNCTION REFERENCES

         LOCATION  GEN TAG   SYM TAG   REFERENCES

STATEMENT NUMBER REFERENCES

         LOCATION  GEN TAG   SYM TAG   REFERENCES

BLOCK NAMES AND LENGTHS

VARIABLE REFERENCES

         LOCATION  GEN TAG   SYM TAG   REFERENCES
         000050    V00005    I         000007
         000053    V00010    II        000016    000032
         000054    V00011    IJ        000021    000022
         000052    V00007    ID        000015    000017
         000055    V00012    IT        000025    000026
         000051    V00006    NNM1      000014    000035

START OF CONSTANTS
000042

START OF TEMPORARIES
000043

START OF INDIRECTS
000045

EXTERNAL REFERENCES
         END

COMPILER SPACE
UNUSED -  010400    USED   -   037400
```

RUNX COMPILER (VER.2.3M)   07/01/76. 20.57.03.

```
                  SUBROUTINE   PMPY(IA,IB,IC,NN)
000007            DIMENSION IA(1),IB(1),IC(1),IR(1)
          *
000007            NA2 = NN + NN
000010            DO 10 I = 1,NA2
000010            IC(I) = 0
000012    10      CONTINUE
          *
000015            DO 30 I=1,NN
          *
000016            IAI = IA(I)
000017            IF(IAI.EQ.0)   GO TO 30
000021            I1 = I - 1
          *
000023            DO 20 J= 1,NN
000024            K = I1 + J
          *        IABK = IAI*IB(J)
000025            IC(K) = IC(K) + IB(J)
000031    20      CONTINUE
          *
000033    30      CONTINUE
          *
          *
000036            DO 40 I = 1,NA2
000036            ICI = IC(I)
000040            ICH = ICI/2
000042            IC(I) = ICI - 2*ICH
000045    40      CONTINUE
          *
000047            RETURN
000050            END
```

```
RUNX COMPILER (VER.2.3M)                07/01/76. 20.57.03.          RMPY

SUBPROGRAM LENGTH
000070

STATEMENT FUNCTION REFERENCES

         LOCATION  GEN TAG   SYM TAG   REFERENCES

STATEMENT NUMBER REFERENCES

         LOCATION  GEN TAG   SYM TAG   REFERENCES
         000033    L00027    30        000020

BLOCK NAMES AND LENGTHS

VARIABLE REFERENCES

         LOCATION  GEN TAG   SYM TAG   REFERENCES
         000061    V00007    I         000010    000015    000033    000036
         000062    V00010    IAI       000017
         000067    V00015    ICH       000041    000043
         000066    V00014    ICI       000040    000043
         000057    A00001    IR        NONE
         000063    V00011    IJ        000022    000024
         000064    V00012    J         000023
         000065    V00013    K         000025
         000060    V00006    NA2       000007    000012    000045

START OF CONSTANTS
000052

START OF TEMPORARIES
000053

START OF INDIRECTS
000055

EXTERNAL REFERENCES
         END
```

```
RUNX COMPILER (VER.2.3M)                    07/01/76. 20.57.03.          PMPY

COMPILER SPACE
UNUSED -  010400    USED   -  037400
```

```
RUNX COMPILER (VER.2.3K)                    07/01/76.  20.57.03.

                   SUBROUTINE BINCOEF(IP,IPA,NA)
000006             DIMENSION IPA(1)
               *
000006             IH = IP
               *
               *
000007             DO 10 I=1,NA
000010             IPA(I) = IH
000012             IH = IH/2
000013      10     CONTINUE
               *
000015             DO 20 I=1,NA
000016             IZ = IPA(I)
000017             IH = IZ/2
000021             IPA(I) = IZ - 2*IH
000024      20     CONTINUE
               *
000026             RETURN
000026             END
```

```
RUNX COMPILER (VER.2.3M)                 07/01/76. 20.57.03.          BINCOEF

SUBPROGRAM LENGTH
000040

STATEMENT FUNCTION REFERENCES

         LOCATION  GEN TAG   SYM TAG   REFERENCES

STATEMENT NUMBER REFERENCES

         LOCATION  GEN TAG   SYM TAG   REFERENCES

BLOCK NAMES AND LENGTHS

VARIABLE REFERENCES

         LOCATION  GEN TAG   SYM TAG   REFERENCES
         000036    V00005    I         000007    000015
         000035    V00004    IH        000006    000011    000020    000022
         000037    V00006    IZ        000017    000022

START OF CONSTANTS
000030

START OF TEMPORARIES
000031

START OF INDIRECTS
000033

EXTERNAL REFERENCES
         END

COMPILER SPACE
UNUSED -  010500    USED   -  037300
```

```
                                     IDENT  COR
                                     ENTRY  COR
                           ***
                           *  ARGUMENTS ARE:
                           *    C(B1) G = INITIAL CONDITIONS POLYNOMIAL
                           *    C(B2) F = ASSOCIATED POLYNOMIAL
                           *    C(B3) IPERIOD = PERIOD OF C POLYNOMIAL
                           *    C(B4) IRHC = NET MINIMUM NUMBER OF DISAGREEMENTS OR N(1)
                           *    C(B5) LWINDOW = SLIDING WINDOW FOR PARTIAL CORRELATION
                           *
                           *    B7 = 1
                           *    X0 = 1
                           *    X1 = GLEFT
                           *    X2 = F
                           *    X3 = GRIGHT
                           *    X4 = IPERIOD
                           *    X5 = LWINDOW  THEN  USED FOR MIN
                           *    X6 - NET COUNT
                           *    X7 = MIN COUNT
                           ***
0 03172200000000000005               VFD    42/0LCOR,18/5
1                          COR       BSS    1              ENTRY/EXIT LINE
2 6170000001                         SB7    1              PUT 1 IN B7
           76070                     SX0    B7              AND IN X0
                56550                SA5    B5             FETCH LWINDOW TO X5
3 56430                              SA4    B3             FETCH IPERIOD TO X4
      0315000005+                    NZ     X5,OK          IF A SLIDING WINDOW IS DEFINED, OK
                10544                BX5    X4             OTHERWISE COMPUTE ONLY
4 76400                              SX4    B0              SINGLE WINDOW
5 14555                    OK        BX5    -X5            CHANGE SIGN FOR LOOP WINDOW COUNT
      76600                          SX6    B0             INITIALIZE NET ONES COUNT
           56110                     SA1    B1             FETCH G FOR LEFT END POINT
                56220                SA2    B2             FETCH F
6 10311                              BX3    X1             COPY G FOR RIGHT END POINT
7 0321000010+              LOOPW     PL     X1,NONE        IF LOW ORDER OF G IS 0 SHIFT ONLY
           36660                     IX6    X6+X0          OTHERWISE COUNT
                13112                BX1    X1-X2            AND DIVIDE
```

```
                        *
                        *                          CONSTANT TERM GUARANTEED IN
                        *                          ASSOCIATED POLYNOMIAL
                        *                          REMOVES LOW ORDER
                        *
 10 20101               NONE    LX1    1           NOW SHIFT
        36550                   IX5    X5+XC       INCREMENT LOOP WINDOW COUNT
            0335000007+         NG     X5,LOOPW    IF COUNTER STILL NEGATIVE, LOOP
 11 10766                       BX7    X6          INITIALIZE MINIMUM ONES COUNT
        0314000020+             ZR     X4,STR      IF THERE IS NO WINDOW, STORE RESULTS
                  14444         BX4    -X4         OTHERWISE CHANGE SIGN FOR LOOP COUNT
 12 0321000013+         LOOP    PL     X1,NONE1    IF LOW ORDER OF GLEFT IS 0 SHIFT ONLY
            36600               IX6    X6+X0       OTHERWISE ADD COUNT
                  13112         BX1    X1-X2         AND DIVIDE
 13 20101               NONE1   LX1    1           NOW SHIFT
        0323000015+             PL     X3,NONE3    IF LOW ORDER OF GRIGHT IS 0 SHIFT ONLY
                  37060         IX6    X6-XC       OTHERWISE SUBTRACT COUNT
 14 13332                       BX3    X3-X2         AND DIVIDE
 15 20301               NONE3   LX3    1           NOW SHIFT
        37567                   IX5    X6-X7       IF NET IS GREATER THAN
            0325000017+         PL     X5,CONT       MINIMUM CONTINUE
 16 10766                       BX7    X6          OTHERWISE DEFINE NEW MIN COUNT
 17 36440               CONT    IX4    X4+XC       INCREMENT LOOP COUNT
        0334000012+             NG     X4,LOOP     IF COUNTER STILL NEGATIVE, LOOP
 20 56740               STR     SA7    B4          OTHERWISE STORE RESULTS
        0400000001+             EQ     COR          AND RETURN
 21                             END

      42760 STORAGE USED      64 STATEMENTS      9 SYMBOLS
```

```
SYMBOLIC REFERENCE TABLE.

 CONT         17  PROGRAM*    3/21        3/23 L
 COR           1  PROGRAM*    1/09        2/22 L     3/26
 LOOP         12  PROGRAM*    3/12 L      3/24
 LOOPW         7  PROGRAM*    2/35 L      3/08
 NONE         10  PROGRAM*    2/35        3/06 L
 NONE1        13  PROGRAM*    3/12        3/15 L
 NONE3        15  PROGRAM*    3/16        3/15 L
 OK            5  PROGRAM*    2/27        2/30 L
 STR          20  PROGRAM*    3/10        3/25 L
```

APPENDIX E. 5

TABLE OF PREFERRED PAIRS OF MAXIMAL POLYNOMIALS OF DEGREE 11, 13, 15, 18, 19

PREFERRED PAIRS OF DEGREE 11

4005	4445
4445	6015
4215	4563
4055	5623
6015	6233
7413	7335
4143	5263
4563	6637
4053	5221
5023	5747
5623	7627
4577	6227
6233	7431
6673	5265
7237	5607

PREFERRED PAIRS OF DEGREE 11

7335	4603
4505	7041
5337	4173
5263	5463
5361	5625
5171	4053
6637	4707
7173	5531
5711	7243
5221	4731
6307	6651
6211	7317
5747	6765
4533	7655
4341	5545

PREFERRED PAIRS OF DEGREE 13

36515	32437
26077	31303
35673	25775
20635	27217
33763	23077
25745	27051
36575	33343
26653	34641
21133	22675
22441	36501
30417	35567
32517	22233
37335	33163
25327	24031
23231	31327

PREFERRED PAIRS OF DEGREE 13

20033	23261
23261	30741
24623	21277
23517	34723
30741	31425
21643	26077
30171	33763
21277	26653
27777	30417
35051	25327
34723	26533
34047	27271
32535	21103
31425	32311
37505	30711

PREFERRED PAIRS OF DEGREE 15

117423	146637
106341	103145
161007	115135
174003	174443
113337	145573
126007	103125
105257	123023
114467	177541
177207	162375
147047	160521
111511	147363
114633	176561
133663	176133
102171	117143
170465	173661

ORIGINAL PAGE IS
OF POOR QUALITY

PREFERRED PAIRS OF DEGREE 15

100003	102043
102043	102067
110013	177775
102067	103251
104307	112611
100317	117423
177775	174003
103451	126007
110075	177207
102061	102171
114725	161615
103251	123067
163005	125235
112611	171737
120265	122231

PREFERRED PAIRS OF DEGREE 18

1000047	1431503
1000077	1763717
1000115	1443125
1000173	1072617
1000201	1325427
1000333	1032067
1000347	1703227
1000355	1176621
1000407	1324243
1000517	1571527
1000621	1530521
1000743	1623325
1000751	1100233
1000757	1060065
1001013	1022541

ORIGINAL PAGE IS
OF POOR QUALITY

PREFERRED PAIRS OF DEGREE 18

1001023	1707137
1001141	1025051
1001165	1305335
1001253	1301323
1001361	1402335
1001427	1101533
1001453	1133015
1001455	1162577
1001567	1560655
1001607	1657733
1001625	1754267
1001631	1774153
1001651	1574603
1001661	1753301
1001705	1452077

PREFERRED PAIRS OF DEGREE 18

1007121	1363535
1007165	1141703
1007171	1771735
1007263	1230121
1007315	1131677
1007417	1716201
1007501	1054121
1007543	1615575
1007637	1201011
1007705	1766061
1007777	1640727
1010045	1260711
1010051	1243565
1010133	1530723
1010163	1604575

ORIGINAL PAGE IS
OF POOR QUALITY

PREFERRED PAIRS OF DEGREE 18

1010211	1733241
1010313	1125611
1010463	1743317
1010551	1101063
1010613	1207077
1010615	1763515
1010727	1156337
1010741	1205651
1011041	1323607
1011055	1613463
1011245	1525001
1011261	1073733
1011267	1021101
1011333	1760247
1011347	1116115

PREFERRED PAIRS OF DEGREE 19

2000605	2105575
2000635	2146157
2000641	2105121
2000655	2106753
2000663	2164223

ORIGINAL PAGE IS
OF POOR QUALITY

PREFERRED PAIRS OF DEGREE 19

2000047	2020471
2000077	2060063
2000107	2021131
2000123	2061313
2000131	2041173
2000143	2022743
2000157	2022107
2000175	2043343
2000223	2165127
2000257	2125273
2000341	2106645
2000503	2025777
2000541	2007265
2000553	2024055
2000565	2047005

PREFERRED PAIRS OF DEGREE 19

2001557	2032367
2001637	2175617
2001645	2112435
2001651	2113527
2001711	2112543
2001727	2172501
2001733	2173475
2001735	2150163
2001763	2177277
2002067	2243311
2002121	2263405
2002165	2260165
2002177	2241477
2002211	2327617
2002221	2366261

ORIGINAL PAGE IS
OF POOR QUALITY

PREFERRED PAIRS OF DEGREE 19

2002265	2366451
2002271	2367727
2002323	2346323
2002331	2366333
2002435	2260507

APPENDIX F. 5

COMPUTER PROGRAM LISTING FOR GENERATION OF PREFERRED PAIRS OF MAXIMAL PN SEQUENCES

```
RUNX COMPILER (VER.2.3M)                12/27/75. 14.07.16.

                      PROGRAM IG3(INPUT,OUTPUT)
                C
                C   CODE COMPONENTS PROGRAM
                C
000004                DIMENSION IPA(254),IPB(254),IPC(7),IPD(7),IPR(127)
000004                ACCEPT NR
000011                DO 500 ID=1,64
000013                IPA(1) = 0
000014                IOCT = ID - 1
000016                DO 110 I1=2,7
000017                IPA(I1) = IOCT .AND. 1B
000021                IOCT = IOCT/2
000022          110   CONTINUE
000024                DO 120 I=1,7
000025                IPB(I) = 1
000026          120   CONTINUE
000030                CALL SE02A7(IPA,IPB,NR,IPC,IPD,IPR)
000034                IF (MOD(ID,12).EQ.1) PRINT 150,NR
000047          150   FORMAT(1H1 *BALANCED CODE COMPONENTS OF LENGTH* I4)
000047                PRINT 200, (IPC(I),I=1,7)
000061                PRINT 200, (IPD(I),I=1,7)
000073                PRINT 200, (IPR(I),I=1,NR)
000106          200   FORMAT(1H 80I1)
000106          500   CONTINUE
000110                STOP
000112                END
```

ORIGINAL PAGE IS
OF POOR QUALITY

```
RUNX COMPILER (VER.2.3M)                     12/27/75. 14.07.16.

                SUBROUTINE SEQ2A7(IPA,IPB,NR,IPC,IPD,IPR)
000011          DIMENSION IPA(254), IPB(254), IPC(7), IPD(7), IPR(127)
000011          CALL SEQ37(IPA)
000012          CALL SEQ1237(IPB)
          C
          C  2**N-1 = 127 FOR N=7
          C
000017          ICOMP = 127 - NR
000024          ISUM = 0
000025          DO 120 I=1,ICOMP
000025          ICOUNT = 1
000030          IF (IPA(I).EQ.IPB(I)) ICOUNT=-1
000034          ISUM = ISUM + ICOUNT
000036     120  CONTINUE
000040          M2 = 127 + ICOMP
000041          DO 140 I=ICOMP,M2
000041          IF (ISUM.EQ.0) GO TO 400
000043          I2 = I + 1
000044          I1 = I2 - ICOMP
000046          ICOUNT1 = 1
000047          IF (IPA(I1).EQ.IPB(I1)) ICOUNT1=-1
000053          ICOUNT2 = 1
000054          IF (IPA(I2).EQ.IPB(I2)) ICOUNT2=-1
000060          ISUM = ISUM - ICOUNT1 + ICOUNT2
000062     140  CONTINUE
          C     DISPLAY *EVEN NUMBER OF 1*S AND 0*S NOT FOUND*
000065          DO 200 I=1,7
000067          IPC(I) = IPD(I) = 0
000073     200  CONTINUE
000075          DO 210 I=1,NR
000076          IPR(I) = 0
000077     210  CONTINUE
000101          RETURN
000102     400  CONTINUE
          C     DISPLAY *COMPARISION FOUND AFTER*, I, *TERMS*
000102          ISTART = I
000104          DO 410 I=1,7
```

```
RUNX COMPILER (VER.2.3M)                    12/27/75. 14.07.16.        SEC2A7

000105             IPC(I) = IPA(ISTART+I)
000110             IPD(I) = IPB(ISTART+I)
000113       410   CONTINUE
000115             DO 420 I=1,NR
000117             IPP(I) = MOD( IPA(ISTART+I) + IPB(ISTART+I) , 2 )
000130       420   CONTINUE
000133             RETURN
000133             END
```

ORIGINAL PAGE IS
OF POOR QUALITY

```
RUNX COMPILER (VER.2.3M)                12/27/75. 14.07.16.

                  SUBROUTINE SEQ37(IPA)
000003            DIMENSION IPA(254)
000003            DO 120 I=8,254
000005            IPA(I) = MOD( IPA(I-3) + IPA(I-7) , 2 )
000013      120   CONTINUE
000015            RETURN
000016            END
```

RUNX COMPILER (VER.2.3M)   12/27/75. 14.07.16.

```
                SUBROUTINE SEQ1237(IPB)
000003          DIMENSION IPB(254)
000003          DO 120 I=8,254
000005          IPB(I) = MOD(
000005         1 IPB(I-1) + IPB(I-2) + IPB(I-3) + IPB(I-7) , 2 )
000016     120  CONTINUE
000020          RETURN
000021          END
```

APPENDIX G-5

CODE LIBRARY FOR FORWARD LINK RANGE CHANNEL

MAXIMAL PN CODES OF PERIOD 2^{18}-1 HAVING SIX OR LESS FEEDBACK TAPS IN THE GENERATING SHIFT REGISTER

SHIFT REGISTERS WITH LESS THAN OR EQUAL NUMBER OF TAPS THAN 6

1022005
1022027
1022055
1022131
1022145
1022225
1022311
1022443
1022461
1022621
1023045
1023103
1023111
1023221
1023405
1024017
1024027
1024063
1024065
1024305
1025105
1025141
1026023
1026043
1026061
1030145
1030161
1030215
1030303
1030311
1030321
1030341
1030407
1034013
1034051
1034105
1035021
1040043
1040051
1040117
1040205
1040247
1040361
1040463
1040465
1040545
1040645
1040721
1041011
1041035
1041207
1041225
1041423
1041445
1041451
1041505

APPENDIX H-5

ALTERNATE CODE LIBRARY FOR MODE 1 RETURN LINK

MAXIMAL PN CODES OF PERIOD $2^{18}-1$ HAVING SIX OR LESS FEEDBACK TAPS IN THE GENERATING SHIFT REGISTER

1000115	1004455
1000743	1004545
1000751	1004623
1001013	1004643
1002031	1004645
1002061	1004711
1002075	1005035
1002133	1005213
1002171	1005225
1002211	1005305
1002241	1005341
1002441	1005431
1002623	1005451
1002705	1005521
1002741	1006113
1003011	1006161
1003035	1006605
1003053	1007031
1003215	1010045
1003451	1010051
1003461	1010463
1003521	1010551
1004073	1010613
1004163	1010615
1004205	1010741
1004313	1011041
1004405	1011245
1004447	